

From sample to smartphone: consumer-operable analytical devices for multiplex allergen detection

Georgina M.S. Ross

Thesis committee

Promotor

Prof. Dr M.W.F. Nielen

Special Professor Analytical Chemistry with a special emphasis on the detection of food contaminants

Wageningen University & Research

Co-promotor

Dr G. IJ. Salentijn

Assistant Professor at the Laboratory of Organic Chemistry

Wageningen University & Research

Other members

Prof. Dr HJ. Wichers, Wageningen University & Research

Prof. Dr C.T. Elliott, Queen's University Belfast, United Kingdom

Prof. Dr E.M.J. Verpoorte, University of Groningen

Dr Bert Pöpping, FOCOS, GbR, Alzenau, Germany

This research was conducted under the auspices of the Graduate School VLAG (Advanced studies in Food Technology, Agrobiotechnology, Nutrition and Health Sciences).

From sample to smartphone: consumer-operable analytical devices for multiplex allergen detection

Georgina M.S. Ross

Thesis

submitted in fulfilment of the requirements for the degree of doctor
at Wageningen University
by the authority of the Rector Magnificus,
Prof. Dr A.P.J. Mol,
in the presence of the
Thesis Committee appointed by the Academic Board
to be defended in public
on Friday 12th March 2021
at 1 p.m. in the Aula.

Georgina M.S. Ross

From sample to smartphone: consumer-operable analytical devices for multiplex allergen detection

274 pages

PhD thesis, Wageningen University, Wageningen, NL (2021)

With references, with summary in English

DOI: [10.18174/541188](https://doi.org/10.18174/541188)

ISBN: 978-94-6395-701-4

**Science and everyday life
cannot and should not
be separated**

Rosalind Franklin

Table of Contents

1	Introduction	11
2	Consumer-friendly food allergen detection: moving towards smartphone-based immunoassays	39
3	Rapid antibody selection using surface plasmon resonance for high-speed and sensitive hazelnut lateral flow prototypes	97
4	A critical comparison between flow-through and lateral flow immunoassay formats for visual and smartphone-based multiplex allergen detection	125
5	Interconnectable solid-liquid protein extraction unit and chip-based dilution for multiplexed consumer immunodiagnosics	161
6	Unraveling the hook effect: a comprehensive study of high antigen concentration effects in sandwich lateral flow immunoassays	191
7	General discussion	229
	Summary	257
	Curriculum Vitae	261
	Acknowledgements	265
	Overview of completed training activities	271

Abbreviations

(c)BCPI	(corrected)Blue Channel Pixel Intensity
ALARA	As Low as Reasonably Achievable
ASSURED	Affordable, Sensitive, Specific, User-friendly, Rapid, Equipment-free, Deliverable
AuNPs	Gold Nanoparticles
BB	Borate Buffer
BC	Blank Cookie
BCA	Bicinchoninic acid assay
BSA	Bovine Serum Albumin
CAD	Computer Aided Design
CCD	Charge Coupled Device
CIP	Clean in Place
CMOS	Complementary Metal Oxide Semiconductor
CMYK	Cyan, Magenta, Yellow, Key
CNP-mAb	Carbon nanoparticle-labelled monoclonal antibodies
CNPs	Carbon Nanoparticles
CPUs	Central Processing Units
DF	Dilution Factor
EC	European Commission
ECSA	European Citizen Science Association
ELISA	Enzyme Linked Immunosorbent Assay
EU	European Union
EW	Evanescent Wave
FARRP	Food Allergy Research and Resource Program
Fc-IgG	Fc-receptor specific antibody
FDA	Food & Drug Administration
FDM	Fused Deposition Modelling
FO	Fiber Optic
fps	Frames per second
GAMaB	Goat anti-mouse antibody
GPS	Global Positioning System
GUI	Graphical User Interface
HA	Hazelnut Assay
HC	Hazelnut Cookie
HPC	Hazelnut, Peanut, Control; LFIA
IgG	Immunoglobulin
LED	Light Emitting Diode
LFIA	Lateral Flow Immunoassay
LOAEL	Lowest Observable Adverse Effect Limit
LOC	Lab on a Chip
LOD	Limit of Detection
mAb	Monoclonal Antibody
MFC	Miniaturized Flow Cytometry
MIP	Molecularly Imprinted Polymers

MQ	MilliQ Water
NOAEL	No Observable Adverse Effect Limit
PA	Peanut Assay
pAb	Polyclonal Antibody
PAL	Precautionary Allergen Labeling
PBS	Phosphate Buffered Saline
PC	Peanut Cookie
PDMS	Polydimethylsiloxane
PHC	Peanut, Hazelnut, Control; LFIA
PoC	Point of Care
PPE	Personal Protective Equipment
ppm	parts per million
QD	Quantum Dots
RASFF	Rapid Alert System Food & Feed
RB	Running Buffer
RGB	Red, Green, Blue
RIU	Refractive Index Unit
ROI	Region of Interest
RSD	Relative Standard Deviation
RU	Response Unit
SB	Storage Buffer
SEM	Scanning Electron Microscopy
SLA	Stereolithography
SPR	Surface Plasmon Resonance
THP	Total Hazelnut Protein
TIR	Total Internal Reflection
TLC	Thin Layer Chromatography
TPP	Total Peanut Protein
ULOC	Unibody Lab on a Chip
USB	Universal Serial Bus
UV-VIS	Ultra-Violet Visible Spectrophotometry
VITAL	Voluntary Incidental Trace Allergen Labeling
WB	Washing Buffer
WHO	World Health Organization
μPAD	Micro Paper Analytical Device

CHAPTER 1

1

Introduction

1 Introduction

Food allergies represent a significant and increasingly prevalent health concern affecting the lives of over 220 million people worldwide^{1,2}. Allergies are typically caused by proteins that are naturally present in many foods, but they can also be towards food additives (e.g., sulphites). These so-called food allergens are capable of eliciting an adverse immune response in sensitized individuals. While people can become or sensitized, to almost any food, the majority of food allergies are caused by 14 allergens: milk, eggs, peanuts, tree-nuts, fish, shellfish, soy, wheat celery, mustard, sesame, sulphur dioxide/sulphites, lupine and mollusk (see Figure 1.1). Allergic symptoms can range from mild, such as rashes, itching, stomach pains and diarrhea, to severe including shortness of breath, loss of consciousness and even fatal anaphylaxis³.

The 14 Allergens



Figure 1.1. Icons of the 14 regulated allergens.

Under European Commission (EC) legislation (Directive 2003/89/EC), food products containing any of the 14 allergens must explicitly state so on the food packaging⁴. In 2014 a further amendment specified the requirement for allergen labeling of non-packaged foods containing the 14 legislated allergens. This regulatory framework safeguards individuals from exposure to known allergenic foods. However, it is the presence of undeclared allergens that have been inadvertently introduced into a food product that are the biggest risk for the allergic consumer; traces of allergens that occur due to cross-contamination are not regulated by the EU⁵. To prevent allergen cross-contact, manufacturers must stick to strict clean-in-place (CIP) procedures, especially when allergen-containing and allergen-

free foods or foods containing different allergens are manufactured/processed in the same facility⁶. Even with dedicated sanitation procedures, trace amounts of allergenic proteins can still infiltrate other food products. To reduce the risk of unintentional exposure to allergens, food manufacturers can voluntarily incorporate precautionary allergen labeling (PAL) on pre-packaged food (e.g., 'May Contain X' labels)⁷; but this comes with its own risks such as, consistently changing ingredient formulations⁸, global labeling differences⁹, lack of agreed regulatory threshold levels¹⁰ and inconsistent terminology/readability¹¹ of the label¹². Even with regulatory frameworks, voluntary PAL statements, mandatory allergen declarations and CIP procedures, a rising number of international food-related recalls are due to mislabeling of food products containing undeclared allergens^{5,13}. These allergens are infiltrating our global food supply-chain, putting the allergic community at constant risk.

In the past, most people trusted the food industry and governments to maintain food safety and to control for the presence of allergens, but with the increasing number of food-allergen related recalls, that perception is shifting. This growing consumer distrust is understandable, especially when government agencies responsible for public food safety (e.g., the FDA) announce temporary ingredient and food labeling alterations that leave allergic individuals inadequately protected^{8,12}. Providing consumers with the analytical tools to test for trace allergens themselves could give them an additional layer of security and assurance that their food is safe to eat¹⁴. This would require the development of consumer-operable devices that can detect allergens in a safe and accessible way.

For too long, industrial quality assurance/control procedures, labeling initiatives and governmental regulations have fell short of providing protection for food allergic individuals. As consumers become more aware of the potential risks of undeclared allergen presence, we are witnessing a paradigm shift in food allergen testing with the emergence of inexpensive, sensitive and portable citizen-science focused tests capable of on-the-go allergen detection, taking the analysis out of the lab and literally into the hands of allergic individuals. Portable analytical systems capable of executing simplified sample extraction, preparation, and multi-allergen detection, with minimal user-input will enable consumers to carry out their own allergen analysis¹⁵. The World Health Organization (WHO) outlined the necessary criteria for decentralized testing as being affordable, sensitive, specific, user-friendly, rapid, equipment-free and deliverable (ASSURED)^{16,17}. Combining disposable, paper-based colorimetric tests, such as lateral flow immunoassays (LFIA) that are already readable by the naked eye, with a digital device capable of recording photos or videos can empower consumers to perform their own food safety testing and automate data analysis¹⁵. Scientific developments that make on-site screening for trace allergens accessible, allowing for data storage, interpretation, connectivity and reporting, should reduce the number of food allergy related hospitalizations¹⁸.

At the same time, such devices will likely increase the percentage of allergen-based recalls, as consumers hold food manufacturers more accountable. Exploiting ubiquitous devices such as smartphones or tablets as analytical detectors offers an attractive approach because of the global reach of these technologies¹⁹. Smartphones are well-positioned for on-site analytical chemistry because of their powerful central processing units (CPUs), advanced optical sensors (camera), embedded flash functions, global positioning systems (GPS), portability and their ability to connect to the internet through Bluetooth and WiFi for Cloud based data storage¹⁸⁻¹⁹. Further, smartphone sensors are already commercially available for food allergen detection¹⁸, but typically these rely on proprietary diagnostic kits/reagents¹⁹, ultimately negating one of the key benefits of smartphone-based detectors, affordability.

For personalized food allergen testing to become accessible to all, some key requirements must be addressed such as assay affordability, speed, sensitivity, portability, simplicity - including sample preparation; and the ability to extract and detect multiple allergens from a single solid sample. The science and technology behind a device capable of integrating sample preparation, immunosensing and smartphone detection requires input from multiple disciplines as evident from Figure 1.2.

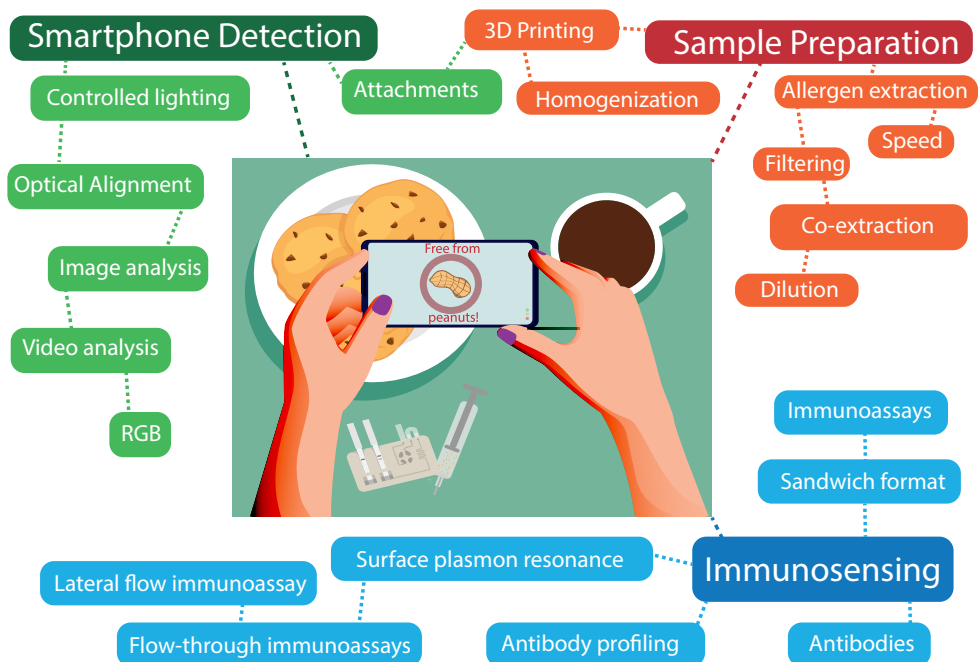


Figure 1.2. Schematic depiction of “from sample to smartphone”. Overview of the key themes of this thesis for the development of consumer operable immunodiagnosics for food allergen detection.

This introduction (Chapter 1) provides the necessary context, terminology and methodologies for this thesis, including an introduction to: sample preparation, immunosensing, smartphone detection and 3D-printing. More details about the current state-of-the-art for consumer-friendly food allergen detection can be found in the review presented in Chapter 2.

2 Sample Preparation

Before a food product can be tested for the presence of allergens, it is necessary to separate allergenic proteins from their food matrices into a testable liquid. In the case of a solid food sample, allergen extraction is typically carried out in the laboratory, first requiring the sample to be homogenized to a fine powder and incubated in a liquid buffer for an extended period of time, before filtering the resulting extract through a series of low-protein binding syringe filters. The ideal sample preparation protocol should enable extraction recovery of 100% of the target compound, but for food allergens the situation is more complicated because the extractability of these proteins can be altered by food processing techniques²⁰.

Usually, the recovery afforded by a given extraction is compared and benchmarked against other extraction methods using standardized certified reference materials. However, while several food allergen reference materials have been developed to-date, these do not yet allow certification according to international standards (ISO) requirements²¹.

Lengthy and complicated sample preparation is a paradox compared with the relative speed and simplicity characteristic of many on-site allergen screening assays and cannot be considered consumer-friendly²². One portable allergen test (iTube) requires food samples to first be ground and incubated for 10 min in extraction buffer (50-60°C) followed by a further 10 min incubation with assay reagents (conjugate, substrate and stop solution) before the sample is ready for testing²³. Longer extraction times and multi-step sample preparation might be appropriate for some allergen analyses, but not when the intention is for rapid, on-site screening. Even the fastest allergen tests have extractions of over 3 min and require multiple sample handling steps, increasing the safety risk for consumers when involving irritating or harmful reagents and the risk of human error^{24, 25}.

Even after allergens have been extracted from their matrix, concentrated samples still require dilution with assay running buffer (RB) into the appropriate dynamic working range to prevent adverse high concentration dependent effects. Sample dilution is particularly important when considering optical detection with paper-based immunoassays (discussed further section 2.1), because concentrated samples can lead to false negative results due to the "hook-effect"²⁶. Further, it is unrealistic to expect allergic individuals to

have the equipment or technical skill to carry out multi-step sample handling procedures, making sample preparation a pivotal bottleneck when considering consumer-operable allergen testing¹⁸. Micro-paper analytical devices (μ PADs) or lab-on-a-chip devices that integrate safe, multi-step sample handling and automated dilution in a single handheld device present an interesting option for portable sample preparation²⁷.

While it is widely acknowledged that simplified sample preparation is a dire necessity for on-site food safety testing, currently there is only one commercial allergen sensor capable of achieving this²⁸. The gluten and peanut sensors from Nima Labs accomplish integrated sample preparation through disposable capsules that allow for the grinding, mixing and solid-liquid extraction of either gluten or peanut proteins within minutes²⁹. Still, this cutting-edge extraction technology only allows for the extraction of a single analyte (e.g., gluten or peanut) with separate sensors being required for each analyte, and the \$5 disposable capsules come at a significant cost. To make consumer allergen analysis accessible to all a combined, inexpensive, miniaturized extraction device capable of handling sample homogenization, multi-allergen extraction and dilution is needed.

The emergence of affordable 3D-printing platforms (discussed in section 4) has reformed the rapid prototyping of disposable devices for integrated sample handling and miniaturized analytical chemistry^{30,31}; but until now, these devices have focused on membrane separation, solid-phase extraction and liquid-liquid extraction^{24,32-35}, leaving samples requiring solid-liquid extraction, such as foods, still requiring extensive sample pre-treatment.

2.1 Immunosensing

Immunosensors or immunoassays are affinity-based analytical assays that rely on the interaction between an antibody and a specific antigen³⁶. Immunoassays can be singleplex and only detect a single antigen or can be multiplex and use a number of different antibodies or a polyspecific antibody to detect several antigens. Many people suffer from more than one food allergy, with even unrelated allergens experiencing cross-reactivity towards other structurally similar but distinct allergens³⁷. The high prevalence of co-allergies means that is necessary to develop multiplex immunosensors capable of simultaneously detecting different allergens from a single sample, saving the consumer time and money compared with performing multiple singleplex tests. Still, there are only a handful of simplified immunosensors capable of multiplex allergen detection³⁸⁻⁴⁰. For further detail, readers should refer to the comprehensive review on multiplex immunosensors recently provided by Anfossi⁴¹.

This section introduces some of the fundamental terms and concepts for immunosensing including immunoreagent selection and characterization by surface plasmon resonance (SPR), key immunoassay formats, screening assay validation, smartphone detection and 3D-printing.

2.1.1 Immunoreagents

Antibodies or immunoglobulins (Ig) are Y shaped proteins comprised of two heavy (H) and two light (L) chains and a variable binding site (paratope) which dictates which specific epitope on the antigen that particular antibody can interact with⁴² (see Figure 1.3A). As antibodies are produced by the immune system to counteract the presence of foreign compounds (antigens) in the blood, they are only formed against targets big enough to elicit an immune response, such as food allergens⁴³. Because of their ability to specifically target and bind with proteins, antibodies have been widely used as biorecognition elements in a range of detection immunoassays.

Monoclonal antibodies (mAbs) are produced from fusing the the antibody producing cells from mice exposed to the target antigen with an immortal cancer cell (hybridoma). Because the hybridoma is specialized for antibody secretion and can be directed with pre-determined specificity towards a particular target antigen; it allows for the continuous production of identical clones, making mAbs excellent choices for commercial immunodiagnosics⁴⁴⁻⁴⁵. The allergen specific mAbs applied in this research were previously developed by immunizing mice with extracted hazelnut or peanut protein (obtained from roasted or combination of roasted and raw hazelnut/peanut) and isolating the mAbs from raw cell culture media by precipitation and affinity chromatography^{46,47}.

Immunoassays typically rely on the use of a specific mAb (or pair of mAbs) to detect the target antigen (e.g., an allergen) as well as a secondary species-specific antibody to amplify the assay signal and/or act as a control region.

2.1.2 Sandwich Format Immunoassays

The two formats of immunoassay used for food allergen detection are competitive and sandwich immunoassays. Competitive immunoassays are typically used for low molecular weight compounds but can also be used for some allergens⁴⁸. They are based on the competition between a free analyte and a labeled detector antigen for a limited number of capture antibody binding sites. Comparably, sandwich format immunoassays use two antibodies to capture their target antigen and as such can support the detection of larger compounds and proteins such as food allergens due to the presence of multiple binding epitopes (see Figure 1.3B)^{49 50,51}. In sandwich or two-site immunoassays, one mAb is immobilized onto a surface (capture mAb) and a secondary mAb is conjugated to an optical label/reporter molecule such as a nanoparticle or enzyme (detector mAb). Labels should retain their properties when conjugated with immunoreagents, be detectable at low levels and be stable over a prolonged time period. Some labels such as, gold nanoparticles, colored polystyrene beads, carbon nanoparticles, selenium nanoparticles and silver nanoparticles elicit a direct optical signal that can read with the naked eye⁵². Other labels including quantum dots, up-converting phosphors, and fluorophores require

a UV light source to make them visible; while other reporter molecules (e.g., enzymes) require the addition of a substrate to generate a detectable signal.

When testing a sample containing the target antigen, the antigen will be captured between the immobilized mAb and the labelled detector mAb to produce an optical signal, or between the immobilized mAb, labelled mAb and substrate to catalyze a readable color change. In an assay's dynamic working range, the signal intensity increases alongside antigen concentration as more antigen and detector antibody are captured by the immobilized capture antibody.

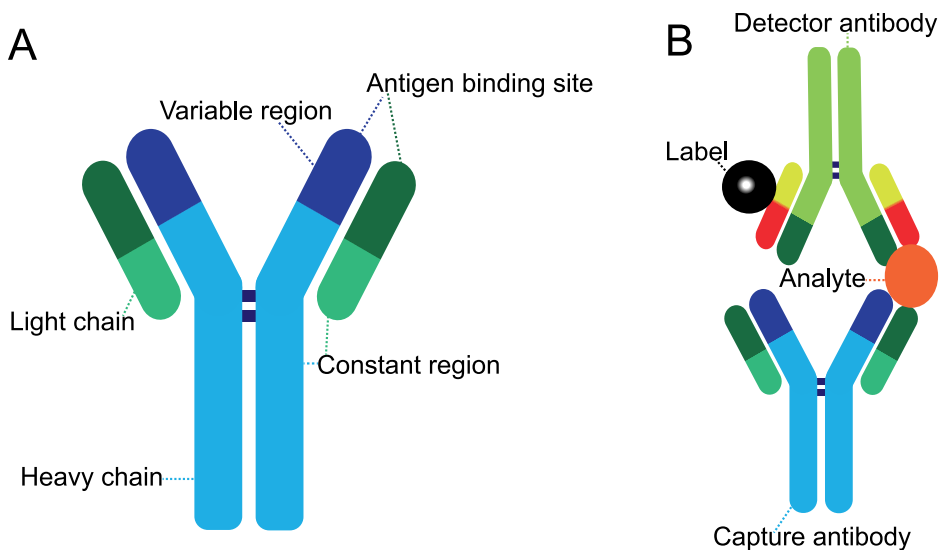


Figure 1.3. Annotated graphic showing antibody regions and binding. (A) Depiction of relevant antibody features (B) Schematic of antibody sandwich pair binding where the capture antibody binds the analyte which in turn binds the detector antibody that carries the optical label.

2.2 SPR-based Immunosensing

The selection of an appropriately matched mAb sandwich pair, capable of specifically and rapidly detecting the target antigen at low levels, is crucial for successful immunoassay development. One way to compare mAbs for their specificity, sensitivity, speed and sandwich pair binding potential is to measure them by surface plasmon resonance (SPR). SPR is label-free and allows for monitoring of biomolecular interactions, such as antibody-antigen binding, in real-time.

In SPR-based immunosensors, antibodies are immobilized onto a gold chip surface over which the sample of interest is injected. When plane-polarized (P-polarized) light is

reflected from a thin gold film surface, under total internal reflection (TIR) conditions an evanescent wave (EW) is generated⁵³. The EW is absorbed by free electrons on gold chip surface creating surface plasmons which cause a shift in the intensity of the reflected light (called the resonance angle)⁵³. The SPR signal is generated from the changes in refractive index at the gold surface of the sensor chip. The increase in mass caused by a binding event (e.g., antibody-antigen binding) resulting in a shift in the refractive index which is observed as an increase in response⁵⁴. The response is directly proportional to the number of molecules bound at the surface and is measured as response units (RUs)⁵⁵.

Sensorgrams are the output from SPR and show RU's versus time allowing for label-free, real-time detection of analytes⁵⁶ (see Figure 1.4). Using the sensorgrams, detailed information about antibody-antigen binding kinetics and affinity (rate of association and rate of dissociation) can be elucidated⁵⁴.

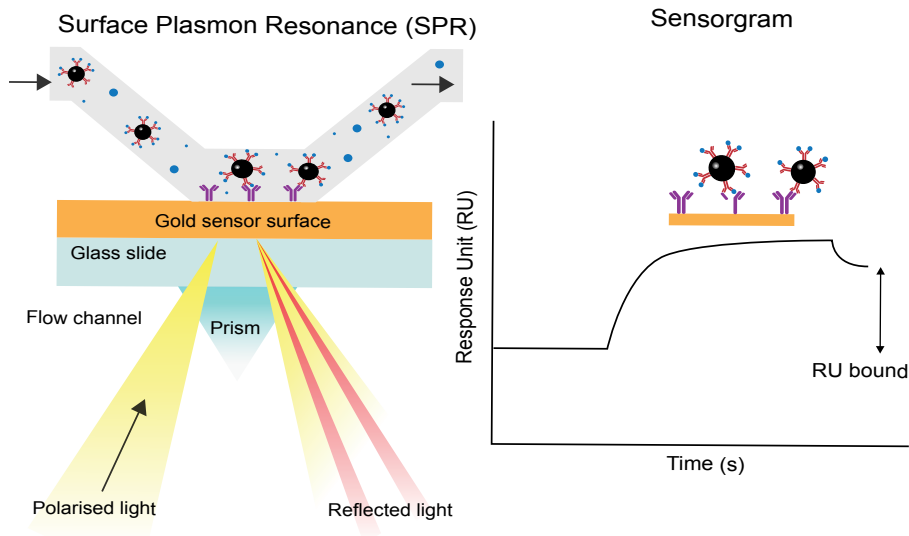


Figure 1.4. Schematic of an SPR-based biosensor and sensorgram output. (A) SPR-based biosensing; a capture antibody (purple) is immobilized on the gold sensor surface with analyte (blue) being injected across the surface; when antibody-analyte binding at the gold surface occurs, this causes a change in refractive index. (B) SPR sensorgram showing the binding response, or response units (RUs) in real-time. The increasing curve shows the association (binding response) of the antigen for the immobilized capture antibody, the plateau indicates the binding is at steady-state and the subsequent dip shows the antigen dissociating (unbinding) with the capture antibody following the termination of injection; the arrow shows the RUs or antigen bound at the end of the assay.

2.3 Microplate-based Immunoassays

Microplate-based immunoassays such as enzyme-linked immunosorbent assays (ELISAs) are the gold standard for laboratory-based food allergen detection²². In ELISA, the allergen-specific capture antibody is immobilized onto surface of microwell. When the plate is incubated with liquid sample containing allergen, the allergenic proteins present in the sample bind with the capture antibody. After washing steps, a secondary enzyme-labelled antibody is added, this catalyzes a colorimetric change upon addition of a substrate (see Figure 1.5). This color change can then be measured using a microplate reader, with increasing signal intensity directly correlating with increasing allergen concentration.

Despite being the most widely used method for food allergen analysis, ELISA is restricted to a centralized laboratory test by its multiple sample handling steps, lengthy duration (up to 3.5 hours) and need for specialized equipment such as multi-channel pipettes, 96-well plates, plate-readers and considerable sample/reagent consumption²³. These limitations, and the necessity for technical skills makes microplate-based ELISA's unsuitable for consumer-based allergen detection.

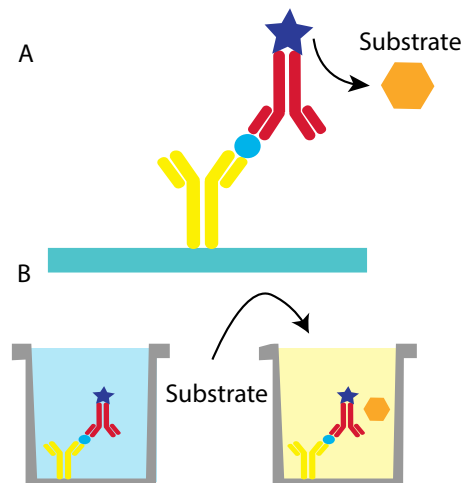


Figure 1.5. Schematic showing a sandwich format ELISA. (A) A capture antibody (yellow) immobilized in a microwell binds the antigen (blue circle) which then binds a secondary antibody conjugated to an enzyme (blue star) labelled antibody (red), when a substrate is added the enzyme catalyzes a color change (orange hexagon). (B) Depiction of the color change observed upon adding substrate.

An alternative approach to ELISA is to integrate microfluidic chips which allow for immunoreagent pre-storage and controlled reagent interaction with digital optical detection⁵⁷⁻⁵⁹. Miniaturized analytical fluidic systems substantially reduce the sample/reagent consumption, assay duration and cost compared with traditional ELISA⁶⁰. Yet,

ELISA can be made even more affordable, portable and disposable when converting it from a microplate/chip-based assay to a paper-based format⁶¹.

2.4 Paper-based Immunoassays

In microplate-based immunoassays, mAbs are directly immobilized onto the solid support of the microwell⁶²; in paper-based immunoassays, the capture mAb is shaped into a test region. Paper-based immunoassays benefit from being affordable, disposable and porous, resulting in capillary action that is beneficial for transporting liquid samples²⁷.

2.4.1 Lateral Flow Immunoassay (LFIA)

LFIA have revolutionized point-of-care diagnostics, translating traditional laboratory-based immunoassays into affordable and accessible home testing devices. The science underpinning LFIA is derived from the latex agglutination assay, which was first developed in 1956⁶³, with the technology becoming increasingly popular with the application to pregnancy testing^{64,65}. While the home pregnancy test remains the most successful application of LFIA⁶⁶, rapid on-site LFIA have been developed for a multitude of food-safety^{38,39,67}, biomedical^{68,69}, forensic^{70,71} and environmental⁷² needs.

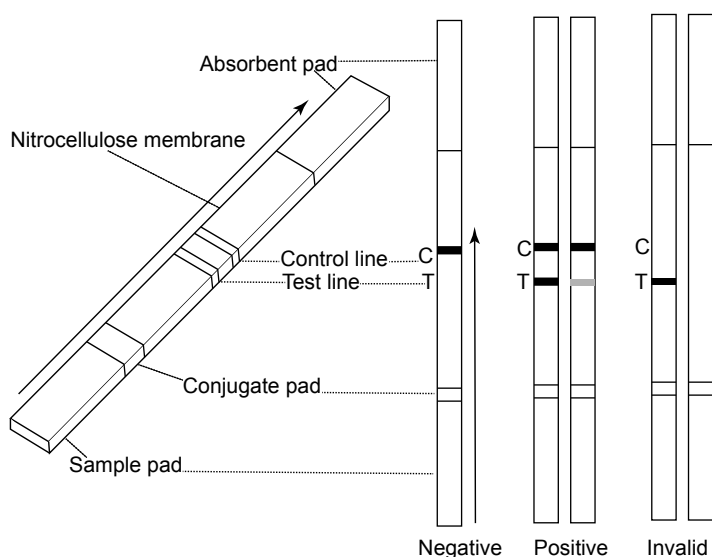


Figure 1.6. Schematic overview of the components in a typical singleplex LFIA and the possible results, where the arrows represent sample flow direction. (A) LFIA components: sample flows through the sample pad to the conjugate pad where any antigen in the sample interacts with labelled antibodies, the labeled antigen-analyte complex flows up the nitrocellulose membrane and is captured by the test line (T) and the control line (C), the absorbent pad acts as the fluid driving force for the LFIA. (B) LFIA tested in different sample types: C only means a sample is negative, C and T of any intensity means a sample is positive, only a T or no lines at all is indicative of an invalid sample concentration or LFIA.

The core component of a LFIA is the paper nitrocellulose (NC) membrane on which the immunoreagents are immobilized and the immunochemical reaction occurs. The type of NC membrane used for an LFIA depends on specific assay requirements such as desired test duration and sensitivity. The pore size and porosity of the NC determine the LFIA's capillary flow rate, dictating how quickly the sample front moves up the LFIA. This is usually measured as seconds per cm and correlates with the NC pore size, with the flow rate proportionally increasing along with pore size. Comparably, slower NC membranes with smaller pores increase the available binding opportunity for optical labels/labeled [antigen-antibody complexes] to bind at the test line, which can increase the assay sensitivity. In most cases, LFIA developers select a mid-speed NC membrane as a compromise between assay speed and sensitivity. In addition to the capture mAb(s) immobilized as test line(s), a secondary species-specific antibody, capable of binding the labeled detection mAb is immobilized as a control line. Typically, test and control lines are sprayed using a low volume dispenser, such as the BioDot instruments. The NC membrane is overlaid at one end by an absorbent pad which acts as the sink for the assay, directing fluid by capillary action and maintaining a consistent flow rate (see Figure 1.6). The NC membrane and absorbent pad are secured by a plastic backing. If the assay requires it, a sample pad and a conjugate pad impregnated with labeled-antibodies can also be added.

Unlike microplate-based assays, LFIA's mostly can be read by the naked eye making them suitable for on-site testing. Further, LFIA's can be semi-quantified when combined with an optical detector⁷³. In addition to being drastically faster and portable, LFIA's are also comparable or superior to microplate immunoassays in terms of development time, simplicity, cost and versatility⁷⁴.

2.4.1.1 LFIA Mechanism

When allergen extract diluted with running buffer and detection mAb comes into contact with an LFIA, it moves passively up the LFIA strip towards the absorbent pad. The allergen is captured by the immobilized test line antibody, and the detection mAb forms a sandwich complex with the antigen and capture antibody, giving a measurable optical signal. Remaining free labelled- secondary mAb moves up the LFIA where it is captured at the control line, resulting in the appearance of two lines for a positive result in a singleplex LFIA, or more lines in a multiplex LFIA (see Figure 1.7). In an LFIA's dynamic working range, as the concentration of analyte increases the intensity of the test line also increases. However, as the concentration of analyte increases beyond the dynamic working range, it begins to influence the development of signal on both the control and test lines, with extreme concentrations even leading to the complete loss of test line, known as the hook-effect^{75,76}.

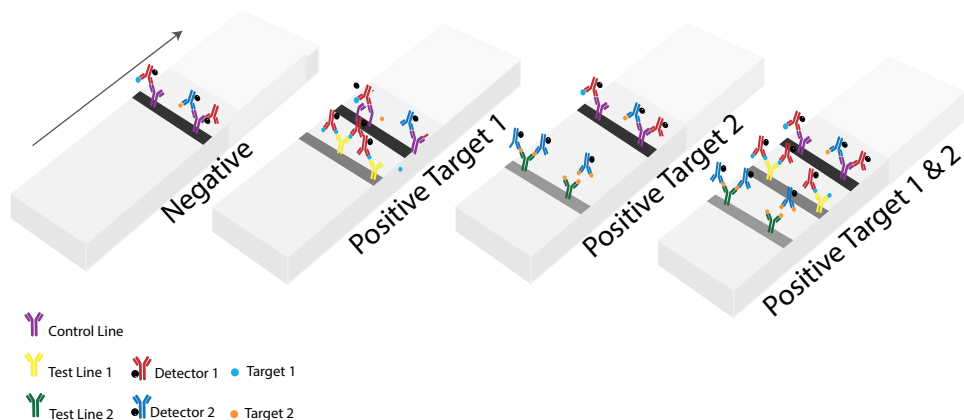


Figure 1.7. Schematic of multiplex lateral flow immunoassays (LFIA) tested (left to right) in a negative sample, a sample positive for target 1, a sample positive for target 2, a sample positive for both targets. The arrow represents the flow direction.

There are several mitigation strategies employed by assay developers to minimize and monitor for high-concentration LFIA effects, such as the hook-effect. The most common strategy is to test the sample both undiluted and diluted; if the diluted sample gives a more intense signal than the undiluted sample, the latter sample can be considered as at hook-effect levels⁷⁷. Diluting a sample means that the dynamic working range of the LFIA can be adjusted but testing both diluted and undiluted samples invokes additional sample preparation, time and expenses. Other approaches for avoiding the hook-effect change the physical design of the LFIA, allowing for antigen and immunoreagents to be delivered to the detection areas at different times or supplementing the LFIA with additional test lines to optimize the reagents^{78,79}. Further, real-time optical monitoring of the LFIA signal development allows for differentiation between artificially low and truly low antigen concentrations⁷⁶.

2.4.2 Flow-Through Immunoassays

Flow-through immunoassays are an alternative format of paper-microarray offering high-speeds and sensitivities⁴⁰. Flow-through assays can take many formats with the shared characteristic being that sample and reagents are flowed through an assay membrane, rather than across such as in LFIA. Compared to multiplex LFIA which can be subject to cross-reactivity between different targets due to their close geometry; flow-through assays generally allow greater freedom in geometric design⁸⁰. Flow-through assays typically exploit a circular NC membrane with a large surface area allowing for spatial separation of immunoreaction dots, facilitating the simultaneous measurement of multiple isolated analytes with no signal interference.

Passive flow-through assays consist of LFIA materials, but in a stacked arrangement, with the membrane biofunctionalized with capture antibodies on top, and the conjugate and absorbent pads layered underneath^{81,82}. In passive flow-through, the absorbent pad physically draws any fluid through the assay membrane. An alternative is the active vertical flow-through approach where a biofunctionalized membrane inserts into a syringe filter holder and manual or mechanical pressure is applied to the syringe to actively control the vertical flow of the reagents and the sample^{81,83}. While such “lab-in-a-syringe” formats demonstrate efficient multiplexing capabilities, they require large sample volumes (in mL range) with substantial dead volumes, and their manual operation makes them subject to intra/inter-use variability^{83,84}.

Flow-through immunoassays housed in custom 3D-printed cassettes with pre-stored reagents can limit the sample volume required for analysis and minimize signal variations by enabling uniform flow rates⁸⁵. However, unless using an already liquid sample, flow-through immunoassays are still limited by the need for sample pre-preparation, same as the LFIA and other assays.

2.5 Validation of Screening Assays

According to EC regulation No 519/2014 all semi-quantitative screening methods such as LFIA should be effectively validated by standardized procedures, preferably using a certified reference material⁸⁶. Certified standardized allergen reference materials are food matrices certified by an instrumental method to contain a known amount of target allergen. Lack of such materials for food allergens prevents consistency when validating novel detection assays⁸⁷. Still, in-house validation is a crucial step in the development of any novel screening immunoassay. Extensive validation demonstrates a screening method's fitness for purpose by assessing several assay performance characteristics including sensitivity, selectivity and precision. By far the most important performance characteristic is the false compliance rate. In paper-based sandwich format immunoassays, a false positive is when a negative control sample (blank matrix) or non-target analyte gives a positive result. Comparably a false negative, which can result from the hook-effect described earlier, is when a positive sample gives a blank or artificially low response. The minimum number of different samples required for false compliance validation is 20 homogenous negative control samples and 20 homogeneous positive control samples containing the target analyte at the screening target concentration (STC), here the STC for hazelnut and peanut is defined at 1 ppm. Ideally, consumer-focused screening assays should have a 0% false compliance rate but a false negative/positive rate of up to 5% is typically considered acceptable²². Although legally a 5% false compliance rate is tolerated, consumer-operable tests should aim to be more reliable or provide an inexpensive way to monitor for presence of false negative results.

3 Smartphone Detection

Smartphones have emerged as portable detectors for optical paper-based tests such as LFIAs and flow-through assays. Their connectivity and processing power makes them suited for combining with cloud-based apps and their ubiquity, portability and widespread usage means they are accessible in even challenging environments¹⁹ (see Figure 1.8). However, smartphones also have some limitations as analytical sensors, including the multitude of constantly upgrading models and the significant differences between different operating systems (e.g., Android vs iOS) complicating app design. Preferably consumer-focused tests should be based around a smartphone application with a simplified graphical user interface (GUI). The app should allow the user to record an image or video while it automatically performs the image analysis and data interpretation, before providing the user with a clear binary result: yes or no; safe or unsafe. Currently, most optical smartphone-based detection devices work by taking a photo of a developed assay, wirelessly transferring the image to a computer and then using a powerful image analysis software determine the analyte concentration based on the intensity of the test areas^{18,19,88}. Optical smartphone detectors have already been applied for numerous food-safety, biomedical, environmental and forensic needs. A comprehensive review of using smartphones for food allergen detection is provided in Chapter 2.

3.1 Image Analysis

Most often, smartphones are used to acquire images of developed paper-based immunoassays, and the images must then be subsequently analyzed to calibrate the assay intensity to analyte concentration. Typically, this is done by taking an intensity reading from the test, control and background of an LFIA. This intensity is then correlated to a particular concentration of analyte in a given sample. LFIA results can be normalized for lighting differences or positioning of the smartphone by dividing the test line intensity by the control line intensity (called the T/C ratio)⁸⁹. The color system used by the complementary metal oxide semiconductor (CMOS) image sensor of modern smartphones is the red, green, blue (RGB) color model⁹⁰. In RGB, all colors are formed from a combination of these three channels, with each channel expressing a value between 0-255. Typically, after images are recorded on a smartphone, they are transferred to an image processing software such as ImageJ⁹¹ to split them into individual RGB channels.

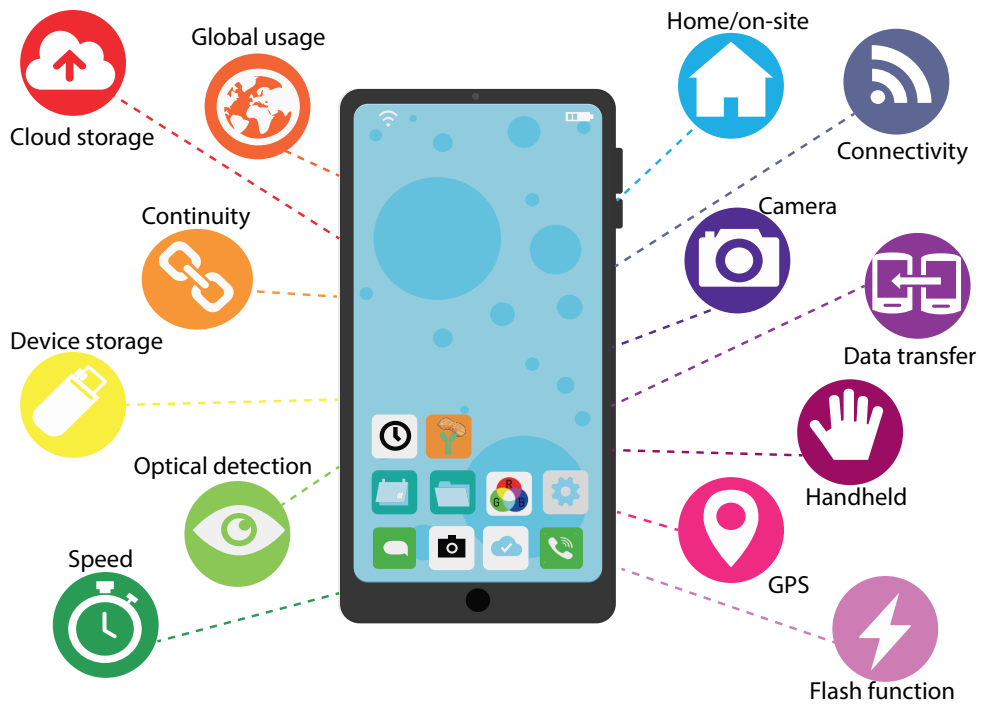


Figure 1.8. Graphic showing some of the key features that make smartphones well-suited as portable analytical devices.

The RGB model can be translated into other color spaces such as *cieLAB*. In *cieLAB*, L indicates luminosity or lightness of a region and A and B are chromatic co-ordinates¹⁹. As such, the L value of this color space is suitable for measuring intensity-based changes. Still, the RGB model is preferred for colorimetric quantification owing to its simplicity for splitting up images and quantifying their red, green, blue components⁹². Unlike other color models, which still use RGB as their base model, it does not need to be further converted to another color space.

3.2 Video Analysis

Rather than basing analysis on a single picture ('frame'), using a smartphone to record the entirety of the LFIA signal development may provide a real-time profile of LFIA binding characteristics. Based on the timing of signal development and based on whether the signal develops first on the test or control line it is possible to distinguish if a LFIA is in its dynamic working range or at high concentrations that could result in a false negative⁷⁶. Still, optical smartphone-based detection can be limited by the resolution and focus of the camera as well as by inconsistencies in ambient lighting. While using the smartphone's

ambient light sensor (ALS) instead of the camera might overcome the issues of lighting differences⁹³; lighting is most often controlled through a 3D-printed attachment¹⁸.

4 3D-Printing

The accessibility of computer aided design (CAD) software and affordable 3D-printing platforms has paved the way for the rapid development of custom smartphone-attachments⁹⁴, disposable cartridges^{95,96}, and lab on a chip (LOC) devices⁹⁷⁻¹⁰³. CAD software allows prototypes to be efficiently 'sketched' out in 2D and extruded to make 3D structures. When the 3D design is complete, the file is exported as an STL file and sent to the printer for assembly; the final 3D object is a series of different polymer layers stacked on top of each other. 3D-printing benefits from relative affordability of the platform and materials, a rapid design-to-prototype timeline, reproducibility and from being easy-to-learn¹⁰⁴. Further, 3D-printing can combine with and benefit from paper-based assays¹⁰¹, making it suitable for the development of portable, miniaturized analytical chemistry solutions.

It is essential to select the most appropriate 3D-printer based on the requirements of the final 3D-printed object (e.g., material type, necessary final resolution, strength, composition, transparency, biocompatibility etc.)¹⁰⁵. Two of the most popular 3D-printing systems are referred to as Fused Deposition Modelling (FDM) and Stereolithography (SLA). FDM is one of the most affordable types of 3D-printing and works by extruding a thread of molten thermoplastic polymer through the heated nozzle dispenser of the print head³¹. The thread of filament is deposited onto a movable print bed. After the initial 2D layer is drawn on the print bed, the print head lifts up, and the second layer is deposited on top of the original. This layering continues until the 3D object is complete. FDM is suitable for printing affordable, disposable devices and for larger, less detailed devices. Contrastingly, SLA typically has superior resolution compared with FDM with improved mechanical strength, surface finish, layer deposition and greater freedom in printing complex architectures. In SLA, the printer build platform lowers into a resin tank containing photosensitive liquid polymer that hardens on contact with a UV light. A UV laser draws the first layer of the object and then the platform is lowered into the resin tank again, with the process repeating until the final object is complete. Still, SLA has some limitations including the printer and resin costs – compounded by the use of proprietary resins with generally poor chemical and biocompatibility, the print time, limited print area, and the necessity for removal of residual resin through post-print processing with solvents^{21,105}.

5 Outline of Thesis

To develop consumer-operable immunodiagnosics that allow for the total analysis of food allergens, from sample to smartphone, several key science and technology challenges need to be addressed (summarized in Table 1.1). Based on these challenges, the structured and systematic development of a consumer-operable, affordable, rapid, sensitive and portable system combined with interconnectable solid-liquid protein extraction and on-chip enabled sample handling, dilution and reagent storage for multiplex allergen immunosensing, is presented in this thesis. Chapter 2 provides a comprehensive critical review of allergen immunoassays and the requirements needed for the future of consumer-operable smartphone-based allergen immunosensors. Chapter 3 addresses the barriers of speed, sensitivity and affordability in allergen sensing, by developing an SPR screening method for selecting rapid and sensitive hazelnut specific antibodies for high-speed LFIA. Carbon nanoparticles (CNPs) are used as a low-cost optical label and a free software app is applied for smartphone analysis. Chapter 4, explores how different immunoassay formats, using the same bioreagents, influence allergen detectability. This chapter details multiplex detection of total hazelnut and peanut protein in two formats of flow-through microarray and two configurations of LFIA. Chapter 5 introduces an interconnectable, handheld unit for solid-liquid extraction of peanut and hazelnut allergens from a solid sample into a LFIA testable liquid. The unit integrates with a 3D-printed device allowing on-chip bioreagent storage and sample handling for consumer-operable allergen detection; and the development of a reusable, adjustable 3D-printed smartphone holder for recording LFIA development under controlled lighting. The smartphone holder is also used in Chapter 6 for real-time monitoring of LFIA signal development for digitally distinguishing between low concentration and false negative results in LFIA caused by the hook and other concentration-dependent effects. Chapter 7 contains an overarching summary of the work reported in this thesis and future perspectives for the development of consumer immunodiagnosics.

Table 1.1. Advantages and limitations of LFIA and solutions provided by this thesis

Advantages of LFIA	Challenges of LFIA	Science and technology (this thesis)
Fast, specific and affordable	Selecting optimal bioreagents can be expensive and time-consuming	Created an SPR method for rapid profiling of unpurified antibodies for their speed, specificity and sandwich pairing abilities; greatly facilitating the screening process (Chapter 3)
Qualitative, visual readout	(Semi)-quantification requires expensive LFIA readers/immovable flatbed scanners	In-parallel with visual readout and as an affordable alternative to LFIA readers, smartphone-based readout was used for semi-quantification of singleplex LFIA results (Chapter 3), multiplex LFIA and flow-through results (Chapter 4), for dynamic real-time detection (Chapter 5) and for monitoring high-concentration LFIA effects (Chapter 6).
Versatile format	Individual tests, low throughput	Experimented with different multiplex LFIA and flow-through assay configurations (Chapter 4), developed a smartphone-device holder allowing for the simultaneous screening of 3 independent LFIAs as they develop increasing the throughput (Chapters 5 & 6)
No sample pre-treatment necessary for liquid samples except for dilution	Sample pre-treatment necessary for solid samples	Developed a combined system for extracting solid proteins into LFIA testable liquid which interconnects with a lab on a chip device for on-chip sample dilution (Chapter 5)
Sensitive at low analyte concentrations	Prone to the hook-effect at high analyte concentrations which can lead to false negatives	Provided a real-time smartphone method for distinguishing between truly low concentrations and false negatives (Chapter 6)

References

1. Prescott, S.L.; Pawankar, R.; Allen, K.J.; Campbell, D.E., et al. A global survey of changing patterns of food allergy burden in children, *World Allergy Organ J* **2013**, *6*, 21-21, 10.1186/1939-4551-6-21.
2. Manea, I.; Ailenei, E.; Deleanu, D. Overview of food allergy diagnosis, *Clujul Med* **2016**, *89*, 5-10, 10.15386/cjmed-513.
3. Yue, D.; Ciccolini, A.; Avilla, E.; Wasserman, S. Food allergy and anaphylaxis, *J Asthma Allergy* **2018**, *11*, 111-120, 10.2147/JAA.S162456.
4. Reese, I.; Holzhauser, T.; Schnadt, S.; Dölle, S., et al. Allergen and allergy risk assessment, allergen management, and gaps in the European Food Information Regulation (FIR), *Allergo Journal International* **2015**, *24*, 180-184, 10.1007/s40629-015-0066-0.
5. EC, RASFF - The Rapid Alert System for Food and Feed - Annual Report 2019: Luxembourg, 2020.
6. Jackson, L.S.; Al-Taher, F.M.; Moorman, M.; Devries, J.W., et al. Cleaning and Other Control and Validation Strategies To Prevent Allergen Cross-Contact in Food-Processing Operations, *Journal of Food Protection* **2008**, *71*, 445-458, 10.4315/0362-028x-71.2.445.
7. Soon, J.M.; Manning, L. "May Contain" Allergen Statements: Facilitating or Frustrating Consumers?, *Journal of Consumer Policy* **2017**, *40*, 447-472, 10.1007/s10603-017-9358-8.
8. Szybist, L. In: United States (U.S.) Department of Health and Human Services, Food and Drug Administration, 2020.
9. Gendel, S.M. Comparison of international food allergen labeling regulations, *Regulatory Toxicology and Pharmacology* **2012**, *63*, 279-285, <https://doi.org/10.1016/j.yrtph.2012.04.007>.
10. Ballmer-Weber, B.K.; Fernandez-Rivas, M.; Beyer, K.; Defernez, M., et al. How much is too much? Threshold dose distributions for 5 food allergens, *Journal of Allergy and Clinical Immunology* **2015**, *135*, 964-971, <https://doi.org/10.1016/j.jaci.2014.10.047>.
11. Cornelisse-Vermaat, J.R.; Voordouw, J.; Yiakoumaki, V.; Theodoridis, G., et al. Food-allergic consumers' labeling preferences: a cross-cultural comparison, *European Journal of Public Health* **2007**, *18*, 115-120, 10.1093/eurpub/ckm032.
12. Allen, K.J.; Turner, P.J.; Pawankar, R.; Taylor, S., et al. Precautionary labeling of foods for allergen content: are we ready for a global framework?, *World Allergy Organization Journal* **2014**, *7*, 1-14, 10.1186/1939-4551-7-10.
13. Bucchini, L.; Guzzon, A.; Poms, R.; Senyuva, H. Analysis and critical comparison of food allergen recalls from the European Union, USA, Canada, Hong Kong, Australia and New Zealand, *Food Additives & Contaminants: Part A* **2016**, *33*, 760-771, 10.1080/19440049.2016.1169444.
14. du Toit, G.; Tsakok, T.; Lack, S.; Lack, G. Prevention of food allergy, *Journal of Allergy and Clinical Immunology* **2016**, *137*, 998-1010, <https://doi.org/10.1016/j.jaci.2016.02.005>.
15. Popping, B.; Allred, L.; Bourdichon, F.; Brunner, K., et al. Stakeholders' Guidance Document for Consumer Analytical Devices with a Focus on Gluten and Food Allergens, *JAOC Int* **2018**, *101*, 185-189, 10.5740/jaoacint.17-0425.

16. Martinez, A.W.; Phillips, S.T.; Whitesides, G.M.; Carrilho, E. Diagnostics for the Developing World: Microfluidic Paper-Based Analytical Devices, *Analytical Chemistry* **2010**, *82*, 3-10, 10.1021/ac9013989.
17. Peeling, R.W.; Mabey, D. Point-of-care tests for diagnosing infections in the developing world, *Clinical Microbiology and Infection* **2010**, *16*, 1062-1069, <https://doi.org/10.1111/j.1469-0691.2010.03279.x>.
18. Ross, G.M.S.; Bremer, M.G.E.G.; Nielen, M.W.F. Consumer-friendly food allergen detection: moving towards smartphone-based immunoassays, *Anal Bioanal Chem* **2018**, *410*, 5353-5371, 10.1007/s00216-018-0989-7.
19. Nelis, J.L.D.; Tsagkaris, A.S.; Dillon, M.J.; Hajslova, J., et al. Smartphone-based optical assays in the food safety field, *TrAC Trends in Analytical Chemistry* **2020**, 115934, <https://doi.org/10.1016/j.trac.2020.115934>.
20. Sayers, R.L.; Johnson, P.E.; Marsh, J.T.; Barran, P., et al. The effect of thermal processing on the behaviour of peanut allergen peptide targets used in multiple reaction monitoring mass spectrometry experiments, *Analyst* **2016**, *141*, 4130-4141, 10.1039/c6an00359a.
21. (ISO), I.O.f.S. In *Guidance for the characterization and assessment of the homogeneity and stability of the material* ISO 2017.
22. Tsagkaris, A.S.; Nelis, J.L.D.; Ross, G.M.S.; Jafari, S., et al. Critical assessment of recent trends related to screening and confirmatory analytical methods for selected food contaminants and allergens, *TrAC Trends in Analytical Chemistry* **2019**, *121*, 115688, <https://doi.org/10.1016/j.trac.2019.115688>.
23. Coskun, A.F.; Wong, J.; Khodadadi, D.; Nagi, R., et al. A personalized food allergen testing platform on a cellphone, *Lab on a Chip* **2013**, *13*, 636-640, 10.1039/C2LC41152K.
24. Lin, H.Y.; Huang, C.H.; Park, J.; Pathania, D., et al. Integrated Magneto-Chemical Sensor For On-Site Food Allergen Detection, *ACS Nano* **2017**, *11*, 10062-10069, 10.1021/acsnano.7b04318.
25. Ito, K.; Yamamoto, T.; Oyama, Y.; Tsuruma, R., et al. Food allergen analysis for processed food using a novel extraction method to eliminate harmful reagents for both ELISA and lateral-flow tests, *Anal Bioanal Chem* **2016**, *408*, 5973-5984, 10.1007/s00216-016-9438-7.
26. Butch, A.W. Dilution Protocols for Detection of Hook Effects/Prozone Phenomenon, *Clinical Chemistry* **2000**, *46*, 1719-1720, 10.1093/clinchem/46.10.1719.
27. Salentijn, G.I.J.; Grajewski, M.; Verpoorte, E. Reinventing (Bio)chemical Analysis with Paper, *Analytical Chemistry* **2018**, *90*, 13815-13825, 10.1021/acs.analchem.8b04825.
28. Taylor, S.L.; Nordlee, J.A.; Jayansa, S.; Baumert, J.L. Evaluation of a Handheld Gluten Detection Device, *Journal of Food Protection* **2018**, *81*, 1723-1728, 10.4315/0362-028x.Jfp-18-184.
29. Zhang, J.; Portela, S.B.; Horrell, J.B.; Leung, A., et al. An integrated, accurate, rapid, and economical handheld consumer gluten detector, *Food Chemistry* **2019**, *275*, 446-456, <https://doi.org/10.1016/j.foodchem.2018.08.117>.
30. Manzanares Palenzuela, C.L.; Pumera, M. (Bio)Analytical chemistry enabled by 3D printing: Sensors and biosensors, *TrAC Trends in Analytical Chemistry* **2018**, *103*, 110-118, <https://doi.org/10.1016/j.trac.2018.03.016>.

31. Gross, B.; Lockwood, S.Y.; Spence, D.M. Recent Advances in Analytical Chemistry by 3D Printing, *Analytical Chemistry* **2017**, *89*, 57-70, 10.1021/acs.analchem.6b04344.
32. Zhu, C.; Hu, A.; Cui, J.; Yang, K., et al. A lab-on-a-chip device integrated DNA extraction and solid phase PCR array for the genotyping of high-risk HPV in clinical samples, *Micromachines* **2019**, *10*, doi:10.3390/mi10080537.
33. Park, M.; Seo, T.S. An integrated microfluidic device with solid-phase extraction and graphene oxide quantum dot array for highly sensitive and multiplex detection of trace metal ions, *Biosensors and Bioelectronics* **2019**, *126*, 405-411, <https://doi.org/10.1016/j.bios.2018.11.010>.
34. Heub, S.; Tschärner, N.; Monnier, V.; Kehl, F., et al. Automated and portable solid phase extraction platform for immuno-detection of 17 β -estradiol in water, *Journal of Chromatography A* **2015**, *1381*, 22-28, <https://doi.org/10.1016/j.chroma.2014.12.076>.
35. Yin, J.; Suo, Y.; Zou, Z.; Sun, J., et al. Integrated microfluidic systems with sample preparation and nucleic acid amplification, *Lab on a Chip* **2019**, *19*, 2769-2785, 10.1039/C9LC00389D.
36. Malhotra, B.D.; Ali, M.A. In *Nanomaterials for Biosensors*, Malhotra, B. D.; Ali, M. A., Eds.; William Andrew Publishing, 2018, pp 1-74.
37. Worm, M.; Jappe, U.; Kleine-Tebbe, J.; Schäfer, C., et al. Food allergies resulting from immunological cross-reactivity with inhalant allergens: Guidelines from the German Society for Allergology and Clinical Immunology (DGAKI), the German Dermatology Society (DDG), the Association of German Allergologists (AeDA) and the Society for Pediatric Allergology and Environmental Medicine (GPA), *Allergo journal international* **2014**, *23*, 1-16, 10.1007/s40629-014-0004-6.
38. Anfossi, L.; Di Nardo, F.; Russo, A.; Cavallera, S., et al. Silver and gold nanoparticles as multi-chromatic lateral flow assay probes for the detection of food allergens, *Anal Bioanal Chem* **2018**, 1905-1913, <https://doi.org/10.1007/s00216-018-1451-6>.
39. Galan-Malo, P.; Pellicer, S.; Pérez, M.D.; Sánchez, L., et al. Development of a novel duplex lateral flow test for simultaneous detection of casein and β -lactoglobulin in food, *Food Chemistry* **2019**, *293*, 41-48, <https://doi.org/10.1016/j.foodchem.2019.04.039>.
40. Ross, G.M.S.; G.J.J.; Nielen, M.W.F. A Critical Comparison between Flow-through and Lateral Flow Immunoassay Formats for Visual and Smartphone-Based Multiplex Allergen Detection, *Biosensors (Basel)* **2019**, *9*, 10.3390/bios9040143.
41. Anfossi, L.; Di Nardo, F.; Cavallera, S.; Giovannoli, C., et al. Multiplex Lateral Flow Immunoassay: An Overview of Strategies towards High-throughput Point-of-Need Testing, *Biosensors (Basel)* **2018**, *9*, 10.3390/bios9010002.
42. Chiu, M.L.; Goulet, D.R.; Teplyakov, A.; Gilliland, G.L. Antibody Structure and Function: The Basis for Engineering Therapeutics, *Antibodies (Basel)* **2019**, *8*, 55, 10.3390/antib8040055.
43. Huby, R.D.J.; Dearman, R.J.; Kimber, I. Why Are Some Proteins Allergens?, *Toxicological Sciences* **2000**, *55*, 235-246, 10.1093/toxsci/55.2.235.
44. Liu, J.K.H. The history of monoclonal antibody development - Progress, remaining challenges and future innovations, *Ann Med Surg (Lond)* **2014**, *3*, 113-116, 10.1016/j.amsu.2014.09.001.
45. Nelson, P.N.; Reynolds, G.M.; Waldron, E.E.; Ward, E., et al. Monoclonal antibodies, *Mol Pathol* **2000**, *53*, 111-117, 10.1136/mp.53.3.111.

46. Bremer, M.G.E.G.; Smits, N.G.E.; Haasnoot, W. Biosensor immunoassay for traces of hazelnut protein in olive oil, *Anal Bioanal Chem* **2009**, *395*, 119-126, 10.1007/s00216-009-2720-1.
47. Haasnoot, W.; Smits, N.G.E.; Kemmers-Voncken, A.E.M.; Bremer, M.G.E.G. Fast biosensor immunoassays for the detection of cows' milk in the milk of ewes and goats, *Journal of Dairy Research* **2004**, *71*, 322-329, 10.1017/S0022029904000317.
48. Badran, A.A.; Morais, S.; Maquieira, Á. Simultaneous determination of four food allergens using compact disc immunoassaying technology, *Anal Bioanal Chem* **2017**, *409*, 2261-2268, 10.1007/s00216-016-0170-0.
49. Miles, L.E.M.; Lipschitz, D.A.; Bieber, C.P.; Cook, J.D. Measurement of serum ferritin by a 2-site immunoradiometric assay, *Analytical Biochemistry* **1974**, *61*, 209-224, [https://doi.org/10.1016/0003-2697\(74\)90347-9](https://doi.org/10.1016/0003-2697(74)90347-9).
50. Liang, T.; Robinson, R.; Houghtaling, J.; Fridley, G., et al. Investigation of Reagent Delivery Formats in a Multivalent Malaria Sandwich Immunoassay and Implications for Assay Performance, *Analytical chemistry* **2016**, *88*, 2311-2320, 10.1021/acs.analchem.5b04222.
51. Taylor, S.L.; Nordlee, J.A.; Niemann, L.M.; Lambrecht, D.M. Allergen immunoassays--considerations for use of naturally incurred standards, *Anal Bioanal Chem* **2009**, *395*, 83-92, 10.1007/s00216-009-2944-0.
52. Sajid, M.; Kawde, A.-N.; Daud, M. Designs, formats and applications of lateral flow assay: A literature review, *Journal of Saudi Chemical Society* **2015**, *19*, 689-705, <https://doi.org/10.1016/j.jscs.2014.09.001>.
53. Zhao, H.; Schuck, P. Kinetic Binding. In *Handbook of Surface Plasmon Resonance (2)*; The Royal Society of Chemistry, 2017, pp 27-59.
54. Zhao, H.; Schuck, P. Intro to SPR. In *Handbook of Surface Plasmon Resonance*; The Royal Society of Chemistry, 2017, pp 1-26.
55. Schasfoort, R.B.M. SPR instruments. *Handbook of Surface Plasmon Resonance 2ed.*; Royal Society of Chemistry 2017.
56. Prabowo, B.A.; Purwidyantri, A.; Liu, K.-C. Surface Plasmon Resonance Optical Sensor: A Review on Light Source Technology, *Biosensors* **2018**, *8*, 80, 10.3390/bios8030080.
57. Weng, X.; Gaur, G.; Neethirajan, S. Rapid detection of food allergens by microfluidics ELISA-based optical sensor, *Biosensors* **2016**, *6*, doi:10.3390/bios6020024.
58. Huang, W.-Y.; Chou, S.-T.; Chen, C.-H.; Chou, S.-Y., et al. An automatic integrated microfluidic system for allergy microarray chips, *Analyst* **2018**, *143*, 2285-2292, 10.1039/C8AN00247A.
59. Costantini, F.; Sberna, C.; Petrucci, G.; Manetti, C., et al. Lab-on-chip system combining a microfluidic-ELISA with an array of amorphous silicon photosensors for the detection of celiac disease epitopes, *Sensing and Bio-Sensing Research* **2015**, *6*, 51-58, <https://doi.org/10.1016/j.sbsr.2015.11.003>.
60. Weng, X.; Neethirajan, S. Ensuring food safety: Quality monitoring using microfluidics, *Trends in Food Science & Technology* **2017**, *65*, 10-22, <https://doi.org/10.1016/j.tifs.2017.04.015>.
61. Cheng, C.-M.; Martinez, A.W.; Gong, J.; Mace, C.R., et al. Paper-Based ELISA, *Angewandte Chemie International Edition* **2010**, *49*, 4771-4774, 10.1002/anie.201001005.

62. Hoofnagle, A.N.; Wener, M.H. The fundamental flaws of immunoassays and potential solutions using tandem mass spectrometry, *J Immunol Methods* **2009**, *347*, 3-11, 10.1016/j.jim.2009.06.003.
63. Plotz, C.M.; Singer, J.M. The latex fixation test. I. Application to the serologic diagnosis of rheumatoid arthritis, *Am J Med* **1956**, *21*, 888-892.
64. Boyko, W.L.; Barrett, B. Detection and Quantitation of the β -Subunit of Human Chorionic Gonadotropin in Serum by Radioimmunoassay, *Fertility and Sterility* **1980**, *33*, 141-150, [https://doi.org/10.1016/S0015-0282\(16\)44534-6](https://doi.org/10.1016/S0015-0282(16)44534-6).
65. Vaitukaitis, J.L.; Braunstein, G.D.; Ross, G.T. A radioimmunoassay which specifically measures human chorionic gonadotropin in the presence of human luteinizing hormone, *Am J Obstet Gynecol* **1972**, *113*, 751-758, 10.1016/0002-9378(72)90553-4.
66. Koczula, K.M.; Gallotta, A. Lateral flow assays, *Essays Biochem* **2016**, *60*, 111-120, 10.1042/EBC20150012.
67. Deng, X.; Wang, C.; Gao, Y.; Li, J., et al. Applying strand displacement amplification to quantum dots-based fluorescent lateral flow assay strips for HIV-DNA detection, *Biosensors and Bioelectronics* **2018**, *105*, 211-217, <https://doi.org/10.1016/j.bios.2018.01.039>.
68. Anfossi, L.; Di Nardo, F.; Profiti, M.; Nogarol, C., et al. A versatile and sensitive lateral flow immunoassay for the rapid diagnosis of visceral leishmaniasis, *Anal Bioanal Chem* **2018**, *410*, 4123-4134, 10.1007/s00216-018-1067-x.
69. Liang, R.-L.; Xu, X.-P.; Liu, T.-C.; Zhou, J.-W., et al. Rapid and sensitive lateral flow immunoassay method for determining alpha fetoprotein in serum using europium (III) chelate microparticles-based lateral flow test strips, *Analytica Chimica Acta* **2015**, *891*, 277-283, <https://doi.org/10.1016/j.aca.2015.07.053>.
70. Old, J.B.; Schweers, B.A.; Boonlayangoor, P.W.; Reich, K.A. Developmental Validation of RSID™-Saliva: A Lateral Flow Immunochromatographic Strip Test for the Forensic Detection of Saliva, *Journal of Forensic Sciences* **2009**, *54*, 866-873, 10.1111/j.1556-4029.2009.01055.x.
71. Schweers, B.A.; Old, J.; Boonlayangoor, P.W.; Reich, K.A. Developmental validation of a novel lateral flow strip test for rapid identification of human blood (Rapid Stain Identification (TM)-Blood), *Forensic Science International-Genetics* **2008**, *2*, 243-247, 10.1016/j.fsigen.2007.12.006.
72. Koets, M.; Sander, I.; Bogdanovic, J.; Doekes, G., et al. A rapid lateral flow immunoassay for the detection of fungal alpha-amylase at the workplace, *Journal of Environmental Monitoring* **2006**, *8*, 942-946, 10.1039/B605389K.
73. Nelis, J.L.D.; Zhao, Y.; Bura, L.; Rafferty, K., et al. A Randomized Combined Channel Approach for the Quantification of Color- and Intensity-Based Assays with Smartphones, *Anal Chem* **2020**, 10.1021/acs.analchem.0c01099.
74. Kasetsirikul, S.; Shiddiky, M.J.A.; Nguyen, N.-T. Challenges and perspectives in the development of paper-based lateral flow assays, *Microfluidics and Nanofluidics* **2020**, *24*, 17, 10.1007/s10404-020-2321-z.
75. Ryall, R.G.; Story, C.J.; Turner, D.R. Reappraisal of the causes of the "hook effect" in two-site immunoradiometric assays, *Analytical Biochemistry* **1982**, *127*, 308-315, [https://doi.org/10.1016/0003-2697\(82\)90178-6](https://doi.org/10.1016/0003-2697(82)90178-6).

76. Rey, E.G.; O'Dell, D.; Mehta, S.; Erickson, D. Mitigating the Hook Effect in Lateral Flow Sandwich Immunoassays Using Real-Time Reaction Kinetics, *Anal Chem* **2017**, *89*, 5095-5100, 10.1021/acs.analchem.7b00638.
77. Namburi, R.; Kancherla, V.; Ponnala, A. High-dose hook effect, *Journal of Dr. NTR University of Health Sciences* **2014**, *3*, 5-7, 10.4103/2277-8632.128412.
78. Oh, Y.K.; Joung, H.-A.; Han, H.S.; Suk, H.-J., et al. A three-line lateral flow assay strip for the measurement of C-reactive protein covering a broad physiological concentration range in human sera, *Biosensors and Bioelectronics* **2014**, *61*, 285-289, <https://doi.org/10.1016/j.bios.2014.04.032>.
79. Hu, J.; Choi, J.R.; Wang, S.; Gong, Y., et al. Multiple test zones for improved detection performance in lateral flow assays, *Sensors and Actuators B: Chemical* **2017**, *243*, 484-488, <https://doi.org/10.1016/j.snb.2016.12.008>.
80. Jiang, N.; Ahmed, R.; Damayantharan, M.; Ünal, B., et al. Lateral and Vertical Flow Assays for Point-of-Care Diagnostics, *Advanced Healthcare Materials* **2019**, *8*, 1900244, 10.1002/adhm.201900244.
81. Oh, Y.K.; Joung, H.-A.; Kim, S.; Kim, M.-G. Vertical flow immunoassay (VFA) biosensor for a rapid one-step immunoassay, *Lab on a Chip* **2013**, *13*, 768-772, 10.1039/C2LC41016H.
82. Eltzov, E.; Marks, R.S. Colorimetric stack pad immunoassay for bacterial identification, *Biosensors and Bioelectronics* **2017**, *87*, 572-578, <https://doi.org/10.1016/j.bios.2016.08.044>.
83. Chinnasamy, T.; Segerink, L.I.; Nystrand, M.; Gantelius, J., et al. Point-of-Care Vertical Flow Allergen Microarray Assay: Proof of Concept, *Clinical Chemistry* **2014**, *60*, 1209-1216, 10.1373/clinchem.2014.223230.
84. Nunes Pauli, G.E.; de la Escosura-Muñiz, A.; Parolo, C.; Helmuth Bechtold, I., et al. Lab-in-a-syringe using gold nanoparticles for rapid immunosensing of protein biomarkers, *Lab on a Chip* **2015**, *15*, 399-405, 10.1039/C4LC01123F.
85. Joung, H.-A.; Ballard, Z.S.; Ma, A.; Tseng, D.K., et al. Paper-based multiplexed vertical flow assay for point-of-care testing, *Lab on a Chip* **2019**, *19*, 1027-1034, 10.1039/C9LC00011A.
86. EC. In *519/2014*, Union, E., Ed.; European Commission 2014.
87. Holzhauser, T.; Johnson, P.; Hindley, J.P.; O'Connor, G., et al. Are current analytical methods suitable to verify VITAL® 2.0/3.0 allergen reference doses for EU allergens in foods?, *Food and Chemical Toxicology* **2020**, *145*, 111709, <https://doi.org/10.1016/j.fct.2020.111709>.
88. Rateni, G.; Dario, P.; Cavallo, F. Smartphone-based food diagnostic technologies: a review, *Sensors* **2017**, *17*, doi:103390/s17061453.
89. Foyzal, K.H.; Seo, S.E.; Kim, M.J.; Kwon, O.S., et al. Analyte Quantity Detection from Lateral Flow Assay Using a Smartphone, *Sensors (Basel)* **2019**, *19*, 4812, 10.3390/s19214812.
90. Priye, A.; Ball, C.S.; Meagher, R.J. Colorimetric-Luminance Readout for Quantitative Analysis of Fluorescence Signals with a Smartphone CMOS Sensor, *Analytical chemistry* **2018**, *90*, 12385-12389, 10.1021/acs.analchem.8b03521.
91. Schneider, C.A.; Rasband, W.S.; Eliceiri, K.W. NIH Image to ImageJ: 25 years of image analysis, *Nature Methods* **2012**, *9*, 671-675, 10.1038/nmeth.2089.

92. Rezazadeh, M.; Seidi, S.; Lid, M.; Pedersen-Bjergaard, S., et al. The modern role of smartphones in analytical chemistry, *TrAC Trends in Analytical Chemistry* **2019**, *118*, 548-555, <https://doi.org/10.1016/j.trac.2019.06.019>.
93. Pol, R.; Diez, L.; Gabriel, D.; Baeza, M. Versatile Three-Dimensional-Printed Platform for Nitrite Ion Analyses Using a Smartphone with Real-Time Location, *Analytical Chemistry* **2019**, *91*, 13916-13923, [10.1021/acs.analchem.9b03409](https://doi.org/10.1021/acs.analchem.9b03409).
94. Chen, Y.; Fu, Q.; Li, D.; Xie, J., et al. A smartphone colorimetric reader integrated with an ambient light sensor and a 3D printed attachment for on-site detection of zearalenone, *Anal Bioanal Chem* **2017**, *409*, 6567-6574, [10.1007/s00216-017-0605-2](https://doi.org/10.1007/s00216-017-0605-2).
95. Salentijn, G.I.J.; Oleschuk, R.D.; Verpoorte, E. 3D-Printed Paper Spray Ionization Cartridge with Integrated Desolvation Feature and Ion Optics, *Analytical Chemistry* **2017**, *89*, 11419-11426, [10.1021/acs.analchem.7b02490](https://doi.org/10.1021/acs.analchem.7b02490).
96. Salentijn, G.I.J.; Permentier, H.P.; Verpoorte, E. 3D-Printed Paper Spray Ionization Cartridge with Fast Wetting and Continuous Solvent Supply Features, *Analytical Chemistry* **2014**, *86*, 11657-11665, [10.1021/ac502785j](https://doi.org/10.1021/ac502785j).
97. Park, J.; Park, J.-K. Integrated microfluidic pumps and valves operated by finger actuation, *Lab on a Chip* **2019**, *19*, 2973-2977, [10.1039/C9LC00422J](https://doi.org/10.1039/C9LC00422J).
98. Comina, G.; Suska, A.; Filippini, D. Autonomous Chemical Sensing Interface for Universal Cell Phone Readout, *Angewandte Chemie International Edition* **2015**, *54*, 8708-8712, [10.1002/anie.201503727](https://doi.org/10.1002/anie.201503727).
99. Zeraatkar, M.; Filippini, D.; Percoco, G. On the Impact of the Fabrication Method on the Performance of 3D Printed Mixers., *Micromachines* **2019**, *10*.
100. Comina, G.; Suska, A.; Filippini, D. Low cost lab-on-a-chip prototyping with a consumer grade 3D printer, *Lab on a Chip* **2014**, *14*, 2978-2982, [10.1039/c4lc00394b](https://doi.org/10.1039/c4lc00394b).
101. Tsagkaris, A.S.; Pulkrabova, J.; Hajslova, J.; Filippini, D. A Hybrid Lab-on-a-Chip Injector System for Autonomous Carbofuran Screening, *Sensors (Basel)* **2019**, *19*, 5579, [10.3390/s19245579](https://doi.org/10.3390/s19245579).
102. Eriksson, E.; Lysell, J.; Larsson, H.; Cheung, K.Y., et al. Geometric Flow Control Lateral Flow Immunoassay Devices (GFC-LFIDs): A New Dimension to Enhance Analytical Performance, *Research* **2019**, *2019*, 8, [10.34133/2019/8079561](https://doi.org/10.34133/2019/8079561).
103. Suska, A.; Filippini, D. Autonomous lab-on-a-chip generic architecture for disposables with integrated actuation, *Scientific Reports* **2019**, *9*, 20320, [10.1038/s41598-019-55111-z](https://doi.org/10.1038/s41598-019-55111-z).
104. Zastrow, M. 3D printing gets bigger, faster and stronger, *Nature* **2020**, *578*, 20-23, [10.1038/d41586-020-00271-6](https://doi.org/10.1038/d41586-020-00271-6).
105. Salentijn, G.I.J.; Oomen, P.E.; Grajewski, M.; Verpoorte, E. Fused Deposition Modeling 3D Printing for (Bio)analytical Device Fabrication: Procedures, Materials, and Applications, *Analytical Chemistry* **2017**, *89*, 7053-7061, [10.1021/acs.analchem.7b00828](https://doi.org/10.1021/acs.analchem.7b00828).

CHAPTER 2

2

Consumer-friendly food allergen detection: moving towards smartphone-based immunoassays

Adapted from:

Ross, G.M.S., Bremer, M.G.E.G, Nielen, M.W.F., 2018. Consumer-friendly food allergen detection: moving towards smartphone-based immunoassays. Analytical and Bioanalytical Chemistry. 410 (22). 5353-5371. doi: 10.1007/s00216-018-0989-7

In this critical review, we provide a comprehensive overview of immunochemical food allergen assays and detectors in the context of their user friendliness, through their connection to smartphones. Smartphone based analysis is centered around citizen science, putting analysis into the hands of the consumer. Food allergies represent a significant worldwide health concern and consumers should be able to analyze their foods, whenever and wherever they are, for allergen presence. Owing to the need for a scientific background, traditional laboratory-based detection methods are generally unsuitable for the consumer. Therefore, it is important to develop simple, safe and rapid assays which can be linked with smartphones as detectors to improve user accessibility. Smartphones make excellent detection systems due to their cameras, embedded flash functions, portability, connectivity and affordability. Therefore, this review has summarized traditional laboratory-based methods for food allergen detection such as enzyme-linked-immunosorbent assay, flow cytometry and surface plasmon resonance and the potential to modernize these methods by interfacing them with a smartphone readout system, based on the aforementioned smartphone characteristics. This is the first review focusing on smartphone-based food-allergen detection methods designed with the intention of being consumer friendly.

1 Introduction

An allergen is a protein capable of eliciting an immune response in sensitized individuals. Food allergies represent a significant international health problem. Worldwide, allergies toward foods affect 2% of the adult population and 5-8% of the children population^{1,2}. There are many existing methods for food allergen detection, which can be split into two general categories: protein-based and DNA based detection. For a general and in-depth explanation on all in-vivo and in-vitro allergen assays, refer to the review by Poms et al³. General and quantitative methods for allergen detection have been reviewed by Kirsch et al and Walker et al^{2,4}. Additionally, an overview on commercially available rapid immuno-analytical allergen detectors has been presented by Schubert-Ulrich⁵. All immunochemical and DNA based methods were reviewed by Monaci & Visconti and Slowianek & Majak^{6,7}. Further discussion into allergen detection methods with a particular focus on proteomic mass-spectrometry has been given by Prado et al⁸. The most recently published food allergen review⁹ focused on the use of biosensors for detection, so only limited attention will be paid to them in this review.

Although analytical methods such as mass spectrometry can provide a wealth of information when used complementarily with immuno-methods; current allergen analysis trends are moving away from lab methods and toward point-of-care diagnostics (PoC) and a citizen science approach¹⁰. Point-of-care diagnostics allow instant on-site testing for food allergens by individuals, whilst citizen science centers around consumer-friendly devices which allow the user to carry out their own PoC allergen analysis. It is of particular importance that food allergen detection devices are consumer friendly as allergic individuals will need to carry out testing at home or in restaurants prior to eating. Many allergic individuals suffer with more than one food allergy, due to cross-reactivity, where antibodies against one allergen recognize a structurally related epitope of another similar allergen¹¹. Due to allergens being cross-reactive, it is necessary to develop multiplex devices which can detect a range of allergens within a single sample, saving time and money and making sure that the consumer is confident that their food does not contain any undesired allergens. For the purpose of this review, a consumer can be considered as the end-user of the assay/detector, and thus the terms consumer and user are used synonymously. The authors define consumer friendly to mean that any adult of average intelligence would be able to perform the assay safely and effectively with minimal instruction. One way of making allergen testing more user-friendly is to link the assays with a smart detector such as: a smartphone, tablet or wearable device. Although some of the existing allergen assay formats are simple to perform, linking these tests to a smart detector will make them more accessible for the general public. As the majority of the population already own a smartphone, with the number rising, smartphones represent a source of analytical equipment that can reach even the most desolate areas of the globe, making them ideal for sensors¹².

Smartphones are ideal to use as detector systems because of their powerful internal computers, optical sensors, global positioning systems (GPS) and most importantly, their ability to connect to the internet, through Bluetooth and WiFi¹³⁻¹⁵. Connectivity is a key benefit of smartphones as results can instantaneously be uploaded to Cloud databases and results can be disseminated as spatio-temporal maps across the globe¹⁶. Since their development in 1992 and first use as analytical devices in 2008, smartphones have already been used as sensors, for light microscopy, single-molecule microscopy, cell imaging, bacteria detection, colorimetric detection, enzyme linked immunosorbent assay (ELISA) and lateral flow immunoassays (LFIA); which exemplifies their capabilities as detectors in rapid diagnostics^{12,17-26}. For an in-depth review into all existing smartphone based diagnostic devices, Quesada-Gonzalez & Merkoci can be referred to²⁷. For a more focused review concerning biosensors and bioelectronics on a smartphone see Zhang & Liu²⁸. General approaches to smartphone-based food diagnostics have been recently reviewed by Rateni et al²⁹ and Choi¹² which addressed the necessity and market-gap for user-friendly food detection. This is particularly important in the field of food allergen analysis where detection methods must be consumer-friendly so that the allergic individual can apply analysis themselves in the comfort of their home and/or at a restaurant. The present review specifically focuses on how successful lab-based methods can be based on smartphones to enable consumer-friendly allergen detection.

Up until now, the literature has lacked specific focus on consumer-friendly food allergen detection devices. To that end, literature has been reviewed from the period of 2002 to the end of 2017 using the SciFinder, Scholar, Scopus and Web of Science databases and key words such as: food allergen, detection, smartphone OR cell phone, multiplex, lateral flow, immunoassay, flow-through, microfluidics, strip reader and ELISA. Section 1 of the review will provide a general background of food allergens and the legislations that control the labeling procedures. The study will then discuss the concept of consumer friendliness in section 2. In Section 3 there will be focus on traditional laboratory-based methods for food allergen analysis and how these methods could improve their consumer friendliness through coupling to a smartphone as a detector. Section 4 will discuss assays/devices which have been designed with the intention of being consumer friendly, including commercial consumer-friendly allergen detectors. Finally, the conclusion will summarize the findings of the review.

2 Background on Food Allergens

2.1 Types of Food Allergens

Food allergies can be debilitating, and food requires proper monitoring to ensure sensitized individuals are not exposed to allergens. Symptoms of food allergy can include:

itching, diarrhea, stomach pains, eczema, shortness of breath as well as more significant effects such as loss of consciousness and anaphylactic shock, which can be fatal³⁰. The prevalence of food allergies is increasing, but awareness of allergies is growing even faster with dedicated events such as 'Food Allergy Awareness Week' in the USA³¹. The Codex Alimentarius Standard listed eight allergens with international variants which require mandatory labeling³². These are referred to as the Big 8 and consist of: peanuts, tree-nuts, milk, eggs, fish, crustacean, soya and wheat³³. Wheat contains a variety of proteins which have been implicated as allergens (see Table 2.1). In addition to wheat allergy, other wheat related disorders include the autoimmune disorder, celiac disease. Celiac disease is triggered by gluten, a protein mixture of prolamins and glutenins, which can be found in wheat, rye and barley and their cross-breeds³⁴. Allergic reactions are provoked by many different proteins within the allergenic foods. Those allergenic proteins which have been repeatedly referenced in the literature and databases (e.g. allergen.org) as causing an allergic reaction in the majority of sensitized individuals are described in Table 1 below.

Allergenic proteins can result in hypersensitivity of the immune system, arbitrated by allergen specific immunoglobulin E (IgE) (type I allergies); but allergies can also be cell-mediated (non-IgE) (type II allergies)^{9,35}. Disruption of the structure of allergens by food processing can lead to an increase or decrease in their immunogenicity, altering how an allergic individual might react to the protein³⁶. The modification of allergenic proteins is dependent on the processing procedure applied. For example, by hydrolyzing or thermally treating an allergen the structure is altered, which can result in either a reduction in immunogenicity of the allergen, or the formation of a neo-allergen. The method used for processing a food will affect the extractability of the allergens from their matrix³⁷. When extracting gluten for example, it is crucial to have a homogenized sample so that particulates can be extracted. As ethanol-based extractions result in the incomplete extraction of gluten, it is desirable to use a cocktail extraction solution which contains a reducing agent and alcohol, which is capable of extracting monomeric and polymeric proteins from gluten³⁸⁻⁴⁰. Extraction procedures have been a detriment in the past, where hazardous and environmentally damaging extraction solutions such as 2-mercaptoethanol (2-ME) have been applied in food allergen extraction⁴¹. In order to step toward consumer-friendliness it is necessary to have extraction buffers which are safe to use and easy to dispose of. Many traditional allergen analysis methods use environmentally harmful reagents, which contain additives that improve allergen solubility/extractability and reduce background interference from the food matrix⁴². It is desirable to use eco-friendly extraction buffers, but these must first be compared and validated against traditional buffers to ensure that they are as effective in allergen extraction.

All assays and detectors need to be effectively validated by standardized procedures. Certified reference materials in raw and processed foods need to be developed for food

allergens as well as reference methods for allergen analysis^{67,68}. Current lack of standardized reference materials for allergens in foods means that there is a lack of consistency between different allergen detection methods as each test kit is calibrated in a different way. Reference materials are critical for quality assurance of allergen detection methods, but their production is complicated in food allergen analysis owing to the changes in allergen protein structure during food processing procedures⁶. When standardized reference materials are developed, they should be based on a whole protein extract as allergens are a mixture of non-defined proteins in complex matrices⁶⁹. Having a set of standards for allergen testing devices will ensure that effective and smart detection devices can be created, validated and benchmarked against each-other, allowing consumer science to be achieved by providing individuals with personalized smart-detection platforms for food allergens.

2.2 Worldwide Legislation and Mandatory Labeling

Worldwide, dietary differences and the big 8 influence which allergens require mandatory labeling. Some countries include additional mandatory and recommended allergens for labeling depending on the staple diet of that particular country⁷⁰. Despite worldwide communication, significant variance exists in different countries regulatory labeling framework. This can be problematic due to the high percentage of international food trade and individual peoples travelling patterns⁷¹. The European Commission (EC) produced legislation in 2003 (Directive 2003/89/EC) covering a list of 14 allergens which require mandatory labeling, the legislation is commonly referred to as the "allergen-labeling-directive"⁷².

If a manufacturer uses any of the allergens listed, it must be stated, with clear labeling, on the packaging⁷³. This is a crucial amendment, as labeling of the presence of allergenic ingredients is currently the only way allergic individuals can effectively maintain strict avoidance diets⁷⁴. Proper labeling of allergens is crucial as it informs consumers what products are safe to eat. In 2014, the EU Regulation amendment 1169/2011 came officially into effect, this amendment stipulated that even non-prepackaged foods require allergen labeling, meaning in practice that all food retailers must provide allergen information^{72,75}. Food manufacturers and retailers are responsible for the proper labeling of their products; when an allergen has been labelled it then becomes the consumers responsibility to avoid this food⁶⁸. As a large amount of food allergic reactions happen to individuals when they are abroad, it is vital that consumers are aware of the differences in which allergens require labeling in other countries (SI Table S2.1). However, it is undeclared food allergens that are accidentally introduced into non-allergenic foods, through cross-contamination, that pose the biggest risk to the consumer⁷⁶. The EU does not currently provide guidance on labeling for allergens which may have unintentionally been introduced into the product via shared facilities⁷².

Table 2.1. The main allergenic proteins in foods within the 'Big 8' plus 'gluten'

Food	Allergenic Protein	Ref
Cow's Milk	B-lactoglobulin (Bos d 5)	43
	Casein (Bos d 8)	44
	α-Lactalbumin (Bos d 4)	45
Egg	Ovomucoid (Gal d 1)	46
	Ovalbumin (Gal d 2)	46
	Ovotransferrin (Gal d 3)	47
	Lysozyme (Gal d 4)	48
	α-Livetin (Gal d 5)	49
Crustacean	Tropomyosin (Pen a 1)	50
Fish	B-Parvalbumin (Lep w 1; Pon 1 4; Pon 1 7; Seb m 1; Xip g 1)	51
Peanut	Ara h1	52
	Ara h2	53
	Ara h3	54
	Arah h4-9	55
Tree Nuts		
Hazelnut	Cor a 1; Cor a 2; Cor a 8; Cor a 9; Cor a 11; Cor a 12; Cor a 13;	56
Brazil Nut	Cor a 14	57
Cashew	Ber e 1; Ber e 2	58
Almond	Ana o 1; Ana o 2; Ana o 3	59
Walnut (Black)	Pru du 3; Pru du 4; Pru du 5; Pru du 6	51
Walnut (English)	Jug n 1; Jug n 2; Jug n 4	51
Pecan	Jug r 1-6	51
Pistachio	Car i 1; Car i 2; Car i 4	51
	Pis v 1; Pis v 2; Pis v 3; Pis v 4; Pis v 5	
Soybean	Gly m Bd 30K	60
	Gly m Bd 60K	61
	Gly m Bd 28K	61
Wheat	Tri a 12	62,63
	Tri a 14	62,64
	Tri a 18	62,65
	Tri a 25	62,65,66
Gluten*	Gluten (Tri a 26 & Tri a 36)	51,62
	Gliadin (Tri a 19 & Tri a 20)	51,62

**Although not an allergen, gluten has been included in this table to show the toxic portion of the protein responsible for gluten's autoimmune effects.*

2.3 Precautionary Labeling and Thresholds

The EU has a zero-tolerance policy for allergen labeling, and any foods listed in the legislation (see Supplementary Information (SI) Table S2.1) must be stated on the food packaging when they are used as ingredients or processing aids in the food. However, the EU has no obligation to label any allergens which are not part of the recipe and may have accidentally been introduced by cross-contamination⁶⁷. Some countries have set



threshold levels, and any food containing allergens above those levels require labeling. For example, in Japan any foods containing any of the legislated allergens (see SI Table S2.1) above 10 ppm must be declared on the packaging, meaning that the majority of the allergic population are protected from exposure⁷⁰. However, due to individual differences in sensitivities to allergens, having such a low labeling threshold may further restrict the diet of individuals who are less sensitive to those allergens. Switzerland have taken an alternative approach, not mandating allergen labeling for any product containing less than 1000 ppm of allergen⁷⁷. The Swiss approach can be detrimental to the allergic individual, with many people experiencing allergic reactions at levels far lower than 1 g/kg for particular allergens⁷⁸. The Swiss allergen labeling legislation illuminates the requirement for consumers to be able to test their own foods for allergen presence so that they do not have to solely rely on labeling legislations.

In addition, it is also common practice for food manufacturers to include precautionary allergen labeling (PAL) on their foods for protection against unintentional presence of allergens. There is a lack of consistency in the wording of PAL, which can be confusing to the allergic consumer and reduces the consumers ability to make informed food choices⁶⁸. Labels such as “may contain nuts”, are used if there is any risk the product may have come into contact with an allergen⁷⁷. Food manufacturing companies have highlighted their desire for standardized PAL on food packaging to avoid misinterpretation⁷⁹. Although advisory labeling is well intentioned, excessive use of warnings can lead to individuals taking risks with what they eat by ignoring the labels⁸⁰⁻⁸². Currently, most countries PAL is not on a threshold-based criterion, and manufacturers include labels for any potential allergen.

There is an evident requirement for threshold-based action levels, to properly assess the risk of an unintentional allergen being introduced to a food, and to establish when and where advisory labeling is necessary and beneficial to the allergic consumer. These action levels should be science based. Clinical information regarding minimum eliciting doses has been translated into lowest-observed-adverse-effect-levels (LOAEL) and no-observed-adverse-effect-levels (NOAEL)^{78,83,84}. Developing effective thresholds using LOAELs is a safety-assessment based approach that protects the majority of the allergic population. The Allergen Bureau of Australia & New Zealand (ABA) are global leaders in regulation of labeling and have already established voluntary labeling thresholds for the major allergens, based on LOAELs, which protect 95% of allergic population from severe reactions^{82,85}. Voluntary Incidental Trace Allergen Labeling (VITAL) aims to limit the use of excessive, unnecessary PAL in foods; and has also incorporated reference dose information into the LOAEL action levels for allergen labeling^{82,86}. The reference dose in VITAL is defined as milligrams of total protein from an allergenic food that only the most sensitive individual would be likely to experience an adverse reaction toward⁸⁷. If the individual reference dose

is exceeded in an un-labelled food, VITAL recommends precautionary labeling⁶⁷. In 2011, a scientific expert committee including the food allergy research and resource program (FARRP), revised VITAL to develop VITAL 2.0 which uses action levels based on reference doses⁸⁸. The action levels provide a clear indication on when “may contain” labeling should be applied. Despite Australia and New Zealand being at the forefront of allergen labeling regulation, further implementation and standardization in PAL is required⁸⁵.

Regardless of dedicated labeling procedures, presence of undeclared allergens still remains the greatest cause for food-based recalls globally^{31,89}. Large scale recalls can have a significant socio-economic burden on a country⁹⁰. The Rapid Alert System for Food and Feed (RASFF) is a European food safety risk assessment system which has experienced an increased volume of notifications regarding undeclared allergens in recent years⁹¹. When an allergen has been mislabeled it must be reported to the competent authority as well as recalled in the notifying country and then RASFF issues an alert informing that the product contains a mislabeled allergen⁹². It is an option to notify RASFF about allergens that may have been unintentionally introduced into a product by cross contamination, however, this is not mandatory as it is not regulated by the EU. Risk communication is expected within the food industry, but it is not mandatory so providing the industry with sensitive tests that can detect allergens at concentrations as-low-as-reasonably-achievable (ALARA) is the best way to ensure that unintentional allergen presence in food is monitored. In order for consumers to be entirely confident that their food is free from allergens, it is necessary to manufacture easy to use assays to detect for unwanted allergen presence so that consumers do not have to rely on recall or notification data to maintain their avoidance diets^{93,94}. A consumer-friendly allergen test which can be based on a smart-detector could provide consistent, essential information for the allergic individual, regardless of the quality of product labeling.

2.4 Criteria for Consumer-Friendliness

As the world moves towards personalized testing and diagnosis, the need for user-friendly devices becomes more apparent. Whilst many products claim to be ‘for the consumer’, in reality only a low percentage of these devices actually are. It is useful to consider the parameters that make an assay usable for the general population. Recently, stakeholder guidance into the development of consumer-orientated allergen analytical devices has highlighted the need for standardization of instructions for assay use and for transparency in validation procedures in consumer assays⁹⁵. For a truly user-friendly assay, the majority of the adult population should be able to perform it successfully, using the device should be self-explanatory or require minimal instruction. When linking an assay to a smartphone app it is possible to include safety information and instructions for application within the app, limiting the need for an instruction manual. Alongside being easy-to-use, the assay should be safe and not contain toxic chemicals, it should also not be able to stain the

user/damage clothing and therefore should not require the use of personal protective equipment (PPE). There should be no toxic waste produced, and preferably the assay should be environmentally friendly and recyclable, there should be instructions on how to dispose on any waste that does come from the assay⁹⁵.

The assay/detector should require minimal external equipment. By having to use scientific equipment such as precision pipettes and centrifuges, the manufacturer introduces the need for further training/explanation to negate human error. In addition, requiring basic laboratory skills (such as pipetting), prevents individuals with no scientific background from being able to use the device. External equipment increases the overall cost of the assay and affordability is a prerequisite for user-friendly assays. Pre-containing reagents within the assay eliminates pipetting steps and allows waste to be minimized and cost reduced. As the consumer cannot rely solely on the visual readout of a screening assay, another major cost in many assays is the requirement for a specialized detector/reader⁹⁵. Next-generation citizen science detectors such as smartphones reduce cost significantly, as most people already own at least one smartphone. Often the assay can be performed with relative ease (e.g., LFIA) but it is the result interpretation, such as differentiating between lighter and darker lines, which is difficult for the consumer and can be negatively affected by personal bias. In general, LFIA readers are expensive and are not something that a consumer would own and carry around with them, whereas smartphones are universally present across the globe. The smartphone as a readout system makes most assays more consumer friendly as the majority of people are accustomed to using smartphone applications. A significant benefit of using the smartphone is that the results can be instantly uploaded to cloud databases/sent to relevant stakeholders, which can be particularly useful for remote quality control. Conversely, it should be considered that when using a smartphone-based analytical device in a low resource setting that the wireless system may suffer with low connectivity and so the smartphone application must be able to support asynchronous data transmission¹². Linking an assay to a smartphone detector goes a long way to making the assay more portable. Portability means that the assay can be taken anywhere and applied under in-field conditions, such as in a restaurant.

Another key component of a user-friendly device is that it should provide results quickly. Consumers do not want to wait for extended periods for results, so rapid tests are desirable. The assay should provide results as quickly as reasonably possible without compromising the sensitivity or reliability of the test. The speed of an assay can be optimized by first carrying out detailed kinetics studies to select antibodies with rapid association rates and high affinities to the allergen of interest, for use in the assay. The reaction rate can also be increased by proper orientation of the antibodies, so that the relevant binding sites are directed away from the surface where they can better interact with the targets. Assays can be further sped up by using internal microfluidics, which also limits the

necessity for excessive sample handling/preparation as mixing can be achieved in the fluidics system. Microfluidics often increase the speed of the assay as mixing, pumping and directional flow can be carried out at precise locations in the assay itself, limiting the need for operator interaction⁹⁶. Proper mixing can also speed up the assay by increasing the rate of diffusion of the sample. The assay should not have significant cross-reactivity with different allergens, so that the user can be certain that their results are correct. Proper characterization of antibodies ensures that the assay is selective for the target allergen. In addition to being selective, the assay should be sensitive and able to detect allergens at their LOEL.

Multiplexing allows multiple allergens to be detected in a single sample, which is desirable, saving time and money in comparison with using several singleplex assays⁹⁷. Furthermore, a proportion of the allergic population suffer with more than one allergy, due to cross-reactivity with similarly structured allergens, so it is attractive to test more than one allergen at a time⁹⁶⁻⁹⁹. An individual who suffers with multiple allergies should be able to test for all of them using a singular device. As allergens are structurally different proteins, they may require different extraction procedures, when testing for multiple allergens the extraction buffer will likely be a compromise between maximum extraction efficiency and the ability to co-extract different allergens from the matrix. Truly personalized allergen testing where a consumer selects the allergen panel, they want included in the assay would come at an expense, but this could be lowered if companies start including more allergens in multiplex assays. The current proof-of-concept allergen multiplex assays are displayed in SI Table S2.2.

It is critical for user-friendly assays to be reproducible so that the user is confident in the result. In order for this to be achieved, assays should be validated by intra and inter laboratory testing and benchmarked against successful commercial allergen assays. By proper validation, the reliability of the assay can be proven, and consumer confidence can be attained. Popping et al suggests that consumer devices should first go through single-laboratory-validation, followed by independent laboratory validation and proficiency testing in parallel, including being tested by untrained personnel/consumers⁹⁵. It would improve the affordability of the assay if the assay were reusable such as when using an SPR chip, however if the assay cannot be reused (LFIA) the smartphone attachment and app should be able to be reused for a number of cycles and the assay should be recyclable. The ideal device for consumers would therefore be easy to use, safe, recyclable, affordable, a smartphone-based detector or other smart device with connectivity possibilities, portable, rapid, sensitive, multiplexed where appropriate and properly validated and benchmarked.

3 Food Allergen Detection Using Smartphone Readout

Immunochemical methods for allergen detection focus around the complementary interaction of an allergen-specific antibody and an allergen. An overview of commercial laboratory-based allergen assays is provided in SI Table S2.3. Lab based methods are highly sensitive, selective and accurate. However, lab-based methods require trained personnel, scientific knowledge and often expensive equipment. By linking traditional lab-based methods with a smartphone readout system they become more user-accessible. A comparison of lab and smartphone-based methods is given in SI Table S2.4. The most popular optical approach to smartphone detectors is based on colorimetric reactions such as in LFIA or ELISA²⁸. Colorimetric smartphone-based sensing conventionally relies on the phones complementary metal oxide semiconductor (CMOS) filters to assign red, green, blue (RGB) values to light. Therefore, smartphone-based sensors are able to detect changes, in optical density or intensity of analyte-reagent complexes over a range of wavelengths¹². The majority of the population have and are familiar with smartphones, so interfacing a scientific method with a simple smartphone app improves consumer friendliness.

3.1 Lateral Flow Immunoassays

Lateral flow immunoassays (LFIA) are immuno-chromatographic test strips designed to be easy to use, as has been exemplified by their success as pregnancy tests¹⁰⁰. Many food manufacturers utilize LFIA's to test their clean-in-place (CIP) procedures and to ensure that their production lines are free from allergens. Cross contamination can be monitored for instance using LAB-2-GO, a user-friendly test toolkit developed by Zeulab (Zaragoza, Spain) to prove good manufacturing practice (GMP)¹⁰¹. The standard components of an LFIA are the sample filter pad, the conjugate pad, the membrane, the absorption pad and the test/control lines¹⁰².

In a sandwich format LFIA, the conjugate pad contains a pre-sprayed antibody which is specific to the allergen of interest. This specific antibody is labelled with colored or fluorescent moieties. The test line contains an immobilized allergen-specific antibody, which binds to a different epitope on the allergen than the labelled antibody. The control line contains an antibody raised against the animal species of the labelled antibody. When a sample containing the target allergen is added to the sample pad, the target binds with the labelled antibody in the conjugate pad, forming a labelled complex. The labelled complex flows via capillary action, driven by the absorption pad, laterally up the membrane. When the test line is reached, the complex is captured by the immobilized allergen specific antibody. The target analyte is sandwiched between the labelled and the capture antibodies, which results in the appearance of a colored line in the test region. The remaining labelled antibody binds with the immobilized anti-species antibody at

the control line, resulting in the appearance of a second colored line in this region. In a sandwich assay the color intensity of the test line is directly proportional to the concentration of the target allergen in the sample. Whilst the test line informs the user of the relative concentration of the allergen in the sample, the control line proves that the assay is functioning correctly.

3.1.1 Multiplex Dipstick Tests

Lateral flow immunoassays can also be multiplexed through the addition of multiple test lines. Each test line corresponds to the target analytes to be detected¹⁰³. Detecting a range of allergens in a sample is attractive as it reduces analysis time and reagent waste, as multiple analytes can be assessed under the same conditions. Structures other than simple strip tests can also be applied in multiplexing. Fenton et al has shown that two-dimensional shaping of capillary driven membrane assays into candelabra or other structures can improve the spatial discrimination of the assay¹⁰⁴. Assays for different analytes can be positioned on separate arms of the device which can be directly labelled to minimize user confusion. Currently much of the attention of multiplex flow assays has been focused on mycotoxin analysis¹⁰⁵. It is expected that future research will focus on incorporating multiplex into the food allergen field in order to make food allergen analysis more user-friendly. When multiplex dipsticks are constructed for food allergens, they should be designed to fit the criteria of consumer friendliness. Lateral flow immunoassays are easy-to-use, safe, affordable, portable, rapid, sensitive and can be quantitative when linked with a dipstick reader such as a smartphone.

3.1.2 Smartphone Lateral Flow Immunoassay Readers

Although LFIA results can be visually detected with the naked eye, by integrating LFIA with a smartphone detector system, a quantitative result can be achieved. Owing to their simple structure, LFIAs are fairly simple to interface with smartphones, as the results can be easily detected via the phone's camera. Smartphone dipstick readers can be categorized based on their light source; some rely on LED's as the external light source whilst others utilize the internal flash in the phone. Mudanyali et al described a smartphone readout system termed rapid diagnostic test reader (RDS)²⁵. The reader is made up of a 3D-printed 65 g mechanical attachment which consists of: a LFIA strip holder, an inexpensive lens, 3 LED's and 3 AAA batteries. The device captured images of the LFIA, which were digitally processed within the related smartphone app. The linked central database received and stored the processed results in a world map through geo-time stamping. This device was validated by using commercially available malaria, tuberculosis and HIV LFIAs²⁵. Another example applying LED's as an external light source, was described by Lee et al for using a smartphone-based readout system integrated with a LFIA reader for the detection of Aflatoxin B1. The device described a LFIA reader consisting of: a close up lens, white LEDs and batteries. A smartphone camera was positioned over the lens of the LFIA reader where

the camera recorded images of the optical density of the LFIA test and control lines. Lee et al further refined this LED based format of LFIA reader and smartphone app for image capture and data acquisition for Salmonella detection²⁴. This format of LFIA strip readers utilize LED's as light sources which requires external battery packs for power.

Another format of smartphone LFIA readers utilize the smartphones embedded camera flash as the light source. Oncescu et al developed a smartphone readout system for the colorimetric detection of changes of pH in sweat and saliva¹⁰⁶. The device used a 3D printed phone case, which housed a slot for the indicator pH strip, a reference strip, and room to store up to 6 spare pH test strips. The attachment applied PDMS light diffusers to allow for reproducible illumination from the camera flash. The strips were photographed and the RGB (red, green, blue) values were analyzed and converted to a hue spectrum. Hue more appropriately fits the range of color for pH strips. In another study Oncescu et al advanced the use of the internal flash of a phone camera for reading of LFIA for cholesterol testing¹⁰⁷. This device is referred to as the smartCARD and it monitors the colorimetric change resulting from an cholesterol enzymatic interaction on a test strip. The phone flash and camera are then used to record images of the colorimetric reaction, which is then digitally processed in the related app. The attachment has a slot for the test strip and a PDMS light diffuser. The device converts recorded RGB values to hue, luminosity and saturation values within the app and is capable of quantifying cholesterol over all physiological values^{106,107}. A further example of an embedded flash based LFIA smartphone reader for screening thyroid stimulating hormone (TSH) was described by You et al¹⁰⁸. This device used an opto-mechanical 3D printed attachment which directed the light from the phone camera, via an optical fiber to a collimating lens to illuminate the LFIA. The study emphasized the importance of minimizing the Mie scattering of the nitrocellulose membrane particles and maximizing the Raleigh scattering of the gold nanoparticles of the test/control lines, increasing the signal in these regions. The improved signal to noise ratio allowed very sensitive LOD's to be achieved with this readout system. Although these examples have not yet been applied to allergen testing, the technology could easily be translated for allergen analysis.

Commercial companies are now finding ways to advance their traditional LFIAs by interfacing them with smartphone technology. R-Biopharm's (Darmstadt, Germany) RIDA QUICK lateral flow assays are compatible with the RIDA SMART App, which acts as an embedded flash smartphone based lateral flow strip reader. Currently, the mycotoxin strip test range has been converted for use with the app but it is expected that soon all RIDA QUICK assays (including the extensive allergen range) will be compatible with the app¹⁰⁹. Once a sample has been tested with the LFIA, a strip cover with the color calibration required by the app to distinguish the differences in test/control line intensity, is placed over the strip. The strip and cover are placed in a cardboard enclosure, this box is to control

ambient light conditions and ensure that consistent results are achievable. The app uses the smartphone camera to capture a photo of the strip. The results are automatically stored within the app database/and or can be exported to email or printed via a Wi-Fi connected/Bluetooth printer. The major benefit of the app is the ability to quantify results, however, when testing for food allergens a semi-quantitative result would be sufficient as there are currently no set threshold levels for allergens EU legislation. Although the company also makes quantitative readers, using a smartphone is significantly more affordable and user-friendly for the general consumer. A major limitation for this set-up is that it is currently only suitable for use with the Android platform (5.1-8.0 OS) and on a limited number of smartphone models (Google NEXUS 6, NEXUS 6P & Pixel XL)¹⁰⁹.

Lateral flow fits the criteria of being affordable, portable, disposable and rapid. The popularity of using smartphones as LFIA readers has also been highlighted by commercial companies, such as Novarum and Mobile Assay who develop bespoke smartphone apps for the reading of established LFIAs¹¹⁰⁻¹¹³.

3.2 ELISA

Enzyme linked immunosorbent assays (ELISAs) are the most routinely used method of allergen analysis in the food industry^{5,114}. Commercially available allergen ELISA's are listed in SI Table S2.3. ELISA's exist in both competitive format (suitable for low molecular weight proteins) or sandwich format, which is the prominent choice for food allergens⁸³. Both formats of ELISA are based on the interaction of an enzyme labelled allergen specific antibody with an antigen. An antibody is labelled with an enzyme which initiates a measurable colorimetric change upon the addition of the substrate. The reaction is measured by an ELISA plate reader¹¹⁵. In sandwich ELISAs, the measured response is directly proportional to the concentration of allergen in the sample. Due to the laboratory-based nature of ELISA which involves following a standard operating procedure and technical instructions, the requirement for scientific equipment/trained personnel and the long incubation steps, ELISA cannot be considered consumer-friendly¹¹⁶. Nevertheless, a few smartphone interfaces have been designed for use in resource limited settings.

3.2.1 Smartphone 96 Well Microplate Readers

Microplate readers are one of the most used instruments in routine immunochemical analysis. However, they are relatively expensive, require maintenance and are non-portable, making them inaccessible for in-field testing¹¹⁷. It is possible to create smartphone-based spectrophotometers using the smartphone camera^{25,117-119}. In a 2016 study, Fu et al described the development of a smartphone-based microplate reader capable of detecting biomarkers in the absorbance range of 340-680nm^{120,121}. This research relied upon established commercial ELISA's and compared the results with microplate reader Synergy H1 Hybrid Multi-mode Microplate Reader (BioTek Instruments; Winooski,

USA) for validation. Once the assay was complete, the 96 well plate was introduced to the smartphone-based microplate reader, which was attached to the camera of the smartphone. The related app stores calibration curves which convert the transmitted light intensity to absorbance values and then to analyte concentrations¹²⁰. The results obtained were slightly lower than with the commercial microplate reader.

Another example was described by Berg et al from Ozcan's group of University of California, Los Angeles (UCLA), which describes a microplate reader based on a Windows phone (Lumia 1020, Nokia) with 3D printed attachment and a data processor connected to the cloud¹¹⁷. The colorimetric reader used a 3D printed opto-mechanical attachment with a light emitting diode (LED) to illuminate 96 well plates. The light from the LEDs is transmitted through 96 individual optical fibers which redirect the light to a collection lens, which then transmits the captured images of the samples to the custom designed app for signal reading. The processing algorithm focuses on finding two centroids to use as references in the 96 well plate and pixel intensity thresholding to separate wells for independent analysis. The device was successful and was able to match the performance of a food and drug administration (FDA) approved microplate reader¹¹⁷.

The use of smartphones as microplate readers will make ELISA technologies more accessible; by making them portable, able to connect to Wi-Fi and upload results to the cloud in real-time. This adaptation will be significantly beneficial in low resource settings such as in developing countries. As ELISA requires multiple reagent handling steps it is necessary for the user to be able to use a pipette. Long incubation steps and multiple washing steps prevent the method from being consumer friendly. Even if on a smartphone app there was a step-by-step guide showing which reagents to use at each interval, the method would still not be that consumer friendly. The detection method on the smartphone is however more user friendly in the sense that it is affordable, portable and can connect wirelessly so it is suitable for in-field conditions.

3.2.2 Smartphone 8 Well-Strip Microplate Reader

In some scenarios the user may only want to analyze a small number of samples rather than a whole 96 well plate, in these circumstances a smartphone detector which analyses a strip of 8 microwells may be more appropriate. The iTube is a novel allergen testing platform also developed by Ozcan's laboratory at UCLA. The device is a 3D printed opto-mechanical attachment that is connected to the existing camera of a smartphone (Fig. 2.1)¹²². The approach is based on a 8 well strip of the commercial Neogen peanut ELISA. The platform consists of a 3D printed attachment that holds the microwells and the smartphone reader, and a related 'iTube' app which converts transmission images received from the camera to relative absorption values, which can be related to the concentration of allergen present within the sample¹²². The attachment weighs around 40 g and is made up of: a

plano-convex lens, two LED's, two light diffusers and circular apertures to allow control of the field of view. Once the peanut assay has been performed, transmission intensities are recorded using the smartphone camera and the images are digitally processed. The digital processing in the app occurs by converting the transmission images of the light through the test tubes into binary mask images. The detector is semi-quantitative, giving a positive signal for samples containing over 1 ppm peanut and negative results for lower concentrations.

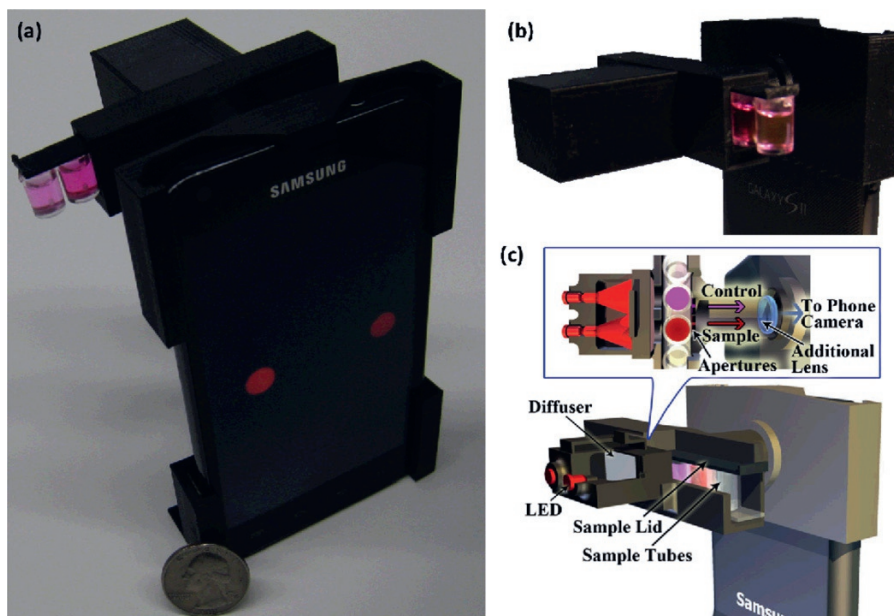


Figure 2.1. (a) An image of the iTube platform, using a Neogen Peanut ELISA 8-well strip and a smartphone based digital reader, is displayed. (b) The 3D printed opto-mechanical attachment which is connected to the rear-facing camera on the smartphone. (c) A schematic of the iTube is shown. Reproduced from (Coskun et al. 2013) with permission of The Royal Society of Chemistry.

Another example of a single-strip 3D printed smartphone microplate reader was successfully explored by Wang et al for the detection of herbicide 2,4 dichlorophenoxyacetic acid which further clarifies that in some situations only a limited number of samples require analyses¹⁹. Like most smartphone based analytical devices, the iTube has the ability to upload results to servers through its app. This means that a personalized allergen testing database can be constructed, and users can monitor tests they have carried out on different foods, in varied locations, creating a spatio-temporal allergen map. Using anonymized 'big data' in this way not only assists allergic sufferers, but also helps those involved in food manufacturing, product design and official regulators to better understand allergens from a consumer point of view.

3.3 Flow Cytometry: Bead Suspension Array

Flow cytometry (FC) in suspension array format, uses microbeads as solid phase support systems for capture antibodies to be immobilized onto. The bead-antibody complex can be identified by its fluorescent/colored profile by a flow cytometer¹²³. Flow cytometry can be used for both in-vivo and in-vitro quantitative allergen analysis^{124,125}. Garber et al and Cho et al have shown that by using magnetic bead sets it is possible to detect 14 food allergens (and gluten) in 12 different samples, within 6 hours, with a similar LOD to existing ELISA methods (<5 ng/mL)^{97,126}. However, their methods required two extraction procedures, so although the assay could be multiplexed, the extraction could not. Otto et al combined a competitive format ELISA with flow cytometry (BD Accuri® C6 apparatus, Becton-Dickinson; Vianen, The Netherlands) to develop an assay capable of detecting 5 different allergens in a cookie matrix¹²⁷. The assay could detect in the range of 2-10 ppm for all the allergens in the test. Cho et al further described the usefulness of FC for cross-reactivity profiling between 23 legumes and 12 tree nuts¹²⁸.

3.3.1 Miniaturized Flow Cytometry

Despite their success, FC's are not portable, are relatively expensive, require trained personnel, and are therefore unsuitable for in-field analysis. In response to this, FC was miniaturized. Miniaturization of FC involves focusing the flow of the particles to be analyzed within a microfluidic channel, reducing the size of both the microfluidics and the optics, and integrating them with a signal readout device¹²⁹.

The portability of miniaturized flow cytometry (MFC) makes it an attractive technique for in-field routine analysis. Connecting MFC to a smartphone readout system further strengthens its portability. Ozcan's UCLA group have worked since 2008 to develop on-chip cytometers that are capable of interfacing with smartphones as the detector¹³⁰. Zhu et al has further substantiated the ability to combine MFC and optical microscopy with a smartphone interface¹³¹. The study integrated a microfluidic chip with a syringe pump that controlled the transport of sample to the imaging field, where a photo was captured by a smartphone camera. This example uses an opto-mechanical attachment, featuring simple lenses, plastic color filters, LED's and batteries. Further development on this study yielded a smartphone based MFC interfaced with an optical microscope for the counting of fluorescently labelled blood cells¹³².

Despite these examples being for the healthcare sector they provide an excellent basis for future design of smartphone-based cytometers for application to food allergen analysis. Similarly, MFC has been used in contaminant and residue monitoring in milk samples¹³³. An assay was designed to detect growth promotor bovine somatotropin (rbST). Biomarker specific antibodies (anti-rbST) were coupled with quantum dots (QD), which were immobilized on paramagnetic microspheres. The device relied on an optical-mechanical

attachment consisting of a phone holder (for alignment of optics), a sample tray to hold the cover slides, 12 UV excitation LEDs, white LEDs, an optical filter, a de-magnifying lens and a lid to prevent introduction of ambient light¹³³. The smartphone camera was used to record images of the fluorescence emitted from the QD's. This assay still takes a substantial amount of time to carry out owing to incubation steps so it cannot be classified as a rapid assay. An even more sophisticated multiplexed smartphone approach based on the original rbST microsphere assay was presented for biomarkers in milk (Fig. 2.2)¹³⁴. Although this technology has currently only been applied to food diagnostics, focusing this approach could allow it to be applied more specifically for food allergens.

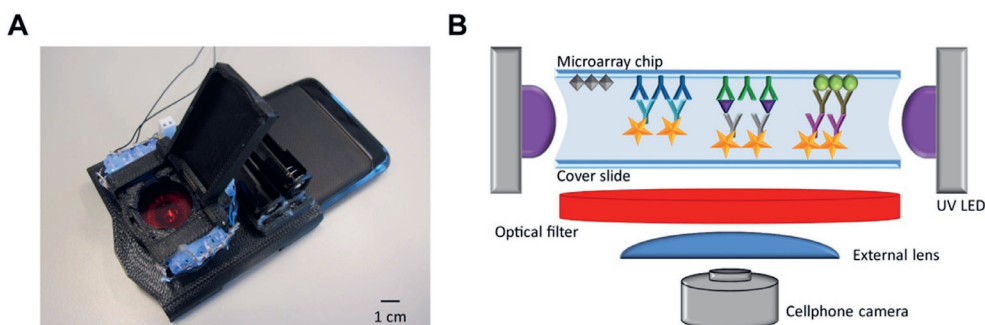


Figure 2.2. (A) Photo of 3D printed optical attachment on the smartphone used for testing. (B) Schematic representation of the smartphone biomarker detection platform. Reproduced with permission from authors (Ludwig et al. 2015).

3.4 Multiplex Surface Plasmon Resonance Based Food Allergen Biosensor

This review has averted biosensors, due to the in-depth review on using biosensors for food allergen analysis published in 2016 and another 2016 review focusing specifically on smartphone-based biosensors^{9,28}. Only brief attention will be paid here to biosensors. Surface plasmon resonance (SPR) monitors changes in the refractive index based on the dielectric properties of a thin layer of sample containing solution, near the gold metal surface of the sensor region. The energy transfer from polarized light to surface plasmons results in characteristic reflected light patterns which can be monitored label free, in real-time through a sensorgram (the angle at which the dip is observed versus time)¹³⁵. Analyte specific antibodies are immobilized onto the metal layer of the sensor chip, mounted onto a glass prism with an integrated flow cell that is then placed in the instrument. When polarized light is shone through the prism, the light is reflected by the metal layer, resulting in an angle of incidence capable of inducing surface plasmon resonance and causing a dip in the reflected light intensity¹³⁶. The refractive index near the metal surface will change as proteins are adsorbed onto the metal surface and then the amount of adsorbed protein

can then be determined. Unfortunately, current 'portable' SPR's still require a laptop or small computer to operate¹³⁷.

Imaging SPR (iSPR) has the benefit of being able to simultaneously detect multiple analytes in a single sample. Raz et al described an iSPR linked with an allergen-antibody array for the detection of 12 food allergens within 12 minutes¹³⁸. The rapid, multianalyte, method is quantitative and detects food allergens at 2 mg/kg. The procedure allowed for total allergen profiling within food, providing a unique fingerprint for which allergens each commercially available food contained. The optical devices laboratory of Linköping University (Sweden) described a smartphone-based angle resolved localized SPR device¹³⁹. The device used the phone screen as the light source; the phone camera to record images and a disposable optical coupler made of PDMS/epoxy which matched the refractive index of glass¹³⁹. The polymer surface contained glass coated with a layer of gold, as the thin metal surface, which simple or more complex microfluidic systems are compatible with. The app allowed a red-rectangle on the phone screen to frame the region of interest (ROI) to be photographed, which ensured that the images were all captured under the same conditions, in the right ROI, minimizing test-to-test variation. The camera shutter and exposure were set using a simple app developed for iOS 5. When the light was reflected from the gold chip surface the SPR signal was transported to the front camera of the phone where it was conditioned by deflection via a PDMS prism. The method was validated using a commercial β -microglobulin assay but should be compatible with numerous other targets.

Guner et al described interfacing a smartphone with disposable Blu-ray discs as SPR chips and a 3D-printed iSPR attachment²⁶. Detection limits were reported as comparable with commercial instruments. The SPR attachment recorded measurements from over 20,000 individual pixels based on an intensity interrogation mechanism. An additional study applying fiber-optic SPR (FO-SPR) using a smartphone platform has achieved results consistent with commercial SPR instruments¹⁴⁰. Although the FO-SPR interfaced with the smartphone is portable and allows precise detection and sophisticated optical calibration, due to the need to compensate for alignment issues in the app, the platform cannot be classified as consumer-friendly.

3.5 Section Summary

The food allergen detection methods that have been discussed so far do not fully satisfy the criteria for consumer friendliness (see section 2.4) and are therefore not currently suitable for citizen science. In order to be consumer-friendly the technique should be easy to carry out, requiring minimal training. Of the methods discussed so far, dipsticks are generally considered to be user-friendly with many people being accustomed to using home pregnancy tests, which are historically the first example of LFIA¹⁰⁰. The majority of the population would be capable of carrying out a strip test with minimal instruction,

and when linking the test to a smartphone reader, would be able to interpret the results. However, smartphone dipstick readers have not yet been developed for food allergen detection and although the general consumer could carry out the LFIA easily, they would not have a quantitative strip reader so the results would only be qualitative. But for food allergen analysis, it is not fundamental to have a quantitative result as long as the result is semi-quantitative within a small range, as there are currently no set threshold levels for food allergens (excluding gluten). If a consumer wanted to use their screening results in court, for example to sue a company for the presence of an undeclared allergen, it would first be necessary to use orthogonal approaches to confirm the result with instrumental analysis such as mass spectrometry anyway¹⁴¹.

Whilst LFIA are simple to carry out, methods such as ELISA, FC and SPR all require training to perform. The methods require understanding of laboratory practice and experience in data interpretation to achieve meaningful results. Even when linking with a smartphone readout system, ELISA still requires laboratory skills, such as using precision pipettes, to carry out. Performing an ELISA is time consuming owing to the incubation steps and need for external equipment. As the assay uses open test tubes, it is possible that there could be spillage of chemicals, which would mean the user carrying out the test would require PPE, which further limits its potential as a user-friendly device. ELISA has the disadvantage of currently being non-reusable, non-recyclable and produces chemical waste. Flow cytometry is a multiplex laboratory-based method, meaning that it is not portable. It requires scientific skill and good laboratory practice to stay safe and uses expensive instrumentation. The advancement of MFC with a smartphone-based readout makes FC more user-friendly by providing an inexpensive platform, which can be easily operated and re-used, decreasing the cost of the assay. An additional benefit of MFC is that it is portable and so therefore can be used in field. Of the discussed methods, smartphone SPR may be the most promising for citizen science as it has the benefit of having limited sample preparation steps owing to its label free nature and results in real-time and the ability to re-use the sensor chip. Interfacing with a smartphone also makes SPR portable and suitable for in-field use.

All of the methods, except for LFIA and SPR, require trained personnel, take a prolonged period of time to carry out, have complex data acquisition and need to be completed under laboratory conditions. This means that the general population would not be able to efficiently carry out these tests and so they cannot be classified as user friendly.

4 Consumer-Friendly by Design

Whilst the previous section discussed scientific methods for food allergen analysis, this section will focus on methods which have specifically been designed with the intention of

being consumer friendly. The devices are compared in Table 2.2 below. Consumer-friendly devices are needed as allergic individuals require devices which can be easily operated whilst at home or in a restaurant. Consumer-friendly detectors will allow the road to be paved for citizen science, as the general population of allergic sufferers will be able to perform their own food analysis.

4.1 Portable Gluten Sensor

NIMA (San Francisco, USA) is a commercial portable gluten detector based on an immunochromatographic dipstick and a sensor. The device provides a testing platform for individuals with celiac disease/gluten intolerance to be able to perform their own gluten analysis. The device is portable, sensitive and rapid, taking only 2-3 minutes for a result in the consumer-friendly form of an LED smiley face (gluten free) or a wheat grain (containing gluten)¹⁴². It has fully integrated sample handling inside single use test capsules, which makes it attractive for the general consumer, especially when considering its use in a setting such as a restaurant. The test is based on gluten antibodies (13-F6 & 14-G11) against the toxic 33-fragment of the protein, which have been immobilized as the test line of the strip test¹⁴². This is the fragment widely considered responsible for the autoimmune effects of gluten, so its detection is crucial¹⁴³. The majority of celiac/gluten intolerant individuals can tolerate gluten levels up to 20 ppm and the assay detects below this level^{144,145}. However, it should be considered that if analyzing whole grains for gluten, that contamination is localized to particular 'hot spots' rather than being ubiquitous to the whole sample, which could result in false positives/negatives with the sensor, so it is necessary to first homogenize the sample before testing¹⁴⁶.

To operate the device, the user puts some chopped food into the one-use capsule. Once the food is inside the capsule, the user turns the head of capsule operating the grinding mechanism and homogenizing the food. The final twist of the lid introduces the food homogenate to the pre-contained extraction buffer and an internal rotating-motor acts as a mini-centrifuge to mix the food and buffer, solubilizing and extracting any gluten from the food¹⁴². After a few minutes, the electronic sensor will determine whether there is gluten present in the sample. An algorithm then converts this information to a smiley face icon for gluten free or a wheat icon for products containing gluten. The sensor costs \$279 and includes 3 one-use buffer containing capsules, a charger and a carrier pouch¹⁴⁷. Each single-use capsule can only test the food portion that you put into the capsule. To test multiple components of a meal at a restaurant, a user would need multiple test capsules, increasing the overall cost of the meal.

This set-up can be considered as user-friendly in the sense that the assay is easy to use, the results are easily interpretable, it is safe, rapid, sensitive and portable. NIMA has a related app, which allows consumers to create a map of local restaurants or compilation

of products that are truly gluten-free, which can help lessen the economic and restrictive burden of an avoidance diet. NIMA has a large social media presence, utilizing the hashtag #nimatested to denote restaurants and foods that have been tested using the device. The use of social media allows users of the device to communicate and opens a discussion between gluten intolerant individuals. In addition, the product website has a wealth of information on how to operate the device, what can and cannot be tested, limits of detection and a customer support service. A major disadvantage is the overall cost of the device, which will prevent it from becoming the first choice for every gluten intolerant consumer, although the sensor is reusable the one-use capsules are not and cost \$5 each. An additional disadvantage is that it cannot be multiplexed, and its designers are making a separate sensor and assay for major peanut allergens, which further increases the cost to the consumer particularly if they suffer with co-allergies. As a result of lack of published validation studies, it is plausible that false negatives could prove dangerous to individuals with celiac/gluten intolerance and false positives from the sensor could adversely affect the food industry⁷⁹. Lack of evidence-based literature surrounding the product makes it difficult to assess its reliability.

4.2 Molecularly Imprinted Polymer Allergen Sensor

The Allergy Amulet (AA; Boston, USA) is a rapid, portable food allergen and ingredient detection device that is currently being developed, intended for commercial release in Winter 2018¹⁴⁸. This device has been included in this review as a state-of-the-art consumer targeted allergy detection and management device. The device is initially being designed to target peanut protein in the concentrations of 1-2 ppm. The device uses molecularly imprinted polymers (MIP) which are synthetic receptors which can be designed to recognize a specific target allergen¹⁴⁹. If the allergen is present, the selective cavities in the MIP capture the allergen through a 'lock and key' mechanism and a signal on the device then alerts the user to the allergen presence¹⁴⁸. The device works in theory by inserting a test strip probe directly into the food or liquid to be assessed. The website states that no sample preparation is required, however this is difficult to believe when considering inserting a probe into samples such as peanuts or cookies. Following exposure to the sample, the probe is then inserted into its MIP containing covering sheath, and then the sheath is inserted into the amulet reader, which resembles a USB stick. If the target allergen is present, an LED in the amulet case will light up, promptly alerting the user to the allergen-presence within a matter of seconds. The results are also sent via a smartphone interface to the AA app, which allows users to compare test results creating a personalized allergen database. This helps users to connect with other food allergic individuals and compare results based on what they have eaten. It is truly portable and can be worn as a necklace or keychain. This device is consumer-friendly in the sense that it is portable, (claims to) require minimal sample preparation/extraction, it is quick, sensitive and selective. However, as there is not more evidence-based information available about

the cost, reusability and the validation/benchmarking of the device at this stage, it is impossible to state how suitable it is for citizen science.

4.3 Portable Electrochemical Multiplex Allergen Sensor

The integrated exogenous antigen testing (iEAT) is a state-of-the-art, electrochemical, magnetic bead-based food allergen detection sensor. It works by conjugating the desired allergen antibody onto a magnetic bead¹⁵⁰. The bead suspension containing the immobilized antibodies is then incubated with the extracted food for around 3 minutes before re-suspending with horseradish peroxidase (HRP)-conjugated isotype IgG antibodies, as a label. The HRP-bead complex can then be mixed with substrate (TMB) and added to the electrode. The entire assay takes less than 10 minutes, including extraction time. The iEAT allows singleplex or multiplex analysis when using the multichannel electrode, which can detect up to 8 different allergens (Fig. 2.3). The current device tests for major allergenic proteins (see SI Table S2.1) in peanut, hazelnut, wheat, egg-whites and milk.

The assay includes a disposable extraction kit which allows immuno-magnetic enrichment of the allergen antigens concentrating food antigens from food. The kit contains a disposable extraction device, and the extraction buffers and wash solutions that are needed in pre-measured volumes. The lid of the extraction vial has a magnetic sheathed bar attached to allow for capture of allergen-magnetic beads. This bar allows easy transfer of the antibody-bead complex to the washing/labeling stages and then for loading onto the magnetic electrode making sample handling easier for the consumer. The reader centers around a microcontroller unit linked with digital-to-analog converters and a potentiostat, which controls the potential difference between the reference and working electrodes. The sensor was benchmarked against the commercial potentiostat SP-200 Bio-Logic (Seyssinet-Pariset, France) and the two systems were reported to be excellently matched¹⁵⁰.

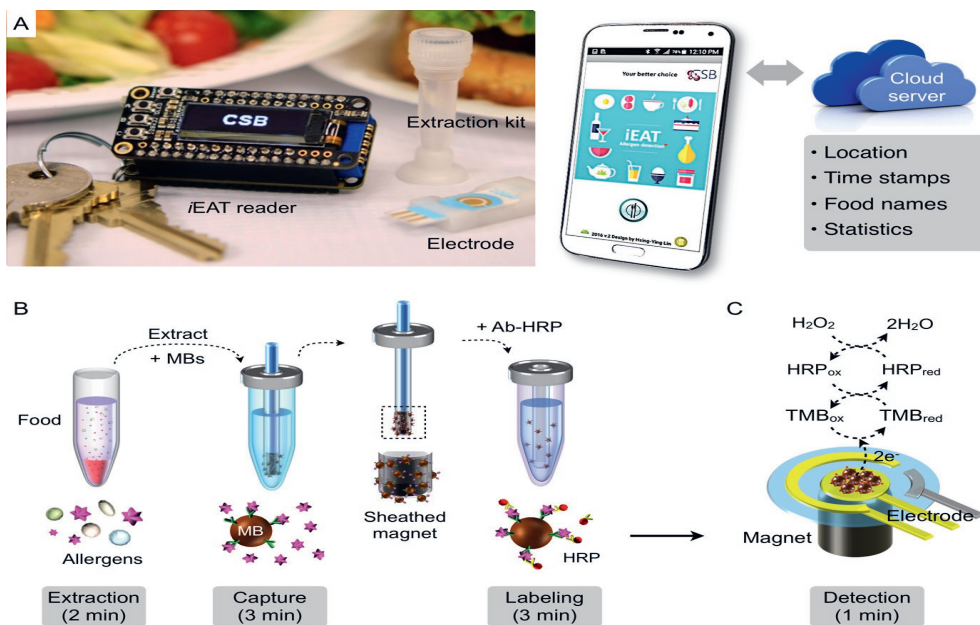


Figure 2.3. The iEAT platform. (A) The keychain sized detector, the multi-channel electrode chip and the disposable extraction kit which is linked with a smartphone app as the readout system. (B) Antigen extraction; antigens are captured on magnetic beads (MB) and labelled with allergen specific antibodies labelled with oxidizing agent HRP (horseradish peroxidase). The disposable kit contains a sheathed magnetic bar which collects and relocates MBs. (C) Signal detection is achieved by mixing HRP-labelled MBs with substrate (TMB, 3,3',5,5'-tetramethylbenzidine) and moved to the electrode. The HRP catalyzes the oxidation of TMB. When TMB is oxidized (ox) or reduced (red) on/near the electrode, measurable electrical currents are given off. Reproduced with permission from (Lin 2017). Copyright 2017 American Chemical Society.

The reader is operated via a Bluetooth connection to a related Android app. The app also takes sample photos and records data such as timestamp, analyte concentrations and GPS information. The research suggests that a future development of the test will be to use the pressure-sensitive screen of the phone as a weighing-scale. By reducing the need for extra equipment/instrumentation the consumer-friendliness of the device will be even further improved. The low cost of the assay, the speed, and the ability to be multiplexed, orientate the assay to consumer friendliness. The use of a magnetic bar for the transfer of the target to each step of the assay eliminates the need for use of precision pipettes, making it more accessible to non-scientists. However, in addition to multiple sample handling steps, the assay uses harmful mutagenic chemicals such as TMB, and so would need to be carried out under careful lab conditions with PPE. The electronic key chain sensor is reusable, and the extraction device is disposable. However, assay would produce toxic waste, preventing it

from being environmentally friendly and limiting its consumer-friendliness as the general user will not be accustomed to disposing of chemical waste.

Table 2.2. Consumer-friendly by Design: Comparison of Devices

Criteria	Smartphone Readout	Consumer-friendly by Design		
	RIDA Smart App	NIMA	Allergy Amulet	iEAT
Safe	Y	Y	Y	N
Portable	Y	Y	Y	Y
Quantitative	Y	Y	Y	Y
Speed (min)	<10	<3	Not Stated	<10
LOD (ppm)	Low mg/kg range	2	1-2	Gliadin: 0.075 mg/kg Ara h1: 0.007 mg/kg Cor a1: 0.089 mg/kg Casein: 0.170 mg/kg Ovalbumin: 0.003 mg/kg
Multiplex?	N	N	Not Stated	Y (x5)
Sample Prep	Homogenization & extraction prior to analysis	Integrated in disposable capsule	Stated as 'Not Necessary'	Extraction with TECP/ sarkosyl at 60°C followed by labeling & mixing steps
Mechanism	LFIA strip reader with smartphone display	LFIA strip reader with sensor display and transmission to smartphone	MIP strip reader with sensor display	Magnet-electrochemical sensing with an electronic keychain reader
Connectivity	WiFi, Bluetooth	WiFi, Bluetooth (through App)	WiFi, Bluetooth (through App)	Bluetooth & Smartphone app
Cost	€12.75 per strip test (box of 20) & €150 for sensor	\$279 + \$5 for each use	Not Stated	<\$40 for device & <\$4 per antigen
Validation	N	Yes, against R-Biopharm	N	Potentiostat SP-200 Bio-Logic using potassium ferrocyanide standard solution

5 Conclusions and Future Perspectives

This review has targeted the recent advances toward citizen science through immuno-based food allergen analysis, with a particular focus on novel smartphone-based

detection strategies. Traditional immunochemical detection methods for food-allergens have been assessed for consumer-friendliness. Applying smartphone-based technologies to traditional lab-based immunochemical methods has been explored. This review has underlined the necessity for more user focused assays that can be based on smartphones for simple food allergen analysis. By providing an easy to use, safe, affordable, portable, smartphone based, rapid, sensitive and multiplexed assays, citizen science can be achieved.

The popularity of using smartphone-based analytical devices has greatly improved in recent years; as can be ascertained by the increasing number of publications. However, there are still a number of developments that can be made to improve the capabilities of smartphones as detectors. One area which needs to be addressed in every smartphone-based assay is the control of ambient light conditions. Many authors have attempted to control light by using an attachment, such as a box which controls the field of light or a lid on a 3D-printed attachment that means that photos can be captured in consistent conditions. Alternatively, it has been suggested that a more appropriate way to control differences in lighting conditions would be to include a normalization algorithm in the app to allow optimum image capture through controlling the lighting bias¹². Currently, most assays/apps are based on a singular platform, but for a detector to be truly consumer-friendly it should be compatible with all the major smartphone platforms (iOS, Android and Windows) so that the user does not need to purchase a specific model. Future developments should concentrate on making a multi-platform system. It must be considered when transferring from one model or platform to another, that smartphone models have variance in the number of megapixels, different positions of their front/rear facing cameras and altered position of their flash.

Future devices should aim for embedded storage of pre-contained dry reagents so that minimal user interference is required. Future applications should focus on designing a sampling interface which would allow the sample collection and detection to be carried out in one device. Such an integrated device could limit sample preparation steps as these could be carried out within the attachment, greatly improving its consumer friendliness.

This review has shown that despite the current lack of truly consumer orientated devices, the allergen diagnostics industry is taking the first steps to become more user-friendly. Devices such as NIMA, AA, iEAT, and the RIDA smartphone range are designed with the consumer in mind and exemplify the change in attitude in industry to move towards citizen science. Food allergies are personal and by engaging the consumer with their own diagnostic analysis food allergen analysis will be improved as more people will take responsibility for their own food safety and big data can be collected. Currently the burden for food allergies lies heavily on food manufacturers and labeling legislations, but

by developing devices that can detect multiple allergens in a sample, consumers can take analysis into their own hands. It is desirable for standardized reference materials for both raw and processed allergens to be developed and utilized at assay development stages so that consumer-friendly devices can be properly benchmarked and validated. Having well validated consumer-friendly assays paves the way to the future of citizen science.

References

1. Bonini, S. Introduction, *Allergy* **2001**, *56*, 5-6, 10.1034/j.1398-9995.2001.00103.x-i1.
2. Kirsch, S.; Fourdrilis, S.; Dobson, R.; Scippo, M.-L., et al. Quantitative methods for food allergens: a review, *Analytical and Bioanalytical Chemistry* **2009**, *395*, 57-67, 10.1007/s00216-009-2869-7.
3. Poms, R.K., CL. Anklam, E. . Methods for allergen analysis in food: a review, *Food Additives & Contaminants* **2004**, *21*, 1-31.
4. Walker, M.C., P. Elahi, S. Lumley, I. . Food Allergen Detection: A Literature Review 2004-2007, *Journal of the Association of Public Analysts* **2008**, *36*, 1-18.
5. Schubert-Ullrich, P.; Rudolf, J.; Ansari, P.; Galler, B., et al. Commercialized rapid immunoanalytical tests for determination of allergenic food proteins: an overview, *Analytical and Bioanalytical Chemistry* **2009**, *395*, 69-81, 10.1007/s00216-009-2715-y.
6. Monaci, L.; Visconti, A. Immunochemical and DNA-based methods in food allergen analysis and quality assurance perspectives, *Trends in Food Science & Technology* **2010**, *21*, 272-283, <https://doi.org/10.1016/j.tifs.2010.02.003>.
7. Slowianek, M.M., I. . Methods of allergen detection based on DNA analysis, *Biotechnology and Food Science* **2011**, *75*, 39-44.
8. Prado, M.; Ortea, I.; Vial, S.; Rivas, J., et al. Advanced DNA- and Protein-based Methods for the Detection and Investigation of Food Allergens, *Critical Reviews in Food Science and Nutrition* **2016**, *56*, 2511-2542, 10.1080/10408398.2013.873767.
9. Alves, R.C.; Barroso, M.F.; González-García, M.B.; Oliveira, M.B.P.P., et al. New Trends in Food Allergens Detection: Toward Biosensing Strategies, *Critical Reviews in Food Science and Nutrition* **2016**, *56*, 2304-2319, 10.1080/10408398.2013.831026.
10. Nitride, C.L., V. Baricevic-Jones, I. Adel-Patient, K. Baumgartner, S. Mills, ENC. . Integrating Allergen Analysis Within a Risk Assessment Framework: Approaches to Development of Targeted Mass Spectrometry Methods for Allergen Detection and Quantification in the iFAAM Project, *Journal of AOAC International* **2018 in press**, *101*, <https://doi.org/10.5740/jaoacint.17-0393>.
11. Popescu, F.-D. Cross-reactivity between aeroallergens and food allergens, *World Journal of Methodology* **2015**, *5*, 31-50, 10.5662/wjm.v5.i2.31.
12. Choi, J. In *Sensing Techniques for Food Safety and Quality Control*, RSC, Ed.; RSC: London, 2017, pp 332-358.
13. Fan, Y.; Liu, J.; Wang, Y.; Luo, J., et al. A wireless point-of-care testing system for the detection of neuron-specific enolase with microfluidic paper-based analytical devices, *Biosensors and Bioelectronics* **2017**, *95*, 60-66, <http://dx.doi.org/10.1016/j.bios.2017.04.003>.
14. Korpilo, S.; Virtanen, T.; Lehvävirta, S. Smartphone GPS tracking—Inexpensive and efficient data collection on recreational movement, *Landscape and Urban Planning* **2017**, *157*, 608-617, <http://dx.doi.org/10.1016/j.landurbplan.2016.08.005>.
15. McCracken, K.E.; Yoon, J.-Y. Recent approaches for optical smartphone sensing in resource-limited settings: a brief review, *Analytical Methods* **2016**, *8*, 6591-6601, 10.1039/c6ay01575a.

16. Ravikumar, N.; Metcalfe, N.H.; Ravikumar, J.; Prasad, R. Smartphone Applications for Providing Ubiquitous Healthcare Over Cloud with the Advent of Embeddable Implants, *Wireless Personal Communications* **2016**, *86*, 1439-1446, 10.1007/s11277-015-2999-5.
17. Martinez, A.W.; Phillips, S.T.; Whitesides, G.M. Three-dimensional microfluidic devices fabricated in layered paper and tape, *Proceedings of the National Academy of Sciences* **2008**, *105*, 19606-19611, 10.1073/pnas.0810903105.
18. Lee, S.A.; Yang, C. A smartphone-based chip-scale microscope using ambient illumination, *Lab on a Chip* **2014**, *14*, 3056-3063, 10.1039/c4lc00523f.
19. Gopinath, S.C.B.; Tang, T.-H.; Chen, Y.; Citartan, M., et al. Bacterial detection: From microscope to smartphone, *Biosensors and Bioelectronics* **2014**, *60*, 332-342, <http://dx.doi.org/10.1016/j.bios.2014.04.014>.
20. Yetisen, A.K.; Martinez-Hurtado, J.L.; Garcia-Melendrez, A.; da Cruz Vasconcellos, F., et al. A smartphone algorithm with inter-phone repeatability for the analysis of colorimetric tests, *Sensors and Actuators B: Chemical* **2014**, *196*, 156-160, <http://dx.doi.org/10.1016/j.snb.2014.01.077>.
21. Stedtfeld, R.D.; Tourlousse, D.M.; Seyrig, G.; Stedtfeld, T.M., et al. Gene-Z: a device for point of care genetic testing using a smartphone, *Lab on a Chip* **2012**, *12*, 1454-1462, 10.1039/c2lc21226a.
22. Long, K.D.; Yu, H.; Cunningham, B.T. Smartphone instrument for portable enzyme-linked immunosorbent assays, *Biomedical Optics Express* **2014**, *5*, 3792-3806, 10.1364/boe.5.003792.
23. Lee, S.; Kim, G.; Moon, J. Performance Improvement of the One-Dot Lateral Flow Immunoassay for Aflatoxin B1 by Using a Smartphone-Based Reading System, *Sensors* **2013**, *13*, 5109.
24. Lee, S.K., G. Moon, J. Development of a smartphone based reading system for lateral flow immunoassay *Journal of Nanoscience and Nanotechnologies* **2014**, *14*, 8453-8457.
25. Mudanyali, O.; Dimitrov, S.; Sikora, U.; Padmanabhan, S., et al. Integrated rapid-diagnostic-test reader platform on a cellphone, *Lab on a Chip* **2012**, *12*, 2678-2686, 10.1039/c2lc40235a.
26. Guner, H.; Ozgur, E.; Kokturk, G.; Celik, M., et al. A smartphone based surface plasmon resonance imaging (SPRi) platform for on-site biodetection, *Sensors and Actuators B: Chemical* **2017**, *239*, 571-577, <http://dx.doi.org/10.1016/j.snb.2016.08.061>.
27. Quesada-González, D.; Merkoçi, A. Mobile phone-based biosensing: An emerging "diagnostic and communication" technology, *Biosensors and Bioelectronics* **2017**, *92*, 549-562, <https://doi.org/10.1016/j.bios.2016.10.062>.
28. Zhang, D.; Liu, Q. Biosensors and bioelectronics on smartphone for portable biochemical detection, *Biosensors and Bioelectronics* **2016**, *75*, 273-284, <http://dx.doi.org/10.1016/j.bios.2015.08.037>.
29. Rateni, G.; Dario, P.; Cavallo, F. Smartphone-Based Food Diagnostic Technologies: A Review, *Sensors* **2017**, *17*, 1453.
30. Smith, P.K.; Hourihane, J.O.B.; Lieberman, P. Risk multipliers for severe food anaphylaxis, *World Allergy Organization Journal* **2015**, *8*, 30, 10.1186/s40413-015-0081-0.
31. Spatz, K. Allergens: An Enhanced Focus, *Journal of AOAC International* **2018 in press**, *101*, <https://doi.org/10.5740/jaoacint.17-0435>.
32. CODEX. Codex Alimentarius Commission, Food and Agriculture Organisation and World Health Organisation: Rome, Italy, 2010.

33. Hadley, C. Food allergies on the rise? Determining the prevalence of food allergies, and how quickly it is increasing, is the first step in tackling the problem, *EMBO Reports* **2006**, *7*, 1080-1083, 10.1038/sj.embor.7400846.
34. Fric, P.; Gabrovska, D.; Nevoral, J. Celiac disease, gluten-free diet, and oats, *Nutrition Reviews* **2011**, *69*, 107-115, 10.1111/j.1753-4887.2010.00368.x.
35. Roth-Walter, F.; Pacios, L.F.; Gomez-Casado, C.; Hofstetter, G., et al. The Major Cow Milk Allergen Bos d 5 Manipulates T-Helper Cells Depending on Its Load with Siderophore-Bound Iron, *PLOS ONE* **2014**, *9*, e104803.
36. Shokouhi Shoormasti, R.; Fazlollahi, M.R.; Barzegar, S.; Teymourpour, P., et al. The Most Common Cow's Milk Allergenic Proteins with Respect to Allergic Symptoms in Iranian Patients, *Iranian Journal of Allergy, Asthma and Immunology* **2016**, *15*, 5.
37. Chen, F.-M.; Lee, J.-H.; Yang, Y.-H.; Lin, Y.-T., et al. Analysis of α -lactalbumin-, β -lactoglobulin-, and casein-specific IgE among children with atopic diseases in a tertiary medical center in northern Taiwan, *Journal of Microbiology, Immunology and Infection* **2014**, *47*, 130-136, <http://dx.doi.org/10.1016/j.jmii.2012.08.009>.
38. Caubet, J.-C.; Wang, J. Current understanding of egg allergy, *Pediatric Clinics of North America* **2011**, *58*, 427-443, 10.1016/j.pcl.2011.02.014.
39. Tong, P.; Gao, J.; Chen, H.; Li, X., et al. Effect of heat treatment on the potential allergenicity and conformational structure of egg allergen ovotransferrin, *Food Chemistry* **2012**, *131*, 603-610, <http://dx.doi.org/10.1016/j.foodchem.2011.08.084>.
40. Jacobsen, B.; Hoffmann-Sommergruber, K.; Have, T.T.; Foss, N., et al. The panel of egg allergens, Gal d 1–Gal d 5: Their improved purification and characterization, *Mol. Nutr. Food Res.* **2008**, *52*, S176-S185, 10.1002/mnfr.200700414.
41. Chokshi, N.S., SH. . Molecular diagnosis of egg allergy: an update, *Expert Reviews of Molecular Diagnosis* **2015**, *15*, 895-906.
42. Mohamad Yadzir, Z.H.; Misnan, R.; Bakhtiar, F.; Abdullah, N., et al. Tropomyosin and Actin Identified as Major Allergens of the Carpet Clam (*Paphia textile*) and the Effect of Cooking on Their Allergenicity, *BioMed Research International* **2015**, *2015*, *6*, 10.1155/2015/254152.
43. WHO/IUIS. WHO/IUIS <http://www.allergen.org/viewallergen.php?aid=796>, 2017.
44. Chruszcz, M.; Maleki, S.J.; Majorek, K.A.; Demas, M., et al. Structural and Immunologic Characterization of Ara h 1, a Major Peanut Allergen, *The Journal of Biological Chemistry* **2011**, *286*, 39318-39327, 10.1074/jbc.M111.270132.
45. Keet, C.A.; Johnson, K.; Savage, J.H.; Hamilto, R.G., et al. Evaluation of Ara h2 IgE thresholds in the diagnosis of peanut allergy in a clinical population, *The Journal of Allergy and Clinical Immunology: In Practice* **2013**, *1*, 101-103, 10.1016/j.jaip.2012.08.007.
46. Jin, T.; Guo, F.; Chen, Y.-w.; Howard, A., et al. Crystal structure of Ara h 3, a major allergen in peanut, *Molecular Immunology* **2009**, *46*, 1796-1804, <http://dx.doi.org/10.1016/j.molimm.2009.01.023>.
47. Ratnaparkhe, M.B.; Lee, T.-H.; Tan, X.; Wang, X., et al. Comparative and Evolutionary Analysis of Major Peanut Allergen Gene Families, *Genome Biology and Evolution* **2014**, *6*, 2468-2488, 10.1093/gbe/evu189.

48. Blanc, F.; Bernard, H.; Ah-Leung, S.; Przybylski-Nicaise, L., et al. Further studies on the biological activity of hazelnut allergens, *Clinical and Translational Allergy* **2015**, *5*, 26, 10.1186/s13601-015-0066-7.
49. Alcocer, M.R.; Larsson, G. . Ber e 1 protein: the versatile major allergen from Brazil nut seeds *Biotechnology Letters* **2012**, *34*, 597-610.
50. Mattison, C.P.; Bren-Mattison, Y.; Vant-Hull, B.; Vargas, A.M., et al. Heat-induced alterations in cashew allergen solubility and IgE binding, *Toxicology Reports* **2016**, *3*, 244-251, <http://dx.doi.org/10.1016/j.toxrep.2015.12.009>.
51. Willison, L.N.; Zhang, Q.; Su, M.; Teuber, S.S., et al. Conformational epitope mapping of Pru du 6, a major allergen from almond nut, *Molecular Immunology* **2013**, *55*, 253-263, <http://dx.doi.org/10.1016/j.molimm.2013.02.004>.
52. Tsai, J.C., CY. Liao, EC. . Comparison of allergenicity at Gly m 4 and Gly m Bd 30K of Soybean after genetic modification, *Journal of Agricultural and Food Chemistry* **2017**, *65*, 1255-1262.
53. Wu, Y.-M.; Guan, R.-X.; Liu, Z.-X.; Li, R.-Z., et al. Synthesis and Degradation of the Major Allergens in Developing and Germinating Soybean Seed, *Journal of Integrative Plant Biology* **2012**, *54*, 4-14, 10.1111/j.1744-7909.2011.01092.x.
54. Radauer, C.; Nandy, A.; Ferreira, F.; Goodman, R.E., et al. Update of the WHO/IUIS Allergen Nomenclature Database based on analysis of allergen sequences, *Allergy* **2014**, *69*, 413-419, 10.1111/all.12348.
55. Pastorello, E.F., L. Pravettoni, V. Scibilia, J. Conti, A. Fortunato, D. Borgonovo, L. Banomi, S. Primavesi, L. Ballmer-Weber, B. Maize food allergy: lipid-transfer proteins, endochitinases, and alpha-zein precursor are relevant maize allergens in double-blind placebo-controlled maize-challengepositive patients, *Analytical and Bioanalytical Chemistry* **2009**, *395*, 93-102.
56. Palacin, A.; Quirce, S.; Armentia, A.; Fernández-Nieto, M., et al. Wheat lipid transfer protein is a major allergen associated with baker's asthma, *Journal of Allergy and Clinical Immunology* **2007**, *120*, 1132-1138, <https://doi.org/10.1016/j.jaci.2007.07.008>.
57. Weichel, M.; Vergoossen, N.J.; Bonomi, S.; Scibilia, J., et al. Screening the allergenic repertoires of wheat and maize with sera from double-blind, placebo-controlled food challenge positive patients, *Allergy* **2006**, *61*, 128-135, 10.1111/j.1398-9995.2006.00999.x.
58. Weichel, M.; Glaser, A.G.; Ballmer-Weber, B.K.; Schmid-Grendelmeier, P., et al. Wheat and maize thioredoxins: A novel cross-reactive cereal allergen family related to baker's asthma, *Journal of Allergy and Clinical Immunology* **2006**, *117*, 676-681, <https://doi.org/10.1016/j.jaci.2005.11.040>.
59. Spergel, J.M. Nonimmunoglobulin E-Mediated Immune Reactions to Foods, *Allergy, Asthma & Clinical Immunology* **2006**, *2*, 78, 10.1186/1710-1492-2-78.
60. EFSA. Scientific Opinion on the evaluation of allergenic foods and food ingredients for labeling purposes, *EFSA Journal* **2014**, *12*, 1-286.
61. Gomaa, A.R., S. Boye, J. Detection of allergens in a multiple allergen matrix and study of the impact of thermal processing *Journal of Nutrition & Food Sciences* **2012**, *9*, 1-6.

62. Garcia, E.M., L. Hermando, A. Kieffer, R. Wieser, H. Mendez, E. . Development of a general procedure for complete extraction of gliadins for heat processed and untreated foods, *European Journal of Gastroenterology & Hepatology* **2005**, *17*, 529-539.
63. Wieser, H. Chemistry of gluten proteins, *Food Microbiology* **2007**, *24*, 115-119, <https://doi.org/10.1016/j.fm.2006.07.004>.
64. Mena, M.C.; Lombardía, M.; Hernando, A.; Méndez, E., et al. Comprehensive analysis of gluten in processed foods using a new extraction method and a competitive ELISA based on the R5 antibody, *Talanta* **2012**, *91*, 33-40, <https://doi.org/10.1016/j.talanta.2011.12.073>.
65. Ito, K.; Yamamoto, T.; Oyama, Y.; Tsuruma, R., et al. Food allergen analysis for processed food using a novel extraction method to eliminate harmful reagents for both ELISA and lateral-flow tests, *Analytical and Bioanalytical Chemistry* **2016**, *408*, 5973-5984, 10.1007/s00216-016-9438-7.
66. Lasekan, A.; Nayak, B. Effects of buffer additives and thermal processing methods on the solubility of shrimp (*Penaeus monodon*) proteins and the immunoreactivity of its major allergen, 2016, p 146-153.
67. Waiblinger, H.S., G. Action Levels for Food Allergens: An Approach for Official Food Control in Germany *Journal of Agricultural and Food Chemistry* **2018 in press**, *101*, <https://doi.org/10.5740/jaoacint.17-0383>.
68. Walker, M.G., MH. Points, J. . Managing Food Allergens in the UK Retail Supply Chain, *Journal of AOAC International* **2018 in press**, *101*, <https://doi.org/10.5740/jaoacint.17-0385>.
69. Lacorn, M.; Immer, U. Allergen determination in food: reference materials and traceability of results, *Accreditation and Quality Assurance* **2011**, *16*, 449-452, 10.1007/s00769-011-0786-x.
70. Shoji, M.A., R. Akiyama, H. Japanese Food Allergen Labeling Regulator: An Update, *Journal of AOAC International* **2018 in press**, *101*.
71. Gendel, S.M. Comparison of international food allergen labeling regulations, *Regulatory Toxicology and Pharmacology* **2012**, *63*, 279-285, <http://dx.doi.org/10.1016/j.yrtph.2012.04.007>.
72. Popping, B.D.-A., C. European Regulations for Labeling Requirements for Food Allergens and Substances, *Journal of AOAC International* **2018 in press**, *101*, <https://doi.org/10.5740/jaoacint.17-0381>.
73. EC. Directive 2003/89/EC of the European Parliament and of the Council of 10 November 2003 Amending Directive 2000/13/EC as Regards Indication of the Ingredients Present in Foodstuffs, *Official Journal of the European Union* **2003**, *308*.
74. Sheth, S.S.; Wasserman, S.; Kagan, R.; Alizadehfar, R., et al. Role of food labels in accidental exposures in food-allergic individuals in Canada, *Annals of Allergy, Asthma & Immunology* **2010**, *104*, 60-65, 10.1016/j.anai.2009.11.008.
75. EC. 2011.
76. Khuda, S.E.; Sharma, G.M.; Gaines, D.; Do, A.B., et al. Survey of undeclared soy allergen levels in the most frequently recalled food categories with or without precautionary labeling, *Food Additives & Contaminants: Part A* **2016**, *33*, 1274-1282, 10.1080/19440049.2016.1207809.
77. Allen, K.J.; Turner, P.J.; Pawankar, R.; Taylor, S., et al. Precautionary labeling of foods for allergen content: are we ready for a global framework?, *The World Allergy Organization Journal* **2014**, *7*, 10-10, 10.1186/1939-4551-7-10.

78. Taylor, S.L.; Moneret-Vautrin, D.A.; Crevel, R.W.R.; Sheffield, D., et al. Threshold dose for peanut: Risk characterization based upon diagnostic oral challenge of a series of 286 peanut-allergic individuals, *Food and Chemical Toxicology* **2010**, *48*, 814-819, <http://dx.doi.org/10.1016/j.fct.2009.12.013>.
79. Yeung, J.R., MC. Challenges and Path Forward on Mandatory Allergen Labeling and Voluntary Precautionary Allergen Labeling for a Global Company, *Journal of AOAC International* **2018 in press**, *101*, <https://doi.org/10.5740/jaoacint.17-0391>.
80. Turner, P.J.; Kemp, A.S.; Campbell, D.E. Advisory food labels: consumers with allergies need more than “traces” of information, *BMJ* **2011**, *343*, 10.1136/bmj.d6180.
81. Barnett, J.; Leftwich, J.; Muncer, K.; Grimshaw, K., et al. How do peanut and nut-allergic consumers use information on the packaging to avoid allergens?, *Allergy* **2011**, *66*, 969-978, 10.1111/j.1398-9995.2011.02563.x.
82. Taylor, S.L.; Baumert, J.L.; Kruizinga, A.G.; Remington, B.C., et al. Establishment of Reference Doses for residues of allergenic foods: Report of the VITAL Expert Panel, *Food and Chemical Toxicology* **2014**, *63*, 9-17, <https://doi.org/10.1016/j.fct.2013.10.032>.
83. Baumert, J.L.; Crevel, R.W.R.; Mills, C.; Taylor, S.L. In *Risk Management for Food Allergy*; Academic Press: San Diego, 2014, pp 215-226.
84. Taylor, S.L.; Hefle, S.L.; Bindslev-jensen, C.; Atkins, F.M., et al. A consensus protocol for the determination of the threshold doses for allergenic foods: how much is too much?, *Clin. Exp. Allergy* **2004**, *34*, 689-695, 10.1111/j.1365-2222.2004.1886.x.
85. Koeberl, M.C., D. Allen, K.J. Fleming, F. Katzer, L. Lopata, AL. Said, M. Scheelings, P. Shepherd, N. Sherlock, R. Roberts, J. . Food Allergen Management in Australia, *Journal of AOAC International* **2018 in press**, *101*, <https://doi.org/10.5740/jaoacint.17-0386>.
86. Zurzolo, G.A.; Mathai, M.L.; Koplin, J.J.; Allen, K.J. Precautionary allergen labeling following new labeling practice in Australia, *J Paediatr Child Health* **2013**, *49*, E306-E310, 10.1111/jpc.12138.
87. Taylor, S.C., G. Grinter, K. Sherlock, R. Warren, L. . The Allergen Bureau VITAL Program *Journal of AOAC International* **2018 in press**, *101*, <https://doi.org/10.5740/jaoacint.17-0392>.
88. Bureau, A., Bureau, A., Ed.; Allergen Bureau Australia, 2011.
89. FDA. www.fda.gov, 2010.
90. Frewer, L.J.; Voordouw, J.; Schenk, M.F.; van Putten, M.C., et al. In *Multidisciplinary Approaches to Allergies*; Springer Berlin Heidelberg: Berlin, Heidelberg, 2012, pp 449-459.
91. EC. European Commission, 2017.
92. RASFF, RASFF Annual Report 2016; European Union Luxembourg, 2016.
93. Le, T.-M.; van Hoffen, E.; Kummeling, I.; Potts, J., et al. Food allergy in the Netherlands: differences in clinical severity, causative foods, sensitization and DBPCFC between community and outpatients, *Clinical and Translational Allergy* **2015**, *5*, 8, 10.1186/s13601-015-0051-1.
94. du Toit, G.; Tsakok, T.; Lack, S.; Lack, G. Prevention of food allergy, *Journal of Allergy and Clinical Immunology* **2016**, *137*, 998-1010, <http://dx.doi.org/10.1016/j.jaci.2016.02.005>.

95. Popping, B.A., L. Bourdichon, F. Brunner, K. Galan-Malo, P. Lacorn, M. North, J. Parisi, S. Rogers, A. Sealy-Voyksner, J. Yeung, J. . Stakeholder's Guidance Document for Consumer Analytical Devices with a Focus on Gluten and Food Allergens, *Journal of AOAC International* **2018 in press**, 101, <https://doi.org/10.5740/jaoacint.17-0425>.
96. Duncombe, T.A.; Tentori, A.M.; Herr, A.E. Microfluidics: reframing biological enquiry, *Nature Reviews Molecular Cell Biology* **2015**, 16, 554-567.
97. Eric A. E. Garber, C.H.P., Sara M. Handy, Chung Y. Cho, Rakhi Panda, Mansour Samadpour, Danica H. Reynaud, and George C. Ziobro Presence of Undeclared Food Allergens in Cumin: The Need for Multiplex Methods, *Journal of Agricultural and Food Chemistry* **2016**, 64, 1202-1211.
98. Valenta, R.; Hochwallner, H.; Linhart, B.; Pahr, S. Food Allergies: The Basics, *Gastroenterology* **2015**, 148, 1120-1131.e1124, 10.1053/j.gastro.2015.02.006.
99. Hofmann, C.; Scheurer, S.; Rost, K.; Graulich, E., et al. Cor a 1-reactive T cells and IgE are predominantly cross-reactive to Bet v 1 in patients with birch pollen-associated food allergy to hazelnut, *Journal of Allergy and Clinical Immunology* **2013**, 131, 1384-1392.e1386, <http://dx.doi.org/10.1016/j.jaci.2012.10.037>.
100. Leuvering, J.H.W.; Goverde, B.C.; Thal, P.J.H.M.; Schuurs, A.H.W.M. A homogeneous sol particle immunoassay for human chorionic gonadotrophin using monoclonal antibodies, *Journal of Immunological Methods* **1983**, 60, 9-23, [https://doi.org/10.1016/0022-1759\(83\)90330-7](https://doi.org/10.1016/0022-1759(83)90330-7).
101. Zeulab. LAB2GO - detection of allergens on work surfaces. 2013. Available at: <http://www.zeulab.com/products.html/allergens/180-lab2go-2.html> . Accessed 21Nov 2017
102. Wang, Y.D., R. Zhang, G. Li, Q. Yang, J. Li, Z. Hu, X. . Rapid and sensitive detection of the food allergen glycinin in powdered milk using a lateral flow colloidal gold immunoassay strip test., *Journal of Agricultural and Food Chemistry* **2015**, 63, 2172-2178.
103. Song, S.L., N. Zhao, Z. Ediage, EN. Wu, S. Sun, C. Saeger, SD. Wu, A. . Multiplex Lateral Flow Immunoassay for Mycotoxin Determination, *Analytical Chemistry* **2014**, 86, 4995-5001.
104. Fenton, E.M., MR. Lopez, GP. Sibbett, SS. . Multiplex lateral-flow test strips fabricated by two-dimensional shaping., *ACS Applied Materials & Interfaces* **2009**, 1, 124-129.
105. Zhang, X.Y., X. Wen, K. Li, Chenglong, L. Mari, GM. Jiang, H. Shi, W. Shen, J. Wang, Z. . Multiplex Lateral Flow Immunoassays Based on Amorphous Carbon Nanoparticles for Detecting Three *Fusarium* Mycotoxins in Maize, *Journal of Agricultural and Food Chemistry* **2017**, 65, 8063-8071.
106. Oncescu, V.; O'Dell, D.; Erickson, D. Smartphone based health accessory for colorimetric detection of biomarkers in sweat and saliva, *Lab on a Chip* **2013**, 13, 3232-3238, 10.1039/c3lc50431j.
107. Oncescu, V.M., M. Erickson, D. Cholesterol testing on a smartphone, *Lab on a Chip* **2014**, 14, 759-763.
108. You, D.P., TS. Yoon, JY. . Cell-phone-based measurement of TSH using Mie scatter optimised lateral flow assays *Biosensors and Bioelectronics* **2013**, 40, 180-185.
109. R-Biopharm. RIDA®SMART APP. 2015. Accessible at: <http://app.r-biopharm.com/> . Accessed 24 Jul 2017.
110. MobileAssay. Mobile diagnostics. 2017. Accessible at: <https://mobileassay.com/> . Accessed 2 Aug 2017.

111. Novarum. Novarum: mobile reader solutions. 2017. Available at: <https://www.novarumdx.com/>. Accessed 27 Jul 2017.
112. Hydrosense. Hydrosense Smartphone reader. 2017. Available at: <https://www.hydrosense-legionella.com/smartphone-reader/>. Accessed 27 Jul 2017.
113. OmegaDiagnostics. VISITECT CD4. Omega Diagnostics Group PLC. 2017. Available at: <http://www.omegadiagnostics.com/Products/Infectious-Diseases/HIV/CD4>. Accessed 2 Aug 2017.
114. Wang, X.; Young, O.A.; Karl, D.P. Evaluation of Cleaning Procedures for Allergen Control in a Food Industry Environment, *Journal of Food Science* **2010**, *75*, T149-T155, 10.1111/j.1750-3841.2010.01854.x.
115. Cox, K.D., V. Kriauciunas, A. Manetta, J. Montrose, C. Sittampalam, S. . *Assay Guidance Manual* Eli Lilly & Company and the National Center for Advancing Translational Sciences 2014.
116. Lacron, M.L., S. Siebeneicher, S. Weiss, T. Commercial ELISA Measurement of Allergens and Gluten: What We Can Learn From Case Studies, *Journal of AOAC International* **2018 in press**, *101*, <https://doi.org/10.5740/jaoacint.17-0399>.
117. Brandon Berg, B.C., Derek Tseng, Haydar Ozkan, Steve Feng, Qingshan Wei, Raymond Yan-Lok Chan, Jordi Burbano, Qamar Farooqui, Michael Lewinski, Dino Di Carlo, Omai B. Garner, and Aydogan Ozcan. Cellphone-based hand held microplate reader for point-of-care testing of enzyme-linked-immunosorbent assays, *Acs Nano* **2015**, *9*, 7857-7866.
118. Jang, H.; Ahmed, S.; Neethirajan, S. GryphSens: A Smartphone-Based Portable Diagnostic Reader for the Rapid Detection of Progesterone in Milk, *Sensors* **2017**, *17*, 1079.
119. Y Wang, M.M.A.Z., M Yang, R Sun, S Wang, J.N. Smith, C Timchalk, L Li, Y Lin, and D Du. A 3D-Printed, Portable, Optical-Sensing Platform for Smartphones Capable of detecting the Herbicide 2,4-Dichlorophenoxyacetic Acid, *Analytical Chemistry* **2017**, *89*, 9339-9346.
120. Fu, Q.; Wu, Z.; Li, X.; Yao, C., et al. Novel versatile smart phone based Microplate readers for on-site diagnoses, *Biosensors and Bioelectronics* **2016**, *81*, 524-531, <http://dx.doi.org/10.1016/j.bios.2016.03.049>.
121. China, 2016.
122. Coskun, A.F.; Wong, J.; Khodadadi, D.; Nagi, R., et al. A personalized food allergen testing platform on a cellphone, *Lab on a chip* **2013**, *13*, 636-640, 10.1039/c2lc41152k.
123. Kingsmore, S.F. Multiplexed protein measurement: technologies and applications of protein and antibody arrays, *Nature Reviews Drug discovery* **2006**, *5*, 310-320, 10.1038/nrd2006.
124. Santos, A.F.; Douiri, A.; Bécares, N.; Wu, S.-Y., et al. Basophil activation test discriminates between allergy and tolerance in peanut-sensitized children, *Journal of Allergy and Clinical Immunology* **2014**, *134*, 645-652, <http://dx.doi.org/10.1016/j.jaci.2014.04.039>.
125. Rebe Raz, S.; Haasnoot, W. Multiplex bioanalytical methods for food and environmental monitoring, *TrAC Trends in Analytical Chemistry* **2011**, *30*, 1526-1537, <https://doi.org/10.1016/j.trac.2011.04.016>.
126. Cho, C.Y.; Nowatzke, W.; Oliver, K.; Garber, E.A.E. Multiplex detection of food allergens and gluten, *Analytical and Bioanalytical Chemistry* **2015**, *407*, 4195-4206, 10.1007/s00216-015-8645-y.

127. Otto, G.; Lamote, A.; Deckers, E.; Dumont, V., et al. A flow-cytometry-based method for detecting simultaneously five allergens in a complex food matrix, *Journal of Food Science and Technology* **2016**, *53*, 4179-4186, 10.1007/s13197-016-2402-x.
128. Cho, C.Y.; Oles, C.; Nowatzke, W.; Oliver, K., et al. Cross-reactivity profiles of legumes and tree nuts using the xMAP® multiplex food allergen detection assay, *Analytical and Bioanalytical Chemistry* **2017**, 10.1007/s00216-017-0528-y.
129. Ateya, D.A.; Erickson, J.S.; Howell, P.B.; Hilliard, L.R., et al. The good, the bad, and the tiny: a review of microflow cytometry, *Analytical and Bioanalytical Chemistry* **2008**, *391*, 1485-1498, 10.1007/s00216-007-1827-5.
130. Seo, S.; Su, T.-W.; Erlinger, A.; Ozcan, A. Multi-color LUCAS: Lensfree On-chip Cytometry Using Tunable Monochromatic Illumination and Digital Noise Reduction, *Cellular and Molecular Bioengineering* **2008**, *1*, 146, 10.1007/s12195-008-0018-6.
131. Zhu, H.M., S. Coskun, AF. Yaglidere, O. Ozcan, A. . Optofluidic Fluorescent Imaging Cytometry on a Cell Phone, *Analytical Chemistry* **2011**, *83*, 6641-6647.
132. Zhu, H.; Ozcan, A. In *Mobile Health Technologies: Methods and Protocols*, Rasooly, A.; Herold, K. E., Eds.; Springer New York: New York, NY, 2015, pp 171-190.
133. Ludwig, S.K.J.; Zhu, H.; Phillips, S.; Shiledar, A., et al. Cellphone-based detection platform for rbST biomarker analysis in milk extracts using a microsphere fluorescence immunoassay, *Analytical and Bioanalytical Chemistry* **2014**, *406*, 6857-6866, 10.1007/s00216-014-7984-4.
134. Ludwig, S.K.J.; Tokarski, C.; Lang, S.N.; van Ginkel, L.A., et al. Calling Biomarkers in Milk Using a Protein Microarray on Your Smartphone, *PLOS ONE* **2015**, *10*, e0134360.
135. Preechaburana, P.; Suska, A.; Filippini, D. Biosensing with cell phones, *Trends in Biotechnology* **2014**, *32*, 351-355, 10.1016/j.tibtech.2014.03.007.
136. Schasfoort, R. *Handbook of Surface Plasmon Resonance* 2nd ed.; Royal Society of Chemistry London, 2017.
137. Zhao, S.S.; Bukar, N.; Toulouse, J.L.; Pelechacz, D., et al. Miniature multi-channel SPR instrument for methotrexate monitoring in clinical samples, *Biosensors and Bioelectronics* **2015**, *64*, 664-670, <http://dx.doi.org/10.1016/j.bios.2014.09.082>.
138. Raz, S.L., H. Norde, W. Bremer, MGEG. Food Allergen Profiling with an Image Plasmon Resonance-Based Biosensor *Analytical Chemistry* **2010**, *82*, 8485-8491.
139. Preechaburana, P.; Gonzalez, M.C.; Suska, A.; Filippini, D. Surface Plasmon Resonance Chemical Sensing on Cell Phones, *Angew. Chem. Int. Ed.* **2012**, *51*, 11585-11588, 10.1002/anie.201206804.
140. Liu, Y.L., Q. Chen, S. Cheng, F. Wang, H. Peng, W. . Surface Plasmon Resonance Biosensor Based on Smart Phone Platforms *Scientific Reports* **2015**, *5*, 1-9.
141. Daly, M.A., P. Haubl, G. Rogers, A. Brunner, K. . Assessing Almond and Peanut Allergens Using Commercially Available Immunoanalytical kits and LC-MS/MS: A Case Study *Journal of AOAC International* **2018 in press**, *101*, <https://doi.org/10.5740/jaoacint.17-0398>.
142. NIMA (2017) The science behind NIMA: understanding the device. Available at: <https://nimasensor.com/science-nima-understanding-device/> . Accessed 24 Jul 2017
143. Koning, F. Adverse Effects of Wheat Gluten, *Ann Nutr Metab* **2015**, *67*, 7-14.

144. Sapone, A.; Bai, J.C.; Ciacci, C.; Dolinsek, J., et al. Spectrum of gluten-related disorders: consensus on new nomenclature and classification, *BMC Medicine* **2012**, *10*, 13, 10.1186/1741-7015-10-13.
145. Ludvigsson, J.F.; Bai, J.C.; Biagi, F.; Card, T.R., et al. Diagnosis and management of adult coeliac disease: guidelines from the British Society of Gastroenterology, *Gut* **2014**, 10.1136/gutjnl-2013-306578.
146. Allred, L.K., C. Quinn, C. . The Use of Visual Examination for Determining the Presence of Gluten-Containing Grains in Gluten Free Oats and Other Grains, Seeds, Beans, Pulses and Legumes., *Journal of AOAC International* **2018 in press**, *101*, <https://doi.org/10.5740/jaoacint.170414>.
147. NIMA (2017) NIMA starter kit. Available at: <https://shop.nimasensor.com/products/nima-starter-kit> . Accessed 24 Jul 2017
148. AllergyAmulet (2017) Allergy Amulet. Available at: <http://www.allergyamulet.com/the-amulet> . Accessed 24 Jul 2017
149. Haupt, K.; Linares, A.V.; Bompart, M.; Bui, B.T.S. In *Molecular Imprinting*, Haupt, K., Ed.; Springer Berlin Heidelberg: Berlin, Heidelberg, 2012, pp 1-28.
150. Lin, H.H., CH. Park, J. Pathania, D. Castro, CM. Fasano, A. Weissleder, R. Lee, H. . Integrated Magneto-Chemical Sensor for On-Site Food Allergen Detection, *ACS Nano* **2017**, *11*, 10062-10069, 10.1021/acsnano.7b04318.

Supplementary information

Chapter 2

Table S2.1. Food allergens requiring labeling in different countries

	EU	Canada	USA	Australia	China	Hong Kong	Japan	Korea	Taiwan	Argentina	Thailand	Bolivia	Brazil	Chile	Colombia	Costa Rica	Cuba	Mexico	Nicaragua	South Africa	Venezuela	
Milk	X	X	X	X	X	X	X	X	X	X	X	X	X	X	X	X	X	X	X	X	X	X
Eggs	X	X	X	X	X	X	X	X	X	X	X	X	X	X	X	X	X	-	X	X	X	X
Cereal/Wheat	X	X	X	X	X	X	X	-	-	-	X	-	-	X	X	X	X	X	X	X	X	X
Peanut	X	X	X	X	X	X	X	X	X	X	X	X	X	X	X	X	X	X	X	X	X	X
Tree Nuts	X	X	X	X	X	X	-	-	X	X	X	X	X	X	X	X	X	X	X	X	X	X
Fish	X	X	X	X	-	X	-	-	X	X	X	X	X	X	X	X	X	X	X	X	X	X
Crustacean	X	X	X	X	X	X	X	X	X	X	X	X	X	X	X	X	X	X	X	X	X	X
Soy	X	X	X	X	X	X	-	-	X	X	X	X	X	X	X	X	X	X	X	X	X	X
Celery	X	-	-	-	-	-	-	-	-	-	-	-	-	-	-	-	-	-	-	-	-	-
Mustard	X	X	-	-	-	-	-	-	-	-	-	-	-	-	-	-	-	-	-	-	-	-
Lupin	X	-	-	-	-	-	-	-	-	-	-	-	-	-	-	-	-	-	-	-	-	-
Sesame	X	X	-	X	-	-	-	-	-	-	-	-	-	-	-	-	-	-	-	-	-	-
Sulphites	X	X	-	-	-	-	-	-	X	X	X	X	X	X	X	X	-	X	X	-	X	
Other	-	-	-	-	X	-	X	X	X	X	-	X	-	-	-	-	-	-	-	-	-	-

Table S2.2. Proof-of-concept multiplex allergen assays

Assay Format	Allergens Detected	Label Used	Extraction Buffer	LOD	Ref
iSPR	Peanut, hazelnut, soy, casein, egg, pine nut, macadamia nut, brazil nut, cashew, pistachio & pecan.	Label free	RIDASCREEN allergen extraction buffer (R-Biopharm AG)	0.4-4.6 mg/kg	1
Compact Immunoassay	Disc Gliadin, casein, B-lactoglobulin & ovalbumin	Gold nanoparticle amplified by silver enhancement method	40% ethanol in PBST (pH 7.5)	0.04-0.16 mg L ⁻¹	2
Reverse dot immunoassay	blot Peanut, hazelnut & brazil nut	Biotin	PBS with 0.1% (v/v) tween 20 & 4.0% (w/v) skimmed milk powder	0.01-0.02 mg/kg	3
Microfluidics based optical sensor	ELISA- Ara h1 & Gluten	Horseradish peroxidase	Extraction buffers provided in ELISA kits (Indoor Biotechnologies for Ara h1 and Crystal Chem for Gluten)	4.77-15.2 ng/mL	4
Sandwich assay optical biosensor	format Milk, egg, hazelnut, peanut, shellfish & sesame	Label Free	20mM TRIS pH 8.7, 150mM NaCl	1-12.5 µg/kg	5
Flow Cytometry	Casein, soy & gluten	Colored paramagnetic microbeads	super-2-ME in guanine HCl in PBS	Not Specified	6
Flow Cytometry	Crustacean, peanut, egg, milk & mustard	Colored paramagnetic microbeads	PBS (pH 7.5) NaCl (50mM), Na ₂ HPO ₄ (40mM), KH ₂ PO ₄ (5mM) & Na ₃ (1mM)	2-10 mg/kg	7
Flow Cytometry	Crustacean, egg, gluten, milk, peanut, soy, almond, brazil nut, cashew, coconut, hazelnut, macadamia, pine nut, pistachio & walnut	Colored paramagnetic microbeads	PBS-T (nondenatured) and 0.5% SDS/2% B-mercaptoethanol (denatured)	5 ng/mL	8

Flow Cytometry	Soy, pea & soluble proteins	wheat	Colored paramagnetic microbeads	super-carboxylated	20mL PBS (pH 7.4)	0.5-0.6 µg/mL	9
Optical thin film biosensors	Mustard, hazelnut, & sesame	lupine, walnut, hazelnut, celery, almond, oat	Label Free		CTAB extraction buffer (2% CTAB, 1.4 mol/l NaCl, 0.1 mol/l Tris/HCl, 20 mmol/l Na2EDTA pH 8.0)	0.001%	10
DNA Microarray	Hazelnut, peanut, oat, wheat, soybean	peanut & soybean	Label Free		CTAB extraction with 10µL RNase and 10µL proteinase K & column purification	1 µg/g (0.0001%)	11
Decaplex capillary electrophoresis	Hazelnut, oat, wheat, soybean	peanut, pistachio, cashew, barley, pecan	Label Free		Plant genomic DNA isolation kit; and 1.0% agarose gel for electrophoresis	0.005%	12
Tetraplex real-time PCR	Soy bean, mustard & brown	celery, white mustard	Fluorophore		CTAB extraction buffer 20 g/L, 1.4 mol/L sodium chloride, 0.1 mol/L TRIS, 0.02 mol/L Na2EDTA (99+%) pH 8.0 and 60µL proteinase K	2.6-36.8 mg/kg	13
Real-time PCR	Mustard, celery, brazil nut	wheat & rye	Fluorophore		CTAB extraction buffer & lysates centrifuged & purified with chloroform & isoamyl alcohol	5-40 mg/kg	14
Real-time PCR	Sesame, almond, citrus fruits	lupine & brazil nut	& Fluorophore		CTAB extraction precipitation step	with 10 mg/kg	15
Real-time PCR	Citrus Fruits		Fluorophore		Trizol to extract RNA. digested with DNase1. RNA reverse transcribed with random hexamers using Prime-Script first strand cDNA synthesis kit	DNA 20 fg per tube	16

Real-time PCR	Almonds, hazelnuts, cashews, peanuts & sesame seeds	Fluorophore; SYBR®GreenER™	CTAB extraction	0.5-5 pg of DNA	17
One step PCR	Brazil nut & pecan	Not stated	DNeasy plant mini kit column	0.1%	18
Multiplex dependent amplification (MLPA)	Sunflower seed, poppy seed, flaxseed, sesame & soy	Fluorophore	Wizard DNA clean-up system kit	10 mg/kg	19
Multiplex dependent amplification (MLPA)	Sesame, soy, hazelnut, peanut, lupine, gluten, mustard & celery	Fluorophore	DNeasy plant mini kit column	0.001%	20
Multiplex dependent amplification (MLPA)	Peanut, cashew, pecan, pistachio, hazelnut, sesame seeds, macadamia nut, almond, walnut & brazil nut	Fluorophore	CTAB extraction: 2% CTAB, 1.4 M NaCl, 20mm EDTA, 100mM TRIS-OH/HCl and 30µl proteinase K at 65oc overnight	5 mg/kg-1	21
Multiplex dependent amplification (MLPA)	Scallop, fish, gastropod, crustacean, cephalopod & bivalve	Fluorophore	CTAB: 2% CTAB, 1.4 M NaCl, 0.1 M TRIS & 20mm EDTA & proteinase K solution at 65 oc overnight	20-100 mg/kg-1	22
Giant magneto-resistant sensor array	Peanut (Ara h1 & Ara h2) gliadin	Streptavidin conjugated to magnetic microbeads and biotinylated detection antibody	N/A	0.2-7 ng/mL	23

Table S2.3 Commercially Available Food Allergen Assays

Allergenic Food	Product	Target	Assay Format	LOD/LOQ	Time (min)	Company
Cereals with Gluten	RIDASCREEN	Gluten	Sandwich ELISA	0.5mg/kg gliadin; 1.0mg/kg gluten	90	R-Biopharm AG
	RIDASCREEN FAST	Gliadin/gluten	Sandwich ELISA	0.5 mg/kg gliadin; 1.0 mg/kg gluten	30	R-Biopharm AG
	RIDASCREEN Competitive	Gluten	Competitive ELISA	2.3 mg/kg gliadin; 4.6 mg/kg gluten	40	R-Biopharm AG
	RIDAQUICK	Gluten	Lateral Flow Strip	1.3 µg/100cm ² gliadin on surfaces; 2.2 mg/kg gliadin; 3.1 mg/kg gluten	5	R-Biopharm AG
	Gliadin/Gluten ELISA	Gliadin/gluten/wheat/barley	Sandwich ELISA	0.3 mg/kg	60	Immunolab
	Gliadin ESGLISS-48	Gliadin	Sandwich ELISA	2.0-20 mg/kg	Not Stated	ELISA Systems
	VERATOX for Gliadin	Prolamins (wheat gliadin, rye secalin & barley hordein)	Sandwich ELISA	5 mg/kg	30	Neogen
	VERATOX R5	Prolamins (wheat gliadin, rye secalin & barley hordein) in finished food and clean in rinse	Sandwich ELISA	2.5 mg/kg	30	Neogen
	REVEAL 3-D for Gliadin	Gliadin	Lateral Flow Strip (with overflow line)	5 mg/kg; (10ppm gluten); 2 µg/100cm ² gliadin	5	Neogen
	REVEAL 3-D for Gluten	Gluten	Lateral Flow Strip (with overflow line)	5-10 mg/kg; 80 µg/100cm ² swab	5	Neogen
	ALERT for Gliadin	Gliadin/gluten	Sandwich ELISA	10mg/kg gliadin; 20mg/kg gluten	30	Neogen
	ALERT for Gliadin R5	Gliadin/gluten in processed foods/CIP/environmental surfaces	Sandwich ELISA	10 mg/kg gliadin; 20 mg/kg gluten	30	Neogen
	PROTEON for Gluten	Gliadin/gluten	Sandwich ELISA	LOD: 2.5 mg/kg LOQ: 8.9 mg/kg	90	Zeulab
	PROTEON EXPRESS for Gluten	Gliadin/gluten	Lateral Flow Strip	3 mg/kg	10	Zeulab
	EZ™ Gluten	Prolamins & Glutelins of wheat, rye, barley & related grains	Lateral Flow Strip	10 mg/kg	17	ELISA Technologies Inc.

ALLER-TEK™ ELISA	Gluten (Gliadin) ELISA Kit	Prolamins & Glutelins of wheat, rye, barley & related grains	Sandwich ELISA	5 mg/kg	160	ELISA Technologies Inc.
		Gluten, Wheat	Sandwich ELISA	0.26 mg/kg gluten; 0.31 mg/kg wheat	Not Stated	Crystal Chem
		Gluten (Gliadin)	Lateral Flow Strip	5 mg/kg wheat; 4 mg/kg gluten	15	Crystal Chem
		Gluten	Lateral Flow Strip	4 mg/kg	11	Romer Labs
		Gluten	Sandwich ELISA	2 mg/kg	60	Romer Labs
		Gluten	Lateral Flow Strip	3 mg/kg	11	Romer Labs
		Gluten	Sandwich ELISA	0.6 mg/kg	60	Romer Labs
		Gluten/Gliadin	Sandwich ELISA	LOD: Gluten; 0.3mg/kg; Gliadin: 0.15 mg/kg LOQ: Gluten: 2 mg/kg; Gliadin: 1 mg/kg	40	BioFront Technologies
		Gluten	Lateral Flow Strip	5 mg/kg	<20	Biomedal Diagnostics
		Gluten (wheat, barley, rye and OAT)	Lateral Flow Strip	5 mg/kg	<20	Biomedal Diagnostics
		Gluten (G12 antibody)	Lateral Flow Strip	3 mg/kg	<20	Biomedal Diagnostics
		Gluten	Sandwich ELISA	0.6 mg/kg	150	Biomedal Diagnostics
		Gluten (in hydrolysed foods)	Competitive ELISA	3 mg/kg	90	Biomedal Diagnostics
		Gluten	Competitive ELISA	3.6 mg/kg	30	EuroProxima
Soybeans	RIDASCREEN FAST	Soy protein	Sandwich ELISA	0.24 mg/kg	30	R-Biopharm AG
		Soya on Surfaces	Lateral Flow Strip	0.5 µg soya protein/100cm ²	16	R-Biopharm AG
		Soy in processed foods, drinks and CIP	Sandwich ELISA	2.5 mg/kg	30	Neogen
		Soy	Lateral Flow Strip (with overflow line)	5 mg/kg; 2 µg/100cm ² swab	5	Neogen
		Soy	Sandwich ELISA	2.5 mg/kg	30	Neogen

Soy ESSOYPRD-48	Soy Flour Protein	Sandwich ELISA	2.5-25 mg/kg	80	ELISA Systems
Soy ELISA Kit	Soy in raw & processed foods	Sandwich ELISA	0.31 mg/kg	<120	Crystal Chem
AgraQuant® Soy	Soy	Sandwich ELISA	0.016 mg/kg	60	Romer Labs
Monotracer Soy ELISA	Soy	Sandwich ELISA	LOD: 0.23 mg/kg LOQ: 1 mg/kg	40	BioFront Technologies
Soja (Soy) ELISA	Soja trypsin inhibitor	Sandwich ELISA	0.016 mg/kg	60	Immunolab
AlerTox Soy (STI)	Soja trypsin inhibitor	Sandwich ELISA	LOD: 0.016 mg/kg LOQ: 0.05 mg/kg	Not stated	Biomedal Diagnostics
AlerTox Soy	Soy	Lateral Flow Strip	1 mg/kg	10	Biomedal Diagnostics
PROTEON for Soy	Soy	Sandwich ELISA	LOD: 1.1 mg/kg LOQ: 3.5 mg/kg	90	Zeulab
	Soy	Sandwich ELISA	LOD: <0.7 mg/kg LOQ: 2 mg/kg	100	BioCheck (UK) Ltd
Soya Check					
Milk	RIDASCREEN Fast Milk	Casein & B-lactoglobulin	0.7 mg/kg	30	R-Biopharm AG
	RIDASCREEN Fast Casein/caseinates Casein	Sandwich ELISA	0.12 mg/kg casein in ice-cream/chocolate/ beverages; 0.71 mg/kg casein for all other samples	30	R-Biopharm AG
	VERATOX for Casein	Sandwich ELISA	2.5 mg/kg	30	Neogen
	Casein ESCASPRD-48	Sandwich ELISA	1.0-10 mg/kg	45	ELISA Systems
	AgraQuant® Casein	Sandwich ELISA	0.04 mg/kg	60	Romer Labs
	Monotracer Milk ELISA	Sandwich ELISA	LOD: 0.12 mg/kg LOQ: 1 mg/kg	40	BioFront Technologies
	Casein ELISA Kit	Sandwich ELISA	0.31 mg/kg	Not stated	Crystal Chem
	Casein Lateral Flow Kit	Lateral Flow Strip	5 mg/kg	15	Crystal Chem
	BioKits RAPID 3D™ Casein Test	Lateral Flow Strip (with overflow line)	Screening test (no LOD)	5	Tepnel Reserach Products & Services
	AgraStrip® Casein	Lateral Flow Strip	2 mg/kg casein; 5 mg/kg skimmed milk powder	11	Romer Labs
	Casein ELISA	Sandwich ELISA	0.04 mg/kg	60	Immunolab

AlerTox Casein ELISA	Casein	Sandwich ELISA	LOD: 0.05 mg/kg LOQ: 0.20 mg/kg	Not stated	Biomedal Diagnostics
AlerTox Sticks Casein	Casein	Lateral Flow Strip	2.5 mg/kg	10	Biomedal Diagnostics
Casein ELISA Kit	Casein	Sandwich ELISA	0.31 mg/kg	Not stated	Crystal Chem
Milk-Check (Casein)	Casein	Sandwich ELISA	LOD: 0.2 mg/kg; LOQ: 0.8 mg/kg	100	BioCheck (UK) Ltd
RIDASCREEN B-lactoglobulin	Fast B-lactoglobulin	Sandwich ELISA	0.19 mg/kg	30	R-Biopharm AG
R I D A S C R E E N B-lactoglobulin	B-lactoglobulin in hydrolysed products	Competitive ELISA	0.1 mg/kg	165	R-Biopharm AG
Beta Lactoglobulin ESMDRLG-48	B-lactoglobulin	Sandwich ELISA	0.1-1.0 mg/kg	45	ELISA Systems
Beta-Lactoglobulin ELISA Kit	B-lactoglobulin	Sandwich ELISA	0.31 mg/kg	Not Stated	Crystal Chem
BioKits BLG Assay Kit	B-lactoglobulin	Sandwich ELISA	2 mg/kg	120	Neogen
A g r a Q u a n t B-lactoglobulin	B-lactoglobulin	Sandwich ELISA	0.0015 mg/kg	60	Romer Labs
Beta-Lactoglobulin ELISA	B-lactoglobulin	Sandwich ELISA	0.0015 mg/kg	60	Immunolab
AlerTox BLG ELISA	B-lactoglobulin	Sandwich ELISA	LOD: 0.0015 mg/kg LOQ: 0.010 mg/kg	Not stated	Biomedal Diagnostics
AlerTox Sticks BLG	B-lactoglobulin	Lateral Flow Strips	2.5 mg/kg	10	Biomedal Diagnostics
Milk-Check (BLG)	B-lactoglobulin	Sandwich ELISA	LOD: <0.1 mg/kg LOQ: 0.2 mg/kg	100	BioCheck (UK) Ltd
PROTEON Milk ELISA	B-lactoglobulin	Sandwich ELISA	LOD: 0.03 mg/kg LOQ: 0.05 mg/kg	90	Zeulab
PROTEON EXPRESS for Milk	Milk	Lateral Flow Strip	1-2 mg/kg	10	Zeulab
Bioavid Lateral Flow Milk	Milk	Lateral Flow Strip	1 mg/kg	8	R-Biopharm AG
Milk Check	Milk	Sandwich ELISA	LOD: <0.1 mg/kg LOQ: 1 mg/kg	100	BioCheck (UK) Ltd
VERATOX for Total Milk	Casein & Whey	Sandwich ELISA	2.5 mg/kg	30	Neogen
REVEAL for Total Milk	Casein & Whey	Lateral Flow Strip	5 mg/kg	5	Neogen

REVEAL 3-D for Total Milk	Casein & Whey	Lateral Flow Strip (with overflow line)	5 mg/kg	5	Neogen
ALERT for Total Milk Allergen	Total Milk	Sandwich ELISA	5 mg/kg	30	Neogen
Milk ELISA	Milk	Sandwich ELISA	0.005 mg/kg	60	Immunolab
AlerTox Milk ELISA	Milk	Sandwich ELISA	LOD: 0.05 mg/kg LOQ: 0.5 mg/kg	Not stated	Biomedal Diagnostics
Total Milk ESTMLK-48	Casein & Whey	Sandwich ELISA	0.25-2.5 mg/kg	45	ELISA Systems
Egg	FAST Whole Egg Protein	Sandwich ELISA	0.1 mg/kg whole egg powder; 0.03 mg/kg egg white protein	30	R-Biopharm AG
RIDASCREEN FAST Lysozym	FAST Lysozyme	Sandwich ELISA	0.006 mg/kg lysozyme in wine; 0.016 mg/kg lysozyme in cheese + sausage	30	R-Biopharm AG
Lysozyme ELISA	Lysozyme	Sandwich ELISA	0.002 mg/kg	60	Immunolab
AlexTox ELISA	Lysozyme	Sandwich ELISA	LOD: 0.002 mg/kg LOQ: 0.025 mg/kg	Not stated	Biomedal Diagnostics
VERATOX for Egg	Egg	Sandwich ELISA	2.5 mg/kg	30	Neogen
REVEAL 3-D for Egg	Egg	Lateral Flow Strip (with overflow line)	5 mg/kg; 10 µg/100 cm ² egg swab	5	Neogen
AlerTox Egg ELISA	Egg	Sandwich ELISA	LOD: 0.05 mg/kg LOQ: 0.4 mg/kg	Not stated	Biomedal Diagnostics
AlerTox Sticks Egg	Egg	Lateral Flow Strip	1 mg/kg	10	Biomedal Diagnostics
PROTEON Egg ELISA	Egg	Sandwich ELISA	LOD: 0.05 mg/kg LOQ: 0.18 mg/kg	90	Zeulab
PROTEON EXPRESS for Egg	Egg	Lateral Flow Strip	1 mg/kg	10	Zeulab
Egg Check	Egg	Sandwich ELISA	LOD: <0.2 mg/kg; LOQ: 0.4 mg/kg	100	BioCheck (UK) Ltd
BioKits RAPID Egg Test	3D TM Ovomuroid (Gal d 1)	Lateral Flow Strip (with overflow line)	7.6 mg/kg egg white protein; 0.5 mg/kg whole egg powder; 5 µg/25cm ² whole egg powder environmental swab	5	TepeIn Reserach Products & Services
Enhanced Residue Kit	Egg Ovomuroid	Sandwich ELISA	1.0-10 mg/kg	Not Stated	ELISA Systems

	Monotracer Egg ELISA	Ovomucoid	Sandwich ELISA	LOD: 0.3 mg/kg LOQ: 1 mg/kg	40	BioFront Technologies
	Egg (Ovalbumin) ELISA Kit	Ovalbumin	Sandwich ELISA	0.31 mg/kg	Not stated	Crystal Chem
	Egg (Ovalbumin) Lateral Flow Kit	Ovalbumin	Lateral Flow Strip	5 mg/kg	15	Crystal Chem
	BioKits Egg Assay Kit	Ovalbumin	Sandwich ELISA	0.1 mg/kg	75	Neogen
	Ovalbumin ELISA	Ovalbumin	Sandwich ELISA	0.004 mg/kg	60	Immunolab
	AlerTox ELISA	Ovalbumin	Sandwich ELISA	LOD: 0.004 mg/kg LOQ: 0.025 mg/kg	Not stated	Biomedical Diagnostics
	Egg White ELISA	Egg White	Sandwich ELISA	0.05 mg/kg	60	Immunolab
	AgraQuant® White	Egg White	Sandwich ELISA	0.05 mg/kg	60	Romer Labs
	AgraStrip® Egg	Egg (Dried Whole Egg)	Lateral Flow Strip	2 mg/kg	11	Romer Labs
Nuts	RIDASCREEN Mandel/Almond	FAST Almond	Sandwich ELISA	1.2 mg/kg	30	R-Biopharm AG
	Bioavid Lateral Flow Almond	Almond	Lateral Flow Strip	1 mg/kg	10	R-Biopharm AG
	VERATOX for Almond	Almond	Sandwich ELISA	LOD: 0.3 mg/kg LOQ: 2.5 mg/kg	30	Neogen
	REVEAL Almond	3-D for Almond	Lateral Flow Strip (with overflow line)	5 mg/kg almond; 1 µg/100cm ³ protein	5	Neogen
	Almonds ESARD-48	Almond	Sandwich ELISA	0.5-5 mg/kg	50	ELISA Systems
	AgraQuant® Almond	Almond	Sandwich ELISA	0.2 mg/kg	60	Romer Labs
	AgraStrip® Almond	Almond	Lateral Flow Strip	2 mg/kg	11	Romer Labs
	Almond ELISA	Almond	Sandwich ELISA	0.2 mg/kg	60	Immunolab
	Monotracer ELISA	Almond	Sandwich ELISA	LOD: 0.15 mg/kg LOQ: 1 mg/kg	40	BioFront Technologies
	AlerTox Almond ELISA	Almond	Sandwich ELISA	LOD: 0.2 mg/kg LOQ: 0.5 mg/kg	Not stated	Biomedical Diagnostics
	AlerTox Sticks Almond	Almond	Lateral Flow Strip	10 mg/kg	10	Biomedical Diagnostics
	Almond Check	Almond	Sandwich ELISA	LOD: <0.25 mg/kg LOQ: 0.5 mg/kg	100	BioCheck (UK) Ltd

Bioavid Lateral Flow Brazil Nut Brazil Nut	Lateral Flow Strip	1 mg/kg	10	R-Biopharm AG
AgraStrip® Brazil Nut	Lateral Flow Strip	5 mg/kg	11	Romer Labs
Brazil nut ELISA	Sandwich ELISA	0.2 mg/kg	60	Immunolab
Monotrace Brazil Nut ELISA	Sandwich ELISA	LOD: 0.14 mg/kg LOQ: 1 mg/kg	40	BioFront Technologies
RIDASCREEN FAST Cashew	Sandwich ELISA	0.09 mg/kg	30	R-Biopharm AG
Bioavid Lateral Flow Cashew Kernel Cashew Kernel	Lateral Flow Strip	1 mg/kg	10	R-Biopharm AG
Cashew ELISA	Sandwich ELISA	0.2 mg/kg	60	Immunolab
Monotrace Cashew ELISA	Sandwich ELISA	LOD: 0.12 mg/kg LOQ: 1 mg/kg	40	BioFront Technologies
AlerTox Cashew ELISA	Sandwich ELISA	LOD: 0.2 mg/kg LOD: 2 mg/kg	Not stated	Biomedal Diagnostics
Cashew Check	Sandwich ELISA	LOD: <0.2 mg/kg; LOQ: 2 mg/kg	100	BioCheck (UK) Ltd
Bioavid Lateral Flow Coconut	Lateral Flow Strip	1 mg/kg	10	R-Biopharm AG
Coconut ELISA	Sandwich ELISA	0.4 mg/kg	60	Immunolab
Monotrace Coconut ELISA	Sandwich ELISA	0.13 mg/kg	40	BioFront Technologies
AletTox Coconut	Sandwich ELISA	LOD: 0.4 mg/kg LOQ: 2 mg/kg	Not stated	Biomedal Diagnostics
RIDASCREEN FAST Hazelnut	Sandwich ELISA	1.5 mg/kg	30	R-Biopharm AG
Bioavid Lateral Flow Hazelnut	Lateral Flow Strip	1 mg/kg	10	R-Biopharm AG
VERATOX for Hazelnut	Sandwich ELISA	2.5 mg/kg	30	Neogen
REVEAL 3-D for Hazelnut	Lateral Flow Strip (with overflow line)	5-10 mg/kg; 10 µg/100cm2 swab	5	Neogen
Hazelnut ESHRD-48	Sandwich ELISA	0.5-5 mg/kg	35	ELISA Systems

AgraQuant® Hazelnut	Hazelnut	Hazelnut	Sandwich ELISA	0.3 mg/kg	60	Romer Labs
AgraStrip® Hazelnut	Hazelnut	Hazelnut	Lateral Flow Strip	5 mg/kg	11	Romer Labs
Hazelnut ELISA	Hazelnut	Hazelnut	Sandwich ELISA	0.3 mg/kg	60	Immunolab
Monotrace ELISA	Hazelnut	Hazelnut	Sandwich ELISA	0.04 mg/kg	40	BioFront Technologies
AlerTox ELISA	Hazelnut	Hazelnut	Sandwich ELISA	LOD:0.3 mg/kg; LOQ: 1 mg/kg	Not stated	Biomedal Diagnostics
AleTox Sticks	Hazelnut	Hazelnut	Lateral Flow Strip	1 mg/kg	10	Biomedal Diagnostics
Hazelnut Check	Hazelnut	Hazelnut	Sandwich ELISA	LOD:<0.5 mg/kg LOQ: 1 mg/kg	100	BioCheck (UK) Ltd
RIDASCREEN Macademia	FAST Macademia	Macademia	Sandwich ELISA	0.38 mg/kg	30	R-Biopharm AG
Biovid Macademia Nut	Lateral Flow Macademia	Macademia	Lateral Flow Strip	1 mg/kg	10	R-Biopharm AG
AgraStrip® Macademia Nut	Macademia Nut	Macademia Nut	Lateral Flow Strip	2 mg/kg	11	Romer Labs
Macademia Nut ELISA	Macademia Nut	Macademia Nut	Sandwich ELISA	0.1 mg/kg	60	Immunolab
Monotrace Macademia Nut ELISA	Macademia Nut	Macademia Nut	Sandwich ELISA	0.13 mg/kg	40	BioFront Technologies
AlerTox ELISA	Macademia Nut	Macademia Nut	Sandwich ELISA	LOD: 0.1 mg/kg LOQ: 1 mg/kg	Not stated	Biomedal Diagnostics
RIDASCREEN Peanut	FAST Peanut	Peanut	Sandwich ELISA	1.3 mg/kg	30	R-Biopharm AG
Biovid Peanut	Lateral Flow Peanut	Peanut	Lateral Flow Strip	≤1 mg/kg	10	R-Biopharm AG
VERATOX for Peanut	Peanut	Peanut	Sandwich ELISA	2.5 mg/kg	30	Neogen
REVEAL for Peanut	Peanut	Peanut	Lateral Flow Strip	5 mg/kg	10	Neogen
REVEAL 3-D for Peanut	Peanut	Peanut	Lateral Flow Strip (with overflow line)	5 mg/kg; 1 µg/100cm2 swab	5	Neogen
Peanut ESPRDT-48	Peanut (Ara h1 & Ara h2)	Peanut	Sandwich ELISA	1-15 mg/kg	35	ELISA Systems
Peanut Lateral Flow Kit	Peanut	Peanut	Lateral Flow Strip	5 mg/kg	15	Crystal Chem

Peanut ELISA Kit	Peanut	Sandwich ELISA	0.31 mg/kg	Not Stated	Crystal Chem
BioKits Peanut Assay Kit	Peanut	Sandwich ELISA	0.1 mg/kg	75	Neogen
ALERT for Peanut	Peanut	Sandwich ELISA	5 mg/kg	30	Neogen
AgraQuant® Peanut	Peanut	Sandwich ELISA	0.1 mg/kg	60	Romer Labs
AgraStrip® Peanut	Peanut	Lateral Flow Strip	1 mg/kg	11	Romer Labs
Peanut ELISA	Peanut	Sandwich ELISA	0.1 mg/kg	60	Immunolab
Monotrace Peanut ELISA	Peanut	Sandwich ELISA	LOD: 0.24 mg/kg LOQ: 1 mg/kg	40	BioFront Technologies
AlerTox Peanut ELISA	Peanut	Sandwich ELISA	LOD: 0.3 mg/kg LOQ: 1 mg/kg	Not stated	Biomedal Diagnostics
AleTox Sticks Peanut	Peanut	Lateral Flow Strip	1 mg/kg	10	Biomedal Diagnostics
Peanut Check	Peanut	Sandwich ELISA	LOD: <0.5 mg/kg LOQ: 1 mg/kg	100	BioCheck (UK) Ltd
Pistachio Check	Pistachio	Sandwich ELISA	LOD: <0.2 mg/kg LOQ: 1 mg/kg	100	BioCheck (UK) Ltd
Pistachio ELISA	Pistachio	Sandwich ELISA	0.13 mg/kg	60	Immunolab
Bioavid Lateral Flow Pistachio	Pistachio	Lateral Flow Strip	1 mg/kg	10	R-Biopharm AG
Monotrace Pistachio ELISA	Pistachio	Sandwich ELISA	LOD: 0.12 mg/kg LOQ: 1 mg/kg	40	BioFront Technologies
AlerTox ELISA	Pistachio	Sandwich ELISA	LOD: 0.13 mg/kg LOQ: 1 mg/kg	Not stated	Biomedal Diagnostics
AgraStrip® Pistachio	Cashew/Pistachio	Lateral Flow Strip	5 mg/kg	11	Romer Labs
Monotrace Pine Nut ELISA	Pine Nut	Sandwich ELISA	LOD: 0.24 mg/kg LOQ: 1 mg/kg	40	BioFront Technologies
Monotrace Pecan ELISA	Pecan	Sandwich ELISA	LOD: 0.17 mg/kg; LOQ: 1 mg/kg	40	BioFront Technologies
Pecan nut ELISA	Pecan	Sandwich ELISA	0.2 mg/kg	60	Immunolab
Bioavid Lateral Flow Walnut & Pecan Walnut	Walnut & Pecan	Lateral Flow Strip	10 mg/kg	10	R-Biopharm AG

	BioKits Walnut Assay	Walnut	Walnut	Sandwich ELISA	0.25 mg/kg	75	Neogen
	AgraQuant® Walnut	Walnut	Walnut	Sandwich ELISA	0.35 mg/kg	60	Romer Labs
	AgraStrip® Walnut	Walnut	Walnut	Lateral Flow Strip	10 mg/kg	11	Romer Labs
	Walnut ELISA	Walnut	Walnut	Sandwich ELISA	0.35 mg/kg	60	Immunolab
	Monotrace ELISA	Walnut	Walnut	Sandwich ELISA	LOD:0.22 mg/kg LOQ: 1 mg/kg	Not stated	BioFront Technologies
	AlerTox Walnut ELISA	Walnut	Walnut	Sandwich ELISA	LOD: 0.6 mg/kg LOQ: 2 mg/kg	Not stated	Biomedical Diagnostics
	Walnut Check	Walnut	Walnut	Sandwich ELISA	LOD: <1.0 mg/kg LOQ: 2 mg/kg	100	BioCheck (UK) Ltd
	REVEAL Treenut	Multi- Almond, cashew, hazelnut, walnut, pecan & pistachio	Walnut	Lateral Flow Strip	Rinse samples: 5-10 mg/kg; CIP swabs: 20 µg/100cm ²	10	Neogen
Oil Plants	RIDASCREEN Sesame	FAST Sesame	Sesame	Sandwich ELISA	0.2 mg/kg	30	R-Biopharm AG
	Bioavid Sesame	Lateral Flow Sesame	Sesame	Lateral Flow Strip	1 mg/kg	10	R-Biopharm AG
	REVEAL Sesame	3-D for Sesame	Sesame	Lateral Flow Strip (with overflow line)	5 mg/kg	5	Neogen
	Sesame ESSESRD-48	Sesame	Sesame	Sandwich ELISA	0.5-5 mg/kg	65	ELISA Systems
	BioKits Sesame Kit	Sesame Assay	Sesame	Sandwich ELISA	1 mg/kg	180	Neogen
	AgraQuant® Sesame	Sesame	Sesame	Sandwich ELISA	0.2 mg/kg	60	Romer Labs
	AgraStrip® Sesame	Sesame	Sesame	Lateral Flow Strip	5 mg/kg	11	Romer Labs
	Sesame ELISA	Sesame	Sesame	Sandwich ELISA	0.2 mg/kg	60	Immunolab
	Monotrace ELISA	Sesame	Sesame	Sandwich ELISA	0.3 mg/kg	40	BioFront Technologies
	AleTox Sesame	Sesame ELISA	Sesame	Sandwich ELISA	LOD: 0.2 mg/kg LOQ: 2 mg/kg	Not stated	Biomedical Diagnostics
	Sesame Check	Sesame	Sesame	Sandwich ELISA	LOD: <0.2 mg/kg LOQ: 2 mg/kg	100	BioCheck (UK) Ltd
Seafood	RIDASCREEN Crustacean	FAST Tropomyosin	Sesame	Sandwich ELISA	2 mg/kg	30	R-Biopharm AG

Bioavid Lateral Flow Crustacean	Tropomyosin	Lateral Flow Strip	10 mg/kg	10	R-Biopharm AG
VERATOX for Crustacea	Tropomyosin	Sandwich ELISA	2.5 mg/kg	30	Neogen
REVEAL 3-D Crustacea	Tropomyosin	Lateral Flow Strip (with overflow line)	5-10 mg/kg; 40 µg/100cm ² cooked prawn extract	5	Neogen
Crustacea ESCRURD-48	Tropomyosin	Sandwich ELISA	0.05-0.50 mg/kg	60	ELISA Systems
AgraQuant® Crustacea	Tropomyosin	Sandwich ELISA	0.09 mg/kg	60	Romer Labs
Crustacean ELISA	Tropomyosin	Sandwich ELISA	Soy sauce: 0.0017 mg/kg; vegetable soup: 0.0036 mg/kg; bakery products: 0.0009 mg/kg; fish: 0.0085 mg/kg; meat: 0.0103 mg/kg	60	Immunolab
Monotracer ELISA	Crustacea	Sandwich ELISA	LOD: 0.07 mg/kg LOQ: 1 mg/kg	40	BioFront Technologies
AlerTox ELISA	Crustacean	Sandwich ELISA	LOD: 0.001 mg/kg LOQ: 0.020 mg/kg	Not stated	Biomedal Diagnostics
AlerTox Crustacea	Sticks	Lateral Flow Strips	7 mg/kg (dry) 33 mg/kg (wet)	10	Biomedal Diagnostics
Crustacea-Check	Tropomyosin	Sandwich ELISA	LOD: 0.1 mg/kg LOQ: 1.2 mg/kg	100	BioCheck (UK) Ltd
Fish Check	Fish	Sandwich ELISA	LOD: <1.0 mg/kg LOQ: 5 mg/kg	100	BioCheck (UK) Ltd
AlerTox Sticks Fish	Fish	Lateral Flow Strips	0.35 mg/kg (dry) 1 mg/kg (wet)	10	Biomedal Diagnostics
AlerTox Fish ELISA	Fish	Sandwich ELISA	LOD: 1.4 mg/kg LOQ 4 mg/kg	Not stated	Biomedal Diagnostics
Fish ELISA	Fish	Sandwich ELISA	1.4 mg/kg	60	Immunolab
Miscellaneous Lupine RIDASCREEN FAST	Lupin	Sandwich ELISA	0.7 mg/kg	30	R-Biopharm AG
VERATOX for Lupine	Lupin	Sandwich ELISA	2.5 mg/kg	30	Neogen
Lupin ESLFP-48	Lupin Flour Protein	Sandwich ELISA	0.5-5 mg/kg	Not Stated	ELISA Systems
AgraQuant® Lupin	Lupin	Sandwich ELISA	0.2 mg/kg	60	Romer Labs

Lupine ELISA	Lupin	Sausage: 0.2 mg/kg; bread: 0.3 mg/kg; 60 orange juice: 0.7 mg/kg; ketchup: 0.1 mg/kg; croquette: 0.2 mg/kg	Immunolab
Monotrace ELISA	Lupin	LOD: 0.16 mg/kg LOQ: 1 mg/kg	BioFront Technologies
AlerTox Lupine ELISA	Lupin	LOD: 0.2 mg/kg LOD: 2 mg/kg	Not stated
Lupin Check	Lupin	LOD: <0.3 mg/kg LOQ: 2 mg/kg	BioCheck (UK) Ltd
RIDASCREEN Mustard	Mustard (white, yellow, brown & black)	0.22 mg/kg	R-Biopharm AG
Bioavid Lateral Mustard	Mustard	1 mg/kg	R-Biopharm AG
VERATOX for Mustard	Mustard	2.5-25 mg/kg	Neogen
REVEAL Mustard	Mustard	Lateral Flow Strip (with overflow line)	Neogen
Mustard ESMUS-48	Mustard	1-10 mg/kg	Not Stated
AgraQuant® Mustard	Mustard	1 mg/kg	Romer Labs
AgraStrip® Mustard	Mustard	2 mg/kg	Romer Labs
Mustard ELISA	Mustard	1 mg/kg	Immunolab
Monotrace ELISA	Mustard	LOD: 0.13 mg/kg LOQ: 1 mg/kg	BioFront Technologies
AlerTox Mustard ELISA	Mustard	LOD: 1 mg/kg LOQ: 2 mg/kg	Not stated
Mustard Check	Mustard	LOD: <1 mg/kg LOQ: 2 mg/kg	BioCheck (UK) Ltd

Table S2.4. Conventionally lab-based allergen detection methods and their smartphone-based counterparts

Conventional Method	Current Method	Summary
ELISA with microplate reader as detector system	ELISA with smartphone-based microplate reader as detector system	ELISA is a traditionally laboratory based routine allergen detection method, as it requires multiple reagent handling steps, sample extraction and detection from a UV-VIS microplate spectrophotometer. Microplate readers are expensive and non-portable, however using a smartphone as the microplate reader (see section 3.2.1) for detecting the colorimetric reaction makes the method more portable and accessible in low-resource settings.
Lateral flow immunoassay (LFIA) with strip reader	LFIA with smartphone reader	LFIA is a rapid, portable, easy to use, safe and disposable screening method applied in food allergen analysis. LFIA qualitative optical detection is based on the appearance of 1 or 2 lines for absence/presence of allergens. To quantify LFIA results, conventionally a strip test reader is required which is a relatively expensive piece of equipment requiring training/instruction for use and a power source to operate. By using a smartphone as a LFIA reader (see section 3.1.2) quantitative/semi-quantitative results are achievable. Smartphones have the added benefits of being portable, affordable, easy to use and can connect wirelessly to deliver instant results to shareholders.
Flow cytometry	Miniaturised flow cytometry	Flow cytometry is a lab-based immunoassay where antibodies of interest are immobilised onto different colored microbeads, it has the benefit of being able to be easily multiplexed. The flow cytometer is a desk-based instrument. Miniaturised flow cytometry (MFC) reduces the flow channels in the cytometer to microfluidic channels, reducing the overall size of the instrument. MFC is capable of being linked with a smartphone as the readout system (see section 3.3.1), this gives the method the ability to be portable and suitable for on-site detection of allergens, and data processing and results to be disseminated through a customised MFC app.
Surface plasmon resonance (SPR)	Smartphone based SPR	SPR is a traditionally lab-based method which can detect changes in antibody/antigen binding on the gold surface of a sensor chip. SPR is able to detect multiple allergens, simultaneously in real-time and monitor their binding responses in the form of a sensorgram. Smartphone based SPR can be achieved through a 3D printed optical attachment, the phone camera and a PDMS prism for light to be deflected from. By linking with a smartphone, SPR becomes a portable method which requires no analyte labeling, limited sample preparation steps and results which can be seen in real-time.



References

1. Raz, S.L., H. Norde, W. Bremer, MGEG. Food Allergen Profiling with an Image Plasmon Resonance-Based Biosensor *Analytical Chemistry* **2010**, *82*, 8485-8491.
2. Badran, A.A.; Morais, S.; Maquieira, Á. Simultaneous determination of four food allergens using compact disc immunoassaying technology, *Anal Bioanal Chem* **2017**, *409*, 2261-2268, 10.1007/s00216-016-0170-0.
3. Blais, B.W.; Gaudreault, M.; Phillippe, L.M. Multiplex enzyme immunoassay system for the simultaneous detection of multiple allergens in foods, *Food Control* **2003**, *14*, 43-47, [https://doi.org/10.1016/S0956-7135\(02\)00053-1](https://doi.org/10.1016/S0956-7135(02)00053-1).
4. Weng, X.; Gaur, G.; Neethirajan, S. Rapid detection of food allergens by microfluidics ELISA-based optical sensor, *Biosensors* **2016**, *6*, doi:10.3390/bios6020024.
5. Yman, I.M.; Eriksson, A.; Johansson, M.A.; Hellens, K.-E. Food Allergen Detection with Biosensor Immunoassays, *Journal of AOAC International* **2006**, *89*, 856-861.
6. Gomaa, A.; Boye, J. Simultaneous detection of multi-allergens in an incurred food matrix using ELISA, multiplex flow cytometry and liquid chromatography mass spectrometry (LC-MS), *Food Chemistry* **2015**, *175*, 585-592, <https://doi.org/10.1016/j.foodchem.2014.12.017>.
7. Otto, G.; Lamote, A.; Deckers, E.; Dumont, V., et al. A flow-cytometry-based method for detecting simultaneously five allergens in a complex food matrix, *Journal of Food Science and Technology* **2016**, *53*, 4179-4186, 10.1007/s13197-016-2402-x.
8. Cho, C.Y.; Nowatzke, W.; Oliver, K.; Garber, E.A.E. Multiplex detection of food allergens and gluten, *Anal Bioanal Chem* **2015**, *407*, 4195-4206, 10.1007/s00216-015-8645-y.
9. Gomaa, A.R., S. Boye, J. Detection of allergens in a multiple allergen matrix and study of the impact of thermal processing *Journal of Nutrition & Food Sciences* **2012**, *9*, 1-6.
10. Wang, W.; Li, Y.; Zhao, F.; Chen, Y., et al. Optical thin-film biochips for multiplex detection of eight allergens in food, *Food Research International* **2011**, *44*, 3229-3234, <https://doi.org/10.1016/j.foodres.2011.08.013>.
11. Tortajada-Genaro, L.S.-F., S. Morais, S. Gabaldon. Puchades, R. Maquieira, A. . Multiplex DNA detection of food allergens on a Digital Versatile Disk, *Journal of Agricultural and Food Chemistry* **2012**, *60*, 36-43.
12. Cheng, F.; Wu, J.; Zhang, J.; Pan, A., et al. Development and inter-laboratory transfer of a decaplex polymerase chain reaction assay combined with capillary electrophoresis for the simultaneous detection of ten food allergens, *Food Chemistry* **2016**, *199*, 799-808, <https://doi.org/10.1016/j.foodchem.2015.12.058>.
13. Lubber, F.; Demmel, A.; Pankofer, K.; Busch, U., et al. Simultaneous quantification of the food allergens soy bean, celery, white mustard and brown mustard via combination of tetraplex real-time PCR and standard addition, *Food Control* **2015**, *47*, 246-253, <https://doi.org/10.1016/j.foodcont.2014.06.047>.
14. Waiblinger, H.-U.B., B. Naumann, G. Koeppl, R. . Ring trial validation of single and multiplex real-time PCR methods for the detection and quantification of the allergenic food ingredients sesame, almond, lupine and Brazil nut, *Journal of Consumer Protection and Food Safety* **2014**, *9*, 297-310.

15. Waiblinger, H.-U.; Boernsen, B.; Geppert, C.; Demmel, A., et al. Ring trial validation of single and multiplex real-time PCR methods for the detection and quantification of the allergenic food ingredients mustard, celery, soy, wheat and rye, *Journal of Consumer Protection and Food Safety* **2017**, *12*, 55-72, 10.1007/s00003-016-1063-z.
16. Wu, J.C., L. Lin, D. Ma, Zhaocheng. Deng, X. . Development and Application of a Multiplex Real-time PCR Assay as an Indicator of Potential Allergenicity in Citrus Fruits, *Journal of Agricultural and Food Chemistry* **2016**, *64*, 9089-9098.
17. Pafundo, S.; Gulli, M.; Marmioli, N. Multiplex real-time PCR using SYBR® GreenER™ for the detection of DNA allergens in food, *Anal Bioanal Chem* **2010**, *396*, 1831-1839, 10.1007/s00216-009-3419-z.
18. Hubalkova, Z.; Rencova, E. One-step multiplex PCR method for the determination of pecan and Brazil nut allergens in food products, *J. Sci. Food Agric.* **2011**, *91*, 2407-2411, 10.1002/jsfa.4479.
19. López-Calleja, I.M.; García, A.; Madrid, R.; García, T., et al. Multiplex ligation-dependent probe amplification (MLPA) for simultaneous detection of DNA from sunflower, poppy, flaxseed, sesame and soy allergenic ingredients in commercial food products, *Food Control* **2017**, *71*, 301-310, <https://doi.org/10.1016/j.foodcont.2016.06.014>.
20. Mustorp, S.D., SM. Holck, AL. Multiplex, Quantitative, Ligation-Dependent Probe Amplification for Determination of Allergens in Food, *Journal of Agricultural and Food Chemistry* **2011**, *59*, 5231-5239.
21. Ehlert, A.D., A. Hupfer, C. Busch, U. Engel, KH. . Simultaneous detection of DNA from 10 food allergens by ligation-dependent probe amplification, *Food Additives & Contaminants: Part A* **2009**, *26*, 409-418, 10.1080/02652030802593529.
22. Unterberger, C.; Luber, F.; Demmel, A.; Grünwald, K., et al. Simultaneous detection of allergenic fish, cephalopods and shellfish in food by multiplex ligation-dependent probe amplification, *European Food Research and Technology* **2014**, *239*, 559-566, 10.1007/s00217-014-2251-7.
23. Ng, E.; Nadeau, K.C.; Wang, S.X. Giant magnetoresistive sensor array for sensitive and specific multiplexed food allergen detection, *Biosensors and Bioelectronics* **2016**, *80*, 359-365, <https://doi.org/10.1016/j.bios.2016.02.002>.

CHAPTER 3

3

Rapid antibody selection using surface plasmon resonance for high-speed and sensitive hazelnut lateral flow prototypes

Adapted from:

Ross, G.M.S., Bremer, M.G.E.G, Wichers, J.H., Van Amerongen, A., Nielen, M.W.F., 2018. Rapid antibody selection using surface plasmon resonance for high-speed and sensitive hazelnut lateral flow prototypes. Biosensors. 8(4). 130. doi: 10.3390/bios8040130

Lateral Flow Immunoassays (LFIA) allow for rapid, low-cost, screening of many biomolecules such as food allergens. Despite being classified as rapid tests, many LFIA take 10-20 min to complete. For a really high-speed LFIA, it is necessary to assess antibody association kinetics. By using a label-free optical technique such as Surface Plasmon Resonance (SPR), it is possible to screen crude monoclonal antibody (mAb) preparations for their association rates against a target. Herein, we describe an SPR-based method for screening and selecting crude anti-hazelnut antibodies based on their relative association rates, cross reactivity and sandwich pairing capabilities, for subsequent application in a rapid ligand binding assay. Thanks to the SPR selection process, only the fast mAb (F-50-6B12) and the slow (S-50-5H9) mAb needed purification for labeling with carbon nanoparticles to exploit high-speed LFIA prototypes. The kinetics observed in SPR were reflected in LFIA, with the test line appearing within 30 s, almost two times faster when F-50-6B12 was used, compared with S-50-5H9. Additionally, the LFIA have demonstrated their future applicability to real life samples by detecting hazelnut in the sub-ppm range in a cookie matrix. Finally, these LFIA not only provide a qualitative result when read visually, but also generate semi-quantitative data when exploiting freely downloadable smartphone apps.

1 Introduction

Lateral flow immunoassay (LFIA) is a rapid technique which relies on the fast interaction between an antibody and a target antigen¹. These devices have experienced a surge in popularity in the medical and food safety fields, since their birth as home-pregnancy tests². It is preferred for LFIAs to use purified, fast, specific and properly characterized antibodies³. Although LFIAs are classified as a rapid method, they still require 10–20 min to complete⁴. In order to create high-speed LFIAs, it is necessary to test the antibody rate of association towards the target analyte, as well as use a nitrocellulose membrane with a high flow rate. Traditional antibody selection techniques, such as enzyme linked immunosorbent assay (ELISA) and western blot, do not necessarily convert well into LFIAs due to the much faster rate of kinetics in LFIA⁵. As trends move toward rapid on-site testing, with consumer-friendly tests such as LFIA and smartphone-based readout systems, the need for antibodies with rapid association towards their target becomes more apparent⁴. In addition to requiring fast antibodies, it is necessary to have a rational way of quickly comparing and selecting such antibodies. One way of speeding up the antibody screening and LFIA prototyping process is to use a label-free biosensor to compare relative antibody-antigen association binding speeds to facilitate the selection process⁶⁻⁸.

Surface plasmon resonance (SPR) is one such technique. SPR allows label-free, optical monitoring of important kinetic information, such as the association and dissociation rates of antibodies, in real-time⁹. Using SPR it is possible to screen crude antibodies. Herein, the term crude refers to: a mixture of un-purified, cell culture media with variable specific antibody concentrations. Screening crude monoclonal antibodies (mAbs) saves time and money in comparison with first purifying a panel of mAbs and then testing them all for application in LFIA¹⁰. Previously, true kinetic studies have been carried out to select antibodies based on their affinities, association and dissociation rates, for application in a direct SPR biosensor¹¹. In the medical sector there is interest in screening and ranking hybridomas, hybrid cells formed from the antibody producing spleen cell of an immunized animal fused with a myeloma cell, for their affinities. However, studies in the literature have not yet focused on the ranking and selection of antibodies based on their association rates towards food allergens, for application in rapid ligand-binding assays such as LFIA^{6,12,13}. Current antibody selection processes using SPR are affinity based and the antibodies are screened against purified analytes. By contrast, in this study, an unpurified hazelnut extract, which is a complex mixture of heterogeneous proteins of various molecular weights, is the target analyte¹⁴.

When developing sandwich format assays for large molecular weight proteins (e.g., food allergens) it is essential to select appropriate antibody pairs for the capture and detection of the target analyte¹⁵. Hazelnut has been selected as the target for this study, as hazelnut is

considered the most prevalent tree nut allergy in Europe¹⁶. Sandwich pairs are antibodies that are capable of simultaneously binding an antigen. Pre-matched antibody pairs can be purchased from commercial vendors which can save time and resources, or they can be selected through sandwich pairing experiments¹⁷. These pairs are often found using ELISA. However, the results obtained in ELISA do not always predict how the antibodies will perform in LFIA³. Alternatively, antibody pairs can be determined by using a half-stick format LFIA¹⁸. Pairwise selection can also be achieved using biosensors by epitope binning¹⁹. This process assesses whether antibodies bind to overlapping epitopes on the target antigen, or whether they are capable of binding to different epitopes²⁰. Using SPR to select antibody pairs for use in LFIA saves time and can be largely automated for screening large antibody panels for their pairs²⁰.

To the best of the authors' knowledge, this is the first example of using SPR as a screening method for selection of high-quality antibodies from crude samples for application in LFIA. SPR has been utilized for selection of purified mAbs for these characteristics, illuminating its importance as a selection tool in this sector¹⁸. A batch screening method was designed using an FC-specific anti-mouse IgG (FC-IgG) immobilized onto an SPR chip. The FC-IgG captures the anti-hazelnut antibodies of interest on the surface. Subsequently, hazelnut protein extract is injected and the binding between the antibody and hazelnut is monitored. Using an FC-IgG surface offers on chip affinity purification of the crude sample, as it captures the crude anti-hazelnut antibodies in their FC region. This allows the captured crude antibodies to be uniformly distributed, in the assumed correct orientation, without any compromise of their biological activity²¹. Furthermore, using an FC-IgG expedites the regeneration of the chip surface between each cycle for screening subsequent antibodies. Following normalization, to compensate for differences in specific antibody concentrations in crude samples, a visual assessment can be made to compare the relative association rates of each mAb towards hazelnut. The un-purified antibodies can then be ranked based on their fast association, sensitivity, specificity and sandwich pairing. As a result, fast (F) and slow (S) antibody pairs selected by SPR were used to develop a carbon nanoparticle-based LFIA system, to identify whether similar kinetics could be observed in LFIA as was seen in SPR.

Amorphous carbon nanoparticles are excellent labels in LFIA as they are easy and low-cost to prepare; have high signal to background contrast, making them easier to read with the naked eye; and can allow for increased sensitivity compared with other labels²². Even lower LOD's might be achieved for carbon nanoparticle-labelled LFIA's by using a flatbed scanner to determine grey pixel values. An alternative, more consumer-orientated method is to use smartphone apps to determine RGB/CMYK values of the test line region of the LFIA's and to convert these to LAB (where L is Luminance and A and B are color channels) values. Whilst RGB (red, green, blue) and CMYK (cyan, magenta, yellow, key) values are device dependent, LAB values provide device independent information

about the darkness/lightness of a selected region of an image²³. In this way a calibration curve of LAB color values against allergen concentration (ppm) can be plotted for semi-quantification of LFIA results. Furthermore, there are currently no food allergen LFIAs that apply carbon nanoparticles, exemplifying the label novelty in this field²⁴. The LFIA prototypes developed were compared based on their speed and sensitivity and applied to a real food matrix of cookies as a proof-of-concept. Cookies have been selected for a matrix as a 2018 report determined that products such as cookies, chocolate and bread are responsible for the majority of accidental allergic reactions²⁵. Finally, the LFIAs were semi-quantified by a smartphone using freely downloadable color analysis apps.

2 Materials and Methods

2.1 Equipment

All SPR experiments were carried out using a BIACORE 3000 (GE Healthcare, Uppsala, Sweden). An EL x 808 BioSPX Microplate Reader was used for the determination of the Bicinchoninic acid (BCA) results (Beun De Ronde, Abcoude, The Netherlands). A NanoDrop ND-3300 (Isogen Life Sciences, De Meern, The Netherlands) or the DeNovix DS-11 spectrophotometer (DeNovix, Wilmington, DE, USA) was used for all other protein quantifications. A Braun Turbo 600 W Food Processor (Krongberg im Taunus, Germany) was used for homogenizing the food samples. All food extracts were filtered through low-binding syringe filters (5 to 0.45 µm; Pall Life Sciences, Portsmouth, UK). The LFIA strips were sprayed using a Linomat IV TLC-spotter (CAMAG, Berlin, Germany). The CM4000 BioDot Guillotine (Biodot Inc., Irvine, CA, USA) was used to cut the strips. A Bioruptor Plus Diagenode (Diagenode SA, Seraing, Belgium) was used to sonicate the carbon nanoparticle suspensions. All smartphone video recordings and photos were taken using a Google Pixel 2 XL (Google, Mountain View, CA, USA). All smartphone-based color detection was accomplished using 'RGB Color Detector' (version 1.0.35, The Programmer; Google Play Store) and color conversions using 'Nix Pro Color Sensor' (version 1.28; Nix Sensor Ltd., Hamilton, ON, Canada; Google Play Store).

2.2 Chemicals & Reagents

The SPR experiments were carried out using carboxymethylated dextran sensor chips (CM5), HBS-EP buffer (pH 7.4), an amine coupling kit (containing: 0.1 M N-hydroxysuccinimide (NHS), 0.4 M 1-ethyl-3-(3-dimethylaminopropyl)carbodiimide hydrochloride (EDC) and 1 M ethanolamine hydrochloride (pH 8.4)), all purchased from GE Healthcare (Uppsala, Sweden). Bovine serum albumin (BSA) was purchased from Sigma-Aldrich (Zwijndrecht, The Netherlands). Analysis of all SPR results was performed using the BiaEvaluation software (Biacore, Uppsala, Sweden).

The washing buffer (WB) was composed of 5 mM borate buffer (BB) (pH 8.8) diluted from a mixture of 100 mM sodium tetraborate (VWR, Leuven, Belgium) and 100 mM boric acid (Merck, Darmstadt, Germany), and bovine serum albumin (BSA) was added to a final concentration of 1% (w/v). The storage buffer (SB) consisted of 100 mM BB containing BSA to a final concentration of 1% (w/v). The running buffer (RB) was prepared by adding 1% BSA (w/v) and 0.05% Tween-20 (v/v) (Merck, Darmstadt, Germany) to 100 mM BB. TRIS-buffered saline (TBS; pH 8.2) was prepared from 20 mM TRIS (Duchefa Biochemie, Haarlem, The Netherlands) and 300 mM NaCl (Merck, Darmstadt, Germany). Phosphate-buffered saline (PBS) pH 7.4 was purchased from Sigma-Aldrich (Sigma-Aldrich, St Louis, MO, USA). The BCA reagents were purchased from Pierce (Rockford, IL, USA). All solutions were prepared with MQ water from a MilliQ-system (> 18.2 MΩ/cm) purchased from Millipore (Burlington, MA, USA). 'Spezial Schwartz 4' carbon nanoparticles were purchased from Degussa AG (Frankfurt, Germany). Goat anti-mouse IgG Fc specific antibody in PBS (2.4 mg/mL) used in the SPR study was purchased from ThermoFisher Scientific (Landsmeer, The Netherlands). Goat anti-mouse IgG in PBS (pH 7.6) (1.2 mg/mL; AffiniPure F(ab')₂ Fragment GAM IgG Fcγ) used for spraying LFIA control lines was purchased from Jackson ImmunoResearch Laboratories Inc (Sanbio, Uden, The Netherlands). All other antibodies were developed by RIKILT, Wageningen University & Research (Wageningen, The Netherlands), according to the procedure described in^{26,27}. In short, the antibody panel listed in Table 3.1 was produced by immunizing mice with 50 µg extracted hazelnut (mixed) protein, with booster immunizations containing 25 µg extracted hazelnut protein. Antibodies selected for LFIA were purified using a HiTrap Protein G column (GE Healthcare, Uppsala, Sweden). Briefly, antibodies were collected from 1 L of raw cell culture media by ammonium sulphate precipitation and subsequent affinity chromatography purification. Following this method, around 15–20 mg of purified antibodies was obtained from 1 L of raw cell culture medium.

Table 3.1. Antibody ranking based on the visually observed association rates, confirmation by slope analysis in Excel and maximum plateau of Hazelnut bound

Fastest Association (Visual)	Slope Analysis (Excel)	Maximum Plateau
50-7B8	0.0233	50-7B8
50-6B12	0.0215	50-6B12
50-8A3	0.0193	50-8A3
50-1G10	0.0174	50-1G2
50-1G2	0.0166	50-6E1
50-6G7	0.0155	50-6G7
50-6E1	0.0153	50-1G10
50-6B3	0.0145	50-5H9
50-8B11	0.0137	50-8B11
50-5H9	0.0114	50-6B3
50-3A11	0.0110	50-3A11
50-2D9	0.0109	50-2D9

2.3 Allergen Extractions

Certified standardized reference materials for food allergens are not commercially available and so antigen standards require in-house preparation. Allergen extracts were made from a 'blank' matrix of organic whole meal digestive biscuits (containing: flour, palm oil, sugar, barley malt extract, sodium bicarbonate, ammonium bicarbonate, salt; Dove's Farm Organic Whole meal Digestive Biscuits; Dove's Farm, Berkshire, UK), from hazelnut cookies (TimeOut Hazelnoot Granenbiscuits containing: 10% hazelnut, egg, milk & sesame; Albert Heijn, The Netherlands) and from hazelnuts, pecan nuts, pistachio nuts, brazil nuts, peanuts, cashew nuts, almonds, walnuts and macadamia nuts, which were all purchased from a local supermarket. All extracts were filtered through a series (5 μm , 1.2 μm , 0.45 μm) of low protein-binding syringe filters. For the SPR study, whole raw hazelnuts were frozen at $-80\text{ }^{\circ}\text{C}$ for 4 h. The frozen hazelnuts were homogenized to a fine powder using a commercial hand blender. The protein was extracted by adding 10 mL of heated TBS buffer per gram of ground hazelnut. The mixture was vortexed for 30 s before rotating end-over-end for 30 min at $37\text{ }^{\circ}\text{C}$. The solution was centrifuged at room temperature for 15 min at $4000 \times g$. The resulting liquid phase was filtered through a series of low protein-binding syringe filters. Total protein concentrations were determined according to the BCA protein assay using BSA as the standard. All hazelnut protein extracts were aliquoted and stored at $-20\text{ }^{\circ}\text{C}$ until use. For the cross-reactivity study, a universal allergen extraction procedure was applied that can be used to simultaneously extract multiple different food allergens. Extracts were made from hazelnut, peanut, pecan, pistachio, walnut, brazil nut, macadamia nut, almond and cashew following the method described by Raz²⁸. Briefly, nuts were homogenized using a Braun Turbo 600 W Food Processor, and 0.25 g sample portions were weighed out. Twenty-five milliliters of PBS (pH 7.4) was added to the ground samples and incubated at room temperature for 1 hour. Following incubation, extracts were centrifuged at $3,220 \times g$ for 20 min. The extracts were then filtered through a series of low protein-binding syringe filters, aliquoted and stored at $-20\text{ }^{\circ}\text{C}$ until use. The same procedure was applied for the matrix extraction of the 'Blank' matrix and hazelnut cookies but using a 2.5 g ground food in 25 mL PBS. Total protein contents of all allergen/matrix extracts were determined using the NanoDrop.

2.4 Biosensor Chip Preparation

A standard amine coupling procedure was applied at $25\text{ }^{\circ}\text{C}$ to immobilize the Fc-Specific IgG (FC-IgG) onto the CM5 surface. Immobilization pH scouting for coupling of FC-IgG to CM5 chip was performed. The FC-IgG was diluted to $20\text{ }\mu\text{g/mL}$ in 10 mM sodium acetate of varying pH's and tested using the pH scouting wizard in the Biacore 3000 control software (Uppsala, Sweden). A high immobilization level was reached at pH 5.5, so sodium acetate pH 5.5 was selected as the immobilization buffer in the following procedure. The four flow channels, clamped against the carboxymethylated (CM) dextran chip surface, were simultaneously activated by injecting 35 μL of a mixture of EDC and NHS (1:1 v/v)

at a flow rate of 5 $\mu\text{L}/\text{min}$. Then, FC-IgG diluted (20 $\mu\text{g}/\text{mL}$) in coupling buffer (10 mM sodium acetate, pH 5.5) was injected in flow cells 2–4, and FC-IgG was attached to the activated CM-dextran surface via its exposed primary amine groups. Flow cell 1 was used as a reference channel and was left blank and was only activated by EDC/NHS. The coupling was followed by blocking the remaining active ionic groups in all flow cells with ethanolamine (1 M) preventing electrostatic interactions with the CM-dextran surface. Around 10,000 RU of FC-IgG was immobilized in each channel (2–4) using this method; this high level was aimed for in order to properly cover the chip surface with FC-IgG for the subsequent capture of the specific anti-hazelnut mAbs of interest.

2.5 Crude Antibody Screening Assay

The screening analysis was performed at 25 $^{\circ}\text{C}$ using HBS-EP (pH 7.4) as the screening buffer. The crude antibodies were diluted 1/20 in the screening buffer. The hazelnut protein extract was diluted to 20 ppm in the screening buffer. Twenty microliters of each crude antibody dilution was injected at a flow rate of 20 μL per minute for capture. These flow conditions were selected to more accurately reflect the fast flow kinetics observed in LFIAs. Subsequently, 20 μL of 20 ppm hazelnut extract was injected at a flow rate of 20 μL per minute. The surfaces were immediately regenerated with 2 pulses of 5 μL , 5 mM NaOH to return the biosensor signal to baseline²⁹. A range of different regeneration conditions were tested, including glycine, HCl and different strengths, volumes and flow rates of NaOH. Of all the tested regeneration conditions, 2 short NaOH pulses were found to be the most appropriate for removing both strong and weak binders whilst minimizing FC-IgG surface deterioration, and these were applied as the standard regeneration conditions.

Using the Biaevaluation software (Biacore, Uppsala, Sweden), the whole sensorgrams for each crude antibody capture and antigen binding cycle were superimposed. As the antigen in this study is comprised of heterogeneous proteins, the curves do not conform to Langmuir binding models. Therefore, as this study is focused on a rapid screening process, a full kinetic curve fitting was not performed. The sensorgrams were aligned on the x-axis at the hazelnut antigen injection point. A snapshot of the relevant part of the sensorgram, containing the hazelnut association and dissociation data, was made in the software. The sensorgrams were double referenced, first by using flow cell 1 as a blank reference channel for buffer signal subtraction and subsequently by normalizing the hazelnut response by dividing the antigen response by the corresponding crude antibody capture level, as described in¹¹. All sensorgrams were y-axis zeroed to baseline. After data processing and removal of the FC-IgG capture curve and the regeneration peaks, a visual assessment of the association rates of each antibody towards hazelnut could be achieved. The visual assessment of the steepness of the association curves for the crude antibodies toward hazelnut was confirmed using the slope analysis function in Microsoft Excel.

2.6 Cross-Reactivity Testing

Total protein extracts from tree nuts and peanut (in PBS) were protein content determined using the NanoDrop and then were diluted to 100 ppm in HBS-EP. Three different antibodies were captured by the FC-IgG surface, in individual flow cells, at a flow rate of 20 μL per minute. During the first cycle, 20 ppm hazelnut extract was injected as a control to monitor the binding response of these crude antibodies towards hazelnut. Following this, the surface was regenerated with the standard regeneration conditions. Subsequently, the same antibodies were re-captured and 20 μL of one of the other tree nut/peanut protein extracts was injected over the antibodies using the same flow conditions. Following this, the surface was regenerated using 1 or 2 pulses of 5 mM NaOH, depending on the extent of tree nut/peanut binding. The procedure was repeated for all of the tree nut/peanut extracts.

2.7 Sandwich Pairing Assay

Twenty microliters of each of three antibodies was captured in individual flow cells at a flow rate of 20 μL per minute. Next, 20 μL of 20 ppm hazelnut extract was injected over all flow cells simultaneously at flow of 20 μL per minute. Subsequently, 20 μL of one crude antibody was injected over all three flow cells, generating data for one antibody against itself and against two other antibodies. Following this, the surface was regenerated with standard conditions to return the signal to baseline.

2.8 Labeling with Carbon Black Nanoparticles

A 1% suspension of carbon nanoparticles was prepared by adding 1 mL of MilliQ Water (MQ) to 10 mg carbon and sonicating for 10 min. The resulting 1% carbon suspension was diluted five times in 5 mM BB (pH 8.8) to obtain a 0.2% suspension, which was then sonicated for a further 5 min. Next, 350 μg of purified anti-hazelnut antibody was added per 1 mL of 0.2% carbon suspension and stirred overnight at 4 $^{\circ}\text{C}$. The suspension was divided into two aliquots and 500 μL of WB was added to each and centrifuged for 15 min at $13,636 \times g$ at 4 $^{\circ}\text{C}$. Following this, the supernatants were removed, and the pellets re-suspended in WB, this process was repeated 3 times. After the final wash, the supernatants were discarded, and the pellets were pooled together with 1 mL storage buffer and stored at 4 $^{\circ}\text{C}$ until use. Scanning electron microscopy (SEM) images of F-50-6B12-carbon nanoparticle suspension can be seen in the Supplementary Information (SI; Figure S3.1).

2.9 Lateral Flow Immunoassay

2.9.1 Preparation of Lateral Flow Immunoassay Prototype

Lateral flow strips were manufactured using nitrocellulose (NC) membranes (HiFlow Plus HF13502; Millipore, Carrigtwohill, Co. Cork, Ireland) cut to approximately 2.5 cm in length; see SI Figure S3.2 for an SEM image of the NC membrane. The NC membrane was secured on a plastic backing (G & L, San Jose, CA, USA), with 4.5 cm of absorbent pad (Schleicher

& Schuell, Dassel, Germany) overlapping one end of the NC. Four LFIA were prepared for each antibody, with different antibody concentrations dispensed onto the test line to determine the optimum conditions. A TLC spotter was used to dispense the test line (the anti-hazelnut antibody at 0.2 mg/mL, 0.15 mg/mL, 0.1 mg/mL or 0.05 mg/mL) at 1.2 cm and the control line (Goat anti-mouse Fab Fragment at 0.1 mg/mL) at 1.5 cm from the sample application end of LFIA. The TLC spotter used 1 μ L of antibody per 5 mm wide strip, at a speed of 15 μ L per second. The membranes were allowed to dry at room temperature for 30 min. Finally, 5-mm-wide strips were cut using the BioDot Guillotine CM4000 (Biodot Inc., Irvine, CA, USA) and were packaged in aluminum pouches with silica desiccation packs, heat-sealed and stored at room temperature until future use.

2.9.2 Lateral Flow Immunoassay: Limit of Detection

First, the visual limit of detection (LOD) of the strip tests was determined using a decreasing concentration of hazelnut protein extract diluted in PBS. Herein, the visual LOD is defined as the lowest concentration of total hazelnut protein capable of resulting in the appearance of a test line. Both strip batches had the same amount of purified anti-hazelnut antibody immobilized on the test line, and both sets of carbon nanoparticle labelled mAbs had 350 μ g of antibody immobilized per mL of carbon so that a fair comparison could be made between the two sets of antibodies. For dipstick analysis, a strip test was placed in a well of low binding microtiter plate containing 100 μ L running buffer (RB), 1 μ L carbon-antibody conjugate and 1 μ L hazelnut extract (dilution range: 100, 50, 25, 10, 5, 2.5, 1, 0.5, 0.25, 0.1, 0 ppm) and was allowed to run for 5 min. Subsequently, the visual LOD of the dipsticks in a spiked commodity was determined. To test for matrix LOD's, total hazelnut protein extract was spiked into a blank cookie extract in the range of 100 ppm to 0.5 ppm (100 ppm, 50 ppm, 25 ppm, 10 ppm, 5ppm, 2.5 ppm, 1 ppm, 0.5 ppm, 0 ppm). The testing procedure was the same as that described above. Additional matrix LOD determinations were made using 50 μ L RB, 50 μ L spiked commodity and 1 μ L carbon conjugated-mAb in order to reduce further dilution that was caused by adding 100 μ L of running buffer to 1 μ L of sample. In order to establish the real-life applicability of the optimal LFIA, the real-life matrix of a hazelnut cookie extract was also tested (1 μ L sample in 100 μ L RB) spiked into a decreasing dilution in a blank cookie extract in the range of 1:1 to 1:1,000,000.

2.9.3 Lateral Flow Immunoassay: Test Line Kinetics

To compare the antibody to hazelnut association rates in LFIA, it is necessary to time the appearance of the test line. The strips were tested by inserting a test strip into a microwell containing 100 μ L RB, 1 μ L carbon-mAb and 1 μ L of 50 ppm hazelnut protein extract (in PBS). A higher concentration of hazelnut extract was used for the kinetic study, as a higher analyte level results in the appearance of a darker line with a high contrast, making it easy to visualize the line as soon as it forms. Instead of allowing the strips to run for 5 min, as soon as a test line appeared on the strip, this time was recorded. The kinetic experiments

were repeated multiple times ($n = 8$) and were assessed visually and by smartphone video recording for the test line formations.

2.9.4 Semi-quantitative Smartphone Lateral Flow Readout

To obtain RGB/CMYK color values, each LFIA in a calibration range (100 ppm, 50 ppm, 25 ppm, 10 ppm, 5 ppm, 2.5 ppm, 1 ppm, 0.5 ppm, 0 ppm) was analyzed, with 'RGB Color Detector' (version 1.035), by selecting a region of interest in the LFIA test line area using the crosshair function. To obtain fair color values, values were averaged from three distinct points on the test line of the strips ($n = 3$). Color values were also taken from the background (below the test line) to normalize the results. The 'Nix Pro Color' (version 1.28) sensor allows conversion between multiple different color spaces. Therefore, when plugging the RGB or CMYK values obtained in 'RGB Color Detector' into the 'Nix Pro Color' sensor, it is possible to select a conversion to LAB (or cieLAB) color space. Using the obtained LAB values, a calibration curve was plotted for LAB values vs hazelnut extract spiked into blank cookie extract using an ordinary spreadsheet program.

3 Results

3.1 SPR Crude Antibody Screening Assay

As the antibodies being screened for this study were in an un-purified, crude form, a capture method was used to allow for on-chip purification and proper orientation of anti-hazelnut mAbs (see Figure 3.1a). Although the FC-IgG itself may have suffered with orientation issues because a sufficiently high density was immobilized, these concerns could be alleviated as there was still a significant proportion of correctly orientated FC-IgG. Furthermore, the FC-IgG surface allows for the anti-hazelnut mAbs to be captured predominantly in a 'tail-on' orientation, exposing their unoccupied antigen binding sites³⁰. The FC-IgG was immobilized in flow cells 2–4 (flow cell 1 was left blank as a reference surface) to create a homogeneous surface. Then, the crude antibody sample was injected for capture by the immobilized FC-IgG. Following this, the hazelnut extract was injected and allowed to bind with the captured crude antibody sample. Each cycle was performed in duplicate. The duplicate results, across different flow cells, were used to determine the reproducibility of analyte binding levels. The captured antibody/hazelnut complex was completely removed from the FC-IgG specific surface before injecting the next crude antibody sample.

A key benefit of SPR is the ability to re-use the sensor chips. Proper surface regeneration was achieved using standard conditions. These regeneration conditions removed the captured antibody/hazelnut leaving the FC-IgG surface intact. The signal after regeneration only

resulted in a slight loss of baseline response, but subsequent antibody/analyte injections were able to reach response levels within $\pm 10\%$ of the original response levels.

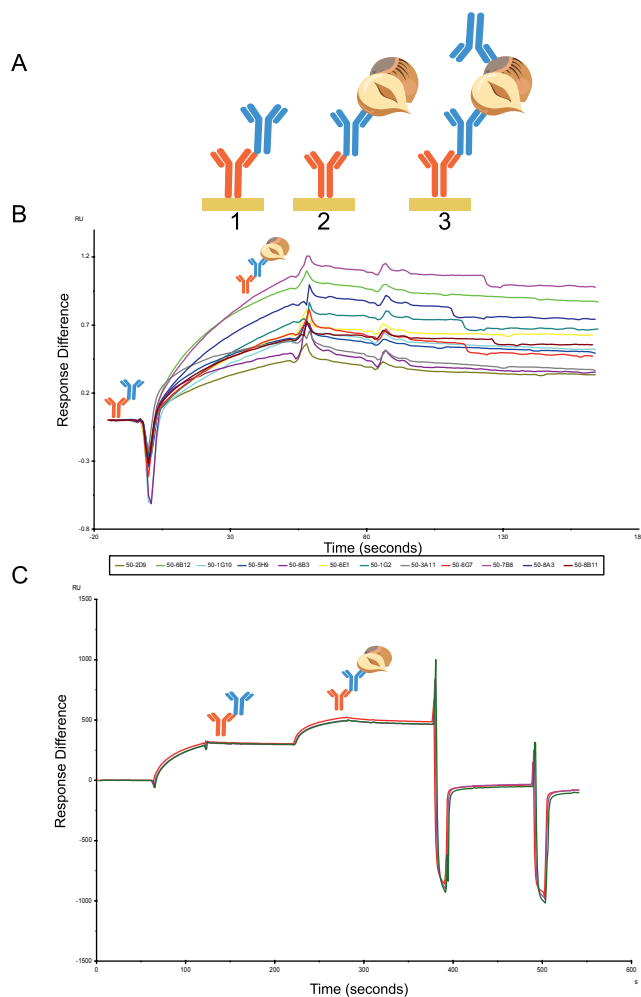


Figure 3.1. (A) SPR screening assay for crude antibodies. The first image shows the capture of a crude anti-hazelnut mAb (blue) via its FC region by the FC specific IgG (orange). The second image shows the binding of total hazelnut protein to the anti-hazelnut mAb. The third image displays the sandwich pairing of an anti-hazelnut mAb (blue) towards hazelnut and another anti-hazelnut mAb (blue). (B) Normalized SPR sensorgrams for 12 crude antibody preparations against 20 ppm hazelnut extract. The hazelnut injection is indicated by the first arrow, which is followed by the association of the crude antibodies towards hazelnut. The second arrow indicates the start of the hazelnut dissociation from the antibodies. (C) Full sensorgram of a crude antibody towards hazelnut in triplicate. The first curve shows the capture of the crude antibody via its FC region, the second curve the binding of hazelnut to that antibody and the following two spikes the regeneration.

Every few cycles, some antibodies were re-injected to ensure that the same levels and binding ratios could be reproduced; for example, S-50-5H9 was re-injected between other antibodies and was able to bind to hazelnut at 87.63, 92.22 and 94.93 RU. For the cross-reactivity study, sometimes only one regeneration pulse was required due to less antigen binding and therefore less protein to remove from the surface.

The overlay plot presented in Figure 3.1b displays sensorgrams with the association curves for 12 different crude antibody preparations against hazelnut (see SI Figure S3.3 for duplicate curve reproducibility across two flow cells). As dissociation is not of primary concern in LFIA, this characteristic was not focused on here. Each sensorgram composed of the crude antibody capture step, followed by the injection of the hazelnut extract and then the subsequent surface regeneration. An example of the full sensorgram before data processing can be seen in Figure 3.1c (data for 1 antibody, overlaid in triplicate) where the first curve represents the capture of the hazelnut antibody, the following curve the binding of the antibody with hazelnut and the subsequent spikes, the standard regeneration conditions. The levels for crude antibody capture ranged from 40-160 RU and the antigen binding response ranged from 20-130 RU; these responses are in correspondence with the range of levels reached in¹¹. The binding curves were normalized as described in the methods section. From Figure 3.1b, a visual interpretation of the association rates of the crude antibodies can be made. The start of the association phase is indicated by the first arrow (Figure 3.1b). Those antibodies with a steeper slope incline at the dip (e.g., 50-7B8) have a faster association towards hazelnut compared with the antibodies with a shallower curve (e.g., 50-2D9). The visual interpretation of the curves was confirmed by slope analysis in Microsoft Excel and was reproducible across two separate cycles in two different flow cells. The crude mAbs were ranked based primarily on association rates (visually and confirmed in Excel) and subsequently on hazelnut binding plateau values as can be seen in Table 3.1. As this study aimed for a quick and simple SPR screening method, no attempt was made to compare the absolute association, dissociation and equilibrium constants of the crude antibodies.

Although the main purpose of this screening method was to select ultra-fast antibodies for a high-speed LFIA, it is also necessary that these antibodies exhibit good sensitivity. Therefore, the antibodies were grouped first according to their association speeds towards hazelnut and then according to the amount of hazelnut that they were able to bind (Table 3.1). Regardless of the extent of hazelnut binding, the most desirable parameter in this study was the speed of mAb to hazelnut binding for final application in LFIA. The experiments were performed in duplicate with identical results. According to this ranking, the three best (fast and able to bind most hazelnut) antibodies selected were 50-7B8, 50-6B12 and 50-8A3. The antibody which was able to bind the least and had the slowest association toward hazelnut was 50-2D9 with the second and third slowest being 50-3A11

and 50-5H9, respectively. Even those crude antibody preparations at the bottom of the table were still capable of binding sufficient hazelnut, meaning that even the less optimal mAbs could be applied as capture ligands in a direct SPR assay.

3.1.1 Cross Reactivity

The cross-reactivity study was carried out with the top two fastest (50-7B8 & 50-6B12) and the two slowest (50-3A11 & 50-2D9) crude antibodies (listed in Table 3.1). The percentage of cross reactivity was determined by dividing the binding response (RU) of the tree nut/peanut extract by the corresponding binding response of hazelnut toward that particular crude antibody (see SI Table S3.1). The fastest antibody (50-7B8) cross reacted with walnut at 17%, making it unsuitable for application in a hazelnut LFIA. The second fastest (F) antibody (F-50-6B12) exhibited no significant cross-reactivity toward the tested tree nut/peanut extracts, so this antibody was selected for further testing for use as the 'best' antibody for the LFIA prototype. Both of the slowest antibodies (50-3A11 & 50-2D9) displayed significant cross-reactivity towards multiple other tree nut/peanut extracts and were capable of binding less hazelnut, making these antibodies unsuitable for LFIA. Therefore, the third slowest (S) antibody (S-50-5H9) was also tested for cross-reactivity and it was found that it did not exhibit significant cross-reactivity toward the tested tree nut/peanut extracts and so was carried forward as the less optimal antibody for LFIA prototyping.

3.1.2 Sandwich Pairing

A different antibody was captured in each of 3 flow cells, leaving flow cell 1 blank as a reference. Hazelnut extract was injected simultaneously over all flow cells, meaning that three hazelnut binding curves were generated per cycle. Succeeding this, one crude antibody was injected simultaneously over all flow cells, attaining sandwich pair information against itself, and against two other crude antibodies.

This method was repeated for all the antibodies to be tested for sandwich pairing. The lack of binding of secondary mAbs, when there was no hazelnut protein bound to the capture mAbs, demonstrated the absence of unwanted binding to unoccupied FC-IgG in the flow cell. Consequently, when binding did occur, following hazelnut injection, this confirmed the formation of a sandwich pair. Although F-50-6B12 and S-50-5H9 could form sandwich pairs both with one another and some of the other antibodies, the most successful pairs (able to bind the most hazelnut and subsequent antibody) were with themselves. In Figure 3.2. the sandwich pairing for F-50-6B12 and itself can be seen. In this sensorgram, the first curve represents hazelnut binding with F-50-6B12 and the subsequent curve shows the binding of F-50-6B12, indicating that F-50-6B12 is capable of binding to two distinct epitopes and can form a sufficient sandwich pair. Furthermore, it appears that F-50-6B12 has very little dissociation, although this is not necessarily an important characteristic

within LFIA, it is indicative of the formation of a stable sandwich pair (see SI Figure S3.4). As the optimal antibody (F-50-6B12) and the less optimal antibody (S-50-5H9) were capable of forming sandwich pairs with themselves, only these antibody preparations were finally purified for application in a LFIA prototype.

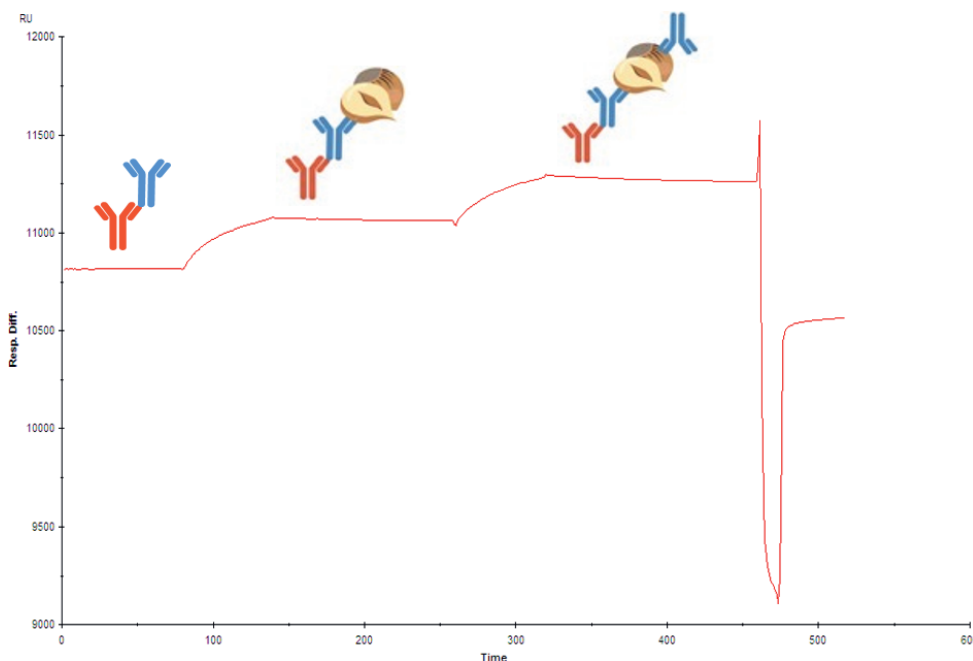


Figure 3.2. SPR based sandwich pairing. Sensorgram depicting crude “good” sandwich pair F-50-6B12 + F-50-6B12. The first curve in the sensorgram represents the hazelnut binding to F-50-6B12. The following curve shows the binding of a second F-50-6B12 to the hazelnut protein extract.

3.2 Lateral Flow Immunoassay Prototypes

First, the optimal mAb test line concentration was determined using the purified antibodies. In order to make a fair comparison between the two antibodies it was necessary to use the same dispensing conditions for each. It was found that the strips with a 0.2 mg/mL mAb at the test line gave a background response in a blank matrix for S-50-5H9, so this concentration was rejected. The 0.05 mg/mL test line strips suffered from a loss of sensitivity for both antibodies. The 0.1 mg/mL test line strips gave no response in the blank but were not as sensitive. Therefore, the optimum test line condition for both mAbs was found to be 0.15 mg/mL. Different control line concentrations were also tested, with the optimal concentration being 0.1 mg/mL. This concentration was selected as it still gave a significant control line response without causing a background response in a blank.

For the optimal antibody (F-50-6B12), an LOD of 0.1 ppm for hazelnut protein extract in spiked buffer was achieved and for the less-optimal antibody (S-50-5H9), an LOD of 2.5 ppm was reached (Figure 3.3 a and b). The results are consistent with the observations made in the SPR experiments, as F-50-6B12 was capable of binding more hazelnut compared with S-50-5H9. As can be seen in Figure 3.3a and b, the naked eye is able to read at a lower limit (visual LOD indicated by the eye icon) compared with the smartphone camera (smartphone LOD indicated by smartphone icon), this is likely owing to ambient light conditions which come into effect when recording the smartphone image. The spiked buffer experiments were reproducible across different days ($n = 3$) with identical visual LOD's being reached for each repetition. As the smartphone images were recorded over different days and times, with no light control mechanism, differences are observed in the ambient lighting conditions in the images.

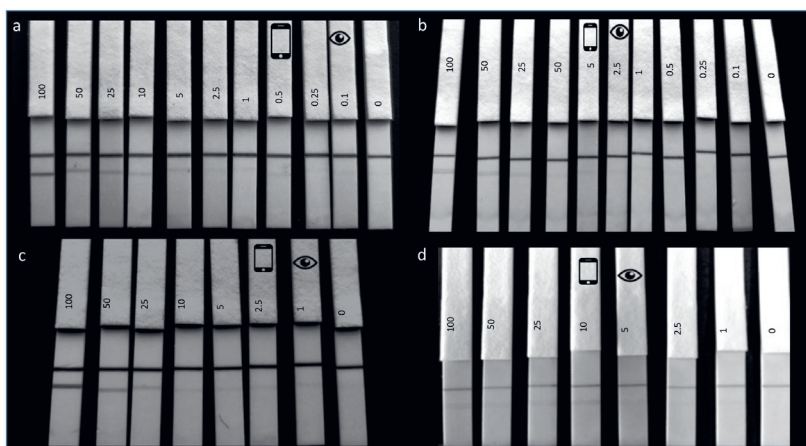


Figure 3.3. Lateral flow immunoassay limit of detection experiments. (a), F-50-6B12, (b), S-50-5H9: LFIA showing the LOD determination of hazelnut protein extract spiked in PBS in the range of 100 ppm to 0.1 ppm with the last LFIA being a blank (0 ppm). In all LFIA, the upper line is the control line and the lower line the test line. The visual LOD is indicated by the eye icon and the detection limit using a smartphone camera is indicated by the smartphone icon. (c), F-50-6B12, (d), S-50-5H9: LFIA showing matrix LOD of hazelnut protein extract spiked in blank cookie extract (1:100 in running buffer) in the range of 100 ppm to 1 ppm (with the last strip representing a blank 0 ppm). The visual LOD is indicated by the eye icon and the detection limit using a smartphone camera is indicated by the smartphone icon.

To understand the LFIA applicability to real life samples, the matrix LOD's were subsequently determined by spiking hazelnut extract into a blank cookie extract. When using $1\mu\text{L}$ of spiked cookie extract in $100\mu\text{L}$ of RB, a matrix LOD of 1 ppm could be achieved for F-50-6B12 (Figure 3.3c) and of 5 ppm for S-50-5H9 (Figure 3.3d). As a much lower LOD was achieved for F-50-6B12 in the spiked buffer experiments, the matrix LOD experiments

were repeated using 50 μL of spiked cookie extract (in RB) and 50 μL of RB in order to try and increase the sensitivity of the LFIA. For the less optimal mAb (S-50-5H9), these assay conditions resulted in a false positive, with even the blank producing a test line signal. However, under these conditions, F-50-6B12 was easily able to detect below 0.5 ppm (see Figure 3.4), making it the most sensitive hazelnut LFIA currently reported. The lowest LOD in spiked matrix for commercially available hazelnut LFIA is currently 1 ppm⁴. This means that the LFIA prototype for the optimal mAb developed in this study is equally or even more sensitive than the currently reported LFIA, even before any further optimization.

To further exemplify future use in real life, the F-50-6B12 LFIA prototype was also tested in a decreasing amount of commercial hazelnut cookie extract, diluted in a blank cookie extract. In this way, F-50-6B12 was still able to detect the presence of the hazelnut cookie even when it was diluted by 106 in a blank cookie.

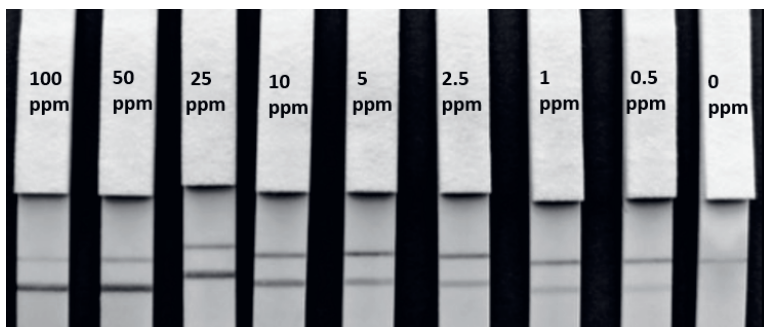


Figure 3.4. F-50-6B12 Lateral flow immunoassay matrix limit of detection. Lateral flow strips for F-50-6B12 showing the matrix LOD of hazelnut protein extract spiked in blank cookie using 50 μL spiked sample and 50 μL RB. A clear LOD of below 0.5 ppm can be visualized both with the naked eye and with a smartphone camera.

In order to determine the kinetics of the LFIA, the strips were tested in a high concentration of hazelnut (50 ppm) and the timing of the appearance of the test line was recorded. Although the test line kinetics were the same when using lower/higher concentration of total hazelnut protein, the appearance of the test line was easier to distinguish when using a higher concentration, making it possible to more accurately record the timing of the line appearance. First, the kinetics were determined for each LFIA batch individually, across different days ($n = 3$), to establish an average visual response time and standard deviation ($n = 8$) for the test line appearance. Subsequently, the two LFIA were one-to-one compared for the speed of the formation of the test lines which was recorded by video using a smartphone recording (see SI Figure S3.5 smartphone video screenshots for video). In SI Figure S3.5, a kinetic comparison between the two different LFIA is

demonstrated. By making time-resolved screenshots from a smartphone video recording (every 5 s) it is possible to distinguish the appearance of the test line of the F-50-6B12 LFIA at a much earlier (30 s) stage than the appearance of the test line for the S-50-5H9 LFIA (60 s). In reality, it is possible to distinguish the test line slightly earlier with the naked eye, compared with the smartphone recording. Therefore, visually the test line for F-50-6B12 first appeared, on average, at 30 s with a standard deviation of ± 1.2 s. The test line for S-50-5H9 appeared on average at 52 s with a standard deviation of ± 2.2 s. The LFIA kinetic results are in direct agreement with the results from the SPR experiments, where F-50-6B12 also exhibited nearly $2 \times$ faster association with hazelnut compared with S-50-5H9 (see Table 3.1; slope analysis). The F-50-6B12 strips could easily be read visually or with a smartphone camera within 2 min and even the S-50-5H9 strips could be read within 5 min.

3.3 Smartphone Detection

The majority of smartphone-based lateral flow readers rely on related assay-specific developed apps^{31,32}. These apps can be used to semi-quantify LFIAs by establishing a calibration curve based on color values for test lines of LFIAs versus analyte concentrations. In the same way, color values can be determined using freely downloadable apps from Google Play Store. More researchers are switching to *cie*LAB/LAB color space analysis, as it has a more extensive color range (gamut), which more accurately represents how humans visually interpret colors and therefore, is device independent. Like RGB, LAB values are composed from three criteria, the L represents luminosity and A and B represent color space; unlike RGB only the L value provides information about the darkness/lightness of the selected region. Using the (L)LAB values obtained from the test lines, it was simple to establish a calibration curve to semi-quantify the strip tests by plotting total hazelnut protein concentration (in blank cookie) against (L)LAB values (see Figure 3.5 below). Background measurements were made from under the test line region on all of the strips, as at this stage a light box was not used to control the ambient lighting conditions of the photos. There is a clear relationship between the (L)LAB values and the concentration of hazelnut present in the sample, with lower hazelnut concentrations corresponding to higher (L)LAB values. The applied method did not utilize any light-box or dedicated algorithm to control ambient lighting conditions, indicating that it is possible to use a smartphone to semi-quantify carbon nanoparticle-based LFIAs without attachments. In this way, it is possible for anybody to perform their own smartphone analysis using only an LFIA calibration range and freely downloadable apps.

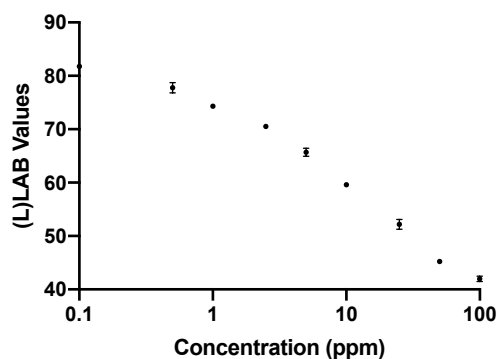


Figure 3.5. A calibration curve showing the relationship between (L)LAB values of test lines of hazelnut LFIA in a decreasing concentration of hazelnut protein (in blank cookie). Error bars have been included to show the standard deviation across multiple ($n = 3$) measurements. An (L)LAB value of 100, (0, 0) corresponds to a true white and of 0 (0,0) to a true black, in this study the lowest L value was 42 and so the L (LAB) axis begins at 40.

4 Discussion

Surface plasmon resonance was used to screen antibodies in their un-purified state based on their fast association, specificity and sensitivity towards hazelnut, for use in LFIA. This method saves significant time and resources compared with selecting mAbs by ELISA. In ELISA, it is preferred to use purified mAbs and the antibody purification process takes approximately one day for each antibody. Considering that in this study, 12 mAbs were ranked by SPR as an analysis tool, if these would have first needed purification, it would have taken over a week longer to get to the antibody assessment stage. As the method only requires small volumes of un-purified mAbs, it is possible to start assessing the mAb characteristics as early as the fusion stage. Additionally, as SPR is a label-free technique, even more time is saved by not having to perform additional labeling experiments, and more unequivocal information is obtained from SPR compared with ELISA.

The SPR results made it possible to select a very good and a less optimal antibody pair for application and comparison in a high-speed LFIA. The two prototype LFIAs displayed a significant difference in the timing of the appearance of the test line, with F-50-6B12's test line appearing at least 20 s before the appearance of the test line on the S-50-5H9 strip. When considering moving towards consumer-friendly food allergen detection, it is desirable to have LFIAs that give accurate, positive results, as quickly as possible, so that food can rapidly be assessed before its consumption. Quick allergen analysis can prevent unnecessary allergic reactions by allowing consumers to determine which portions of

foods are safe to eat and which should be avoided. The proposed screening method could be extremely useful when trying to select antibodies of similar kinetics to use in a multiplex assay. In this way it would be possible to select capture/detector mAbs for a range of targets which have similar association rates towards their targets, so that when they are utilized in a multiplex assay, the T-lines appear within a similar temporal resolution. The optimal F-50-6B12 strips were able to detect the presence of hazelnut at trace levels in spiked buffer, spiked commodity and a real-life hazelnut cookie, highlighting the LFIA's usefulness in real life. The F-50-6B12 LFIA is sensitive enough to protect even for the most sensitive hazelnut allergic individuals. Finally, a semi-quantitative smartphone readout was achieved by using simple and free color analysis apps to obtain device independent LAB values. This proves that even in the absence of additional light-control mechanisms, 3D-printed attachments and dedicated software apps, it is possible for anyone to obtain semi-quantitative LFIA results using their smartphones, provided that mAbs are labelled with carbon nanoparticles. Such apps could also be used to semi-quantify a multiplex assay. This study demonstrates a generically applicable proof-of-concept method for a novel association and sensitivity-based antibody selection procedure that can be applied to crude preparations for consequent application in LFIA with a visual or smartphone readout and an LOD in the low ppm range.

References

1. Posthuma-Trumpie, G.A.; Korf, J.; van Amerongen, A. Lateral flow (immuno)assay: its strengths, weaknesses, opportunities and threats. A literature survey, *Anal Bioanal Chem* **2009**, *393*, 569-582, 10.1007/s00216-008-2287-2.
2. Chan, C.P.-y.; Cheung, Y.-c.; Renneberg, R.; Seydack, M. In *Biosensing for the 21st Century*, Renneberg, R.; Lisdat, F., Eds.; Springer Berlin Heidelberg: Berlin, Heidelberg, 2008, pp 123-154.
3. Brown, M.C. In *Lateral Flow Immunoassay*, Wong, R.; Tse, H., Eds.; Humana Press: Totowa, NJ, 2009, pp 1-16.
4. Ross, G.M.S.; Bremer, M.G.E.G.; Nielen, M.W.F. Consumer-friendly food allergen detection: moving towards smartphone-based immunoassays, *Anal Bioanal Chem* **2018**, *410*, 5353-5371, 10.1007/s00216-018-0989-7.
5. Charlermroj, R.; Oplatoowska, M.; Kumposiri, M.; Himananto, O., et al. Comparison of techniques to screen and characterize bacteria-specific hybridomas for high-quality monoclonal antibodies selection, *Anal. Biochem.* **2012**, *421*, 26-36, 10.1016/j.ab.2011.10.005.
6. Wassaf, D.; Kuang, G.; Kopacz, K.; Wu, Q.-L., et al. High-throughput affinity ranking of antibodies using surface plasmon resonance microarrays, *Anal. Biochem.* **2006**, *351*, 241-253, 10.1016/j.ab.2006.01.043.
7. Markwalter, C.F.; Jang, I.K.; Burton, R.A.; Domingo, G.J., et al. Biolayer interferometry predicts ELISA performance of monoclonal antibody pairs for *Plasmodium falciparum* histidine-rich protein 2, *Anal. Biochem.* **2017**, *534*, 10-13, 10.1016/j.ab.2017.07.010.
8. Liu, M.; Zeng, L.-F.; Yang, Y.-J.; Hu, L.-M., et al. Fluorescent microsphere immunochromatographic assays for detecting bone alkaline phosphatase based on biolayer interferometry-selected antibody, *RSC Advances* **2017**, *7*, 32952-32959, 10.1039/c7ra03756b.
9. Patching, S.G. Surface plasmon resonance spectroscopy for characterisation of membrane protein-ligand interactions and its potential for drug discovery, *Biochim. Biophys. Acta* **2014**, *1838*, 43-55, 10.1016/j.bbamem.2013.04.028.
10. Ndao, D.H.; DT. López-Deber, MP. Davranche, A. Pfeifer, A. Muhs, A. . Binding Affinity Measurement of Antibodies from Crude Hybridoma Samples by SPR., *Bio-protocol* **2014**, *4*, 1-8, 10.21769/BioProtoc.1276.
11. Canziani, G.A.; Klakamp, S.; Myszka, D.G. Kinetic screening of antibodies from crude hybridoma samples using Biacore, *Anal. Biochem.* **2004**, *325*, 301-307, 10.1016/j.ab.2003.11.004.
12. Leonard, P.; Säfsten, P.; Hearty, S.; McDonnell, B., et al. High throughput ranking of recombinant avian scFv antibody fragments from crude lysates using the Biacore A100, *J Immunol Methods* **2007**, *323*, 172-179, 10.1016/j.jim.2007.04.010.
13. Yakes, B.J.; Buijs, J.; Elliott, C.T.; Campbell, K. Surface plasmon resonance biosensing: Approaches for screening and characterising antibodies for food diagnostics, *Talanta* **2016**, *156-157*, 55-63, 10.1016/j.talanta.2016.05.008.

14. Féraudet-Tarisse, C.; Mazuet, C.; Pauillac, S.; Krüger, M., et al. Highly sensitive sandwich immunoassay and immunochromatographic test for the detection of Clostridial epsilon toxin in complex matrices, *PLoS One* **2017**, *12*, 1-23, 10.1371/journal.pone.0181013.
15. Wang, Y.; Li, Z.; Pei, Y.; Li, Q., et al. Establishment of a Lateral Flow Colloidal Gold Immunoassay Strip for the Rapid Detection of Soybean Allergen β -Conglycinin, *Food Analytical Methods* **2017**, *10*, 2429-2435, 10.1007/s12161-017-0800-y.
16. McWilliam, V.; Koplin, J.; Lodge, C.; Tang, M., et al. The Prevalence of Tree Nut Allergy: A Systematic Review, *Curr. Allergy Asthma Rep.* **2015**, *15*, 1-54, 10.1007/s11882-015-0555-8.
17. Ching, K.H. In *ELISA: Methods and Protocols*, Hnasko, R., Ed.; Springer New York: New York, NY, 2015, pp 127-137.
18. Hsieh, H.V.; Dantzler, J.L.; Weigl, B.H. Analytical Tools to Improve Optimization Procedures for Lateral Flow Assays, *Diagnostics* **2017**, *7*, 1-29, 10.3390/diagnostics7020029.
19. Abdiche, Y.N.; Yeung, A.Y.; Ni, I.; Stone, D., et al. Antibodies Targeting Closely Adjacent or Minimally Overlapping Epitopes Can Displace One Another, *PLoS One* **2017**, *12*, doi:10.1371/journal.pone.0169535, 10.1371/journal.pone.0169535.
20. Abdiche, Y.N.; Miles, A.; Eckman, J.; Foletti, D., et al. High-Throughput Epitope Binning Assays on Label-Free Array-Based Biosensors Can Yield Exquisite Epitope Discrimination That Facilitates the Selection of Monoclonal Antibodies with Functional Activity, *PLoS One* **2014**, *9*, doi:10.1371/journal.pone.0092451, 10.1371/journal.pone.0092451.
21. Bergström, G.; Mandenius, C.-F. Orientation and capturing of antibody affinity ligands: Applications to surface plasmon resonance biochips, *Sensors Actuators B: Chem.* **2011**, *158*, 265-270, 10.1016/j.snb.2011.06.017.
22. Posthuma-Trumpie, G.A.; Wichers, J.H.; Koets, M.; Berendsen, L.B.J.M., et al. Amorphous carbon nanoparticles: a versatile label for rapid diagnostic (immuno)assays, *Anal Bioanal Chem* **2012**, *402*, 593-600, 10.1007/s00216-011-5340-5.
23. Nguyen, H.; Sung, Y.; O'Shaughnessy, K.; Shan, X., et al. Smartphone Nanocolorimetry for On-Demand Lead Detection and Quantitation in Drinking Water, *Anal. Chem.* **2018**, *90*, 11517-11522, 10.1021/acs.analchem.8b02808.
24. Gómez-Arribas, L.N.; Benito-Peña, E.; Hurtado-Sánchez, M.d.C.; Moreno-Bondi, M.C. Biosensing Based on Nanoparticles for Food Allergens Detection, *Sensors (Basel, Switzerland)* **2018**, *18*, 1087, 10.3390/s18041087.
25. Blom, M.M.-H., AD. van Os-Medendorp, H. van Duijn, G. de Zeeuw-Brouwer, Ml. Versluis, A. Castenmiller, J.J.M. Noteborn, H.P.J.M. Kruizinga, AG. Knulst, AC. Houben, GF. . Accidental food allergy reactions: products and undeclared ingredients., *J Allergy Clin Immunol* **2018**, [in press], 865-875, 10.1016/j.jaci.2018.04.041.
26. Drs, E.; Baumgartner, S.; Bremer, M.; Kemmers-Voncken, A., et al. Detection of hidden hazelnut protein in food by IgY-based indirect competitive enzyme-immunoassay, *Anal. Chim. Acta* **2004**, *520*, 223-228, 10.1016/j.aca.2004.04.054.
27. Bremer, M.G.E.G.; Smits, N.G.E.; Haasnoot, W. Biosensor immunoassay for traces of hazelnut protein in olive oil, *Anal Bioanal Chem* **2009**, *395*, 119-126, 10.1007/s00216-009-2720-1.

28. Raz, S.L., H. Norde, W. Bremer, MGEG. Food allergen profiling with an imaging surface plasmon resonance-based biosensor *Anal. Chem.* **2010**, *82*, 8485-8491, 10.1021/ac101819g.
29. Hounkamhang, N.; Vongsakulyanon, A.; Peungthum, P.; Sudprasert, K., et al. ABO blood-typing using an antibody array technique based on surface plasmon resonance imaging, *Sensors (Basel, Switzerland)* **2013**, *13*, 11913-11922, 10.3390/s130911913.
30. Trilling, A.B., J. Zuilhof, H. . Antibody orientation on biosensor surfaces: a minireview, *Analyst* **2013**, *138*, 1619-1627.
31. Coskun, A.F.; Wong, J.; Khodadadi, D.; Nagi, R., et al. A personalized food allergen testing platform on a cellphone, *Lab Chip* **2013**, *13*, 636-640, 10.1039/c2lc41152k.
32. Ludwig, S.K.J.; Tokarski, C.; Lang, S.N.; van Ginkel, L.A., et al. Calling Biomarkers in Milk Using a Protein Microarray on Your Smartphone, *PLoS One* **2015**, *10*, 10.1371/journal.pone.0134360, 10.1371/journal.pone.0134360.

Supplementary information

Chapter 3

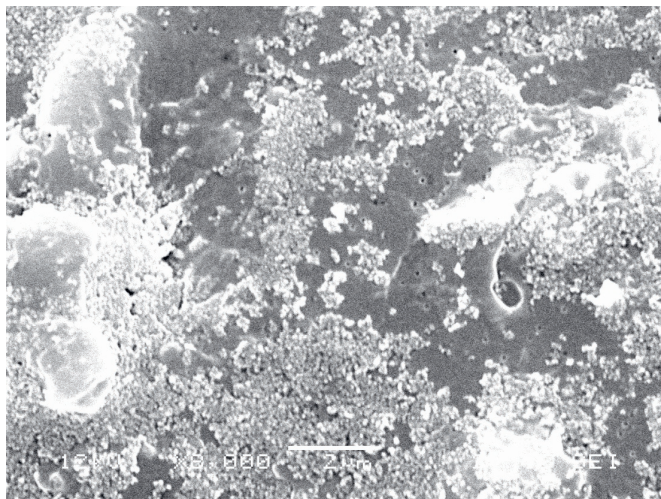


Figure S3.1. Scanning electron microscope (SEM) image of the carbon nanoparticles conjugated to 50-6B12. The images were made by drying a suspension of (1 in 5 dilution of conjugate in 100 mM borate buffer) carbon-50-6B12 onto a Millipore polycarbonate GTTP filter (nominal pore size 0.1 μm) and sputtering it with a fine coating of gold. The SEM conditions were a charge of 12 kV and a magnification of x 8,000. The conjugates are represented by the white grape like structures.

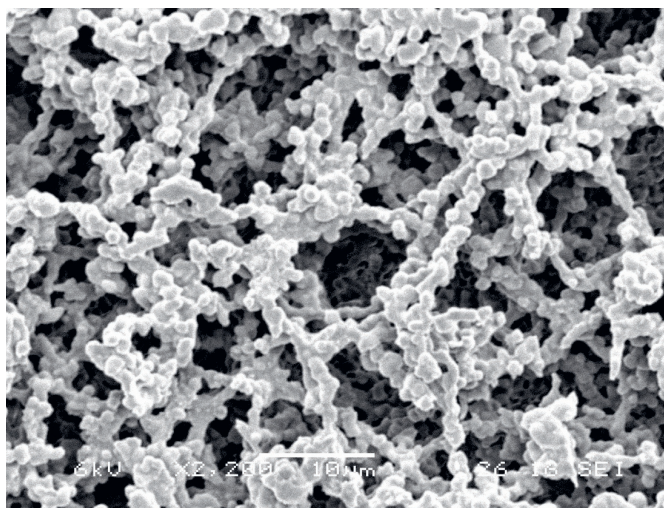


Figure S3.2. SEM image of HF13502XSS nitrocellulose membrane. The SEM conditions for this image were a charge of 6 kV and a magnification of x2,200.

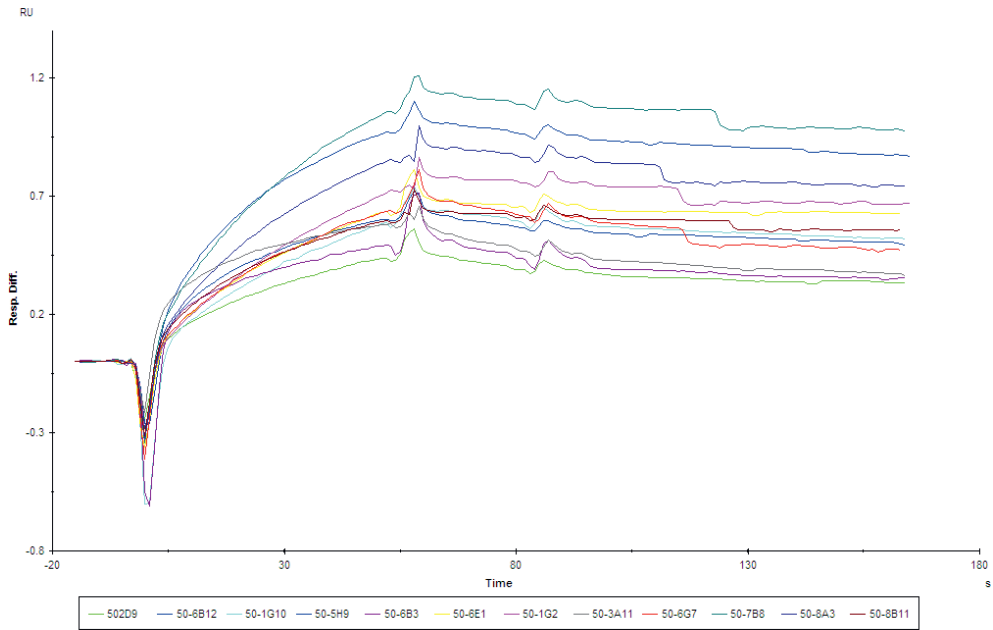


Figure S3.3. Overlay sensorgrams of 12 different hazelnut antibodies towards hazelnut.

Table S3.1. Cross-reactivity of different anti-hazelnut antibodies towards different tree-nut allergen extracts

mAb	Peanut	Pecan	Cashew	Almond	Walnut
50-7B8	N/A	0	N/A	0	17
50-6B12	N/A	4.5	N/A	0	3
50-5H9	N/A	4.7	N/A	2	4.5
50-3A11	N/A	17	N/A	1.7	13
50-2D9	N/A	42	N/A	4	125

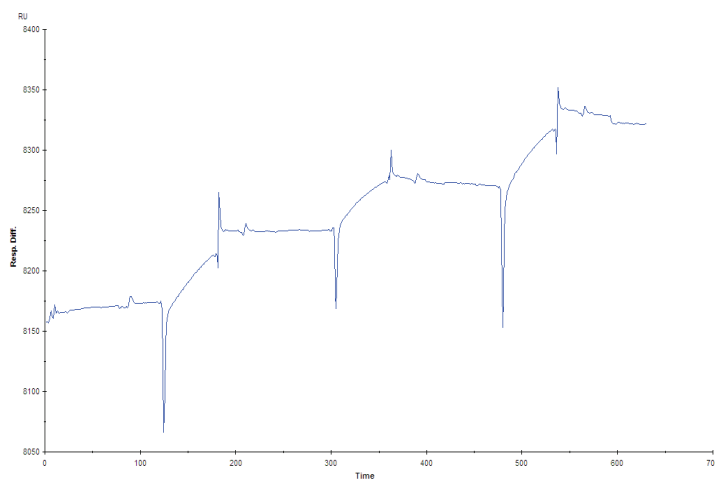


Figure S3.4. Sensorgram depicting the sandwich pairing between 50-5H9 and itself, where the first curve represents the capture of 50-5H9, and the second curve the binding of hazelnut towards 50-5H9 and the third the subsequent binding of 50-5H9.

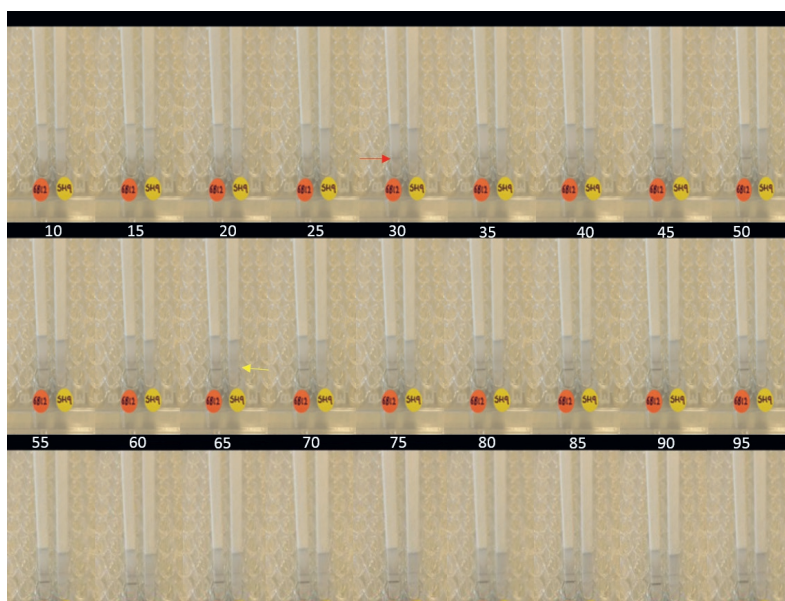


Figure S3.5. Screenshots from smartphone video recording made at 5 second intervals. Lateral flow immunoassay kinetic experiments. Time resolved photos of the appearance of the test and control lines on F-50-6B12 (red) and S-50-5H9 (yellow) LFIA strips. Screen shots taken from the smartphone video recording at 5 second intervals. A clear positive result can be seen for the F-50-6B12 strips within 30 seconds (indicated by red arrow) whilst a positive result for S-50-5H9 can only be seen after 60 seconds (indicated by yellow arrow).

CHAPTER 4

4

A critical comparison between flow-through and lateral flow immunoassay formats for visual and smartphone-based multiplex allergen detection

Adapted from:

Ross, G.M.S., Salentijn, G.IJ., Nielen, M.W.F., 2019. A critical comparison between flow-through and lateral flow immunoassay formats for visual and smartphone-based multiplex allergen detection. Biosensors. 9(4). 143. doi: 10.3390/bios9040143

Background: The lack of globally standardized allergen labeling legislation necessitates consumer-focused multiplexed testing devices. These should be easy to operate, fast, sensitive and robust. **(2) Methods:** Herein, we describe the development of three different formats for multiplexed food allergen detection, namely active and passive flow-through assays, and lateral flow immunoassays with different test line configurations. **(3) Results:** The fastest assay time was 1 min, whereas even the slowest assay was within 10 min. With the passive flow approach, the limits of detection (LOD) of 0.1 and 0.5 ppm for total hazelnut protein (THP) and total peanut protein (TPP) in spiked buffer were reached, or 1 and 5 ppm of THP and TPP spiked into matrix. In comparison, the active flow approach reached LODs of 0.05 ppm for both analytes in buffer and 0.5 and 1 ppm of THP and TPP spiked into matrix. The optimized LFIA configuration reached LODs of 0.1 and 0.5 ppm of THP and TPP spiked into buffer or 0.5 ppm for both analytes spiked into matrix. The optimized LFIA was validated by testing in 20 different blank and spiked matrices. Using device-independent color space for smartphone analysis, two different smartphone models were used for the analysis of optimized assays.

1 Introduction

Food allergens are naturally occurring proteins present in a multitude of foods. Individuals with a food allergy are sensitized towards these proteins, and exposure to them can lead to adverse, sometimes life-threatening, health effects¹. The majority of food allergen-related anaphylaxis in Europe can be attributed to peanut and tree nut allergens². Allergies towards peanuts and tree nuts commonly co-exist, making the simultaneous detection of these problematic allergens desirable^{3,4}.

The only way for allergic individuals to avoid an allergic reaction is for them to stick to an avoidance diet. Such diets are largely reliant upon proper allergen labeling of food products. However, currently in the European Union (EU), only ingredients which have been intentionally incorporated into a food require labeling^{5,6}. This means that allergens that are unintentionally present in food, such as via cross contamination, do not need to be declared, with all associated risks for allergic consumers. As a result, many food manufacturers use voluntary precautionary allergen labeling (PAL) (e.g., 'may contain' statements) in order to safeguard consumers⁷. In theory, PAL statements protect the consumer from potential allergic reactions; in reality the over-use of unregulated PAL has resulted in consumers choosing to ignore these warning statements⁸. Therefore, it is imperative to engage the public with their own food allergen analysis by developing consumer-friendly detection methods^{9,10}. The cornerstones to consumer-friendly allergen detection are speed, sensitivity, ease-of-use, affordability, portability, multiplexing capability and a simple read-out system. Although some specifically consumer-oriented allergen sensors are available, such as the portable gluten and peanut sensors from NIMA, more often these biosensors are still proof-of-concept assays rather than commercial tests designed for consumers¹¹⁻¹⁴, and generally they lack multiplexing and proper validation as screening methods. A shared characteristic of novel allergen detection is the increasing trend to utilize a smartphone as an interface and readout system^{9,14-17}. Using a smartphone readout improves the overall ease of result interpretation by introducing an interface that the consumer is already familiar with, alongside providing a means to wirelessly transmit results to relevant stakeholders, such as food manufacturers and restaurant personnel¹⁸. The Lateral Flow Immunoassay (LFIA) is widely considered the gold standard for easy-to-use, low-cost, sensitive and quick screening for food safety issues. Despite their widespread application, allergen LFIAs are often based on the analysis of a single analyte, owing to the difficulties associated with multiplexing an LFIA, including the need for careful design of test line configuration to prevent upstream detection areas from affecting downstream detection areas^{19,20}. Most multiplex LFIAs for food safety focus upon the detection of low-molecular weight compounds, such as antibiotics and mycotoxins^{21,22}. However, this past year has seen an increase in the development of multiplex food allergen detection LFIAs, with the development of an assay for the detection of hazelnut, ovalbumin and casein in

bakery products within 10 min²³. A further example is the multiplex, low-ppm detection of both β -lactoglobulin and β -casein, two major allergenic milk proteins, within 10 min²⁴.

A major drawback typically associated with LFIAs is the assay duration, which usually is 10–20 min, and is affected by mass transport limitations (MTL) and binding kinetics²⁵. MTLs are caused by the fact that the target analytes need to be carried across a porous membrane, such as nitrocellulose (NC) by passive, capillary flow, and thus affect the detection speed of the assay²⁶. The NC capillary flow rate is measured in the time in seconds it takes the sample front to travel 4 cm. Selection of NC based on this capillary flow rate is a compromise between assay sensitivity and assay speed with mid-speed membranes (120–150 s/4 cm) offering advantages in both areas. When detection speed is not a constraint, a membrane with a slower flow rate and smaller pore size increases the available binding time between the labeled antibody–analyte and the test line antibody which can result in increased assay sensitivity^{27–29}. In order to speed up LFIAs, in combination with NC with a good flow rate, antibodies with fast association rates towards their target should be used. Antibodies can be selected for their binding kinetics by in depth surface plasmon resonance (SPR)-based antibody screening and characterization. In this way a carbon nanoparticle-based hazelnut allergen LFIA has been developed, with a 30 s assay time, which as far as we know is a world record for allergen assay speed³⁰.

In order to overcome restrictions typically associated with LFIAs, a flow-through immunoassay format can be used instead^{31,32}. Flow-through immunoassays are reported to offer the benefits of increased assay speeds, better sensitivities—owing to the use of larger sample volumes, excellent multiplexing capabilities and the absence of the ‘hook-effect’^{27,33,34}. The hook-effect is a phenomenon that is commonly encountered in one-step, sandwich format LFIAs. It occurs where the free analyte and the analyte which is bound to a labeled antibody compete for the limited number of binding sites available on immobilized capture antibodies, leading to a reduction in colorimetric signal and sometimes false negative results^{24,35,36}. Therefore, if the correct assay working range is not determined, it could lead to consumers erroneously believing a food with a high allergen content is safe. Flow-through assays can be prepared in different ways. Passive flow-through assays consist of LFIA materials, but in a stacked arrangement, with the membrane biofunctionalized with capture antibodies on top, and the conjugate and absorbent pads layered underneath or as flow-through enzyme-linked immunosorbent assays (ELISAs)^{37–39}. An alternative flow-through approach is to insert a biofunctionalized membrane into a syringe filter holder, applying manual or mechanical pressure to the syringe to actively control the vertical flow of the reagents and the sample^{40,41}. Although flow-through formats generally allow greater freedom in geometric assay design, they are prone to inter/intra-user variability⁴².

The lack of agreed regulatory allergen thresholds has stalled the development of certified reference materials, preventing true comparisons to be made between various detection methods by different kit manufacturers and researchers⁴³. Therefore, in this study, we use the same bioreagents to compare different geometrically designed, paper-based, flow-through and lateral flow immunoassay configurations for the simultaneous detection of hazelnut and peanut allergens with a smartphone readout system.

2 Materials and Methods

2.1 Reagents and Consumables

Washing buffer (WB) was composed of 5 mM borate buffer (BB) (pH 8.8) diluted from a mixture of 100 mM sodium tetraborate (VWR, Leuven, Belgium) and 100 mM boric acid (Merck, Darmstadt, Germany) and bovine serum albumin (BSA; Sigma-Aldrich, Zwijndrecht, The Netherlands) was added to a final concentration of 1% (w/v). Storage buffer (SB) consisted of 100 mM BB containing BSA to a final concentration of 1% (w/v). Running buffer (RB) was prepared by adding 1% BSA (w/v) and 0.05% Tween-20 (v/v) (Merck, Darmstadt, Germany) to 100 mM BB. Phosphate buffered saline (PBS; 0.01 M; pH 7.4) was purchased from Sigma-Aldrich (Sigma-Aldrich, Zwijndrecht, The Netherlands). All solutions were prepared with water from a MilliQ-system (MQ) (>18.2 MΩ/cm) purchased from Millipore (Burlington, MA, USA). 'Spezial Schwartz 4' carbon nanoparticles were purchased from Degussa AG (Frankfurt, Germany). Goat anti-mouse IgG in PBS (pH 7.6) (1.2 mg/mL; AffiniPure F(ab')₂ Fragment GAM IgG Fcy) used for spraying control lines/spots was purchased from Jackson ImmunoResearch Laboratories Inc. (Sanbio, Uden, The Netherlands). The hazelnut (50-6B12) and peanut (51-2A12 and 51-12D2) antibodies were developed by Wageningen Food Safety Research (WFSR), Wageningen University and Research (Wageningen, The Netherlands) according to the procedure described by Bremer et al⁴⁴. All antibodies were buffer exchanged from PBS (pH 7.4) into 5 mM BB (pH 8.8) using Zeba™ Spin Trap columns (Thermo Scientific; Landsmeer, The Netherlands) prior to use. Passive flow-through assays were developed from a Miriad Rapid Vertical Flow toolkit (MedMira, Halifax, NS, Canada). All active flow-through assays were developed on unbacked Whatman 0.45 μm nylon (GE Healthcare, Eindhoven, The Netherlands) 0.45 μm NC or 0.2 μm NC membranes and inserted into 13 mm Swinny syringe filter holders (Merck, Darmstadt, Germany). The assembled filter holder was attached to a 10 mL syringe (Becton-Dickinson, Utrecht, The Netherlands). Lateral flow immunoassays (LFIA) were developed on 140 CN nitrocellulose membranes (Unisart, Sartorius, Gottinghem, Germany) secured on a plastic backing (G and L, San Jose, CA, USA) overlaid with an absorbent pad (Whatman, GE Healthcare, Eindhoven, The Netherlands). All LFIA were heat-sealed in foil packets with silica beads and stored at room temperature until use.

2.2 Allergen Extraction

Currently, a drawback in allergen detection is that no certified, standardized reference materials are commercially available, and antigen standards and blank matrices need to be prepared in-house⁴⁵. The influence of food processing on the protein conformation of allergens can affect their detectability⁴⁶, but this was not explicitly investigated in this study, as the focus was comparing the performance of the same antibodies applied in different immunoassay formats.

Extracts were made from hazelnuts, peanuts, blank flour, peanut-spiked flour (8 ppm) and 20 truly different biscuits (i.e., 20 different brands and varieties; see Supplementary Information (SI), Table S5.1) free from peanuts/tree-nuts, which were supplied by project partners or purchased from local supermarkets. Raw hazelnuts and unsalted peanuts were frozen whole at -80°C for 1 h. The frozen foods were homogenized using a commercial hand blender (Braun Turbo 600 W Food Processor, Braun, Oss, The Netherlands). A total protein extract was made by adding 10 mL PBS (pH 7.4) per gram of ground sample and incubating at room temperature for 1 h. Following incubation, extracts were centrifuged at $3220\times g$ for 20 min. The extracts were then filtered through a series of low protein-binding syringe filters ($5\ \mu\text{m} > 1.2\ \mu\text{m} > 0.45\ \mu\text{m}$), and the filtrate was aliquoted and stored at -20°C until use. To ensure sample stability, fresh aliquots were defrosted daily for experiments, and protein concentrations were determined using the NanoDrop ND 3300 (Isogen Life Sciences, De Meern, The Netherlands) prior to use. Blank biscuits were homogenized by agitating 0.5 g in a 50 mL tube with ball bearings to a fine powder. Next, 5 mL of 100 mM borate buffer was added to the tubes and agitated for 1 min with the powdered biscuit or flour. The suspension was left at room temperature for 25 min. Afterwards, extracts were filtered through a series of low protein-binding syringe filters ($5\ \mu\text{m} > 1.2\ \mu\text{m} > 0.45\ \mu\text{m}$), aliquoted and stored at -20°C until use. All experiments, except for matrix experiments, were performed using total hazelnut protein (THP) and total peanut protein (TPP) spiked into running buffer. For matrix experiments, 1 μL of 1000 ppm THP and TPP extract was spiked into 999 μL (v/v) of the 20 different blank biscuit extracts.

2.3 Carbon Black Nanoparticle Conjugation

A 1% suspension of carbon nanoparticles (CNPs) was prepared by adding 1 mL of MQ Water to 10 mg carbon and sonicating for 10 min. The resulting 1% carbon suspension was diluted five times in 5 mM BB (pH 8.8) to obtain a 0.2% suspension, which was then sonicated for 5 min. Next, 350 μL purified hazelnut or peanut antibody solution (1 mg/mL in 5 mM BB) was added to 1 mL (to make a total volume of 1.35 mL) of 0.2% carbon suspension and stirred overnight at 4°C . The suspension was split into approximately two equal aliquots (670 μL), and 500 μL of WB was added to each before centrifuging them for 15 min at $13,636\times g$ at 4°C . Following this, the supernatants were removed, and the pellets re-suspended in WB. This process was repeated three times. After the final wash,

the supernatants were discarded, and the pellets were pooled together with 1 mL storage buffer and stored at 4 °C until use.

2.4 Multiplex Passive Flow-Through

The plastic cartridge, biofunctionalized membrane and absorbent pad (absorption volume of 200 μ L) from a Miriad Rapid Vertical Flow technology toolkit was used to create the passive flow-through assays. A schematic representation of the passive flow-through assay is shown in Figure 4.1A.

The membranes were biofunctionalized by manually depositing 0.5 μ L of the peanut, hazelnut and control antibody solutions (1 mg/mL) in three distinct regions using a pipette. The tip of the pipette was touched very lightly against the membrane to dispense a consistent antibody spot. The membranes were dried for 45 min. Once dried, three drops of RB were added via a dropper bottle and allowed to saturate the membrane. Immediately after, 50 μ L of the mixed allergen extract (diluted in RB; 1000 ppm, 100 ppm, 10 ppm, 1 ppm, 0.1 or 0 ppm) was pipetted dropwise onto the membrane and allowed to absorb fully. Next, a 10 μ L suspension of 10 \times diluted carbon labeled-monoclonal antibodies (CNP-mAbs) was pipetted onto the membrane and allowed to absorb fully. Finally, three drops of RB were applied to wash the membranes. The assays were read immediately with the naked eye and an image was acquired with a smartphone camera. LOD values for visual inspection were established at the lowest concentration that reproducibly yielded a signal that could be observed and distinguished from the background by the naked eye.

2.5 Multiplex Active Flow-Through

A schematic representation of the active flow-through assay is shown in Figure 4.1B. First, the most appropriate assays parameters were established including membrane type, pore size, antibody concentration for dispensing and assay conditions.

2.5.1 Simplified Multiplex Flow-Through

Allergen-specific antibody solutions (0.5 μ L of 1 mg/mL mAb solution) and control antibody solution were manually dispensed by lightly touching the tip of the pipette to the membrane onto 0.2 or 0.45 μ m pore size unbacked NC or 0.45 μ m unbacked nylon membranes. The membranes were dried for 45 min and then the membranes were placed in 13 mm syringe filter holders and attached to the 10 mL syringe. The assays were performed by manually and sequentially injecting 500 μ L sample (concentration series 100–0.1 ppm total protein extract diluted in RB), 1 μ L of each CNP-mAb and another 300 μ L of RB as a washing step. In this context, sequentially refers to the sequential loading of the syringe with sample with the CNP-mAbs on top of the sample; these were then pushed through by moving the plunger downwards in a single movement, followed by a final washing step with RB. The membranes were then removed from the filter holder,

dried for 5 min, read with the naked eye and an image was acquired with a smartphone camera.

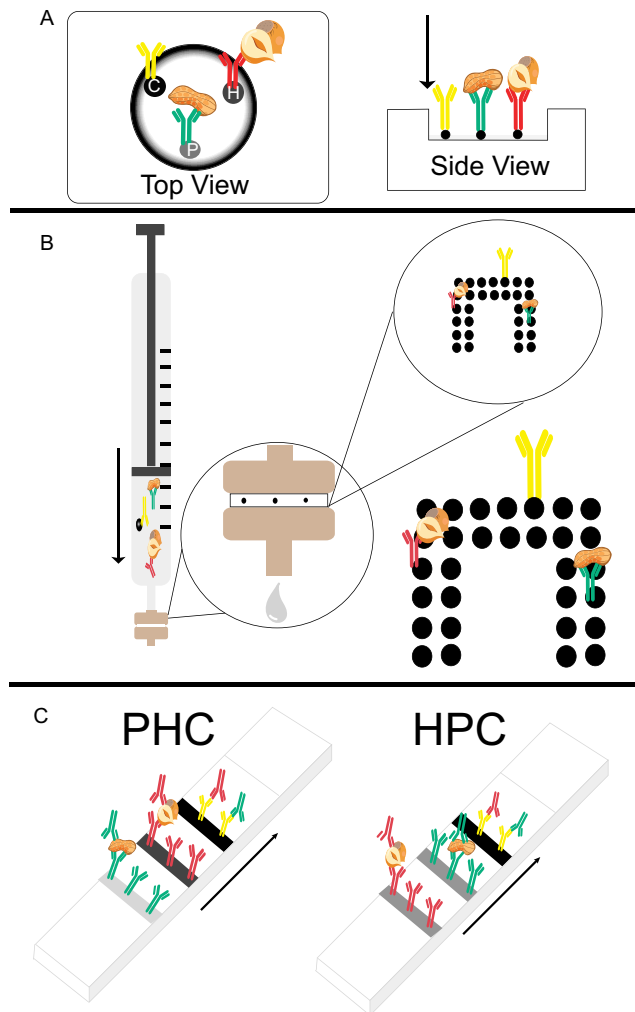


Figure 4.1. Schematic representation (not to scale) of the three flow assay formats developed. Arrows depict the flow direction and C is the control antibody (goat anti-mouse), H is the anti-hazelnut antibody and P is the anti-peanut antibody. Total hazelnut protein (THP) is indicated by the hazelnut graphic and total peanut protein (TPP) is indicated by the peanut graphic. (A) The passive flow assay in top-view and side-view. (B) The active format flow-through assay, where the syringe filter holder is enlarged, and the membrane is further enlarged to show the biofunctionalized area. (C) Both lateral flow immunoassay geometries as defined by the order in which sample will encounter the test and control lines: peanut, hazelnut, control (PHC) and hazelnut, peanut, control (HPC).

2.5.2 Multiplex Flow-Through Iterative Optimization

To establish the optimum active flow-through conditions, a number of alternative assay steps were explored. The experiments aimed to reduce background staining, to improve the signal-to-noise ratio and to improve the assay sensitivity.

2.5.3 Volume Optimization

Different sample and reagent volumes were tested to determine the optimum conditions for flow-through operation. Flow-through assays require larger sample volumes compared with LFIA due to reduced contact time between analyte and capture antibodies⁴². When using sample volumes of less than 500 μL , it was necessary to first 'pre-wet' the membrane with running buffer to ensure that the entire surface would be wetted. Initially, membranes were tested using 500 μL RB, followed by a 300 or 500 μL sample and 0.5 μL of each of the CNP-mAbs solutions followed by 500 μL RB as a washing step. In subsequent experiments, the volume of the CNP-mAb solution was increased to 1 μL for each CNP-mAb to maximize the signal intensity. Finally, experiments were performed using 1 mL of sample, with 1 μL of each CNP-mAb solution dispensed on top of the sample, followed by 500 μL RB.

2.5.4 Pre-Mix Method

The assays were tested by pre-mixing the running buffer and CNP-labeled secondary mAbs with sample and injecting the mixture simultaneously. In this approach, 1 mL of sample, 1 mL of RB and 1 μL of each CNP-mAb were injected across the membrane, effectively causing an additional 50% dilution to the sample, when compared to the sequential method described above. The holder was then dismantled, and the membrane dried for 5 min before visual inspection.

2.5.5 Filter Approach

To improve the uniform wetting of the membrane and reduce the background staining caused by the CNPs, a filter approach was tested. In this method, a 0.45 μm NC filter was placed on top of the functionalized membrane before carrying out the assay sequentially. Following the final wash step, the device was disassembled, the 0.45 μm filter carefully removed and disposed of and the membrane dried for 5 min before visual inspection.

2.5.6 Aspiration Approach

To ensure sufficient wetting of the membrane, and to increase the contact time of the sample and the capture antibodies, an iterative aspiration approach was applied. In this way, when sequentially injecting the sample and CNP-mAbs, the plunger of the syringe was pumped up and down, 1, 5 or 10 times. With the increasing number of aspirations, the flux of the analyte past the membrane, and thus past the immobilized antibodies, was increased. After the final aspiration, the RB was flowed through as a washing step, the

device was disassembled, and the membrane dried for 5 min before visual inspection and photographing with a smartphone camera.

2.5.7 Multiplex Array Layout

The flow-through array was spotted using the XYZ 3060 BioDot Dispense Platform (Irving, CA, USA). The array was composed of 14 (2×7 array) control spots (0.25 mg/mL) and with each analyte having 12 (2×6 array) spots (0.25 mg/mL), with a drop size of 100 nL and an offset of 1 mm between each dot (see Figure 4.1B). The membranes were left to dry overnight prior to testing.

2.5.8 Optimized Active Flow-through Operation Protocol

A 0.45 μm NC filter, acting as a vertical flow diffuser, was placed on top of the biofunctionalized membrane. The filter and membrane were then placed, biofunctionalized side up, into the syringe filter holder. A polytetrafluoroethylene (PTFE) gasket was placed on top of the membrane to seal the fluid pathway, giving the assay an actual flow path of 10 mm. The syringe holder was then attached to a 10 mL Luer-Lock™ syringe. The assay was performed sequentially as described in Section 2.5.1. First, 1 mL of sample topped with 1 μL of each CNP-mAb solution was aspirated 10 times across the membrane (only THP or only TPP or mixture of both diluted in RB at 100, 10, 1, 0.1 and 0 ppm). Following this, 500 μL RB, as a washing buffer, was flowed through the membrane. Finally, the syringe filter holder was disassembled, and the membrane removed and placed on an absorbent pad for drying. To determine whether the immobilized test antibodies suffered from non-specific binding towards the other target, the assays were tested using just THP or just TPP extract spiked into RB. Blank buffer measurements were performed 10 times to test for false positives. The membranes were visually inspected and photographed with a smartphone camera after 5 min. LOD values for visual inspection were established at the lowest concentration that reproducibly yielded a signal that could be observed and distinguished from the background by the naked eye.

2.6 Multiplex Lateral Flow Immunoassay

Lateral flow immunoassays were manufactured using NC (flow rate of 140 s/4 cm) cut to approximately 4 cm length. The NC membrane was secured on a plastic backing, with 4.5 cm of absorbent pad overlapping one end of the NC. Two different test line configurations (as depicted in Figure 4.1C) were designed and produced using the XYZ BioDot dispensing platform. The first configuration had the control line (0.25 mg/mL) dispensed at 10 mm from the absorbent pad, the hazelnut line (0.25 mg/mL) at 5 mm from the control line and the peanut line at 5 mm from the hazelnut line, with 10 mm of blank membrane at the bottom of the strip, hereafter referred to as PHC. The second arrangement had the control line at 10 mm from the absorbent pad, the peanut line at 5 mm from the control line and

the hazelnut line at 7 mm from the peanut line with 8 mm of blank membrane at the bottom of the strip, hereafter referred to as HPC.

2.6.1 Multiplex LFIA Operation Protocol

Firstly, the multiplex LFIAs were tested for non-specific binding by testing 10 × each of the LFIAs in blank running buffer (RB). The LFIAs were inserted into individual microwells of a 96-well plate containing 1 μL of each of the CNP-mAbs and 100 μL of RB (blank). The strips were left to run for 5 min. Next, the LFIAs were tested for specificity by testing in either just THP or TPP extract spiked into RB. LFIAs were placed into the individual microwells of a 96-well plate containing either just THP or TPP (1 μL) spiked into RB, in decreasing concentration with RB (99 μL) and 1 μL of each carbon-labeled mAb. The strips were left to run for 5 min before photographing with a smartphone camera. Finally, the assays were tested using the same conditions in decreasing concentrations (100, 10, 1, 0.5, 0.1 ppm) of both THP and TPP spiked in RB (in triplicate). Calibration series were tested with both formats of the LFIA using (i) 1 μL of sample (diluted in RB) and 99 μL of RB (hereafter, 1:99, sample: RB), (ii) 25 μL of sample (diluted in RB) and 75 μL of RB (hereafter, 25:75, sample: RB), and (iii) 75 μL sample (diluted in RB) and 25 μL of RB (hereafter, 75:25, sample: RB). The 75:25 sample: RB experiments were specifically designed to trigger the hook-effect to determine when the sample volume becomes the limiting factor. The membranes were visually inspected and photographed with a smartphone camera after running for 5 min. LOD values for visual inspection were established at the lowest concentration that reproducibly yielded a signal that could be observed and distinguished from the background by the naked eye.

2.6.2 Smartphone Readout and Data Analysis

Smartphone photographs were acquired using Open Camera (version 4.0.3) and analyzed using a Huawei P20 smartphone (Huawei Technologies, Shenzhen, China) using two freely downloadable apps from the Google Play Store. The red, green, blue (RGB) values were obtained for test regions of assays using the RGB Color Detector (version 1.0.58). Using the crosshair function in the app, test dots on the flow-through membrane or three distinct regions on the test line of the LFIA were selected and the color values were averaged and recorded. Background measurements were also made above and below the test areas to determine an overall background level for subtraction from results.

Alternatively, results were normalized by dividing the value of each test region by the corresponding control region, as has been performed in literature^{35,47,48}. Using 'Nix Pro Color' (version 1.31), the RGB values were converted to luminosity, A, B (LAB) values; a device-independent color space that more accurately represents how humans interpret color intensity. Additionally, to show the device-independent nature of LAB measurements, the optimized assays were also analyzed using a Google Pixel 2 XL smartphone (Google,

Mountain View, CA, USA). The obtained values were used to plot calibration curves for L (luminosity) of the LAB values as a function of allergen concentrations spiked into RB, using Microsoft Excel. LOD values were obtained from these calibration curves by visual evaluation.

2.6.3 Matrix Experiments and Validation

To validate the assays, they were also tested in spiked food matrices. All assays were tested in a decreasing concentration of THP and TPP, spiked directly into a blank biscuit matrix extract to determine the matrix effects. Additionally, the optimized LFIA (PHC) was more extensively validated by testing in 20 truly different blank matrix extracts. In this way, LFIA were placed in individual microwells containing 25 μL blank matrix extract ($n = 20$) and 75 μL RB and left to run for 10 min to determine whether any false positives occurred. Additionally, 1 ppm of THP and TPP was spiked into the 20 different blank matrix extracts (1 μL of 1000 ppm THP and TPP sample into 999 μL (v/v) blank matrix extract) and the LFIA were tested using both 25 μL spiked matrix plus 75 μL RB and 1 μL spiked matrix extract plus 99 μL RB. Assays were left to develop for 10 min. Finally, the optimized LFIA were also tested in blank flour matrix extract and spiked peanut flour matrix extract in both 25:75 and 1:99 dilutions in RB.

3 Results and Discussion

3.1 Multiplex Passive Flow-Through Assay

An overview of conditions, quantitative and qualitative results for spiked buffer experiments for the passive flow-through assay, can be found in Table 4.1. The visual limit of detection (LOD) for the passive flow-through was established by testing in decreasing concentrations of THP and TPP extracts spiked in RB. The visual LODs were determined as 0.1 ppm and 1 ppm and smartphone LODs 1 and 10 ppm for hazelnut and peanut, respectively ($n = 3$), whereas no visible spot was obtained for blanks (see Table 4.1 and SI, Figure S4.1A). Following the addition of the CNP-mAbs to the passive flow-through assay, the positive spots appeared within 5 s, a detection speed which is unparalleled by LFIA.

Even when using the high-speed LFIA described in³⁰ the appearance of the positive result took 30 s, due to MTL limitations of the solution that needs to wick through the membrane before reaching test lines. Three drops of RB were added to the flow-through assay to wash the unbound CNPs from the membrane. Using dropper bottles with pre-defined drop volumes for the delivery of RB makes the assay easy to perform and means that pipettes are unnecessary. A further benefit is that the result can be directly read through the window of the cassette by the naked eye without having to disassemble the device. However, when recording a smartphone image of the membranes, these do need

to be removed from the plastic cassette to avoid shadowing. Despite the washing step, the membranes had variable background staining, which made it impossible to obtain calibration curves from the images acquired with a smartphone.

The reason for the appearance of background staining probably lies with the polydispersity of the CNP, which can form aggregates of several hundred nm, which are too large to be flowed through the pores. A drawback of this specific passive flow assay format is the lack of freedom in geometric assay design as bio-reagents required manual spotting by pipette. However, such a limitation could be easily overcome by biofunctionalization of the membranes before having them cut to the factory-made circular size.

3.2 Multiplex Active Flow-through

An overview of conditions, quantitative and qualitative results for spiked buffer experiments for the active flow-through assay can be found in Table 4.1. The assays using the 0.45 μm pore size nylon and NC membranes were ineffective, and no spots (including control spots) appeared on these membranes. This can be attributed to 0.45 μm being too large a pore size and the majority of the analyte and labeled antibodies passing through the membrane, which is confirmed by the dark coloration of the waste liquid when using this assay membrane. Therefore, the 0.2 μm pore size NC membrane was determined to be the most suitable for this application. During the optimization steps, active flow-through assays were tested using 0.5 μL of each CNP-mAb solution, but this only yielded faint detection spots. In subsequent experiments the volume of the CNP-mAb solution was increased to 1 μL of each CNP-mAb which improved the readability. Additionally, volumes of 500 μL and 1 mL of sample were tested, with the sensitivity improving with the increased sample volume, without the appearance of a hook-effect, even at high concentrations.

Although in this manually spotted initial format, LODs of 0.5 and 0.1 ppm could be reached for peanut and hazelnut (see SI, Figure S4.1B), respectively, false positives were also detected when testing the assays in a blank sample (1 in 5 false positives). Using a pre-mix approach did improve the overall user-friendliness of the assay, as the operator only needed to pass the liquid containing the sample, CNP-labeled mAbs and RB through once without the necessity of removing and reinserting the plunger, but this method consistently resulted in false positives in the blank samples. Contrastingly, using the sequential method increased the difficulty of the assay, but prevented false positives owing to the washing step at the end. The addition of a 0.45 μm NC filter on top of the biofunctionalized membrane increased the (smartphone) readability of the assay.

Table 4.1. Comparison of optimized Flow-through and Lateral Flow parameters

Parameter	Passive flow-through	Active flow-through	PHC**	HPC**
Visual / Smartphone LOD (ppm); Hazelnut (h) Peanut (p)	h: 0.1 / 1 p: 1 / 10	h: 0.05 / 0.5 p: 0.05 / 0.5	h: 0.1 / 0.5 p: 0.5 / 0.5	h: 1 / 5 p: 5 / 10
Working Range (ppm)	1000–0.1	1000–0.05	100–0.1	10,000–0.1
Assay Duration (total assay time, incl. drying)	5 min	10 min	5 min	5 min
Time until result appearance	5 s	5 s	30 s – 1 min	1 min
Extracted volume (µL)	50	1000	25	1
Flexibility of multiplexing	Low—requires manual dispensing bioreagents	High—Printing nL/µL size dots or multi-line	Medium—test line configuration and positioning of antibodies has an influence.	Medium—test line configuration and positioning of antibodies has an influence.
Non-Expert Ease of Use	Easy	Challenging	Easy	Easy
False positives in blank RB (n = number of tested samples within assay working range)	Y (n = 3)	Y (n = 10)	N (n = 10)	N (n = 10)
False negatives in spiked RB (n = number of tested samples within assay working range)	N (n = 3)	N (n = 21)	N (n = 24)	N (n = 18)
Equipment used	Assay cassettes, dropper bottle, pipette	10 mL syringe, syringe filter holder, assay membrane, additional filter, pipette, waste beaker	LFIA, pipettes, microwell plate	LFIA, pipettes, microwell plate
Waste	High plastic consumption (cassettes)	High plastic consumption (syringes) + need for disposal of high volumes liquid waste	Nitrocellulose strips and well plate + disposal of small volume liquid waste	Nitrocellulose strips and well plate + disposal of small volume liquid waste

* All measurements were made using total hazelnut protein and total peanut protein (THP and TPP) spiked into running buffer (RB). ** Where the peanut, hazelnut, control geometry is defined by PHC and the hazelnut, peanut, control geometry is defined by HPC.

Besides filtering the larger sized CNPs, reducing the level of background staining, the filter also acted as a flow diffuser. In this way, uniform wettability of the membrane was achieved, resulting in better reproducibility compared to when it was performed without the filter. Although the filter improved the readability of the membranes, it also further complicated the user-friendliness of the method, as it needed to be carefully removed from the biofunctionalized membrane before the results could be read. The sensitivity of the assay was improved by increasing the number of sample aspirations across the membrane (see SI, Figure S4.2). Flow-through assays are subject to unidirectional flow and require capture antibodies with rapid association rates in order to achieve binding or require extended sample/reagent incubation times. By increasing the number of sample aspirations, the flux of the CNP-mAb-analyte complex past the immobilized antibodies, and the potential of binding, is increased. Of all the tested parameters the most appropriate assay conditions were determined to be a 0.45 μm filter on top a 0.22 μm NC membrane biofunctionalized with 0.25 mg/mL control and test spots and aspirating 1 mL of sample with 1 μL of CNP-mAb solution 10 times back and forth through the membrane. Subsequently, 500 μL of RB was injected as a washing step. Although these conditions allowed for the assay to reach very low LODs, they also meant that this method generated a high volume of chemical waste (1.5 mL), which needs to be safely disposed of.

When testing active flow-through membranes in decreasing concentrations of THP and TPP spiked into RB, visual LODs of 0.05 ppm ($n = 3$) could be reached for both targets, an LOD which is so far un-met by commercially available allergen assays⁸. This LOD is less obvious from the smartphone image (LODs of 0.5 ppm for both THP and TTP) compared with reading by naked eye (see Figure 4.2). Therefore, eye symbols are inserted in Figure 4.2 to designate the lowest concentration that could still be read visually. Despite the active flow-through approach reaching lower LODs than the passive flow-through assay, the assay was more complicated to perform and used a far greater sample volume.

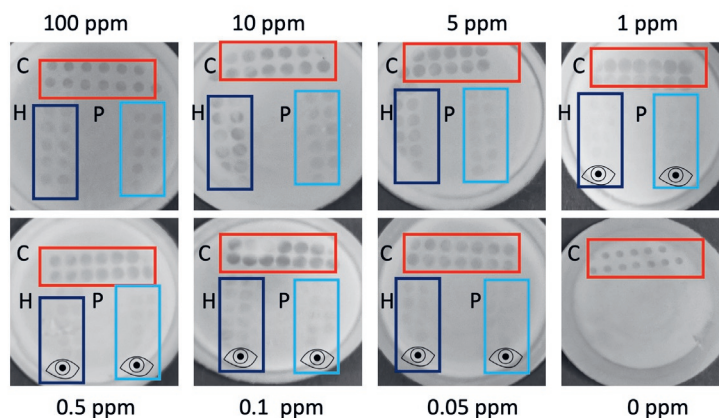


Figure 4.2. Active flow-through assay calibration range. Assays were tested in decreasing concentrations (100–0.05 ppm) of Total Hazelnut Protein (THP), Total Peanut Protein (TPP) spiked into Running Buffer (RB) and in blank RB. The control region is indicated by C and outlined in red, the hazelnut region by H and outlined in dark blue and the peanut region by P and outlined in light blue. There is an evident decrease in test dot intensity as the concentration of total protein in the sample decreases. The eye icon is used to indicate test regions that are visible to the naked eye but more difficult to read in the smartphone image. The visual limit of detection is established at 0.05 ppm for both analytes.

3.3 Multiplex Lateral Flow Immunoassay

An overview of conditions, quantitative and qualitative results for spiked buffer experiments for the LFIA can be found in Table 4.1. The LFIA were both able to achieve single analyte detection and a true blank result every time (0% false positives at 0 ppm; $n = 10$). When testing PHC with 1 μL of sample, 1 μL of each CNP-mAb and 99 μL of RB, visual LODs of 1 and 5 ppm were achieved by the naked eye (see Figure 4.3A) for hazelnut and peanut, respectively, with a clear decrease in intensity in the test line with decreasing concentration of the sample. When the LFIA have a low signal intensity, the naked eye is still superior at distinguishing between a positive or negative signal, and the lower visual LODs are indicated by the eye icon in Figure 4.3. However, these visual readings are performed by a trained person, and the distinction between signal and no signal at the lowest concentrations is not trivial. In comparison, when the same anti-hazelnut antibody was applied in a singleplex LFIA, an LOD of 0.1 ppm in spiked buffer was reached, which suggests that having an additional test line on the LFIA can compromise the overall sensitivity³⁰. Still, the multiplex LODs are in accordance with commercially available allergen single-plex LFIA, which report LODs within this range. However, lack of standardized, certified reference materials in the allergen industry means that each reported assay is developed using antibodies specific to different allergenic components (total soluble protein vs. allergen-specific proteins) and tested and validated using

different analytes^{9,45}, thus underlining that true comparisons can only be made when bioreagents and samples are kept constant, as in this research. To optimize the multiplex LFIA and improve the LOD, the sample volume was increased to 25 μ L (diluted in RB) in 75 μ L RB. By increasing the sample volume to 25 μ L (thus concentrating the sample 25 \times compared with the 1 μ L sample volume) LODs of 0.1 and 0.5 ppm for hazelnut and peanut were reached respectively (see Figure 4.3B).

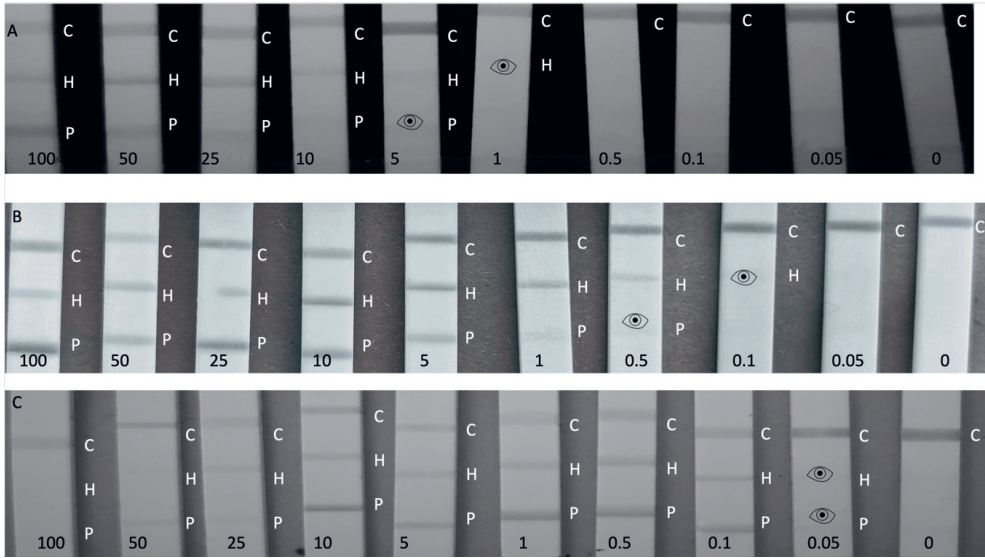


Figure 4.3. Calibration range (100–0.05 ppm) of Total Hazelnut Protein (THP), Total Peanut Protein (TPP) spiked into Running Buffer (RB) and blank RB, where the control line is indicated by C, the hazelnut test line by an H and the peanut test line by a P. A positive result can be still read with the naked eye, but is difficult to see in the smartphone image, thus an eye icon has been used to indicate the visual LOD. (A) Peanut, Hazelnut, Control (PHC) line configuration using 1 μ L of spiked sample and 99 μ L RB. (B) PHC using 25 μ L of spiked sample and 75 μ L RB. (C) PHC using 75 μ L of spiked sample and 25 μ L RB.

Despite the assay sensitivity improving with the increased sample volume, with these conditions at concentrations of 100 ppm and higher, a reduction of the intensity of the upper line (hazelnut) could be observed, as has been witnessed by Galan-Malo et al²⁴. Although this was not considered a false negative, as three distinct lines were still clearly visible, it did warrant further exploration into the extent of the hook-effect in more concentrated samples.

To further investigate the extent of the hook-effect and its potential to limit the upper dynamic range of the LFIA assay, the PHC format was also tested in 75 μ L of sample extract

diluted with 25 μL RB (see Figure 4.3C). These conditions resulted in a more pronounced hook-effect with LFIA tested at 1000 ppm appearing to be false negatives, and at 100–50 ppm exhibiting decreased test line signals. As well as just testing high analyte concentrations, it is important to test different sample-to-RB ratios, as increasing sample volume has a noteworthy influence on the appearance of the hook-effect. In order to avoid the hook-effect it is imperative to use the correct volume of diluted sample. Despite this, PHC in the 75:25 conditions did achieve a lower LOD of 0.05 ppm for both analytes in RB. Therefore, PHC could still be used with 75:25 conditions for testing trace allergen levels, so long as the sample is also tested in the 1:99 and 25:75 conditions to ensure no false negatives arise at high concentrations. The optimum conditions from PHC were determined to be 25:75. When testing HPC in the 1:99 conditions, LODs of 5 and 1 ppm (see SI, Figure S4.3) were reached for peanut and hazelnut, respectively, with the LODs decreasing to 1 and 0.1 with the 25:75 arrangement. But for HPC, the hook-effect was greater in 25:75 compared with PHC with concentrations of 100 and 50 ppm experiencing reduced intensity on both the control and the peanut lines, complicating quantitative analysis. The greater hook-effect in this configuration could be because the upstream (hazelnut) test line comes into contact with the sample first, and this mAb has a rapid association rate and high affinity for THP, and so it becomes quickly saturated³⁰.

So, the optimum condition for HPC was the 1:99 protocol, although this was significantly less sensitive compared with the optimized PHC assay. For this reason, PHC was determined to be the optimum test line configuration with the best working conditions being 25:75 in the working range of 100–0.1 ppm. Therefore, PHC was used for further smartphone quantification and validation experiments.

3.4 Smartphone Readout and Analysis

Smartphones are ever-increasing in popularity for analyzing colorimetric assays. Most often, smartphone analysis is based on specific apps which relate a particular color intensity to a certain concentration of analyte. In the absence of a specific app, it is possible to use freely downloadable apps from the Google Play Store to analyze endpoint smartphone image color intensity values³⁰. By converting RGB values to LAB values, luminosity or intensity can be plotted as a function of concentration in a calibration curve. In sandwich immunoassay formats with CNP labels, a higher L value corresponds to a lower analyte concentration. As LAB color space is device-independent, the same results can be potentially achieved using different smartphone models. For analysis of PHC and HPC (in triplicate) the normalization of the (L)LAB values was carried out by dividing the L values of the test lines by the L values of the control lines. The method of dividing the test line response by the control line response (T/C ratio) is a technique commonly used for the quantification of sandwich LFIA^{35,47-49}. The results for PHC can be found in Figure 4.4, and the HPC smartphone calibration curve can be found in Figure S4.4 in the SI.

Two smartphone models were used for the device independent LAB analysis of PHC assays (in RB in triplicate), as can be seen in Figure 4.4 where A, C and E show the curves for THP in 1:99, 25:75 and 75:25 (sample: RB) and B, D and F show the curves for TPP in 1:99, 25:75 and 75:25 (sample: RB). A higher normalized L value was obtained for hazelnut at 25–100 ppm using the 25:75 conditions, as can be seen in Figure 4.4C. Comparatively, peanut did not appear to be subject to the hook-effect under 25:75. Using 75:25 conditions (see Figure 4.4E), concentrations of 50 and 100 ppm resulted in a higher normalized L value for hazelnut (i.e., weaker signal). Furthermore, under these conditions the hazelnut T/C ratio for 10 ppm and 25 ppm gave the same normalized L value, highlighting that the hook-effect was still evident, even at these lower concentrations. Comparatively, peanut in 75:25 (see Figure 4.4F) gave higher normalized L values at concentrations of 25–100 ppm, again indicating with increasing sample volume and concentration the likelihood of the hook-effect being increased. The only crucial variation between the two smartphone measurements using the different models was obtained for the peanut line using 75:25 at 0.1 ppm (see Figure 4.4F). However, this is the smartphone LOD, and detection spots were already more difficult to read. As well as this, the current method relies on manually selecting regions of interest on the control and test lines, rather than being able to read the values across the whole line. Therefore, please note that the results also include any errors due to not selecting the exact same regions, and this can also cause variations in the obtained color values.

Additionally, to compare different smartphone quantification methods, all smartphone readable assays were also analyzed by making a background subtraction as can be seen in the SI (see Figures S5.5 and S5.6). However, when analyzing the LFAs in this way the differences in background readings, due to discrepancies in lighting conditions caused by recording an image of the entire calibration range simultaneously under ambient lighting conditions, meant that a simple background subtraction was insufficient. However, for active flow-through assays the background subtraction was found to be the most effective analysis method (see SI, Figure S4.6A), whereas the T/C method resulted in larger standard deviations (see SI, Figure S4.6B). This could be attributed to the membranes being photographed independently, so the small membranes were subject to the same ambient lighting conditions and did not have such variable background readings. By using two data processing methods it is evident that the selected data processing method plays a crucial role for the quality of the semi-quantitative information that can be obtained from raw results.

3.5 Matrix Experiments and Validation

To determine their applicability to real life samples, the assays were tested using THP and TPP spiked into blank biscuit matrix extracts. The passive flow-through format was able to achieve visual LODs of 5 and 1 ppm for peanut and hazelnut. These LODs are higher than previously observed in spiked buffer experiments, showing that the matrix extract did have some influence on the detection of the analytes. When testing in this way, the passive flow

membranes had greater background staining compared with in spiked buffer experiments. This can be attributed to the overall reduction of reagents, BSA and tween-20 in the assay buffer, as the sample was spiked into a matrix extract rather than into the RB.

In comparison, the active flow-through membranes did not suffer with increased background staining due to the use of the additional filter on top of the membrane and subsequent washing step. The active-flow assay reached visual LODs of 0.5 and 1 ppm for THP and TPP in spiked matrix extract, however the intensity of the detection spots was fainter compared with spiked buffer samples because of the reduction of buffer reagents responsible for good flow. Therefore, whilst visual readout was possible, the construction of calibration curves based on smartphone images could not be achieved. PHC was tested in both 25:75 and 1:99 of spiked matrix in RB to determine the visual LOD in matrix extract, as can be seen in SI Figure S4.7. When using 25 μL sample (THP and TPP spiked into matrix extract) and 75 μL RB a LOD of 0.5 ppm could be reached for both analytes (see SI, Figure S4.7A). At higher concentrations (100 ppm +) there was decreased intensity for the hazelnut line. This can be attributed to the hook-effect. For the spiked matrix extract experiments, the PHC assays were run for 10 min, due to the reduction of reagents BSA and tween-20 from spiking sample into matrix extract rather than RB, affecting the flow of the sample.

Additionally, PHC was tested in 1 μL of spiked matrix extract:99 μL of RB (see SI, Figure S4.7B). Visual LODs of 10 and 5 ppm were reached for peanut and hazelnut, respectively. The PHC assay was fully validated using 25:75 conditions by evaluating 20 truly different blank matrices and determining that no false positives occurred. Additionally, the 20 blank matrices were spiked with 1 ppm THP and TPP. In the absence of agreed regulatory levels for food allergens, a screening target concentration (STC), based on VITAL 2.0 levels of 1 ppm, was selected^{8,50}. The LFIA's were able to detect the allergens with both visual and smartphone readout at 1 ppm in all 20 samples, as can be seen in Figure 4.5 and as is summarized in Table 4.2. The excellent reproducibility at the STC level clearly suggests that a simple device-independent smartphone readout may provide semi-quantitative data.

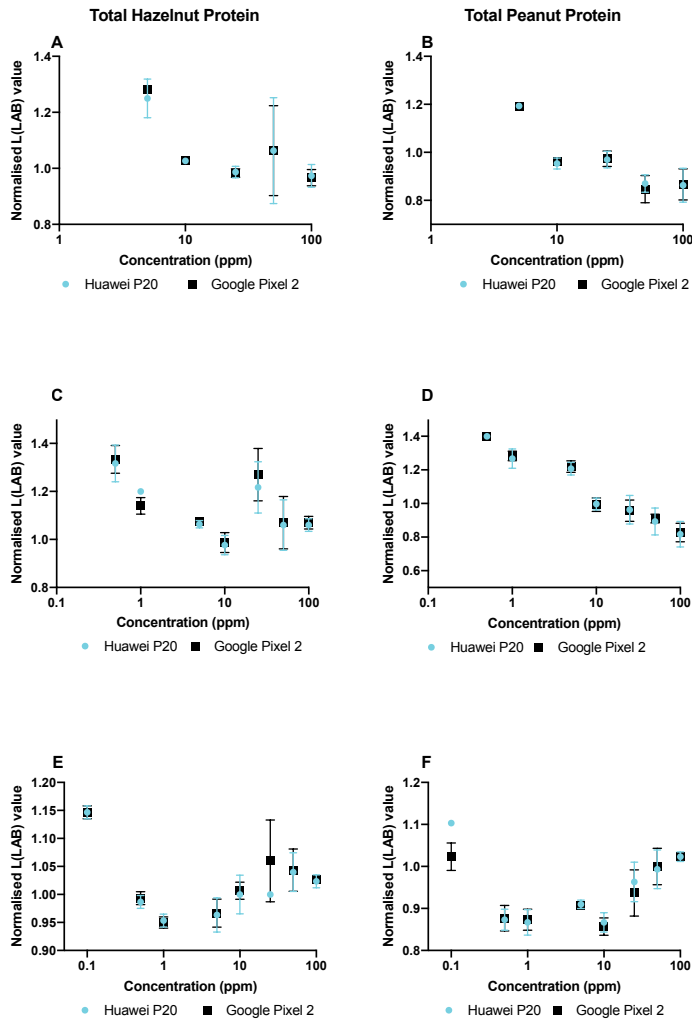


Figure 4.4. Smartphone calibration curves for the normalized (L) LAB values of the test lines of a Peanut Hazelnut Control (PHC) assay as a function of the concentration of Total Hazelnut Protein (THP), and Total Peanut Protein (TPP) (100–0.1 ppm) tested using two different smartphone models. All calibration ranges were performed in triplicate in spiked Running Buffer (RB). All L(LAB) values have been normalized by dividing the test line values by the control line values. (A) Hazelnut tested in 1 μ L of sample in 99 μ L of running buffer (RB) (B) Peanut tested in 1 μ L of sample in 99 μ L of RB. (C) Hazelnut tested in 25 μ L sample in 75 μ L of RB. (D) Peanut tested in 25 μ L sample in 75 μ L of RB. (E) Hazelnut tested in 75 μ L sample in 25 μ L of RB. (F) Peanut tested in 75 μ L of sample in 25 μ L of RB. Error bars show standard deviation (SD) from triplicate measurements.

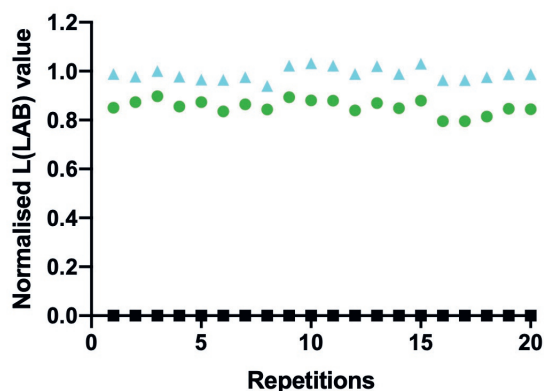


Figure 4.5. Smartphone validation of Peanut Hazelnut Control (PHC) assay using 20 truly different blank biscuit samples (square markers) and 20 truly different biscuit samples spiked at the screening target concentration of 1 ppm Total Hazelnut Protein (THP), and total peanut protein (TPP). Normalized L (LAB) values were obtained by dividing the test line response by the corresponding control line response.

Table 4.2. Matrix experiments for the optimized PHC assay

Parameter	PHC* (Matrix Extract)
LOD	0.5 ppm both analytes
Working range	100–0.5 ppm
Assay duration (total assay time incl. drying)	10 min
Time to result	1.5–2 min
Sample volume	25 μ L
Reproducibility ** (n = 20)	Hazelnut: 2.5% Peanut: 3.4%
False positives (n = 20)	0
False negatives (n = 20)	0

*PHC = Peanut, hazelnut, control geometry lateral flow immunoassay. ** Reproducibility defined as Relative Standard Deviation (RSD) \times 100% 1 ppm of Total Hazelnut Protein (THP), Total Peanut Protein (TPP) spiked into blank biscuit matrix extract (n = 20). Data based on normalized L (LAB) values.

Finally, to confirm the capability of the optimized LFIA in detecting allergens in raw ingredients, blank flour and peanut-spiked flour samples were briefly tested. The LFIAs correctly did not detect either of the allergens in the blank flour (n = 4). Furthermore, PHC specifically detected only peanut in the peanut-spiked flour (n = 4) with no false hazelnut positives being observed. The detection of peanut was not adversely affected by using the accelerated 30 min extraction procedure for the spiked flour. Further developments should include simplified and faster extraction methods.

4 Conclusions

Quick and accurate detection of food allergens is of critical importance for food safety; it is particularly relevant if such testing procedures can be easily performed by the consumer, and therefore, there is an evident requirement for simple and robust testing procedures. Two formats of multiplex flow-through immunoassays have been developed and compared with two test line configurations of LFIA, all developed using the same bioreagents and against the same targets in order to allow a true comparison. Two recent review papers have extensively outlined commercially available and proof-of-concept single-plex and multiplex allergen immunoassays and biosensors, and the assays reported in this study have matched or surpassed these previously reported LODs^{9,51}. All the developed multiplex assays were able to detect both analytes in the low ppm range within minutes. It is important to note here that our screening concentrations always related to total protein extracts from either peanuts or hazelnut, and therefore, the concentration of specific allergenic proteins is expected to be even lower than the reported values. This in turn means that the reported LODs are underestimating the true sensitivity of the immunoassays in this work. The passive flow-through format offered a way to rapidly develop a fast flow-through assay. However, this specific format was limited by the need to manually biofunctionalize the membranes, limiting their reproducibility. The active flow-through assay could achieve very low limits of detection with no false negatives when following the optimization steps. However, it is these optimization steps that made the assay more complicated to perform for a non-expert user such as a consumer. In future versions, the use of a mechanical pump could improve the user-friendliness, although this would introduce an additional and costly element into the procedure, limiting the portability of the assay. It should be reiterated that the assays within this study were performed by a trained scientist, and the active flow-through method is not recommended for untrained users. In comparison, the LFIAs, when using the optimized assay conditions for each configuration, resulted in no false positives. However, outside of working conditions, both configurations of LFIA did experience a hook-effect at high concentrations, a phenomenon commonly encountered in sandwich LFIA, where a falsely low signal occurs at high analyte concentrations. As the hook-effect is concentration-dependent, it can be avoided/limited by assay optimization.

To demonstrate their applicability to real life bakery products and raw ingredients, all assays were tested in decreasing concentrations of analyte spiked into the matrix extract. Additionally, the PHC assay was validated as a screening method in spiked matrix extract, blank matrix extract (n = 20) and incurred spiked flour, proving its capability of detecting the target even in complex matrices. The majority of commercially-available allergen detection LFIA test kits can detect a single analyte at 1–10 ppm^{9,51}. Comparatively, PHC was able to detect both analytes at 0.5 ppm of THP and TPP spiked into a blank biscuit

matrix extract, affirming its place as one of the most sensitive allergen LFIAs. This LOD was in agreement with the LOD using the same hazelnut antibody in a previously reported single-plex assay³⁰. Finally, all assays were (semi-)quantified by smartphone readout. At this stage no additional external equipment was used for the image recording, so the LFIA membranes were subject to ambient lighting conditions. To compensate for the lighting conditions a normalization factor (T/C ratio) was applied. By using device-independent (L) LAB values, it was possible to obtain comparable results using two distinct smartphone models. The ability to use different smartphone models for reading the same assays is a characteristic that is highly desirable, but not often reported, within smartphone analysis. In future developments, researchers should focus on improving the ease of use of these assays by integrating sample preparation, limiting the user interaction with the assay, as well as by developing a consumer-friendly app as a user interface which can directly analyze data with minimal user input.

References

1. O'Keefe, A.W.; De Schryver, S.; Mill, J.; Mill, C., et al. Diagnosis and management of food allergies: new and emerging options: a systematic review, *J. Asthma Allergy* **2014**, *7*, 141-164, 10.2147/jaa.s49277.
2. Weinberger, T.; Sicherer, S. Current perspectives on tree nut allergy: a review, *J. Asthma Allergy* **2018**, *11*, 41-51, 10.2147/jaa.s141636.
3. McWilliam, V.; Koplin, J.; Lodge, C.; Tang, M., et al. The Prevalence of Tree Nut Allergy: A Systematic Review, *Curr. Allergy Asthma Rep.* **2015**, *15*, 1-54, 10.1007/s11882-015-0555-8.
4. Maloney, J.M.; Rudengren, M.; Ahlstedt, S.; Bock, S.A., et al. The use of serum-specific IgE measurements for the diagnosis of peanut, tree nut, and seed allergy, *J Allergy Clin Immunol* **2008**, *122*, 145-151, <https://doi.org/10.1016/j.jaci.2008.04.014>.
5. EC. Directive 2003/89/EC of the European Parliament and of the Council of 10 November 2003 Amending Directive 2000/13/EC as Regards Indication of the Ingredients Present in Foodstuffs, *OJEU* **2003**, 308.
6. EU Regulation No 1169/2011 on the provision of food information to consumers amending Regulations (EC) No 1924/2006 and (EC) No 1925/2006. *OJEU*. **2011**, 304.
7. Allen, K.J.; Turner, P.J.; Pawankar, R.; Taylor, S., et al. Precautionary labeling of foods for allergen content: are we ready for a global framework?, *World Allergy Organization Journal* **2014**, *7*, 1-14, 10.1186/1939-4551-7-10.
8. Soon, J.M.; Manning, L. "May Contain" Allergen Statements: Facilitating or Frustrating Consumers?, *J. Consumer Policy* **2017**, *40*, 447-472, 10.1007/s10603-017-9358-8.
9. Ross, G.M.S.; Bremer, M.G.E.G.; Nielen, M.W.F. Consumer-friendly food allergen detection: moving towards smartphone-based immunoassays, *Anal Bioanal Chem* **2018**, *410*, 5353-5371, 10.1007/s00216-018-0989-7.
10. Choi, J.R.; Yong, K.W.; Choi, J.Y.; Cowie, A.C. Emerging Point-of-care Technologies for Food Safety Analysis, *Sensors* **2019**, *19*, 817.
11. Zhang, J.; Portela, S.B.; Horrell, J.B.; Leung, A., et al. An integrated, accurate, rapid, and economical handheld consumer gluten detector, *Food Chem.* **2019**, *275*, 446-456, <https://doi.org/10.1016/j.foodchem.2018.08.117>.
12. Taylor, S.L.; Nordlee, J.A.; Jayasena, S.; Baumert, J.L. Evaluation of a Handheld Gluten Detection Device, *J. Food Prot.* **2018**, *81*, 1723-1728, 10.4315/0362-028x.jfp-18-184.
13. Alves, R.C.; Barroso, M.F.; González-García, M.B.; Oliveira, M.B.P.P., et al. New Trends in Food Allergens Detection: Toward Biosensing Strategies, *Crit Rev Food Sci Nutr* **2016**, *56*, 2304-2319, 10.1080/10408398.2013.831026.
14. Rateni, G.; Dario, P.; Cavallo, F. Smartphone-Based Food Diagnostic Technologies: A Review, *Sensors* **2017**, *17*, 1453.
15. Lin, H.H., CH. Park, J. Pathania, D. Castro, CM. Fasano, A. Weissleder, R. Lee, H. . Integrated Magneto-Chemical Sensor for On-Site Food Allergen Detection, *ACS Nano* **2017**, *11*, 10062-10069, 10.1021/acs.nano.7b04318.

16. Coskun, A.F.; Wong, J.; Khodadadi, D.; Nagi, R., et al. A personalized food allergen testing platform on a cellphone, *Lab Chip* **2013**, *13*, 636-640, 10.1039/c2lc41152k.
17. Zhang, D.; Liu, Q. Biosensors and bioelectronics on smartphone for portable biochemical detection, *Biosens. Bioelectron.* **2016**, *75*, 273-284, <https://doi.org/10.1016/j.bios.2015.08.037>.
18. Morón, M.J.; Luque, R.; Casilari, E. On the capability of smartphones to perform as communication gateways in medical wireless personal area networks, *Sensors (Basel, Switzerland)* **2014**, *14*, 575-594, 10.3390/s140100575.
19. Gantelius, J.; Bass, T.; Sjöberg, R.; Nilsson, P., et al. A lateral flow protein microarray for rapid and sensitive antibody assays, *Int. J. Mol. Sci.* **2011**, *12*, 7748-7759, 10.3390/ijms12117748.
20. Anfossi, L.; Di Nardo, F.; Cavallera, S.; Giovannoli, C., et al. Multiplex Lateral Flow Immunoassay: An Overview of Strategies towards High-throughput Point-of-Need Testing, *Biosensors* **2018**, *9*, 2.
21. Peng, J.; Wang, Y.; Liu, L.; Kuang, H., et al. Multiplex lateral flow immunoassay for five antibiotics detection based on gold nanoparticle aggregations, *RSC Advances* **2016**, *6*, 7798-7805, 10.1039/c5ra22583c.
22. Song, S.; Liu, N.; Zhao, Z.; Njumbe Ediage, E., et al. Multiplex Lateral Flow Immunoassay for Mycotoxin Determination, *Anal. Chem.* **2014**, *86*, 4995-5001, 10.1021/ac500540z.
23. Anfossi, L.; Di Nardo, F.; Russo, A.; Cavallera, S., et al. Silver and gold nanoparticles as multi-chromatic lateral flow assay probes for the detection of food allergens, *Anal Bioanal Chem* **2018**, 10.1007/s00216-018-1451-6.
24. Galan-Malo, P.; Pellicer, S.; Pérez, M.D.; Sánchez, L., et al. Development of a novel duplex lateral flow test for simultaneous detection of casein and β -lactoglobulin in food, *Food Chem.* **2019**, *293*, 41-48, <https://doi.org/10.1016/j.foodchem.2019.04.039>.
25. Cho, D.G.; Yoo, H.; Lee, H.; Choi, Y.K., et al. High-Speed Lateral Flow Strategy for a Fast Biosensing with an Improved Selectivity and Binding Affinity, *Sensors (Basel, Switzerland)* **2018**, *18*, 1507, 10.3390/s18051507.
26. Zhao, M.; Wang, X.; Nolte, D. Mass-transport limitations in spot-based microarrays, *Biomed Opt Express* **2010**, *1*, 983-997, 10.1364/boe.1.000983.
27. Chen, P.; Gates-Hollingsworth, M.; Pandit, S.; Park, A., et al. Paper-based Vertical Flow Immunoassay (VFI) for detection of bio-threat pathogens, *Talanta* **2019**, *191*, 81-88, <https://doi.org/10.1016/j.talanta.2018.08.043>.
28. Bishop, J.D.; Hsieh, H.V.; Gasperino, D.J.; Weigl, B.H. Sensitivity enhancement in lateral flow assays: a systems perspective, *Lab Chip* **2019**, *19*, 2486-2499, 10.1039/c9lc00104b.
29. Katis, I.N.; He, P.J.W.; Eason, R.W.; Sones, C.L. Improved sensitivity and limit-of-detection of lateral flow devices using spatial constrictions of the flow-path, *Biosens. Bioelectron.* **2018**, *113*, 95-100, <https://doi.org/10.1016/j.bios.2018.05.001>.
30. Ross, G.M.S.; Bremer, M.G.E.G.; Wichers, J.H.; Van Amerongen, A., et al. Rapid Antibody Selection Using Surface Plasmon Resonance for High-Speed and Sensitive Hazelnut Lateral Flow Prototypes, *Biosensors* **2018**, *8*, 130.
31. Ekins, R.; Wild, D. In *The Immunoassay Handbook (Fourth Edition)*; Elsevier: Oxford, 2013, pp 109-121.

32. Yetisen, A.K.; Akram, M.S.; Lowe, C.R. Paper-based microfluidic point-of-care diagnostic devices, *Lab Chip* **2013**, *13*, 2210-2251, 10.1039/c3lc50169h.
33. Oh, Y.K.; Joung, H.-A.; Kim, S.; Kim, M.-G. Vertical flow immunoassay (VFA) biosensor for a rapid one-step immunoassay, *Lab Chip* **2013**, *13*, 768-772, 10.1039/c2lc41016h.
34. Reuterswärd, P.; Gantelius, J.; Andersson Svahn, H. An 8 minute colorimetric paper-based reverse phase vertical flow serum microarray for screening of hyper IgE syndrome, *Analyst* **2015**, *140*, 7327-7334, 10.1039/c5an01013f.
35. Rey, E.G.; O'Dell, D.; Mehta, S.; Erickson, D. Mitigating the Hook Effect in Lateral Flow Sandwich Immunoassays Using Real-Time Reaction Kinetics, *Anal. Chem.* **2017**, *89*, 5095-5100, 10.1021/acs.analchem.7b00638.
36. Tate, J.; Ward, G. Interferences in immunoassay, *The Clinical biochemist. Reviews* **2004**, *25*, 105-120.
37. Clarke, O.J.R.; Goodall, B.L.; Hui, H.P.; Vats, N., et al. Development of a SERS-Based Rapid Vertical Flow Assay for Point-of-Care Diagnostics, *Anal. Chem.* **2017**, *89*, 1405-1410, 10.1021/acs.analchem.6b04710.
38. Eltzov, E.; Marks, R.S. Colorimetric stack pad immunoassay for bacterial identification, *Biosens. Bioelectron.* **2017**, *87*, 572-578, <https://doi.org/10.1016/j.bios.2016.08.044>.
39. Samsonova, J.V.; Safronova, V.A.; Osipov, A.P. Rapid flow-through enzyme immunoassay of progesterone in whole cows' milk, *Anal. Biochem.* **2018**, *545*, 43-48, <https://doi.org/10.1016/j.ab.2018.01.011>.
40. Chinnasamy, T.; Segerink, L.I.; Nystrand, M.; Gantelius, J., et al. Point-of-Care Vertical Flow Allergen Microarray Assay: Proof of Concept, *Clin. Chem.* **2014**, *60*, 1209-1216, 10.1373/clinchem.2014.223230.
41. Burmistrova, N.A.; Rusanova, T.Y.; Yurasov, N.A.; Goryacheva, I.Y., et al. Multi-detection of mycotoxins by membrane based flow-through immunoassay, *Food Control* **2014**, *46*, 462-469, <https://doi.org/10.1016/j.foodcont.2014.05.036>.
42. Joung, H.-A.; Ballard, Z.S.; Ma, A.; Tseng, D.K., et al. Paper-based multiplexed vertical flow assay for point-of-care testing, *Lab Chip* **2019**, *19*, 1027-1034, 10.1039/c9lc00011a.
43. Reese, I.; Holzhauser, T.; Schnadt, S.; Dölle, S., et al. Allergen and allergy risk assessment, allergen management, and gaps in the European Food Information Regulation (FIR), *Allergo Journal International* **2015**, *24*, 180-184, 10.1007/s40629-015-0066-0.
44. Bremer, M.G.E.G.; Smits, N.G.E.; Haasnoot, W. Biosensor immunoassay for traces of hazelnut protein in olive oil, *Anal Bioanal Chem* **2009**, *395*, 119-126, 10.1007/s00216-009-2720-1.
45. Walker, M.J.B., D.T. Elliot, C.T. Gowland, M.H. Mills, C.E.N. Is food allergen analysis flawed? Health and supply chain risks and a proposed framework to address urgent analytical needs, *Analyst* **2016**, *141*, 24-35, 10.1039/C5AN01457C.
46. Croote, D.; Quake, S.R. Food allergen detection by mass spectrometry: the role of systems biology, *NPJ systems biology and applications* **2016**, *2*, 16022-16022, 10.1038/npjbsa.2016.22.
47. Zhao, Y.; Wang, H.; Zhang, P.; Sun, C., et al. Rapid multiplex detection of 10 foodborne pathogens with an up-converting phosphor technology-based 10-channel lateral flow assay, *Sci. Rep.* **2016**, *6*, 21342, 10.1038/srep21342.

48. Anfossi, L.; Di Nardo, F.; Giovannoli, C.; Passini, C., et al. Increased sensitivity of lateral flow immunoassay for ochratoxin A through silver enhancement, *Anal Bioanal Chem* **2013**, *405*, 9859-9867, 10.1007/s00216-013-7428-6.
49. Raeisossadati, M.J.; Danesh, N.M.; Borna, F.; Gholamzad, M., et al. Lateral flow based immunobiosensors for detection of food contaminants, *Biosens. Bioelectron.* **2016**, *86*, 235-246, <https://doi.org/10.1016/j.bios.2016.06.061>.
50. Taylor, S.C., G. Grinter, K. Sherlock, R. Warren, L. . The Allergen Bureau VITAL Program *J AOAC Int* **2018** *101*, 1-5, 10.5740/jaoacint.17-0392.
51. Tsagkaris, A.S.; Nelis, J.L.D.; Ross, G.M.S.; Jafari, S., et al. Critical assessment of recent trends related to screening and confirmatory analytical methods for selected food contaminants and allergens, *TrAC Trends in Analytical Chemistry* **2019**, *121*, 115688, <https://doi.org/10.1016/j.trac.2019.115688>.

Supplementary information

Chapter 4

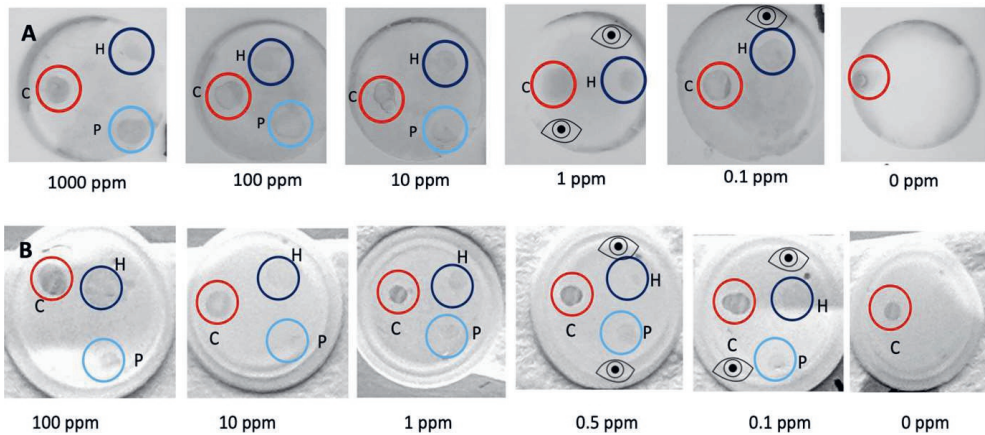


Figure S4.1. Calibration range for multiplex flow-through assays using (A) passive and (B) active flow. For control outlined in red (C), hazelnut outlined in dark blue (H) and peanut outlined in light blue (P). Assays tested in Total Hazelnut Protein (THP) and Total Peanut Protein (TPP) spiked into Running Buffer (RB; 0–1000 ppm in A and 0–100 ppm in B). Membranes were manually spotted with 0.5 μ L of primary antibody (1 mg/mL). Eye icons are used to denote the lowest concentration of TPP or THP the assays are readable by naked eye, but difficult to capture on a smartphone camera.

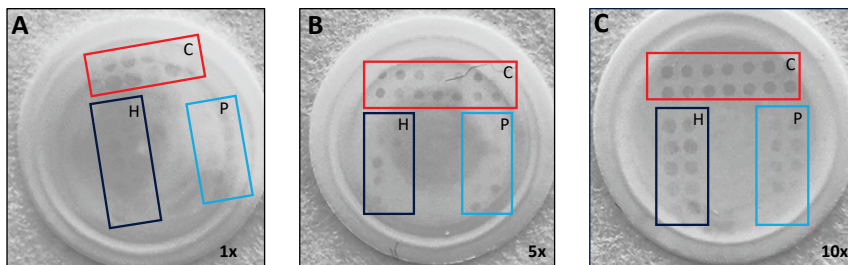


Figure S4.2. Calibration range for multiplex flow-through assay optimization: sample aspirations. Active flow-through assays tested in 10 ppm Total Hazelnut Protein (THP) and Total Peanut Protein (TPP) spiked into Running Buffer (RB) with 1 (A), 5 (B) and 10 (C) aspirations. The control region is outlined in red (C), the hazelnut region in dark blue (H) and the peanut region in light blue (P). There is an increase in surface wetting with the increasing number of aspirations.

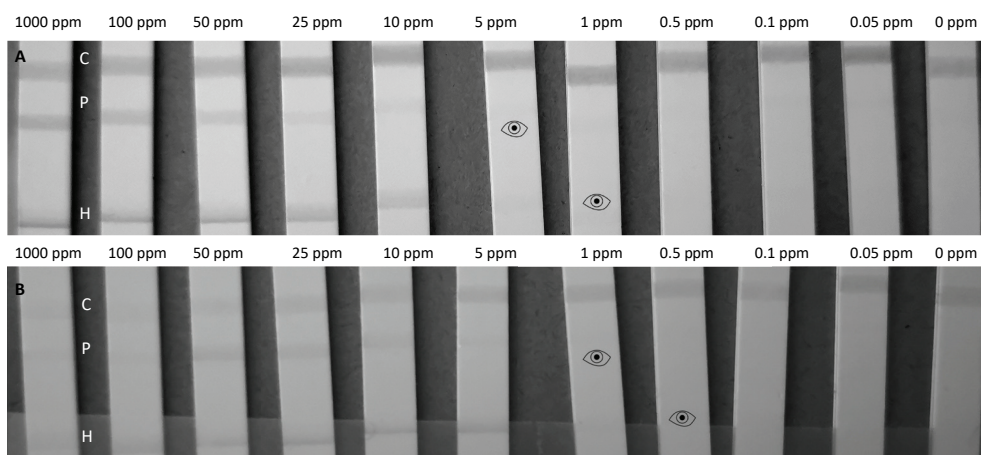


Figure S4.3. Calibration range for lateral flow immunoassay with test line configuration: hazelnut, peanut, control (HPC). The strips were tested with Total Hazelnut Protein (THP) and Total Peanut Protein (TPP) spiked into the Running Buffer (RB) in decreasing concentration. Where C represents the control line, P the peanut line and H the hazelnut line, and the eye icon represents the visual LOD, which is not as clearly readable in the smartphone image. (A) tested in $1\ \mu\text{L}$ of sample in $99\ \mu\text{L}$ of RB, (B) tested in $25\ \mu\text{L}$ of sample in $75\ \mu\text{L}$ of RB.

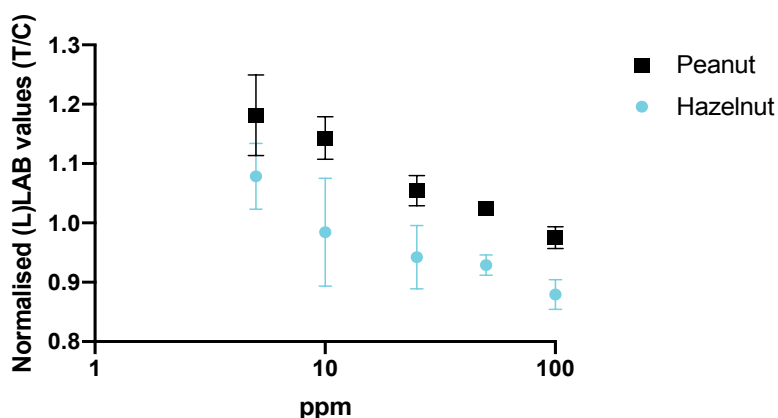


Figure S4.4. Calibration range for smartphone analysis of hazelnut, peanut, control (HPC) lateral flow immunoassay. Smartphone (Huawei P20) analysis, where normalized L (LAB) values (test line intensity/control line intensity; T/C) are plotted as a function of the concentration (100–5 ppm) Total Hazelnut Protein (THP) and Total Peanut Protein (TPP) spiked into Running Buffer (RB) ($1\ \mu\text{L}$ of the given dilution was diluted in $99\ \mu\text{L}$ of RB). Error bars represent the standard deviation ($n = 3$). For experimental details, see the full manuscript.

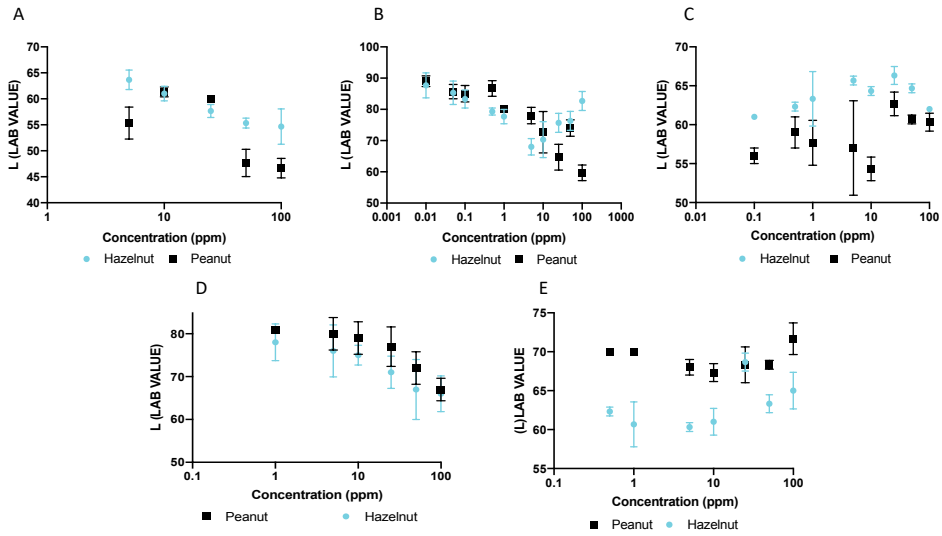


Figure S4.5. Calibration curves for smartphone analysis of lateral flow immunoassays using background subtraction. Smartphone (Huawei P20) analysis for lateral flow immunoassay Peanut Hazelnut Control (PHC) and Hazelnut Peanut Control (HPC) assays, plotted as a function of the concentration of Total Hazelnut Protein (THP) and Total Peanut Protein (TPP) spiked into Running Buffer (RB) (100–0.05 ppm). Where LAB values are obtained by subtraction of the background nitrocellulose values from the test lines. (A) PHC in 1 μL sample: 99 μL Running Buffer (RB) (B) PHC in 25 μL sample: 75 μL RB (C) PHC in 75 μL sample: 25 μL RB (D) HPC in 1 μL sample and 99 μL RB HPC in 25 μL sample: 75 μL RB. Error bars represent the standard deviation ($n = 3$).

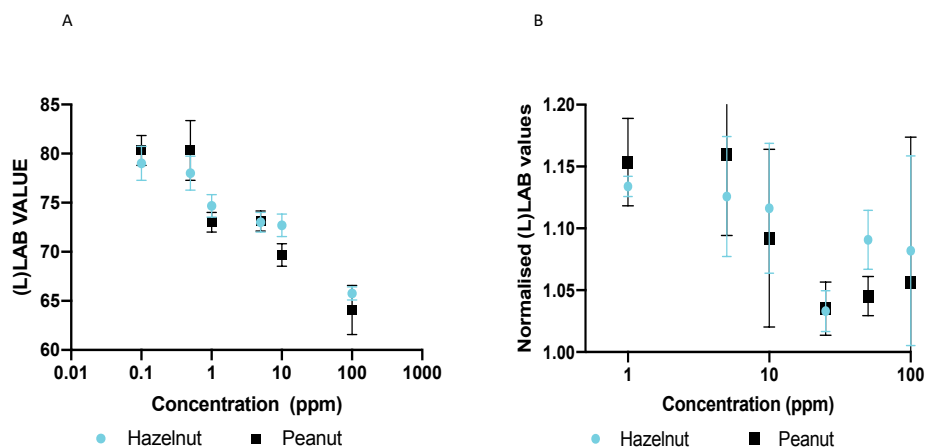


Figure S4.6. Calibration curves for smartphone analysis of active flow-through immunoassay. Smartphone (Huawei P20) analysis of active flow-through immunoassay in a decreasing concentration of Total Hazelnut Protein (THP) and Total Peanut Protein (TPP) spiked in Running Buffer (RB) (100–0.01 ppm) all flow-through assays performed and analyzed in triplicate. (A) Analysis performed by subtracting the background reading from test spots. (B) Analysis performed by normalizing L (LAB) values (test line intensity/control line intensity; T/C). Error bars represent standard deviation ($n = 3$).

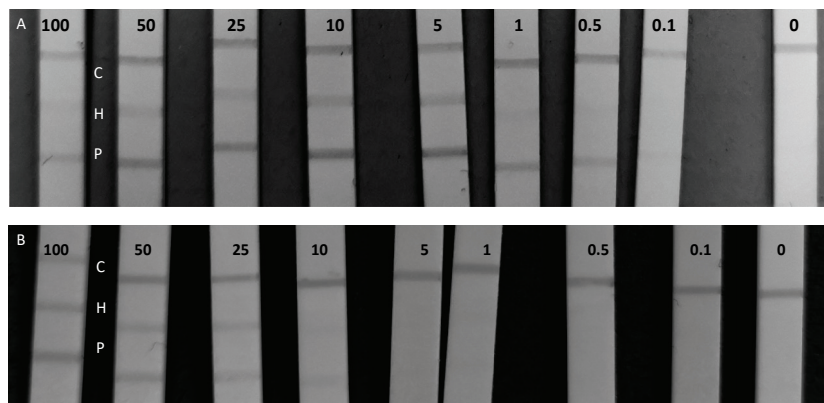


Figure S4.7. Optimized lateral flow immunoassay calibration curve in spiked matrix extract. Peanut Hazelnut Control (PHC) format Lateral Flow Immunoassay tested in a decreasing concentration (100–0.1 ppm) of Total Hazelnut Protein (THP) and Total Peanut Protein (TPP) spiked in matrix extract. The control region is indicated by C, the hazelnut detection region by H and the peanut detection region by P. (A) PHC using optimized assay under optimized conditions of 25 μ L biscuit matrix extract spiked with THP, and TPP and 75 μ L Running Buffer (RB). (B) PHC using optimized assay using 1 μ L of biscuit matrix spiked with THP, TPP and 99 μ L of RB conditions.

Table S4.1. Ingredient and allergen information for the 20 varieties of biscuit used for matrix extract experiments

No.	Ingredients	Allergen Information
1	Sugar, palm oil, glucose-fructose syrup, salt, raising agents: sodium carbonates, ammonium carbonates	40% oat flakes, whole-grain wheat flour, wheat flour May contain: milk, sesame
2	Sugar, sunflower oil, glucose fructose syrup, raising agent (citric acid [E330], sodium carbonate [E500], ammonium carbonate [E503]), salt	33% whole wheat flour, 19% wheat flour, 11% wheat flake Contains: gluten May contain: milk, sesame
3	Sugar, 15% palm oil, glucose fructose syrup, salt, raising agent (sodium carbonate [E500]), ammonium carbonate [E503])	46% wheat flour, wholemeal wheat flour, oat flake Contains: port gluten, wheat gluten May contain: milk, sesame
4	Sugar, vegetable oil (palm, turnip), glucose syrup, leavening agent (diphosphate [E450], sodium carbonate [E503], mono and diglycerides of fatty acids, esterified with monoacetyl and diacetyl tartaric acid [E472e molasses, salt cane, salt	Oat flake, wheat flour, wholemeal wheat flour, barley malt flour Contains: port gluten, wheat gluten, gluten May contain: egg, gluten contain cereals, milk, nuts, peanuts
5	Maize starch, palm fat, cane sugar (16%), maize flour, buckwheat flour (4%), sugar beet syrup, modified tapioca starch, salt, raising agents (ammonium hydrogen carbonate, sodium hydrogen carbonate)	Gluten & Lactose free Soya flour, soya bran (7%) Contains: soy May contain: lupin
6	Sugar, palm oil, salt, glucose-fructose syrup, raising agent, (sodium carbonate [E500], ammonium carbonate [E503]), natural flavor	Wheat flour Contains: wheat gluten May contain: milk, sesame
7	Corn starch, vanilla (sugar, corn starch, vanilla extract), sea salt, raising agent: ammonium carbonates	Wheat flour, butter (26%), free-range eggs Contains: wheat gluten, milk, eggs May contain: soy, almonds, cashews, hazelnut
8	Wheat flour, Sugar, palm oil, salt, glucose-fructose syrup, raising agent, (ammonium carbonate [E503]), natural flavor	Contains: wheat gluten May contain: milk, sesame
9	Maize starch, butter (milk), palm fat, sugar, maize flour, maize starch, sugar beet syrup, modified tapioca starch, salt, whole milk powder, emulsifier (mono- and diacetyl tartaric acid) raising agents (ammonium hydrogen carbonate, sodium hydrogen carbonate)	Gluten free Contains: milk, eggs May contain: soya, lupin

10	Maize starch, maize flour, vegetable margarine [vegetable fats and oils (palm, palm kernel, rape seed)] water, salt emulsifier: mono- and diglycerides of fatty acids (E471); natural flavoring, maltodextrin, modified tapioca starch, sea salt, 2% rice syrup, raising agents: ammonium hydrogen carbonate (E503ii), sodium bicarbonate (E500ii); glucose. Syrup, yeast emulsifier, citric acid, maize starch	Gluten free Soya protein, soya flour Contains: soya May contain: lupin
11	Sugar, palm oil, glucose-fructose syrup, salt, raising agents: sodium carbonates, ammonium carbonates	65% oat flakes, barley malt extract Contains: gluten May contain: sesame seeds, milk
12	Sugar, palm oil, glucose-fructose syrup, salt, raising agents: sodium carbonates, ammonium carbonates, emulsifier lecithin, antioxidant: sodium disulphite	65.5% wheat flour, lactose (milk), lecithin (soya) Contains: wheat gluten, milk, soy May contain: sesame seed
13	Sugar, vegetable oil (palm), glucose syrup, raising agents (sodium carbonates, disodium diphosphate, ammonium carbonates), salt, aromas	Wheat flour, lactose and milk proteins Contains: gluten, milk May contain: egg, soya, sesame seed
14	Sugar, palm oil, inverse sugar syrup, salt, raising agent, (sodium carbonate [E500], ammonium [E503])	40% oat flakes, 18% wholemeal wheat flour Contains: oat gluten, wheat gluten May contain: milk, sesame
15	Gluten free oat flakes 42%, sugar, gluten free oatmeal 17%, vegetable oil (palm), partially inverted sugar syrup, raising agent (sodium carbonates), salt	Gluten free May contain: milk, egg, soya
16	Palm oil, sugar, inversion syrup, salt, raising agents: sodium carbonates, citric acid, ammonium carbonates	48% wheat flour, 14% whole wheat flour Contains: wheat gluten May contain: sesame seed, milk
17	Sugar, palm oil, glucose syrup, raising agents (sodium carbonates, disodium diphosphate, ammonium carbonates), salt, aromas	Wheat flour, milk powder Contains: wheat gluten, milk May contain: egg, soya
18	Sugar, 10% palm oil, glucose fructose syrup, salt, raising agent (sodium carbonate, ammonium carbonate)	40% wheat flour, wholemeal wheat flour, oat flake Contains: gluten, wheat gluten May contain: milk, sesame seeds
19	Sugar, palm oil, salt, glucose-fructose syrup, raising agents: sodium carbonates, ammonium carbonates	60% oat flakes, barley malt extract Contains: gluten May contain: sesame seeds, milk
20	Sugar, palm oil, salt, glucose-fructose syrup, raising agent, (ammonium carbonate, sodium carbonates) natural aromas	Wheat flour, oat flakes Contains: wheat gluten May contain: milk, sesame

CHAPTER 5

5

Interconnectable solid-liquid protein extraction unit and chip-based dilution for multiplexed consumer immunodiagnostics

Adapted from:

Ross, G.M.S., Filippini, D., Nielen, M.W.F., Salentijn, G.IJ., 2020. Interconnectable solid-liquid protein extraction unit and chip-based dilution for multiplexed consumer immunodiagnostics. Analytica Chimica Acta. 1140. 190-198 doi: 10.1016/j.aca.2020.10.01

While consumer-focused food analysis is upcoming, the need for multiple sample preparation and handling steps is limiting. On-site and consumer-friendly analysis paradoxically still requires laboratory-based and skill-intensive sample preparation methods. Here, we present a compact, inexpensive, and novel prototype immunosensor combining sample preparation and on-chip reagent storage for multiplex allergen lateral flow immunosensing. Our comprehensive approach paves the way for personalized consumer diagnostics. The prototype allows for handheld solid-liquid extraction, pipette-free on-chip dilution, and adjustment of sample concentrations into the appropriate assay dynamic working range. The disposable and interconnectable homogenizer unit allows for the extraction and 3D-sieve based filtration of allergenic proteins from solid bakery products in 1 minute. The homogenizer interconnects with a 3D-printed unibody lab-on-a-chip (ULOC) microdevice, which is used to deliver precise volumes of sample extract to a reagent reservoir. The reagent reservoir is implemented for on-chip storage of carbon nanoparticle labeled antibodies and running buffer for dilution. The handheld prototype allows for total homogenization of solid samples, solid-liquid protein extraction, 3D-printed sieve-based filtration, ULOC-enabled dilution, mixing, transport, and smartphone-based detection of hazelnut and peanut allergens in solid bakery products with limited operational complexity. The multiplex lateral flow immunoassay (LFIA) detects allergens as low as 0.1 ppm in real bakery products, and the system is already consumer-operable, demonstrating its potential for future citizen science approaches. The designed system is suitable for a wide range of analytical applications outside of food safety, provided an LFIA is available.

1 Introduction

On-site and personalized food safety tests are growing in popularity, with developments in rapid, affordable, sensitive, and disposable handheld assays driving the move from the laboratory to a consumer-based approach^{1,2}. Consumer detection of food allergens is particularly relevant^{3,4}, and more so now than ever, with the Food and Drug Administration (FDA) announcing temporary changes to food labeling and allowing of ingredient alterations to prevent any disruption to the global food supply chain during the SARS-CoV-2 pandemic⁵. Amendments that overlook hidden or novel allergens put the allergic individual at risk, exemplifying the necessity for personalized, disposable, and simplified analysis of allergens, from sample preparation to detection. To date, the lateral flow immunoassay (LFIA) is the most successful application of consumer diagnostics⁶. Combining LFIAs with smartphones as optical detectors allow for 'on-the-go' decentralized screening⁷ and smartphones can even provide semi-quantitative results by calibrating test and control line intensity values toward a particular antigen concentration⁸.

Despite these advantages, LFIAs also have some disadvantages, including a limited dynamic range, they work only with liquid samples and predominately target only a single analyte. Within a sandwich LFIAs dynamic working range, the test line intensity increases alongside increasing analyte concentration. However, at high analyte concentrations, the signal intensity can paradoxically decrease as the excess of unlabeled analyte saturates the capture and detector antibodies (mAbs) binding sites⁹. The reduction in test line intensity can mimic the signal at a much lower analyte concentration. Dilution to within an assays appropriate concentration range is required to avoid false-negative results. False negatives are particularly problematic for consumers.

Moreover, when analyzing a complex solid matrix such as food, sample preparation, including homogenization of the solid food and extraction of the relevant proteins, as well as reagent storage, are pivotal bottlenecks. Even integrated systems often require pre-treatment¹⁰ or heat-assisted actuation to extract proteins into a testable liquid³. Finally, excluding a few multiplex LFIAs¹¹⁻¹³, allergen LFIAs are restricted to singleplex detection, which is limiting for individuals with co-existing allergies. Sample preparation is a major issue; indubitably, consumers do not have the laboratory skills required for extracting, pipetting, and diluting samples, and fully integrated analytical systems have so far mainly been developed for DNA-based analysis¹⁴⁻¹⁶. Systems with integrated solid-phase extraction for aqueous samples are reported^{10,17}, but the extraction of solid samples is more complex and still requires offline pre-treatment.

In a parallel advancement, the emergence of 3D-printing has revolutionized the rapid prototyping of multifunctional lab-on-a-chip¹⁸ and disposable¹⁹ devices for analytical

chemistry. Modification of Computer-Aided Designs (CADs) takes little cost and time, and prototypes can be refined iteratively multiple times in a single day, outside of a cleanroom environment. A unibody lab-on-a-chip (ULOC)^{18,20} is a monolithic device with all the analytical functionalities in-built on one side, takes less than an hour to manufacture, and is printed in a single step²¹. The ULOC's unibody connectors, ending in unidirectional valves, can be connected to silicon tubing as manual finger pumps²²; or to detachable devices such as syringes or pumps, for pipette-free, active control of sample actuation with volume metering²³. Moreover, 3D-printed devices with on-chip reagent storage^{14,24} can combine with and benefit from the capabilities of paper-based devices^{25,26}.

Here we present a multifunctional and miniaturized sample preparation unit that integrates with a consumer-operable prototype immunosensor for handheld solid-liquid multi-allergen extraction. The interconnectable ULOC then enables on-chip sample handling for equipment-free dilution, transport, and LFIA detection of hazelnut and peanut allergens in the low ppm range in spiked and commercial bakery products.

2 Materials & Methods

2.1 Reagents and Consumables

Multiplex LFIA and carbon nanoparticle labeled antibodies (CNP-mAbs) against hazelnut and peanut have previously been developed, characterized, and validated^{13,27}. Running buffer (RB)/extraction buffer was 100 mM borate buffer (BB) pH 8.8, composed of 100 mM boric acid (Merck, Darmstadt; Germany) and 100 mM sodium tetraborate (VWR, Leuven; Belgium) with 1% (w/v) bovine serum albumin (BSA; Sigma-Aldrich, Zwijndrecht, The Netherlands) and 0.05% tween-20 (v/v) (Merck, Darmstadt; Germany). The 10 mL and 1 mL disposable plastic syringes that were used for the homogenizer and air displacement syringes were purchased from Becton-Dickinson (Utrecht, The Netherlands), and low binding syringe filters used to filter total protein extracts (5 μm ; 1.2 μm ; 0.45 μm) were acquired from Pall Life Sciences (Pall Netherlands B.V., Medemblik; The Netherlands). Silicon tubing for ULOC connectors was purchased from Esska-Tech (Arvika; Sweden). ULOCs were sealed on the open side with adhesive tape (3M Ruban Adhesive Scotch Nastro Adhesive, 3M Europe, Diegem; Belgium). Red food dye solution (consisting of water, propylene glycol, and Carmoisine CI 14720) of unknown concentration used for dilution characterization of the ULOC was purchased from a local supermarket. The clamp used for attaching the smartphone to the holder's frame was purchased from Wolfcraft (Wolfcraft, Kempenich; Germany).

2.2 Reference Material Preparation

Standardized certified reference materials for food allergens are not currently available; therefore, total hazelnut protein (THP), total peanut protein (TPP), and blank cookie (BC)

extracts were prepared in-house^{13,27}. See Supplementary Information (SI) Table S5.1 for ingredient lists and labeling information. Fresh protein aliquots were defrosted on the day of experiments, and the protein content was always checked before use by a NanoDrop (ND 3300, Isogen Life Sciences, De Meern; The Netherlands) protein analyzer. Different range of sample types was utilized to characterize each module of the prototype immunosensor (Table 5.1).

Table 5.1. Reference material and sample classification

Sample type	Matrix	Spike	Concentration range	Used to Characterize
A	Water	Food Dye Solution	N/A	ULOC Dilutor
B	Blank cookie extract	Total hazelnut protein (THP) extract	1 – 1000 ppm (v/v)	LFIA performance
C	Blank cookie	Total hazelnut protein (THP) extract	1 – 1000 ppm (v/w)	Homogenizer
D1	Blank cookie	Hazelnut cookie	0.1 – 100 ppm (w/w)	Total prototype
D2	Blank cookie	Hazelnut cookie & peanut cookie	0.1 – 100 ppm (w/w)	Total prototype

2.3 Design & Fabrication

Computer-aided design (CAD) software Autodesk Fusion 360 (Autodesk Inc. San Rafael, CA; USA) was used for designing 3D-printable parts and converting them to printable .stl files. Figure 5.1 gives a schematic overview of the prototype platform; Figure 5.2 provides an annotated photographic overview of the disassembled (5.2A) and assembled (5.2B) platform. The ULOC dilutor (Figure 5.2C) was printed with a stereolithography (SLA) printer Form3 (FormLabs, Somerville, MA; USA) at 25 μm layer resolution using proprietary clear resin (Type O4, FormLabs). A fused deposition modeling (FDM) model (Hepheststos 2, BQ, Madrid; Spain) was used to print the sieves (Supplementary Information (SI) Figure S5.1), device holder (SI Figure S5.2), and interchangeable LFIA cartridges (SI Figure S5.3).

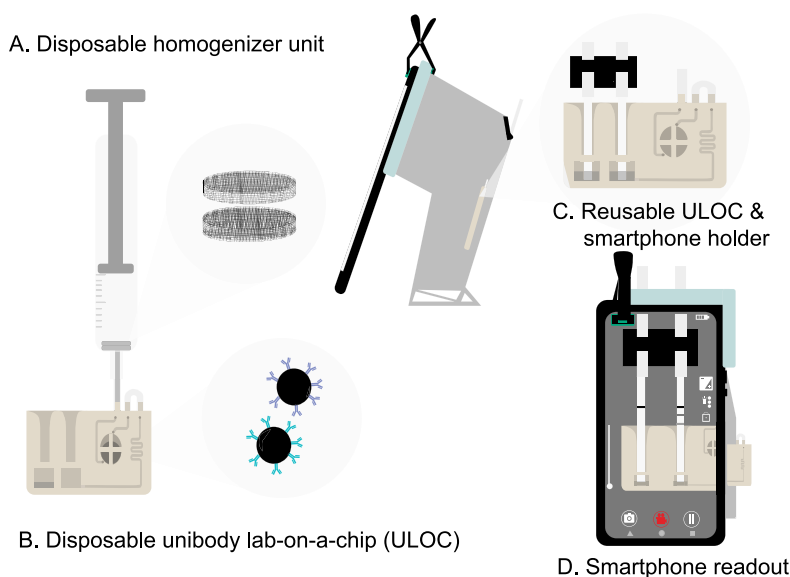


Figure 5.1. Overview schematic of parts of the prototype immunosensor. (A) Disposable homogenizer unit with 3D-printed sieves (B) Disposable unibody lab-on-a-chip (ULOC) for dilution of extracted allergens and mixing with carbon nanoparticle labeled allergen-specific antibodies. (C) Reusable smartphone and ULOC holder. (D) Smartphone readout, as a result, appears in real-time on the screen.

2.4 Homogenizer

The handheld and interconnectable homogenizer unit enables total homogenization and solid-liquid protein extraction from solid food samples. 3D-printed sieves with approximate pore sizes of 0.5 mm were cut by laser (HL40-5g, Full Spectrum Laser LLC, Las Vegas, NV; USA) into discs (18 mm diameter; SI Figure S5.1). Two sieves (Figure 5.1A) insert into a 10 mL syringe at an offset to each other. As the plunger pushes solid material against the first 3D-printed sieve, it breaks into smaller pieces which are subsequently blocked by the second sieve that is kept at an offset, preventing particles from blocking microchannels in the ULOC. Silicon tubing (1.5 mm inner diameter, 40 mm length) connects with the ULOC unibody connector. The tubing can be used as a finger pump or is connected by a second larger piece of silicon tubing (2.5 inner diameter, 20 mm length) to the syringe tip. The syringe pressure is then used for user-controlled actuation.

2.5 ULOC Dilutor

The ULOC dilutor (60 mm W x 40 mm L) has all functional features printed onto a single side. One side is left open, so uncured resin can be removed from 1 mm deep fluidic channels (1 mm wide) by sonicating (FinnSonic m15, FinnSonic Oy, Lahti, Finland) in

ethanol (Sigma Aldrich, Steinheim, Germany) for 30 seconds and air drying. Before sealing the ULOC's open side with adhesive tape, CNP-mAbs and RB were pre-loaded into the reagent reservoir (volume capacity of 250 μL - for flexibility in adjusting RB volume, see Figure S5.4 for bioreagent loading areas) and the reference well (1 μL of CNP-mAb and 100 μL of RB) for control measurements. The RB both stabilized CNP-mAbs for on-chip storage and acted as a dilution buffer for injected samples. The test and reference wells were designed with an internal ledge to prevent any fluid overflow and had a total volume capacity of 200 μL each. Silicon tubing secured the first unibody connector with the homogenizer syringe tip. The remaining two unibody connectors were joined together by silicon tubing (see Figure 5.1B).

2.6 ULOC & Smartphone Holder

The ULOC could be inserted into an opening (50 mm W x 35 mm L) in the 3D-printed device holder, which shielded the assay from ambient light (see SI; Figure S5.2). The LFIA cartridge, which fits 2 LFIAs (4 or 5 mm wide), ensured that the appropriate LFIAs were aligned with the test and reference wells in the ULOC. A smartphone was clamped to the outer frame of the 3D-printed holder overlaying the rear-facing camera and flash.

2.7 Characterization of Prototype Immunosensor

2.7.1 Extraction time

Pre-ground raw hazelnut was incubated in the homogenizer syringe with RB for different periods (1, 2, 3, 5, 10, 20, or 30 minutes) to optimize extraction time and assess 3D-printed sieve efficiency. The total protein concentration was quantified ($n=3$) using the NanoDrop.

2.7.2 ULOC Dilutor

Before characterization, 5 or 10 μL dye was actively injected via a disposable syringe into the manifold. Injections were repeated multiple times for distance verification, with the 5 and 10 μL distances being marked on the ULOC for convenience with subsequent sample loading (see SI Figure S5.5). The ULOC was characterized for its dilution ability by mixing dye with water (sample type A) at various dilution factors (DFs). Adjustable water volumes were pipetted into the ULOC reservoir. Dilution factors of x10, x15, x20, and x40 were achieved by injecting 10 μL of aqueous dye solution to the mark on the ULOC. For comparison with a manually pipetted sample, the same DF dye/water was pipetted into the ULOC reference well. Smartphone images of the ULOC were acquired using OpenCamera (v1.47.3) to keep exposure and focus constant on a Google Pixel 2 XL (Google, California; USA). On and off-chip dilutions were evaluated by comparing the color intensities in the test and reference wells at the end of the manifold²³. Subsequently, images were processed offline using ImageJ²⁸ to split images into their RGB (red, green, blue) color channels. In the blue channel pixel intensity readings were taken from the test and reference wells for direct comparison.

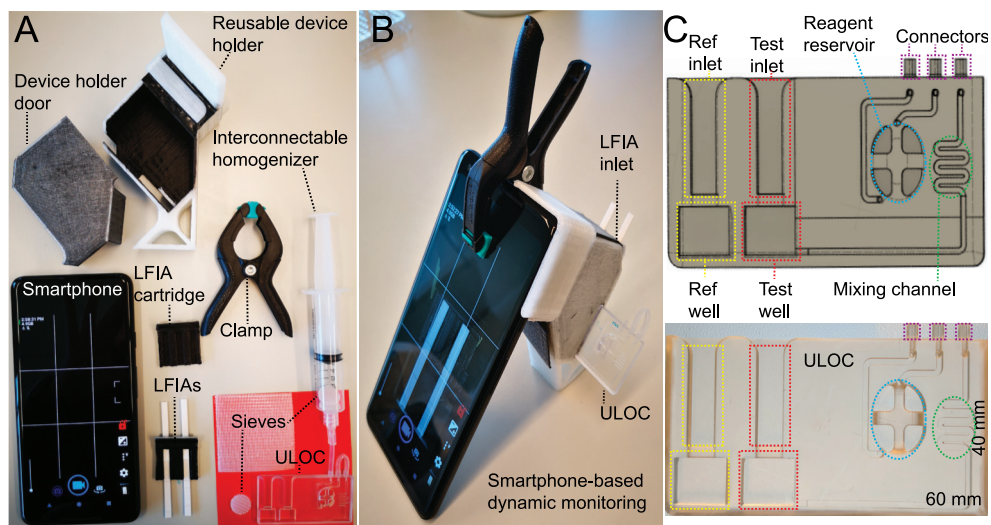


Figure 5.2. Overview of prototype immunosensor. (A) Disassembled prototype immunosensor showing all components. (B) Side view of the assembled device where the Unibody Lab on a Chip (ULOC) slots into the smartphone holder, the smartphone clamps to the holder's frame, the LFIA inserts into the opening, and the results are viewed on the phone. (C) Annotated Computer-Aided Design (CAD) and photo of the ULOC.

2.8 Dynamic Data Acquisition

Images and videos were acquired by smartphone, attached to the holder frame, using OpenCamera to ensure fixed acquisition conditions (fixed focus, locked exposure, controlled illumination, for videos: 30 frames per second (fps), 720 x 480 pixels). LFIA results appeared on the screen as they emerged. Subsequently, videos were split into images of 1 fps using Adapter (v2.1.6), and the resulting time point images were analyzed offline in ImageJ by splitting the images into their color channels. A blue channel pixel intensity (BCPI) reading was taken from below the test line at $t=0$ as a background response; the BCPI measurements from the test and control lines were then subtracted from this to give the corrected BCPI (cBCPI) value. In the assay dynamic working range, cBCPI increases as test and control lines increase in intensity. The T/C ratio is a standard metric used for normalizing sandwich format LFIA results¹¹ and has been applied here.

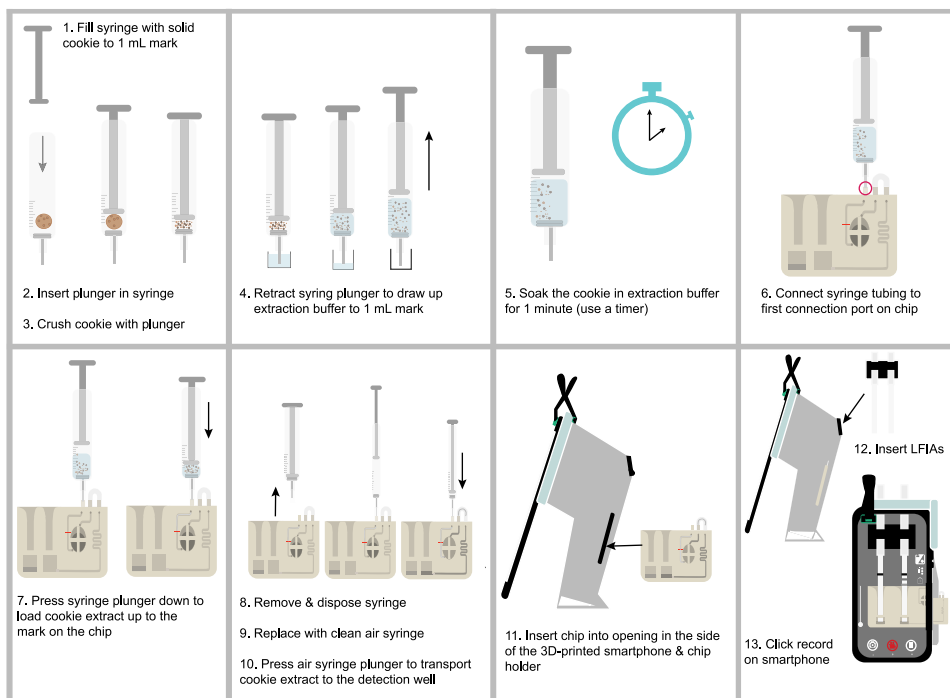


Figure 5.3. Pictogram instructions for operating prototype immunosensor for homogenization, extraction, ULOC-based dilution, transport, and LFIA based detection of food allergens with on-screen smartphone readout. The guidelines have been designed to guide the consumer during citizen science experiments.

2.9 Prototype Immunosensor Characterization

Experiments were performed in triplicate; see Figure 5.3 for the pictogram operation procedure. Before sealing the ULOC with adhesive tape, the reagent reservoir was filled with 2 μL CNP-mAb and 190 μL RB, resulting in a DF x 20 when 10 μL of sample is actively injected into the reservoir. Sample type B was used to characterize the LFIA immunochemistry and smartphone readout. Pre-weighed sample type C was used to evaluate the extraction and filtration by the homogenizer unit by comparing the LFIA result against results obtained with sample type B. To determine the size distribution of the resulting particles crushed by the homogenizer, we tested 3 different solid samples (i.e., BC, HC, and PC; $n=10$) and took 3 individual aliquots and a pooled fraction for each cookie, photographed the particles, and analyzed their size distribution using ImageJ (see SI Protocol S5.1 for full details).

For sample types C and D (approximately 0.25 g), and then incubated with 1 mL RB for 1 minute, before filtering through the 3D-sieves. Finally, to characterize the system for

detecting real-life incurred and processed allergens, sample type D was investigated. The volume of the pre-loaded CNP-mAb was increased to 4 μL (2 μL for the anti-hazelnut mAb-CNP and 2 μL for the anti-peanut mAb-CNP) for multiplex analysis. Here, we consistently injected the sample up to the 10 μL mark on the ULOC to assure the reproducibility of results. However, the sample injection is actively controlled by the user, and they can simply choose to inject the sample further into the ULOC if a greater volume/higher analyte concentration is required. Air displacement transported the sample to the detection well. The ULOC was then inserted into the device holder, the LFIA inserted into the ULOC aligning with the test and reference wells, and the smartphone was set to video record to acquire the data. Here, the immunochromatographic limit of detection (LOD) is the lowest concentration at which two lines (test and control) can be visually, or by smartphone, distinguished compared to a blank sample ($n=3$).

3 Results and Discussion

3.1 Extraction time

A major restriction of allergen analysis is the lengthy extraction process, which typically includes weighing, heating, grinding, and numerous filtering steps^{2,11}. As such, extended extractions delay rapid screening tests such as LFIA. While a 2 minute magneto-assisted allergen antigen extraction has been reported, this still required off-chip microwave pre-heating³. Previously we¹³ described a method for extracting total proteins from cookies and peanut flour at room temperature (RT) in 30 minutes. This method is promising because even with the shorter extraction time and at RT, the extracted samples still required extensive dilution to comply with the LFIA dynamic working range, indicating a much shorter extraction time could still be appropriate for extracting relevant allergenic proteins without delaying the analysis. To test this, we evaluated different extraction times to attempt to reduce the overall assay duration, see Figure 5.4 and SI (Table S5.2). High protein concentrations are extracted even within the first minute (RSD = 1.5%, $n=3$), with the concentration increasing with longer buffer incubation time (first 10 min). The disposable 3D-sieves circumvented the need for further sample filtration, which typically is carried out in a stepwise fashion (see 2.1 & 2.2) to filter out lipids and larger particles. As well as filtering particles, crushing with the 3D-sieves and homogenizer led to reproducible particle size distribution ($n=10$) between the 3 varieties of cookie (0.04 – 1.2 mm particle diameter) with most particles having a diameter between 0.21 – 0.8 mm (see SI Figure S5.6).

Unlike other reported integrated microdevices^{3,10,14}, our extraction requires no sample pre-treatment or heating; the detachable homogenizer unit interconnects with the ULOC, which then executes all outstanding sample handling. Only one other reported

allergen screening device offers solid-liquid internal extraction in less than 4-min¹. These experiments used pre-weighed samples, but to improve consumer-operability, the user can instead simply fill the homogenizer syringe with the solid sample to the 1 mL visual mark, avoiding the need for weighing equipment as this method gave reproducible sample weights ($n=10$) for all 3 variations of cookie tested (see SI Figure S5.7). While this would not result in quantitative results, such an approach is adequate for semi-quantification. Currently, in this early prototype, the extraction buffer is provided in a pre-measured vial containing 1 mL. However, future refinement could include an additional ULOC chamber for on-chip extraction buffer storage.

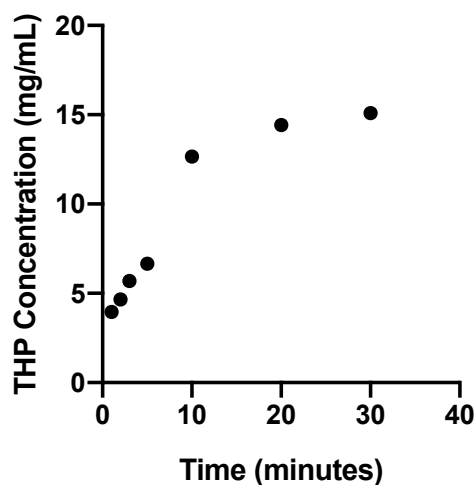


Figure 5.4. Graph showing effects of different buffer incubation times (1, 2, 3, 5, 10, 20 & 30 minutes) on the total hazelnut protein (THP) concentration (mg/mL) in the extract from raw hazelnut ($n=3$ extractions). Error bars are displayed but are too small to see; for standard deviation, see SI Table S5.2.

3.2 ULOC Dilutor

Allergenic proteins exist in foods over a broad dynamic range and must be detected at trace levels for protecting sensitive individuals. Still, it is vital to understand that highly concentrated samples can yield paradoxically low signal intensities, which could easily be misinterpreted by a consumer. However, it is reported that sample dilution (DF \times 10-100) can minimize the occurrence of false-negatives¹¹⁻¹³. While sample dilution is a prerequisite for allergen analysis, we cannot expect the consumer to do this. To circumvent the issue, we have created a system allowing for arbitrary, pipette-free, sample dilution by pre-storing adjustable volumes of RB in the reservoir. When the extracted sample is injected into the reservoir, it efficiently mixes with the pre-stored CNP-mAbs by air displacement and is also diluted in RB by an adjustable DF.

Figure 5.5A compares the BCPIs for on-chip (ULOC-enabled) versus off-chip (manually pipetted) dilutions (dye in water, sample type A, $n=3$) using different DFs. Figure 5.5B indicates where to take the pre-dilution (DF x 0), the mid-dilution (5.5C), and the on-chip and off-chip (5.5D) BCPIs measurements. For consistency, the measurements were always taken below the dye's meniscus. The ULOC DFs invariably matched the manually pipetted DFs, suggesting that the ULOC delivers well-defined sample volumes (see SI Figure S5.5). ULOC devices for other applications have already been extensively characterized for integrated actuation (2-15 μL) with comparable accuracy to pipettes^{23,25}. Injecting the sample causes turbulent mixing (Figure 5.5C) because of the co-injection of air bubbles. Air metering for sample transport is also documented elsewhere¹⁶. The current combined immunosensor benefits from nitrocellulose. When the LFIA touches the turbid liquid, the nitrocellulose wicks the fluid, displacing the air from its pores, without bubbles disrupting the optical measurement.

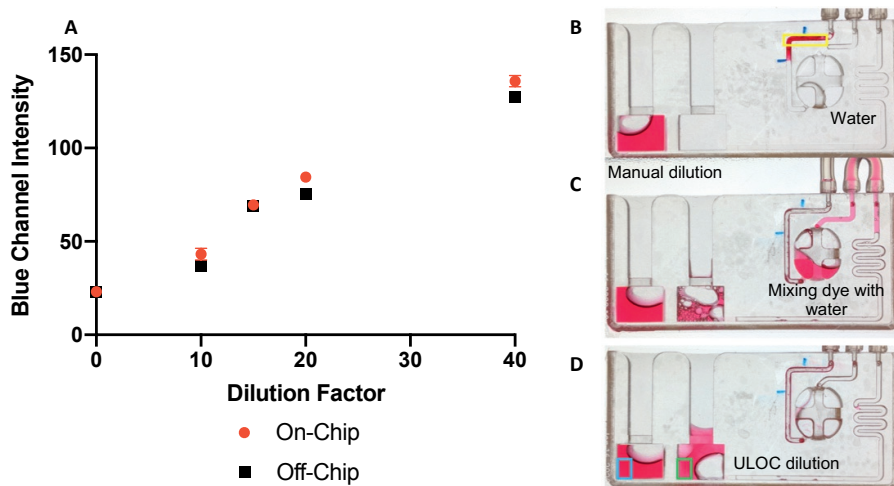


Figure 5.5. ULOC dilutor. (A) Graph depicting the performance of ULOC for unidirectional sample dilution as a function of blue channel intensity. The red circle represents ULOC dilutions. The black square represents manual dilutions. (B) ULOC before dilution, the area where the volume metering reading is taken from is outlined in yellow. (C) ULOC during dilution, the dye mixes with water in the reagent reservoir and is delivered to the test area by the fluidic system. (D) ULOC after dilution, intensity reading for the manual dilution (outlined in blue), and the intensity reading for the ULOC dilution (outlined in green).

3.3 Dynamic Data Acquisition

To investigate the influence of assay duration on the signal development, the LFIAs were readout after 5 (SI Figure [S5.8A]), 10 [S5.8B], 15 [S5.8C], and 20 [S5.8D] minutes

with sample type B (0.1-1000 ppm). From these images, the test and control line signal development [S5.8E] and the T/C ratio development [S5.8F], are each plotted as a function of time (min) in independent calibration curves. At 5 min, the lowest concentration visibly readable is 10 ppm, with the signal improving with increased duration. After 10 min, a 1 ppm signal is readable. However, at 1000 ppm, no signal is generated on either line, even after 10 min. Even with ULOC-enabled sample dilution (DF x 20), high-concentration LFIA effects are observed, affirming the necessity of dilution to avoid false-negative results. The majority of LFIA developers recommend an assay duration of up to 20 min to allow the signal to reach full stability and sensitivity⁸. However, we found that a 15 min duration was suitable for allowing signals to develop for all concentrations, without neglecting highly concentrated samples. In future versions, the ULOC could benefit from having multiple dilution wells for running 3 LFIAs simultaneously across an entire assay dynamic working range, further limiting the occurrence of concentration-dependent effects.

3.4 Total Allergen Protein Detection

Allergenic proteins can be subject to conformational alterations during food processing²⁹. Therefore, biosensors must demonstrate proficiency in detecting allergens in both raw and processed products. Here, solid cookie samples were pre-weighed (0.25 g) for consistency. Still, in real life, the user can instead fill the homogenizer with the cookie to the 1 mL mark to approximately obtain the same sample weight (see SI Figure S5.7). Though this method is less precise, it would suffice for qualitative assessment of bakery products for the presence of allergens. Previously, we found that extracted allergen samples still need extensive dilution before LFIA analysis¹³. Here, a manual DF x 20 (5 μ L of THP in 95 μ L RB) gave clear results at all tested concentrations (see SI Figure S5.9), without compromising detection at the lowest levels, so a DF x 20 was always applied for ULOC-enabled dilutions.

3.5 Total Allergen Protein Extract Screening

See Figure 5.6A for signal development under optimum conditions (e.g., THP extract spiked into RB). For sample B (THP extract spiked into BC extract (v/v); Figure 5.6B), the T/C ratio detection limit is 1 ppm (n=3). Despite using the prototype for analysis, the LOD here is not much higher than in our previous work (0.5 ppm; n=20)¹³, which was obtained using standardized laboratory conditions, pipettes, and equipment. Sample B measurements are reproducible (RSD \pm 2.9%), indicating the ULOC mixes well and delivers persistent volumes, and that the LFIA still works when combined with the ULOC. Solid sample type C (BC spiked with THP extract (w/v); Figure 5.6C) was extracted and analyzed to reflect an actual solid-liquid extraction, with a LOD of 1 ppm (RSD at 1 ppm \pm 3.7%). The slight increase in T/C deviation could be due to the crushing efficacy of the homogenizer. Small differences in buffer incubation times between repeat measurements and non-uniform dispersion of liquid THP extract could be consequential to the somewhat higher variation.

3.6 Incurred Single Allergen Screening

Thermal processing, such as baking, can affect allergen detectability²⁹. See Figure 5.6 to compare signal development for samples using total allergen protein extracts (5.6E) with samples containing incurred allergens (5.6D&F). Testing commercial hazelnut cookies mixed with blank cookies (sample type D1) exemplifies the effectiveness of extracting incurred proteins from a solid matrix into a testable liquid and detecting the allergenic proteins in this liquid. Sample D1 has a LOD of 0.1 ppm (n=3, RSD \pm 3.03%; see Figure 5.6D and F) for processed hazelnut. Compellingly, the D1 LOD is lower than the LOD for sample C. The LFIA is more sensitive towards processed hazelnut. This sensitivity has also been indicated in our singleplex hazelnut LFIA where the same mAb reached the same LOD for HC extract in BC extract²⁷.

In Figure 5.6, high-concentration effects (1000 and 100 ppm) are evident. Even with the faster extraction time and ULOC-dilution concentration-dependent effects still occur, affirming the necessity to dilute allergen samples before analysis^{11,12}. For consumer testing, the loss of the control line (at 1000 ppm) could be problematic, and some tests have additional target lines to limit this¹.

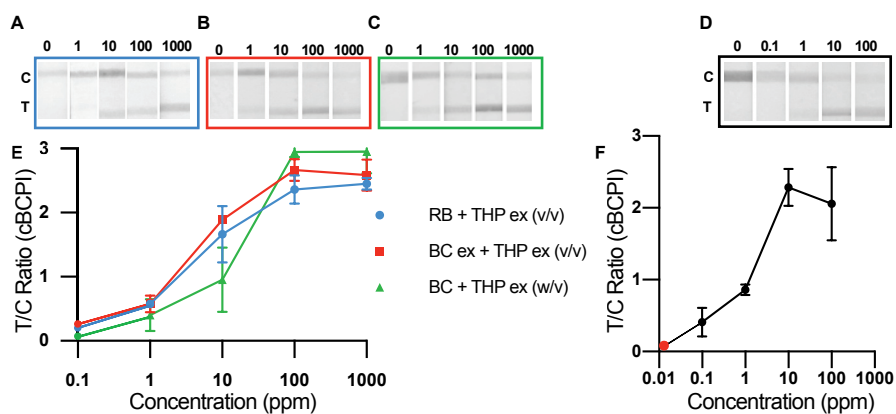


Figure 5.6. Photographs and calibration curves showing LFIA signal development in increasing concentration of analyte where error bars represent standard deviation (n=3) (A) 1-1000 ppm, total hazelnut protein (THP) extract spiked into running buffer (RB)(v/v); (B) 1-1000 ppm, THP extract spiked into a blank cookie (BC) extract (v/v); (C) 1-1000 ppm, BC spiked with THP extract (w/v); (D) 0.1-100 ppm, BC spiked with hazelnut cookie (HC) (w/w); (E) Calibration curve for [A; blue circle], [B; red square] and [C; green triangle] where hollow circles represent the signal at 0 ppm; (F) Calibration curve for D, red circle represents 0 ppm measurement.

Here, we included a reference well in the ULOC pre-containing RB and CNP-mAb for a blank control. The consumer can then use this to directly compare the physical appearance of the test and control lines in real-time. Of course, in a dedicated smartphone-app, any human error would be avoidable, triggering an alert when the LFIA falls outside normality.

3.7 Incurred Multi-Allergen Screening

Sample type D2 (HC and PC in BC (w/w); Figure 5.7) demonstrates the prototype's effectiveness for simultaneously co-extracting and detecting unrelated processed allergens. Both analytes were detectable at 0.1 ppm ($n=3$, $RSD \pm 2.5\%$ and 1.6% for hazelnut and peanut, respectively). There is a slightly lower deviation in multiplex measurements owing to increased control line stability, from using two different CNP-mAbs compared with singleplex analysis. The sensitivity is even better than when using the same LFIAs to detect THP and TPP spiked into BC extract (v/v, LOD 0.5 ppm)¹³ and has similar or higher sensitivity compared to other LFIAs^{11,12}.

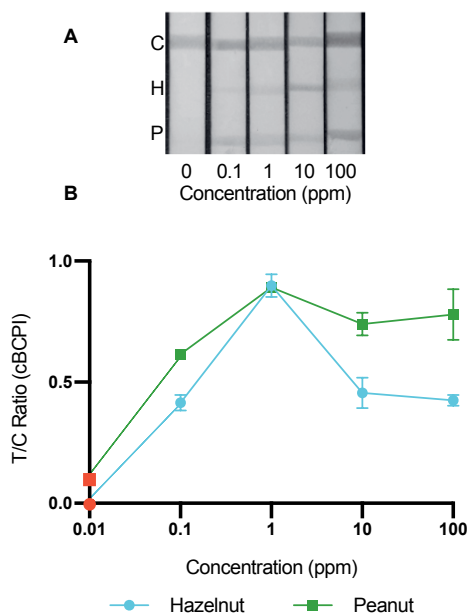


Figure 5.7. Photographs and calibration curves showing multiplex LFIA signal development in increasing concentration of incurred multi-allergen analyte where error bars represent standard deviation ($n=3$). (A) Multiplex calibration range for sample type D2 (i.e., hazelnut cookie and peanut cookie spiked into blank cookie 0.1-100 ppm (w/w)) where C denotes the control line, H the hazelnut test line and P the peanut test line. (B) Calibration curve as a function of the T/C ratio (i.e., test line intensity divided by control line intensity) using corrected blue channel pixel intensities. The red circle represents the T/C ratio in a blank (0 ppm) sample.

3.8 Consumer Diagnostics Potential

The prototype was tested by an independent person with no scientific or technical background to demonstrate consumer-operability. According to the European Citizen Science Association (ECSA), citizen science should involve generating new knowledge that is beneficial to both the citizen and the researcher and with results being made public through open access publications³⁰. We provided the participant with a blank and spiked cookie and two vials with pre-contained volumes of RB, 4 LFIA, and the prototype immunosensor. Following a 5 min explanation and using the pictogram-based standard operating procedure (see Figure 5.3), the participant performed the assay (n=2; see SI Figure S5.10). He then placed the ULOC in the device holder, inserted the reference and test LFIA, and recorded the result on the smartphone. The participant successfully differentiated between the positive and negative results for the spiked and blank samples, signifying the early prototype is already operable by non-skilled individuals after only a short explanation.

4 Conclusions

The reported handheld immunosensor allows for interconnectable sample preparation, solid-liquid protein extraction, dilution, delivery, detection, and smartphone readout of multiple allergens in bakery products. The detachable homogenizer efficiently co-extracts and filters two major but distinct allergens from solid samples in record time. Active injection of the extracted liquid sample into the ULOC mixes the extract with RB for arbitrary sample dilution and with labeled bioreagents before delivery to the detection chamber. This pipette-free dilution limits the occurrence of false-negative results in LFIA. Real-time results are automatically readable as they develop on the phone screen. While the results are readable on the phone screen within 5 minutes, they are optimum after 15 minutes. The interchangeable LFIA cartridge means the reported system with ULOC-enabled sample dilution can easily be applied to test different LFIA targeting various food, biomedical and forensic applications, affirming the value of such a simplified, adjustable, and multifunctional system.

The immunosensor is inexpensive, with current material costs of less than 1\$/USD. The prototype is already consumer-operable, and further advancements, such as image processing in a dedicated smartphone app, will continually improve the usability of the system. The presented handheld system is an encouraging development for affordable, simplified multiplex consumer immunodiagnostics.

Acknowledgments

The authors would like to thank Thomas Tiemens for his participation in citizen science experiments. We would also like to thank Leo van Raamsdonk for making microscope photographs.

References

1. Zhang, J.; Portela, S.B.; Horrell, J.B.; Leung, A., et al. An integrated, accurate, rapid, and economical handheld consumer gluten detector, *Food Chemistry* **2019**, *275*, 446-456, <https://doi.org/10.1016/j.foodchem.2018.08.117>.
2. Tsagkaris, A.S.; Nelis, J.L.D.; Ross, G.M.S.; Jafari, S., et al. Critical assessment of recent trends related to screening and confirmatory analytical methods for selected food contaminants and allergens, *TrAC Trends in Analytical Chemistry* **2019**, *121*, 115688, <https://doi.org/10.1016/j.trac.2019.115688>.
3. Lin, H.Y.; Huang, C.H.; Park, J.; Pathania, D., et al. Integrated Magneto-Chemical Sensor For On-Site Food Allergen Detection, *ACS Nano* **2017**, *11*, 10062-10069, 10.1021/acsnano.7b04318.
4. Ross, G.M.S.; Bremer, M.G.E.G.; Nielen, M.W.F. Consumer-friendly food allergen detection: moving towards smartphone-based immunoassays, *Anal Bioanal Chem* **2018**, *410*, 5353-5371, 10.1007/s00216-018-0989-7.
5. Szybist, L. In: United States (U.S.) Department of Health and Human Services, Food and Drug Administration, 2020.
6. Boxer, J.; Weddell, S.; Broomhead, D.; Hogg, C., et al. Home pregnancy tests in the hands of the intended user, *Journal of Immunoassay and Immunochemistry* **2019**, *40*, 642-652, 10.1080/15321819.2019.1671861.
7. Nelis, J.L.D.; Tsagkaris, A.S.; Dillon, M.J.; Hajslova, J., et al. Smartphone-based optical assays in the food safety field, *TrAC Trends in Analytical Chemistry* **2020**, 115934, <https://doi.org/10.1016/j.trac.2020.115934>.
8. Tsai, T.-T.; Huang, T.-H.; Ho, N.Y.-J.; Chen, Y.-P., et al. Development of a multiplex and sensitive lateral flow immunoassay for the diagnosis of periprosthetic joint infection, *Scientific Reports* **2019**, *9*, 15679, 10.1038/s41598-019-52051-6.
9. Oh, Y.K.; Joung, H.-A.; Kim, S.; Kim, M.-G. Vertical flow immunoassay (VFA) biosensor for a rapid one-step immunoassay, *Lab on a Chip* **2013**, *13*, 768-772, 10.1039/C2LC41016H.
10. Park, M.; Seo, T.S. An integrated microfluidic device with solid-phase extraction and graphene oxide quantum dot array for highly sensitive and multiplex detection of trace metal ions, *Biosensors and Bioelectronics* **2019**, *126*, 405-411, <https://doi.org/10.1016/j.bios.2018.11.010>.
11. Anfossi, L.; Di Nardo, F.; Russo, A.; Cavallera, S., et al. Silver and gold nanoparticles as multi-chromatic lateral flow assay probes for the detection of food allergens, *Anal Bioanal Chem* **2018**, 1905-1913, <https://doi.org/10.1007/s00216-018-1451-6>.
12. Galan-Malo, P.; Pellicer, S.; Pérez, M.D.; Sánchez, L., et al. Development of a novel duplex lateral flow test for simultaneous detection of casein and β -lactoglobulin in food, *Food Chemistry* **2019**, *293*, 41-48, <https://doi.org/10.1016/j.foodchem.2019.04.039>.
13. Ross, G.M.S.; Salentijn, G.I.J.; Nielen, M.W.F. A Critical Comparison between Flow-through and Lateral Flow Immunoassay Formats for Visual and Smartphone-Based Multiplex Allergen Detection, *Biosensors (Basel)* **2019**, *9*, 10.3390/bios9040143.
14. Trinh, K.T.L.; Trinh, T.N.D.; Lee, N.Y. Fully integrated and slidable paper-embedded plastic microdevice for point-of-care testing of multiple foodborne pathogens, *Biosensors and Bioelectronics* **2019**, *135*, 120-128, <https://doi.org/10.1016/j.bios.2019.04.011>.

15. Yin, J.; Suo, Y.; Zou, Z.; Sun, J., et al. Integrated microfluidic systems with sample preparation and nucleic acid amplification, *Lab on a Chip* **2019**, *19*, 2769-2785, 10.1039/C9LC00389D.
16. Du, K.; Cai, H.; Park, M.; Wall, T.A., et al. Multiplexed efficient on-chip sample preparation and sensitive amplification-free detection of Ebola virus, *Biosensors and Bioelectronics* **2017**, *91*, 489-496, <https://doi.org/10.1016/j.bios.2016.12.071>.
17. Zhu, C.; Hu, A.; Cui, J.; Yang, K., et al. A lab-on-a-chip device integrated DNA extraction and solid phase PCR array for the genotyping of high-risk HPV in clinical samples, *Micromachines* **2019**, *10*, doi:10.3390/mi10080537.
18. Comina, G.; Suska, A.; Filippini, D. Low cost lab-on-a-chip prototyping with a consumer grade 3D printer, *Lab on a Chip* **2014**, *14*, 2978-2982, 10.1039/c4lc00394b.
19. Salentijn, G.I.J.; Oomen, P.E.; Grajewski, M.; Verpoorte, E. Fused Deposition Modeling 3D Printing for (Bio)analytical Device Fabrication: Procedures, Materials, and Applications, *Analytical Chemistry* **2017**, *89*, 7053-7061, 10.1021/acs.analchem.7b00828.
20. Comina, G.; Suska, A.; Filippini, D. 3D Printed Unibody Lab-on-a-Chip: Features Survey and Check-Valves Integration., *Micromachines* **2015**, *6*, 437-451.
21. Zeraatkar, M.; Filippini, D.; Percoco, G. On the Impact of the Fabrication Method on the Performance of 3D Printed Mixers., *Micromachines* **2019**, *10*.
22. Park, J.; Park, J.-K. Integrated microfluidic pumps and valves operated by finger actuation, *Lab on a Chip* **2019**, *19*, 2973-2977, 10.1039/C9LC00422J.
23. Suska, A.; Filippini, D. Autonomous lab-on-a-chip generic architecture for disposables with integrated actuation, *Scientific Reports* **2019**, *9*, 20320, 10.1038/s41598-019-55111-z.
24. Reboud, J.; Xu, G.; Garrett, A.; Adriko, M., et al. Paper-based microfluidics for DNA diagnostics of malaria in low resource underserved rural communities, *Proc Natl Acad Sci U S A* **2019**, *116*, 4834-4842, 10.1073/pnas.1812296116.
25. Tsagkaris, A.S.; Pulkrabova, J.; Hajslova, J.; Filippini, D. A Hybrid Lab-on-a-Chip Injector System for Autonomous Carbofuran Screening, *Sensors (Basel)* **2019**, *19*, 5579, 10.3390/s19245579.
26. Salentijn, G.I.J.; Permentier, H.P.; Verpoorte, E. 3D-Printed Paper Spray Ionization Cartridge with Fast Wetting and Continuous Solvent Supply Features, *Analytical Chemistry* **2014**, *86*, 11657-11665, 10.1021/ac502785j.
27. Ross, G.M.S.; Bremer, M.; Wichers, J.H.; van Amerongen, A., et al. Rapid Antibody Selection Using Surface Plasmon Resonance for High-Speed and Sensitive Hazelnut Lateral Flow Prototypes, *Biosensors (Basel)* **2018**, *8*, 10.3390/bios8040130.
28. Schneider, C.A.; Rasband, W.S.; Eliceiri, K.W. NIH Image to ImageJ: 25 years of image analysis, *Nature Methods* **2012**, *9*, 671-675, 10.1038/nmeth.2089.
29. Rahaman, T.; Vasiljevic, T.; Ramchandran, L. Effect of processing on conformational changes of food proteins related to allergenicity, *Trends in Food Science & Technology* **2016**, *49*, 24-34, <https://doi.org/10.1016/j.tifs.2016.01.001>.
30. ECSA. European Citizen Science Association <https://ecsa.citizen-science.net/>, 2020.

Supplementary information

Chapter 5

Table S5.1. Blank biscuit and allergen biscuit ingredients.

Sample	Ingredients	Allergen Information
Blank Cookie	Wheat flour, Sugar, palm oil, salt, glucose–fructose syrup, raising agent, (ammonium carbonate [E503]), natural flavor	Contains: wheat gluten May contain milk, sesame
Hazelnut Cookie	Whole grains, oat flakes, wheat flour, sugar, vegetable oil, glucose fructose syrup, raising agents, salt, emulsifiers, cane sugar molasses	Contains: Hazelnut (10.8%), gluten May contain milk, egg and sesame
Peanut Cookie	Wheat flour, sugar, vegetable oil, center, salt, milk proteins, invert sugar syrup, dextrose, aroma	Contains: Peanut (25%), egg, milk May contain gluten containing grains, nuts

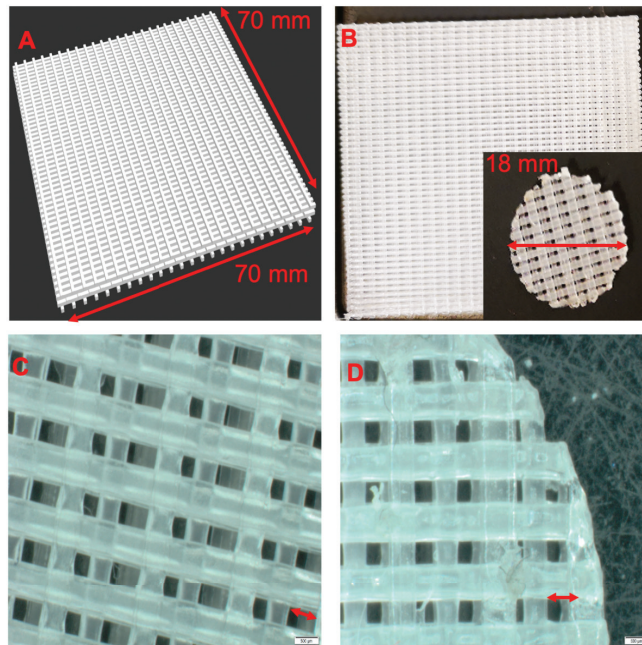


Figure S5.1. 3D-printed sieves. (A) Computer aided design (CAD) of sieve sheet. (B) 3D-print of the sieve sheet. Insert showing the 18 mm diameter laser cut sieves. (C) Microscope image of sieve, scale bar (500 μm) in bottom right-hand corner and indicated by red arrow. (D) Microscope image of edge of laser cut sieve, scale bar (500 μm) in bottom right-hand corner and indicated by red arrow.

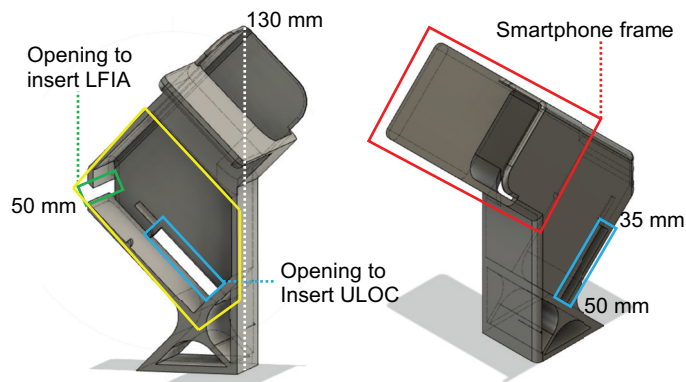


Figure S5.2. Computer aided design (CAD) image for smartphone device holder. Slot to insert ULOC is outlined in blue. The frame for clamping the smartphone to is outlined in red. The area to insert LFIA cartridge is outlined in green. The area which is closed by the door is outlined in yellow.

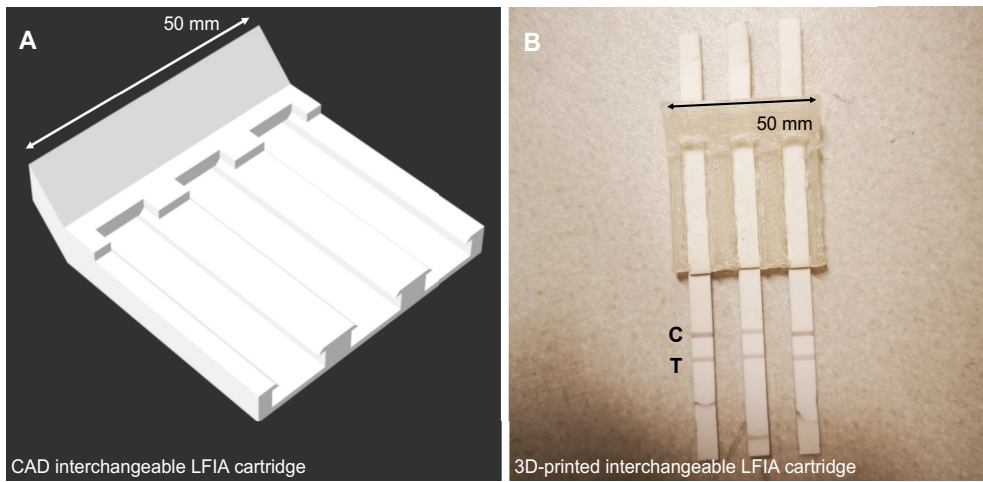
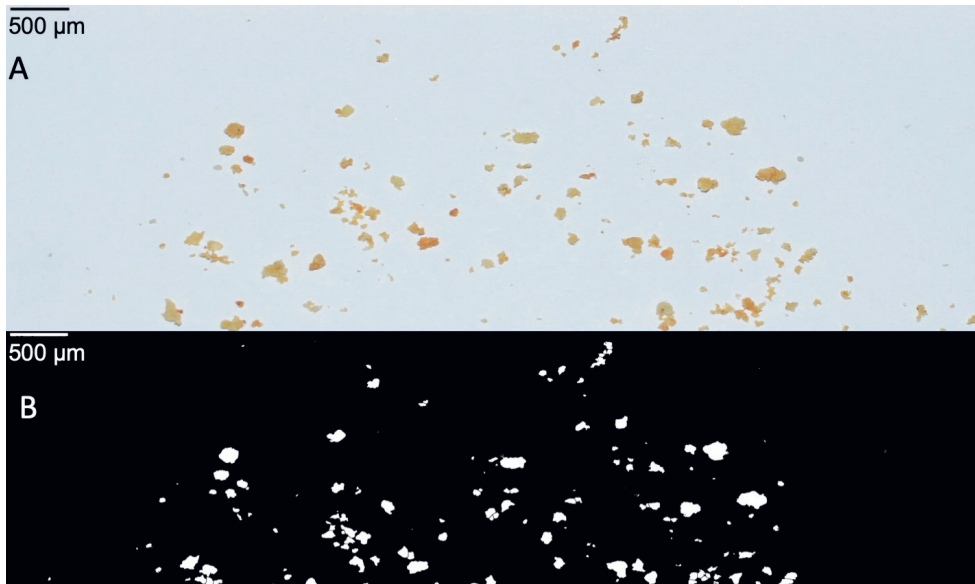


Figure S5.3. LfIA cartridge. (A) Computer aided design (CAD) of 50 mm LfIA cartridge which houses 3 LFIAs of 4 or 5 mm wide. (B) 3D-printed LfIA cartridge with 3 LFIAs inserted.

Protocol S5.1. Procedure for particle analysis using ImageJ.



1. Open image of crushed sample in ImageJ **(A)**
2. Set scale. A line was made along the scale of a ruler (5 mm) in the image and Set Scale function [Analyze>Set Scale] was selected.
3. Region of Interest (ROI). Using the Rectangular tool, a fixed region excluding the scale bar was selected.
4. Crop image. The image was cropped [Image>Crop] based on the defined rectangular ROI.
5. Make image binary. The cropped image was transformed into a binary image **(B)** [Process>Binary>Make Binary]. This makes the outline of the particle visible.
6. Apply Fill Holes [Process>Binary>Fill Holes]. The hollow particles are turned into solid particles.
7. Apply Watershed [Process>Binary>Watershed]. This breaks closely located particles.
8. Apply Particle Analysis [Analyze>Analyze Particles]
9. Copy result of particle sizes to spreadsheet.

Table S5.2. Effect of different incubation times (minutes) on the protein concentration (mg/mL) in the extract of whole raw hazelnut (n=3)

Extraction time	1st	2nd	3rd	%RSD
1	3.94	3.89	4.02	1.5
2	4.64	4.52	4.80	3.0
3	5.58	6.01	5.49	4.9
5	6.59	6.65	6.72	0.9
10	12.42	13.03	12.51	2.5
20	14.68	13.98	14.60	2.6
30	15.11	15.25	14.90	1.1

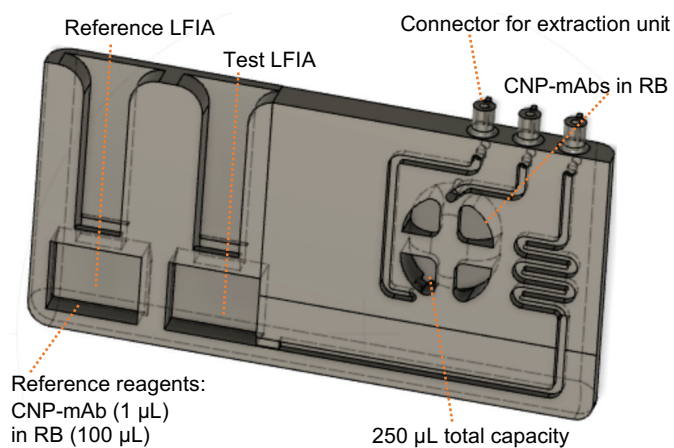


Figure S5.4. Annotated computer aided design (CAD) of the ULOC device indicating where the reference and test LFIA are inserted, where the extraction unit connects to, where the carbon-nanoparticle labelled antibodies (CNP-mAbs) and running buffer (RB) are pre-loaded and where the reference reagents are pre-loaded.

A. 10 μL (n=2)



B. 5 μL (n=2)

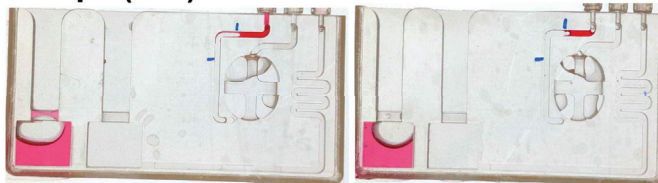


Figure S5.5. *Unibody Lab on a Chip (ULOC) devices showing loading of dye to (A) 10 μL mark (n=2) (B) 5 μL mark (n=2).*

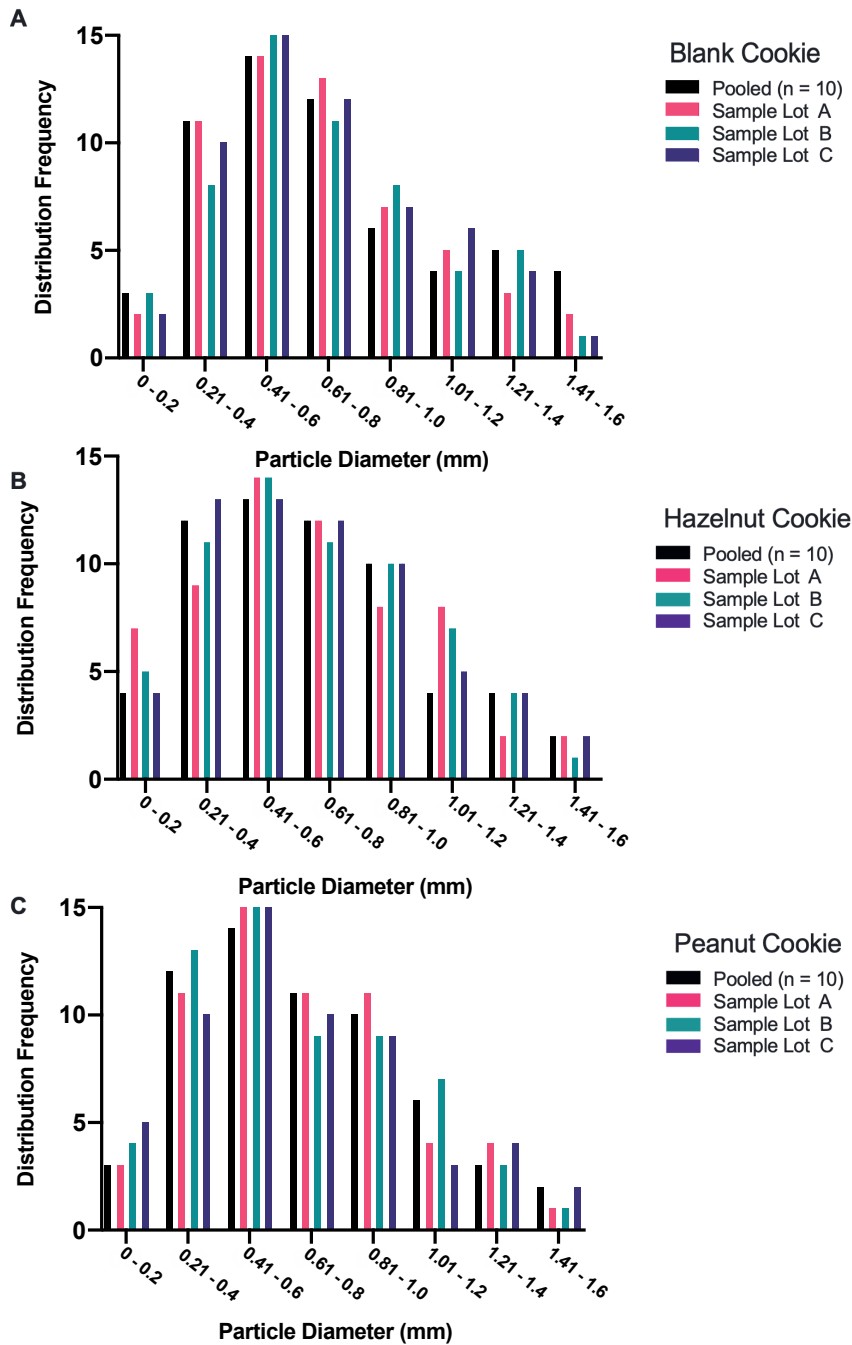


Figure S5.6. Image particle size distribution of 3 varieties of cookie sample (A) blank, (B) hazelnut and (C) peanut cookies, crushed by the homogenizer unit, where the black bars represent the size distribution from a pooled sample ($n=10$), and the pink, teal and purple bars represent 3 individual homogenizations.

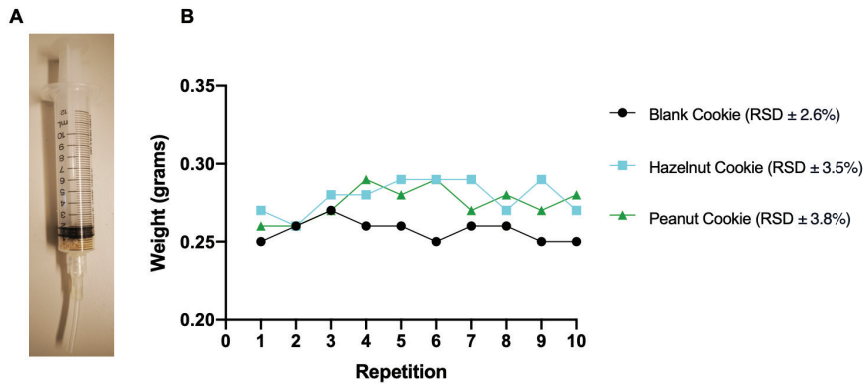


Figure S5.7. Filling the homogenizer syringe to 1 mL mark with cookie (A) photo of syringe filled to 1 mL with blank cookie. (B) Graph showing the variation in weight from filling the syringe to 1 mL mark with blank cookie (black), hazelnut cookie (blue) and peanut cookie (green).

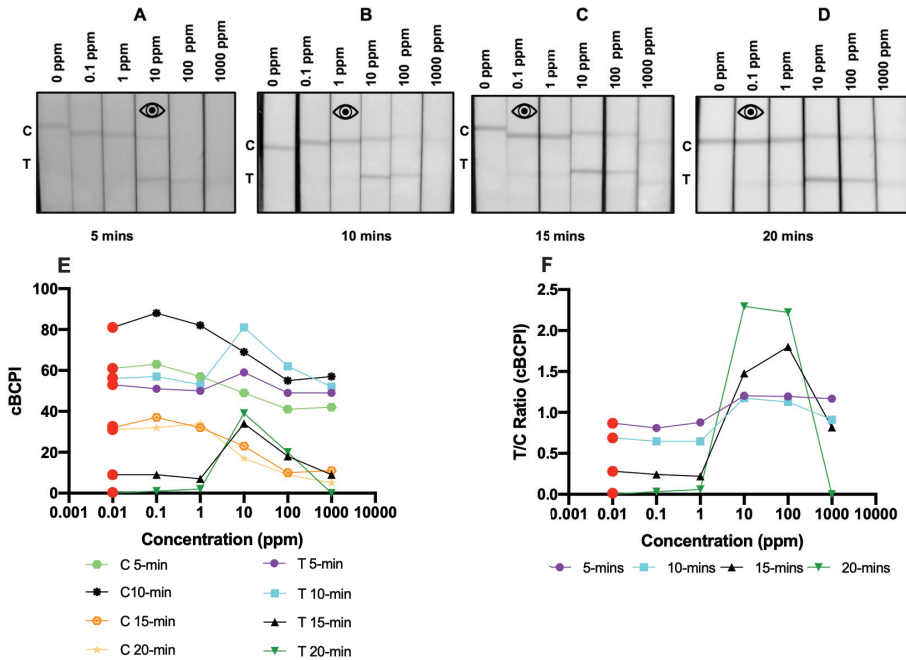


Figure S5.8. Endpoint images and calibration curves showing development of LFIAs tested in an increasing concentration of total hazelnut protein (THP) extract in blank cookie (BC) extract in the range of 0.1-1000 ppm, C represents the control line and T represents the test line, the eye symbol represents the visual LOD at that given time point. All intensities are measured in the blue channel of RGB corrected by subtracting the background response of a blank test. (A) LFIAs after 5 minutes. (B) LFIAs after 10 minutes. (C) LFIAs after 15 minutes. (D) LFIAs after 20 minutes. (E) Calibration curve showing the corrected blue channel pixel intensity (cBCPI) response for the control (C) and test (T) line development (F) Calibration curve showing the test line divided by control line (T/C ratio) development.

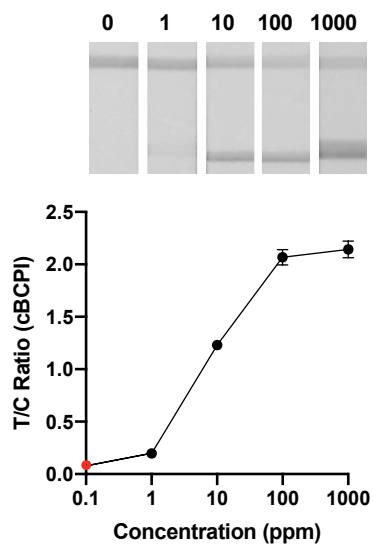


Figure S5.9. Calibration curve for 5 μL of total hazelnut protein (THP) in 95 μL running buffer (RB), a dilution factor (DF) of $\times 20$. Corrected blue channel pixel intensity is plotted by subtracting the blank response and dividing the test line intensity by the corresponding control line intensity value (T/C ratio). The red circle represents the T/C ratio in a blank (0 ppm) sample. Error bars represent the standard deviation ($n=3$).



Figure S5.10. Citizen science experiments ($n=2$). Participant (age 15 years) was provided with a short demo, pictogram instruction sheet, and the prototype to perform experiments.

CHAPTER 6

6

Unraveling the hook effect: a comprehensive study of high antigen concentration effects in sandwich lateral flow immunoassays

Adapted from:

Ross, G.M.S., Filippini, D., Nielen, M.W.F., Salentijn, G.IJ., 2020. Unravelling the hook effect: a comprehensive study of high antigen concentration effects in sandwich lateral flow immunoassay. Analytical Chemistry. 92 (23). 15587-15595 doi:10.1021/acs.analchem.0c0374

Sandwich lateral flow immunoassays (LFIAs) are limited at high antigen concentrations by the hook-effect, leading to a contradictory decrease in test line (**T**) intensity and false-negative results. The hook-effect is mainly associated with the loss of **T**, and research focuses on minimizing this effect. Nevertheless, the control line (**C**) intensity is also affected at higher analyte concentrations, undesirably influencing the **T/C** ratio in LFIA readers. The main aim of this work is to identify and understand such high antigen concentration effects in order to develop ubiquitous strategies to interpret and mitigate such effects. Four complementary experiments were performed: performance assessment of three different allergen LFIAs (two hazelnut, one peanut) over 0.075 – 3500 ppm, LFIAs with **C** only, surface plasmon resonance (SPR) binding experiments on the immobilized control antibody and, smartphone video recording of LFIAs during their development. As antigen concentrations increase, the **C** signal decreases before **T** signal does, suggesting that distinct mechanisms underlie these intensity reductions. Reduced binding at the **C** occurred even in the absence of **T**, so the upfront **T** does not explain loss of **C**. SPR confirmed the **C** antibody favors binding with free labeled antibody compared with labeled-antibody-analyte-complex, indicating that in antigen excess, binding is reduced at **C** before **T**. Finally, a smartphone-based video method was developed for dynamically monitoring LFIA development in real-time to distinguish between different concentration-dependent effects. Digitally analyzing the data allows clear differentiation of highly positive samples and false-negative samples and can conclude whether the LFIA is in the dynamic working range or at critically high concentrations.

1 Introduction

Lateral flow immunoassays (LFIA) have revolutionized consumer diagnostics, translating laboratory-based immunoassays into affordable, accessible home testing devices¹. Sandwich format LFIA utilize two bivalent monoclonal antibodies (mAbs) to capture and detect large multivalent targets, such as allergens². In microplate-based immunoassays, capture mAbs are directly immobilized onto the solid support of the microwell³; in LFIA, the capture mAb is shaped into a test line (**T**). A labeled secondary mAb, which generally binds to a different or repeating epitope on the antigen, forms a sandwich complex with the antigen and capture antibody. The label yields a measurable, often optical signal. In a sandwich LFIA's working range, **T** signal increases with an increase in target antigen concentration; the naked eye can qualitatively read this. However, researchers have known since 1974⁴ that an excess antigen concentration leads to saturation of available binding sites on the bivalent capture and detector mAbs, preventing the formation of a sandwich complex in the **T** area, which in turn leads to a paradoxical loss of **T** signal intensity^{3,5-7}. This disappearance of **T** is known as the hook-effect⁸.

In LFIA, in addition to the capture and detection mAbs, a secondary, species-specific antibody, capable of binding the labeled detection mAb, is immobilized as a control line (**C**)⁹. The **C** informs the user that the test is valid, yielding a signal regardless of the presence of antigen. When analyzing LFIA with a digital optical reader such as a smartphone¹⁰, the ever-present **C** can be used to normalize the **T** against, to correct for experimental variables (**T/C**)¹¹. The use of **T/C** thus assumes that the **C** intensity is constant. However, it has been observed that increasing antigen concentration also leads to a decrease in **C** intensity, while the **T** intensity still heightens¹²⁻¹⁴. Loss of **C** compromises the reliability of the **T/C** at high concentrations, and yet remains to be fully understood. In literature, various concentration-dependent effects are described under the hook-effect definition. See the Supplementary Information (SI) Table S6.1 for a review of the definitions given for the hook-effect and the observed effects in the literature (1974-2020). Despite the qualifying characteristic of the hook-effect being a false-negative result (i.e., the absence of **T**), the definition is frequently also used to describe effects causing loss of the **C**.

There are numerous mitigation strategies to cope with high-concentration effects in sandwich immunoassays:

The most apparent method is testing the sample, both undiluted and diluted¹⁵. If the diluted sample gives a stronger **T** response than the undiluted sample, the undiluted result can be considered as 'hooked'¹⁶. Dilutions allow adjustment of the dynamic working range of an LFIA but also require additional sample preparation, time, and material costs¹⁷. Conversely, changing the physical layout of the assay can prevent high concentration effects^{2,18}, essentially allowing for decoupled reagent delivery¹⁹. Still, separation of

reagent flow is crucial to prevent premature mixing of labeled antibody and analyte²⁰. Alternatively, high-concentration effects can be minimized by optimizing reagents, for example, by supplementing the immunoassay with one or more additional target lines^{6,21,22}. Differentiation between artificially low ('hooked') and truly low concentration samples is possible by real-time monitoring of **T** and **C** development¹⁴ and can allow for LFIA dynamic ranges to be expanded by orders of magnitude²³.

In this work, the aim was to first unravel the hook-effect by comprehensively elucidating how extreme antigen concentrations influence LFIA test line and control line development over time in three different allergen LFIAs. The identification and understanding of how high antigen concentrations influence LFIA signal development is crucial for any sandwich LFIAs and will lead to ways to mitigate such effects, such as by the simplified dynamic smartphone-based method presented here; ultimately leading to more reliable testing.

2 Experimental

Three allergen LFIAs were developed for detecting peanut [PA] and hazelnut [HA1 + HA2]. Each assay has a different sandwich pair of mAbs for their capture (**T**) and detector (carbon nanoparticle-labeled-antibody (CNP-mAb)) mAbs, selected for their differences in sensitivity as observed in prior work²⁴⁻²⁶. All assays used goat-anti mouse (GAMaB) IgG in PBS (pH 7.6; 1.2 mg/mL; AffiniPure F(ab')₂ Fragment) at the **C** line (Jackson Immunoresearch Laboratories Inc., Sanbio, Uden; The Netherlands) and were developed on nitrocellulose membranes (140 CN; Unisart, Sartorius, Gottingen, Germany) overlaid with an absorbent pad (Whatman, GE Healthcare, Eindhoven, The Netherlands) and secured with a plastic backing (G and L, San Jose, CA, USA); see SI Protocol S6.1 and S6.2 for full details on CNP-mAb labeling and LFIA preparation details. For the SPR biosensor assay, an amine coupling kit, pH scouting kit, HBS-EP buffer, and CM5 sensor chips were purchased from GE Healthcare (Uppsala, Sweden); see SI Protocol S6.3 for further detail on the immobilization procedure.

2.1 Reference Materials

Standardized certified reference materials and standard solutions for food allergens are not currently available, and therefore, total protein extracts required in-house preparation²⁷. The procedure for total protein extraction for generating total peanut protein (TPP) and total hazelnut protein (THP) has been described previously^{25,26}. Fresh aliquots were defrosted on the day of experiments, and the protein content was checked with the NanoDrop (ND 3300, Isogen Life Sciences, De Meern; The Netherlands) before use.

2.2 LFIA readout

A qualitative assessment of LFIAs was made by reading the developed signal with the naked eye; quantitative readings were performed by smartphone detection²⁸. A custom 3D-printed smartphone holder was used to shield up to 3 LFIAs from ambient light during optical measurements (See Figure 6.1 and SI Figures S6.1 & S6.2). A smartphone (Google Pixel 2 XL, Google, Mountain View, CA; USA) was used to record images and videos of developing LFIAs. The smartphone was attached to the frame of the holder, supporting the phone during the dynamic measurements (locked exposure, fixed focus, controlled illumination) at 30 frames per second (fps) using OpenCamera (v1.47.3). Adapter (v2.1.6) converted the videos into images of 1 fps. ImageJ²⁹ was used to split the images into their RGB (red, green, blue) color channels. Blue channel intensity values for the **T** and **C** were subtracted from a background reading; the resulting corrected blue channel pixel intensity (cBCPI) increased with increasing line intensity.

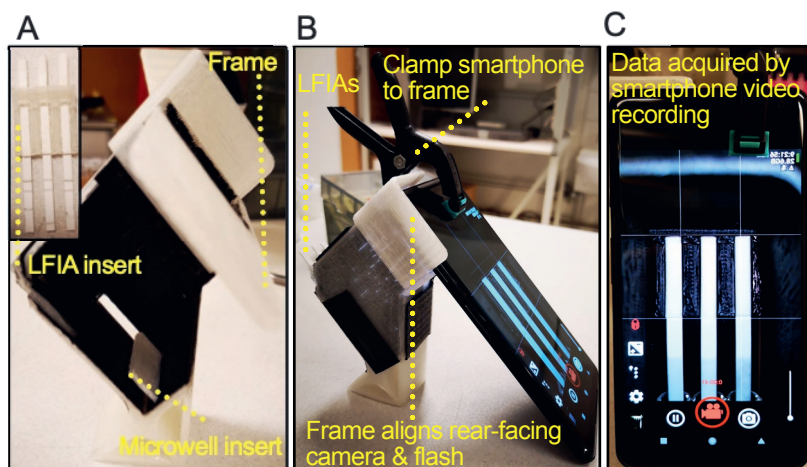


Figure 6.1. Photographs of the 3D-printed smartphone-holder for recording LFIA signal development under controlled lighting: (A) open side view to show where LFIAs and microwells are inserted; (B) closed side view with the LFIAs inserted and smartphone attached; (C) head-on view of LFIA signal development on the phone screen.

2.3 Influence of antigen concentration on LFIA signal development

All three LFIAs were tested in a concentration range spanning 5 orders of magnitude. LFIAs were inserted into microwells containing 99 μ L of antigen in RB (0.0075–3500 ppm of TPP or THP) and 1 μ L of CNP-mAb. Here, endpoint images of **T** and **C** signals were used for calculating **T/C**; LFIAs were left to develop for 40 minutes before the results were recorded by smartphone.

2.4 Influence of antigen concentration on signal development in C only LFIAs

The LFIAs were tested alongside a LFIA with only a GAMaB **C**, at concentrations shown to diminish **C** intensity (5 ppm, 10 ppm, 25 ppm, and 50 ppm) ($n=2$). Additionally, the original LFIAs were ran in a blank as a negative control. LFIAs were developed in a microwell containing 99 μL of antigen in RB (50 ppm TPP, 5 or 50 ppm THP) and 1 μL of CNP-mAb; LFIAs developed for 30 minutes in the 3D-printed smartphone holder (Figure 6.1).

2.5 Sequential and pre-mixed antigen-binding studied by SPR

Biosensor chip immobilization was performed per the manufacturer's instructions; see SI Protocol S6.3 for further details. Using SPR, the influence of increased analyte concentration on the binding characteristics of free CNP-mAb (and subsequently introduced analyte) or pre-mixed immunocomplex ([CNP-mAb-analyte]) towards immobilized GAMaB was evaluated ($n=3$). For sequential measurements, 10 μL of CNP-mAb (diluted 1:99 in HBS-EP) was injected across the GAMaB surface (flow rate of 25 $\mu\text{L}/\text{min}$). After binding, 10 μL analyte solution was injected. For pre-mix experiments, 10 μL of CNP-mAb and analyte solution was injected at 25 $\mu\text{L}/\text{min}$. These experiments were performed at concentrations of 0.1 - 3000 ppm. For regenerating the surface, the flow was adjusted (50 $\mu\text{L}/\text{min}$), and 5 μL 25 mM NaOH was injected, returning the signal to baseline.

2.6 Dynamic monitoring of LFIA signal development

LFIAs were placed in microwells containing 99 μL of antigen in RB (0.0075-3500 ppm of TPP or THP) and 1 μL of CNP-mAb, inserted into the smartphone holder, and were dynamically recorded for 30 minutes. The **T/C** was acquired at set time points (5 - 30 minutes) by selecting frames from the video. This was done for different concentrations ([PA: 0.015-3000 ppm], [HA1: 0.015-3000 ppm], & [HA2: 0.015-2000 ppm]). Alternatively, videos were imported into custom python scripts (Python 3.7) for automated data analysis. In an early video frame, regions of interest (ROI) were positioned over the **T** and **C**, and as a background reading. Data evaluation consisted of averaging the blue pixel intensity in the ROIs across the entire video duration at 1-second data points. The generated responses were exported in a comma-separated value (.csv) format for easy importing into spreadsheet programs. A second, complementary python script corrected the time-response to assess LFIA signal development.

3 Results and Discussion

3.1 Influence of antigen concentration on LFIA signal development

As most reported LFIAs are tested within a limited range and read after up to 20 minutes, high concentration effects are not well documented, but it is known that excess antigen can influence the signal development time. Here, three different LFIAs were tested in a

concentration range spanning 0.0075 – 3500 ppm (Figure 6.2) and developed over 40 minutes before their endpoint image was recorded by smartphone.

In all three assays, the **T** follows the same pattern across the concentration range, as can be observed visually (Figures 6.2 A;D;G) and numerically (Figures 6.2 B;E;H). **T** signal depends on the capture of antigen followed by binding of CNP-mAb, or on the binding of already complexed [CNP-mAb-analyte] to the immobilized antibody. At 0 ppm, there is no analyte present; therefore, no **T** signal develops. As the analyte concentration increases (up to 100 ppm [PA], 10 ppm [HA1], and 10 ppm [HA2]), the **T** intensity increases, by capturing more analyte, and correspondingly, more CNP-mAb or by capturing larger, higher-order immunocomplexes. These complexes form when multivalent antigen, such as hazelnuts and peanuts, with numerous identical or distinct epitopes³⁰, binds several CNP-mAb particles leading to the formation of an intense **T** at high concentrations. Beyond these concentrations, the **T** intensity instead starts decreasing, producing false negatives. This hook-effect is unsurprising because, at extreme antigen-excess, **T** is rapidly saturated by an accumulation of unlabeled antigen, while the remaining, mobile, excess antigen binds with CNP-mAb without being captured on **T**².

Comparably, **C** signal arises due to the binding of CNP-mAb. Therefore, in a blank (0 ppm), a clear **C** is seen. At low concentrations, **C** captures free CNP-mAbs yielding an intense signal, as observed visually (Figures 6.2 A;D;G) and numerically (Figures 6.2 B;E;H). In this range, **C** intensity increases slightly with increasing antigen concentration, possibly due to the binding of multiple CNP-mAbs to the same multivalent allergenic protein, resulting in increased signal intensity³¹. At higher concentrations (roughly above 10 ppm [PA], 0.5 ppm [HA1], and 1 ppm [HA2]), the **C** intensity decreases, while the **T** still becomes more intense. This is reflected in the endpoint **T/C** metric (Figure 6.2 C;F;I). **T/C** increases along with **T** and rises further still at concentrations causing **C** to decrease. This increase in **T/C** widens the LFIA's linear dynamic working range even when **C** is affected by concentration. Only after the hook-effect has occurred, leading to a decrease in **T**, does the **T/C** drastically drop. This trend is consistent across all 3 assays, despite them detecting distinct antigens and using different mAb sandwich pairs with diverse sensitivities and kinetics^{24,25}; as well as from the body of literature describing high concentration effects in LFIA (see SI Table S6.1^{2,12,14}). A decrease in **C** must be caused by a reduction in CNP-mAb binding, which could potentially be due to preventing the arrival of CNP-mAbs at the **C** by the **T** (investigated in the **C** only section below), or by decreasing the avidity of the CNP-mAbs to bind at those sites, which is assessed by the SPR experiments³².

Interestingly, as the concentration further increases (above 100 ppm [PA], 250 ppm [HA1 & HA2]), the **C** intensity partially reappears. At extreme concentrations, multivalent proteins have a propensity to aggregate, potentially masking their epitopes³³. Moreover, these antigen

concentrations probably hinder higher-order immunocomplex formation because there is insufficient CNP-mAb available for binding with the abundant antigen in larger complexes^{12,34}.

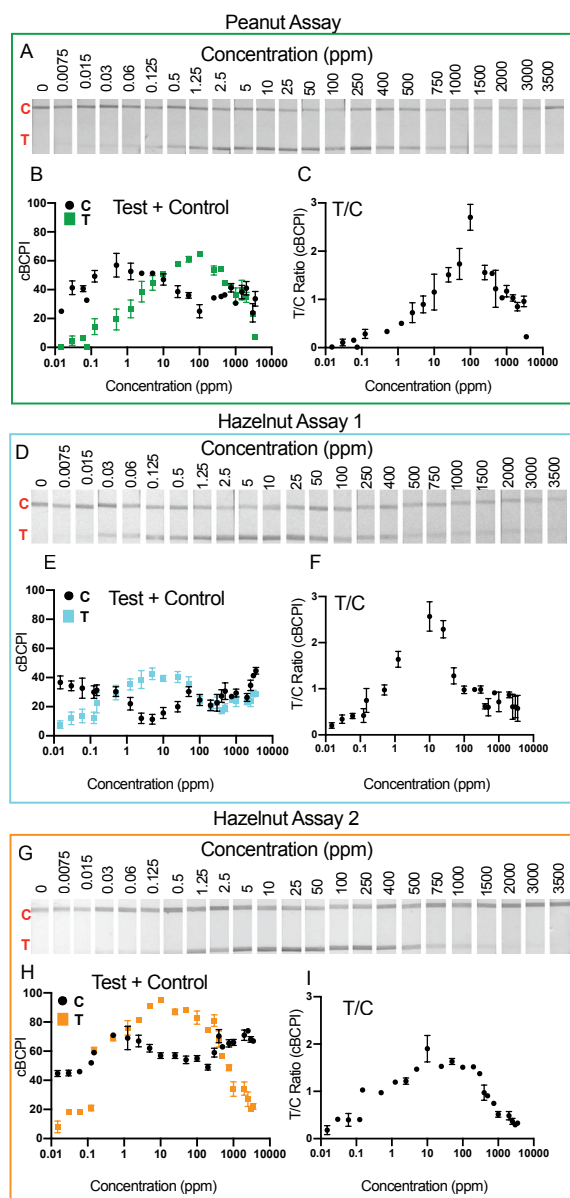


Figure 6.2. Extended calibration range of the 3 LFIA, peanut assay [PA], hazelnut assay 1 [HA1], and hazelnut assay 2 [HA2] in increasing concentration of the analyte (total peanut protein or total hazelnut protein) spiked into RB (0.0075-3500 ppm) ($n=3$). (A, D & G) photographs after 40 minutes. (B, E, H) test and control signal expressed in corrected blue channel pixel intensity (cBCPI) (C, F & I) test line is divided by the control line (T/C Ratio). Error bars represent the standard deviation ($n = 3$).

3.2 Influence of antigen concentration on signal development in C only LFIA

In the extended calibration range, specific concentrations caused the appearance of an intense **T** and a comparably diminished **C**, affecting the **T/C**, as was observed in Figure 6.2 C;F;I. Possibly, at these moderately high concentrations, the antigen, which is bound in immunocomplex with CNP-mAb, binds mostly at the **T**, thus limiting the amount of CNP-mAb that can reach the **C** and can interact with GAMaB. Figure 6.3A-C shows the 3 assays tested at concentrations observed to affect **C** development; Figure 6.3D shows the cBCPIs (n=2) of the **C** from the three variations of the assay, for all three assays. Both in the presence and absence of a **T**, the **C** never reaches the full intensity it would obtain in a blank. Interestingly, the signal for the **C** in the regular LFIA (green [PA], blue [HA1], orange [HA2]), and the **C** only LFIA (checked green [PA], checked blue [HA1], and checked orange [HA2]) are of similar intensity. However, 3D shows that the intensity of **C** in the **C+T** LFIA, is often less than in the **C** only LFIA, indicating that some binding of [CNP-mAb-analyte] at **T** could have a minor contribution to the reduction of binding at **C**. However, there is a more substantial **C** intensity difference between the blank and antigen solutions for each assay, at all tested concentrations. This emphasizes that a reduction of binding at **C** must be due to increased antigen concentrations causing the CNP-mAb to have a decreased avidity for **C**.

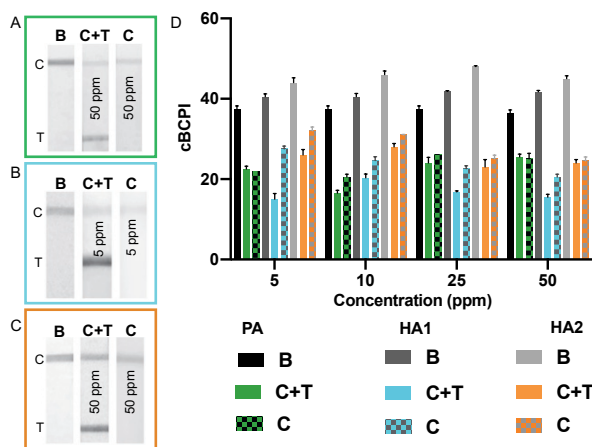


Figure 6.3. Control line only LFIA. Control signal development in LFIA with a control line and a test line (C+T) and LFIA with only a control line (C-only). (A) Peanut assay (PA) C+T signal development in a blank (B), C+T & C-only in 50 ppm total peanut protein (TPP). (B) Hazelnut assay 1 (HA1) C+T & C-only signal development in B and in 5 ppm total hazelnut protein (THP), (C) Hazelnut assay 2 (HA2) C+T & C-only signal development in B and in 50 ppm THP, (D) Signal intensity in B, C+T & C-only across all 3 LFIA as a corrected blue channel pixel intensity (cBCPI).

3.3 Sequential and pre-mixed antigen-binding studied by SPR

Here, using SPR, we set out to elucidate whether increased antigen concentration hinders the labeled [CNP-mAb-analyte] immunocomplex' ability to bind with the GAMaB (pre-mix) compared with whether increased antigen concentration affects the binding of CNP-mAb decoupled from the analyte. SPR typically is label-free²⁴ but antibody labeling can alter essential binding characteristics^{35,36}. In SPR response units (RU's) are generated by the total amount material captured at the surface, compared with LFIA, where the signal is made up solely from the binding of CNP-mAb to **C**. Moreover, it is also important to note that these assays take place on a very different time scale (i.e., LFIA; 40 minutes vs. SPR; 40 seconds).

The RU's reproducibly increased in all 3 assays following the injection of CNP-mAb, as can be seen in Figure 6.4A-C, where the black bar represents the free CNP-mAb binding with GAMaB. Adjusting the concentration of the injected analyte in the second step again leads to a reproducible RU increase in all assays, as can be seen by the colored bar increasing (green [PA], blue [HA1], orange [HA2]). Since these multivalent antigens bind to the captured CNP-mAb, thereby increasing the total mass of material bound to the chip surface, this increase in RU is unsurprising.

Contrastingly, when simultaneously injecting CNP-mAb + antigen (pre-mix), the assays behaved differently (checked green [PA], checked blue [HA1], and checked orange [HA2]) (see SI Figure S6.3 for an example of sequential and pre-mixed TPP sensorgrams). Crucially, the signal intensity in the pre-mix approach is consistently lower versus the sequential approach at all tested antigen concentrations. In excess analyte concentrations, [CNP-mAb-analyte] quickly forms, depleting the free CNP-mAb, which would otherwise interact with **C** with higher avidity than the complex². This explains why high antigen concentrations cause a reduction in binding towards GAMaB in both LFIA and SPR. The **C** signal is consistently reduced at a lower concentration than the **T** signal in LFIA. As soon as an assay is in antigen excess, a prerequisite to enter the hook-range, higher-order immunocomplexes would already have formed in solution. Formation of such complexes would deplete the amount of free CNP-mAb available for binding with **C**.

Therefore, for the hook-effect at **T** to occur, the concentration effect on the **C** must have already taken place.

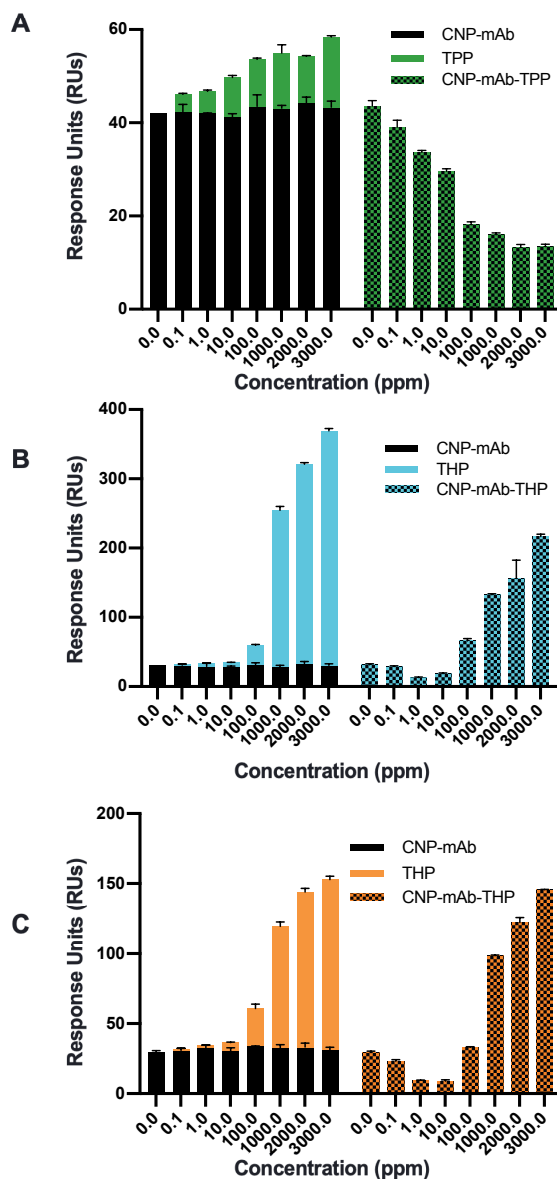


Figure 6.4. SPR responses showing binding to goat anti-mouse antibody of (A) total peanut protein [PA] (B) total hazelnut protein 1 [HA1] (C) total hazelnut protein 2 [HA2] tested by sequentially injecting carbon nanoparticle labelled antibody (CNP-mAb; black) followed by antigen (green [PA], blue [HA1], orange [HA2]) compared against pre-mixed CNP-mAb + antigen (checked green [PA], checked blue [HA1], checked orange [HA2] (n=3). Standard deviation is expressed as error bars (n=3).

The response in both [HA] assays is different from the [PA] assay, although this is not surprising considering that all the assays use different antibodies with varied sensitivities and detect distinct analytes. In the [PA], the total binding decreases as antigen concentration increases, which is consistent with the formation of a higher number of immunocomplexes with reduced avidity to GAMaB. Previously, using SPR, Liang² observed a concentration-dependent decrease in labeled-immunocomplex binding towards **T**; but did not study how concentration influences complex binding at **C**. Here, it is clear there is a decrease in binding at GAMaB with increasing TPP concentrations, seemingly harmonious with a growing number of complexes. In both [PA] formats, a decrease in **C** signal is observed at high concentrations but this stabilizes going up to 3000 ppm. In the LFIA, one additional higher concentration (3500 ppm) was also tested, and at this concentration **C** partially recovered.

Contrastingly, in both [HA] LFIA's we see a reappearance of **C** at much lower concentrations than with [PA], which is logical considering that the [HA] LFIA's are more sensitive than the [PA]. Likewise, both pre-mix HA's initially decrease in RU with increasing concentration (< 100 ppm), consistent with the formation of higher-order complexes with reduced avidity for **C**, these concentrations are also observed to cause a reduction in **C** in all 3 LFIA's (Figure 6.2 (A, B, D, E & G, H) & Figure 6.3 (A, B, C, D)). However, at higher-concentrations both HA assays instead increase in RU; these concentrations likely cause protein aggregation and have a relative scarcity of CNP-mAbs compared to the overabundant antigen, inhibiting the formation of higher-order complexes³⁷.

3.4 Dynamic monitoring of LFIA signal development

The SPR data suggests that the binding of immunocomplexes differs from the binding of free CNP-mAb, resulting in variations of the **C** intensity across broad concentration ranges. The usefulness of **T/C** for normalizing sandwich LFIA results is impeded across this range when considering only endpoint analysis. However, recent research suggests that additional information is available by monitoring the development of the **T/C** over the entire assay duration¹⁴. Figure 6.5 shows the signal development of the **C** (Figure 6.5 A-C), **T** (6.5D-F) and **T/C** (6.5G-I) of the LFIA's at a range of TPP or THP concentrations (0.015-3000 ppm [PA]) (0.015-3000 ppm [HA1] and 0.015-2000 ppm [HA2]) (see SI Figure S6.4 for snapshots from the video recording of developing LFIA's).

Within the assay working range (0.015-5 ppm [PA]) (0.015-0.125 ppm [HA1 & 2]), the **C** always develops faster than or at the same time as the **T**, resulting in a low, stable **T/C** over time. With increasing concentration (10-250 ppm [PA]), (2.5-100 ppm [HA1]), (2.5-400 ppm [HA2]), the speed of binding shifts, with the **T** developing more quickly than the **C**. The **T/C** time-development reflects this with a sharp initial increase (5 min), when mostly a **T** is present, followed by a steady decline as the **C** belatedly develops and the signal balances

out. Outside of the dynamic working range, when **T** or **C** development is influenced by antigen concentration, the final **T/C** becomes an unreliable metric. Recently, Rey¹⁴ presented a method for monitoring LFI signal development, using a different label (i.e., gold nanoparticles), detecting another analyte (C-reactive protein), and similarly observed an initial rise, followed by a decrease in **T/C** over the assay duration at concentrations where the **T** develops before the **C**. Interestingly, here we observed this trend across all 3 LFIsAs, albeit at different concentrations. Unfortunately, Rey's¹⁴ study primarily looked at **T/C**'s in a limited antigen range (120-255 µg/mL) and, as such only tested concentrations that caused a delayed and diminished development of **C** rather than inhibition of **T** development. A recent study²³ consolidated Rey's results by testing a different antigen (hCG) and modeling and observing **T/C** development at different antigen concentrations (0.5 – 500 IU/mL) over 10 min. They found that at low hCG concentrations, **C** initially develops faster than **T**, with **T/C** increasing after **C** is saturated and **T** keeps developing over 10 min. Conversely at high concentrations **T** develops rapidly with **C** developing slowly, causing **T/C** to initially rise and afterwards to steadily decrease over the assay duration as **T** is saturated and **C** still increases. which is in line with our own findings.

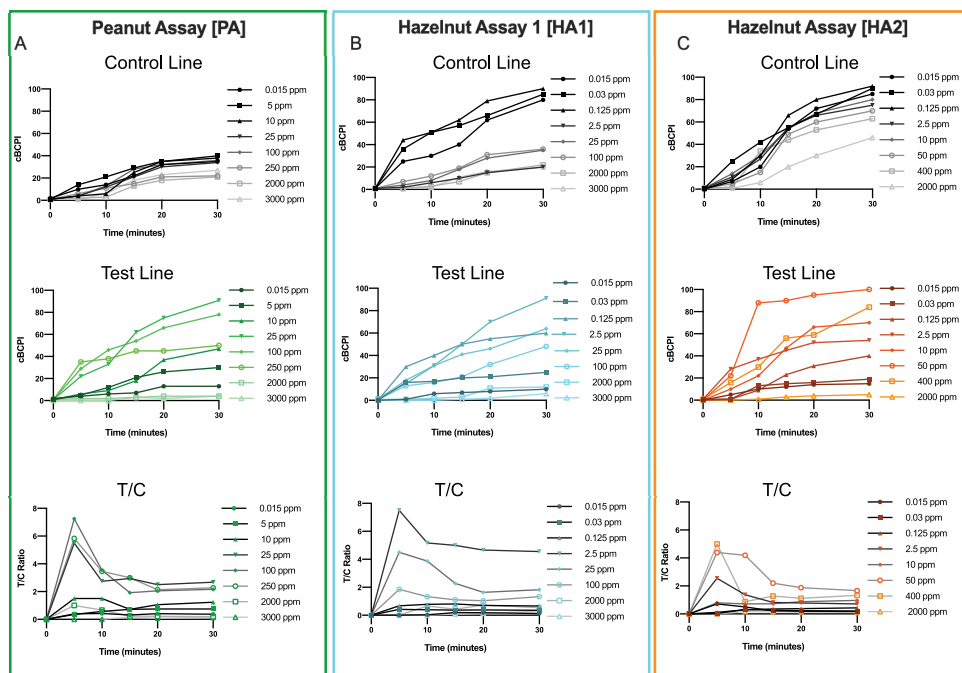


Figure 6.5. Dynamic smartphone monitoring of signal development for total peanut protein (PA), total hazelnut protein 1 (HA1), and total hazelnut protein 2 (HA2) LFIsAs. Control line signal development (A [PA], B [HA1], C [HA2]), test line signal development (D [PA], E [HA1], F [HA2]) and T/C ratio development (G [PA], H [HA1], G [HA2]) over 30 minutes at different concentrations (0.015-5 ppm [PA]) (0.015-0.125 ppm [HA1 & 2]).

Additionally, we found that a delayed and weak **C** development at higher concentrations also occurs when testing LFIA without a **T** (50 ppm [PA], 25 ppm [HA1], and 50 ppm [HA2] (SI Figure S6.5), where the **C** signal only starts developing after 10 min, and then only with diminished intensity. As concluded from the SPR study, reduction in **C** intensity is mainly caused by the formation of (higher-order) immunocomplexes, which have reduced avidity for **C**. While any **T** signal is weak, a diminished and delayed **C** eventually starts to develop after 10 min giving a final low **T/C**.

Critically, at these concentrations, the resulting low final **T/C** overlaps with the **T/C** at much lower concentrations (0.015 ppm [PA], 0.015 & 0.03 ppm [HA1] & [HA2]); misinterpretation of this could lead to reporting of a false negative as can be seen in SI Figure S6.6 where the **T** and **C** signal development and resulting **T/C** is compared for HA1 at 0.015 ppm and 2000 ppm. While the final **T/C**'s at these concentrations are similar, a false negative can be avoided by monitoring when the **T** and **C** develop; at hook-effect concentrations, no signal develops on either line for the first 10 min causing a static **T/C** during this time. Comparatively, at low concentrations in the dynamic working range, the **C** signal develops rapidly and with high intensity. By using dynamic video acquisition, real and artificially low concentration measurements can be differentiated, not only based on signal intensity but additionally based on whether the **C** or **T** develops first (Figure 6.5). Further, it is possible to automatically generate these **T** and **C** development profiles directly from the smartphone video (see SI Figure S6.7 for automatic-profiles for PA compared with manual time-development graphs and Figure S6.8 for a blank assay), using the python script. In addition to dynamic intensity measurements, this allows for BCPI correction and auto background subtraction. Considering that the results generated by the software correlate with the manually plotted time responses, novice users can simply use the automated results rather than carrying out the image analysis, corrections, and background subtraction themselves.

Table 6.1. Summary of results of concentration-dependent effects studied in this work

Experiment	Purpose	Result	Conclusions
Influence of concentration on LFIA signal development	Investigate T & C and T/C development (0.0075-3500 ppm)	C increases at low [conc] T increases at high [conc], at extreme [conc] T is lost (hook-effect) C decreases at lower [conc] than T C partially recovers at extreme [conc]	Hook-effect is reproducible C decreases due to reduced CNP-mAb binding or due to T depleting CNP-mAb
Influence of concentration on signal development in C only LFIAs	Determine how C signal developments without a T	High [conc] prevent C from reaching same intensity as in a blank	High [conc] negatively affect C
Sequential and pre-mixed antigen-binding studied by SPR	Determine the difference between pre-mix and sequential binding of CNP-mAb and antigen to GAMaB (0.1 – 3000 ppm)	Sequential [PA]+[HA1]+[HA2]: at high [conc] Rus increase Pre-mix [PA]: at high [conc] Rus decrease Pre-mix [HA1]+[HA2]: at low [conc] Rus decrease & at high [conc] Rus increase	Free CNP-mAb has better avidity to GAMaB than higher-order [CNP-mAb-analyte-complex]
Dynamic Monitoring of LFIA Signal Development	Investigate T , C and T/C development over time at varying concentrations	Dynamic working range: T & C at similar time High [conc]: T increases faster than C ; T/C increases & then decreases Extreme [conc]: no signal for pprox.. 10 min, then C increases	Dynamic monitoring of T & C can distinguish high concentration effect

4 Conclusions

The experiments, results, and conclusions drawn have been summarized in Table 6.1; a schematic depiction of the complementary experiments can be found in SI Figure S6.9. To unravel the hook-effect, we devised an inexpensive, dynamic, smartphone-based method for directly identifying concentration-dependent effects across three different sandwich LFIAs. We comprehensively elucidated how both antigen concentration and time influence signal development allowing us to differentiate between two distinct concentration effects: (1) the reduced development of a **C** in the presence of a rapidly and intensely developing **T**, which occurs within the first few minutes, and (2) the decrease of signal development on either line for 10 minutes, followed by the development of a **C**

which increases in intensity for the remaining assay duration. These trends were consistent across all three assays.

Indeed, we discovered for the hook-effect to occur on **T**, the concentration effect at **C** must have already happened. Based on our findings, we propose a more appropriate definition for the moderate-high concentrations, which lead to the loss of the **C** in LFIA would be the situation of *free secondary antibody depletion*. In *free secondary antibody depletion*, higher-order [CNP-mAb-analyte] immunocomplexes form, hindering the signal development at **C** by reducing CNP-mAb avidity for binding. As the concentration of analyte increases further, the assay starts to enter the hook-effect range. At these extreme concentrations, the unlabeled analyte rapidly saturates **T**. We have established that while endpoint **T/C** is an appropriate metric within the dynamic working range, outside of this range when the test or control line is falsely diminished, the final **T/C** is negatively influenced. While a prediction algorithm is outside of the scope of this paper, we appreciate that this would be a useful advancement. Here, the automatically generated qualitative binding profiles (SI Figure S6.7) provide a simplified way for novice users to monitor concentration effects without performing any image or data analysis themselves.

Further, the current system can simultaneously analyze 3 LFIAs, making it feasible to include an in-built quality control LFIA; such a control would be highly relevant where non-experts, such as allergic consumers perform LFIAs. Ultimately, the use of dynamic readout provides an inexpensive, direct mechanism for identifying high-concentration effects in LFIA. The digital analysis of dynamic data allows clear differentiation between highly concentrated samples and low concentration results. We foresee that this method should have broad applicability for distinguishing false-negative results in sandwich LFIAs.

References

1. Ross, G.M.S.; Bremer, M.G.E.G.; Nielen, M.W.F. Consumer-friendly food allergen detection: moving towards smartphone-based immunoassays, *Anal Bioanal Chem* **2018**, *410*, 5353-5371, 10.1007/s00216-018-0989-7.
2. Liang, T.; Robinson, R.; Houghtaling, J.; Fridley, G., et al. Investigation of Reagent Delivery Formats in a Multivalent Malaria Sandwich Immunoassay and Implications for Assay Performance, *Analytical chemistry* **2016**, *88*, 2311-2320, 10.1021/acs.analchem.5b04222.
3. Hoofnagle, A.N.; Wener, M.H. The fundamental flaws of immunoassays and potential solutions using tandem mass spectrometry, *J Immunol Methods* **2009**, *347*, 3-11, 10.1016/j.jim.2009.06.003.
4. Miles, L.E.M.; Lipschitz, D.A.; Bieber, C.P.; Cook, J.D. Measurement of serum ferritin by a 2-site immunoradiometric assay, *Analytical Biochemistry* **1974**, *61*, 209-224, [https://doi.org/10.1016/0003-2697\(74\)90347-9](https://doi.org/10.1016/0003-2697(74)90347-9).
5. Petakov, M.S.; Damjanović, S.S.; Nikolić-Durović, M.M.; Dragojlović, Z.L., et al. Pituitary adenomas secreting large amounts of prolactin may give false low values in immunoradiometric assays. The hook effect, *Journal of Endocrinological Investigation* **1998**, *21*, 184-188, 10.1007/BF03347299.
6. Hu, J.; Choi, J.R.; Wang, S.; Gong, Y., et al. Multiple test zones for improved detection performance in lateral flow assays, *Sensors and Actuators B: Chemical* **2017**, *243*, 484-488, <https://doi.org/10.1016/j.snb.2016.12.008>.
7. Ki, H.; Oh, J.; Han, G.-R.; Kim, M.-G. Glycation ratio determination through simultaneous detection of human serum albumin and glycated albumin on an advanced lateral flow immunoassay sensor, *Lab on a Chip* **2020**, *20*, 844-851, 10.1039/C9LC00967A.
8. O'Farrell, B. In *Lateral Flow Immunoassay*, Wong, R.; Tse, H., Eds.; Humana Press: Totowa, NJ, 2009, pp 1-33.
9. Kulabhusan, P.K.; Rajwade, J.M.; Sugumar, V.; Taju, G., et al. Field-Usable Lateral Flow Immunoassay for the Rapid Detection of White Spot Syndrome Virus (WSSV), *PLoS One* **2017**, *12*, e0169012-e0169012, 10.1371/journal.pone.0169012.
10. Nelis, J.L.D.; Tsagkaris, A.S.; Dillon, M.J.; Hajslova, J., et al. Smartphone-based optical assays in the food safety field, *TrAC Trends in Analytical Chemistry* **2020**, 115934, <https://doi.org/10.1016/j.trac.2020.115934>.
11. Foyzal, K.H.; Seo, S.E.; Kim, M.J.; Kwon, O.S., et al. Analyte Quantity Detection from Lateral Flow Assay Using a Smartphone, *Sensors (Basel)* **2019**, *19*, 4812, 10.3390/s19214812.
12. Posthuma-Trumpie, G.A.; Wichers, J.H.; Koets, M.; Berendsen, L.B.J.M., et al. Amorphous carbon nanoparticles: a versatile label for rapid diagnostic (immuno)assays, *Anal Bioanal Chem* **2012**, *402*, 593-600, 10.1007/s00216-011-5340-5.
13. Pilavaki, E.; Demosthenous, A. Optimized Lateral Flow Immunoassay Reader for the Detection of Infectious Diseases in Developing Countries, *Sensors (Basel)* **2017**, *17*, 2673, 10.3390/s17112673.
14. Rey, E.G.; O'Dell, D.; Mehta, S.; Erickson, D. Mitigating the Hook Effect in Lateral Flow Sandwich Immunoassays Using Real-Time Reaction Kinetics, *Anal Chem* **2017**, *89*, 5095-5100, 10.1021/acs.analchem.7b00638.

15. Ruff, L.E.; Sapre, A.A.; Plaut, J.S.; De Maere, E., et al. Selection of DNA nanoparticles with preferential binding to aggregated protein target, *Nucleic Acids Research* **2016**, *44*, e96-e96, 10.1093/nar/gkw136.
16. Anfossi, L.; Di Nardo, F.; Cavalera, S.; Giovannoli, C., et al. Multiplex Lateral Flow Immunoassay: An Overview of Strategies towards High-throughput Point-of-Need Testing, *Biosensors (Basel)* **2018**, *9*, 10.3390/bios9010002.
17. Oh, J.; Joung, H.-A.; Han, H.S.; Kim, J.K., et al. A hook effect-free immunochromatographic assay (HEF-ICA) for measuring the C-reactive protein concentration in one drop of human serum, *Theranostics* **2018**, *8*, 3189-3197, 10.7150/thno.24034.
18. Kim, T.H.; Hahn, Y.K.; Kim, M.S. Recent Advances of Fluid Manipulation Technologies in Microfluidic Paper-Based Analytical Devices (μ PADs) toward Multi-Step Assays., *Micromachines* **2020**, *11*, <https://doi.org/10.3390/mi11030269>.
19. Tsai, T.-T.; Huang, T.-H.; Chen, C.-A.; Ho, N.Y.-J., et al. Development a stacking pad design for enhancing the sensitivity of lateral flow immunoassay, *Scientific Reports* **2018**, *8*, 17319, 10.1038/s41598-018-35694-9.
20. Hemmig, E.; Temiz, Y.; Gökçe, O.; Lovchik, R.D., et al. Transposing Lateral Flow Immunoassays to Capillary-Driven Microfluidics Using Self-Coalescence Modules and Capillary-Assembled Receptor Carriers, *Analytical Chemistry* **2020**, *92*, 940-946, 10.1021/acs.analchem.9b03792.
21. Shin, S.; Choi, M.; Shim, J.; Park, S. Hook effect detection and detection-range-controllable one-step immunosensor for inflammation monitoring, *Sensors and Actuators B: Chemical* **2020**, *304*, 127408, <https://doi.org/10.1016/j.snb.2019.127408>.
22. Oh, Y.K.; Joung, H.-A.; Han, H.S.; Suk, H.-J., et al. A three-line lateral flow assay strip for the measurement of C-reactive protein covering a broad physiological concentration range in human sera, *Biosensors and Bioelectronics* **2014**, *61*, 285-289, <https://doi.org/10.1016/j.bios.2014.04.032>.
23. Sathishkumar, N.; Toley, B.J. Development of an experimental method to overcome the hook effect in sandwich-type lateral flow immunoassays guided by computational modelling, *Sensors and Actuators B: Chemical* **2020**, *324*, 128756, <https://doi.org/10.1016/j.snb.2020.128756>.
24. Bremer, M.G.E.G.; Smits, N.G.E.; Haasnoot, W. Biosensor immunoassay for traces of hazelnut protein in olive oil, *Anal Bioanal Chem* **2009**, *395*, 119-126, 10.1007/s00216-009-2720-1.
25. Ross, G.M.S.; Bremer, M.; Wichers, J.H.; van Amerongen, A., et al. Rapid Antibody Selection Using Surface Plasmon Resonance for High-Speed and Sensitive Hazelnut Lateral Flow Prototypes, *Biosensors (Basel)* **2018**, *8*, 10.3390/bios8040130.
26. Ross, G.M.S.; Salentijn, G.I.J.; Nielen, M.W.F. A Critical Comparison between Flow-through and Lateral Flow Immunoassay Formats for Visual and Smartphone-Based Multiplex Allergen Detection, *Biosensors (Basel)* **2019**, *9*, 10.3390/bios9040143.
27. Marsh, J.T.; Jayasena, S.; Gaskin, F.; Baumert, J.L., et al. Thermal processing of peanut impacts detection by current analytical techniques, *Food Chem* **2020**, *313*, 126019, 10.1016/j.foodchem.2019.126019.

28. Eriksson, E.; Lysell, J.; Larsson, H.; Cheung, K.Y., et al. Geometric Flow Control Lateral Flow Immunoassay Devices (GFC-LFIDs): A New Dimension to Enhance Analytical Performance, *Research* **2019**, 2019, 8, 10.34133/2019/8079561.
29. Schneider, C.A.; Rasband, W.S.; Eliceiri, K.W. NIH Image to ImageJ: 25 years of image analysis, *Nature Methods* **2012**, 9, 671-675, 10.1038/nmeth.2089.
30. Taylor, S.L.; Nordlee, J.A.; Niemann, L.M.; Lambrecht, D.M. Allergen immunoassays—considerations for use of naturally incurred standards, *Anal Bioanal Chem* **2009**, 395, 83-92, 10.1007/s00216-009-2944-0.
31. Qian, S.; Bau, H.H. A mathematical model of lateral flow bioreactions applied to sandwich assays, *Anal Biochem* **2003**, 322, 89-98, 10.1016/j.ab.2003.07.011.
32. Ramos-Vara, J.A.; Miller, M.A. When Tissue Antigens and Antibodies Get Along: Revisiting the Technical Aspects of Immunohistochemistry—The Red, Brown, and Blue Technique, *Veterinary Pathology* **2014**, 51, 42-87, 10.1177/0300985813505879.
33. Shire, S.J.; Shahrokh, Z.; Liu, J. Challenges in the development of high protein concentration formulations, *J Pharm Sci* **2004**, 93, 1390-1402, 10.1002/jps.20079.
34. Koets, M.; Renström, A.; Zahradnik, E.; Bogdanovic, J., et al. Rapid one-step assays for on-site monitoring of mouse and rat urinary allergens, *Journal of Environmental Monitoring* **2011**, 13, 3475-3480, 10.1039/C1EM10658A.
35. Duo, J.; Bruno, J.; Kozhich, A.; David-brown, D., et al. Surface plasmon resonance as a tool for ligand-binding assay reagent characterization in bioanalysis of biotherapeutics, *Bioanalysis* **2018**, 10, 559-576, 10.4155/bio-2017-0271.
36. Duo, J.; Bruno, J.; Piccoli, S.; DeSilva, B., et al. Characterization of labeled reagents in ligand-binding assays by a surface plasmon resonance biosensor, *Bioanalysis* **2017**, 9, 193-207, 10.4155/bio-2016-0204.
37. Bray, D.; Lay, S. Computer-based analysis of the binding steps in protein complex formation, *Proceedings of the National Academy of Sciences of the United States of America* **1997**, 94, 13493-13498, 10.1073/pnas.94.25.13493.

Supplementary information

Chapter 6

Table S6.1. Summary of descriptions of the hook-effect given in literature (1974-2020)

Year	Assay format	Hook-effect definition/description	Observed effect	Mitigation strategy	Ref
1974	Immunoradiometric assay	High analyte concentrations lead to paradoxical fall in dose-response	N/A	Washing step	1
1978	Immunoradiometric assay	Saturation of heterogenous binding sites on capture and detector mAbs	N/A	Kinetic monitoring of binding	2
1982	Immunoradiometric assay	Fall in assay response at high analyte concentrations.	N/A	Bioreagent optimization	3
1989	Immunoradiometric assay	Formation of complex is inhibited at high concentrations. Abnormally elevated concentrations being indistinguishable from low concentrations	N/A	Sample dilution	4
1988	Immunoradiometric assay	High concentrations lead to falsely low results	N/A	Washing step	5
1992	Immunoradiometric assay	Highest analyte concentration gives a value lower than at much lower analyte concentrations	N/A	Sample dilution	6
1998	Immunoradiometric assay	Underestimation of measurements at high concentrations leading to falsely low results	N/A	Sample dilution	7
1998	Chemiluminometric assay	High concentrations lead to falsely low serum concentrations	N/A	Sample dilution	8
2000	ELISA	Prozone effect is when a diluted sample gives a higher signal than an undiluted sample	N/A	Washing step Sample dilution Sample pooling	9
2004	Immunoassay	Excess analyte concentration inhibits sandwich pair formation or lead to non-equivalent binding	N/A	Bioreagent optimization	10
2004	Immunoassay	Free and labelled analyte compete for the same number of binding sites on the capture and detector mAbs leading to a decreased signal response and false negatives	N/A	Bioreagent optimization Sample Dilution	11
2005	Immunodiagnostic devices	Decreased signal response at high analyte concentrations	N/A	Sample dilution	12
2005	Lateral flow test	High concentrations give false negative results if sample is not diluted	N/A	Sample dilution	13

2006	LFI A	When a large proportion of capture and detector mAbs are saturated with analyte, likelihood of tripartite sandwich formation at the test line is reduced.	No loss of T or C in the tested range, but C is diminished at the highest concentrations tested	Bioreagent optimization	14
2007	LFI A	Increased concentration leading to decreased signal	Competitive forma	Bioreagent optimization	15
2008	Rapid Stain Blood (RSIB – LFI A)	Free analyte reaches T first and occupies T binding sites, preventing binding of labeled-analyte-complex.	No loss of T or C in tested range	No hook effect at tested concentrations	16
2009	Rapid Stain Salvia (RSIS – LFI A)	Unlabeled analyte blocks T binding sites, preventing complex binding.	No loss of T or C in tested range	No hook effect at tested concentrations	17
2009	LFI A	Reduction in T intensity at high analyte concentrations	No loss of T or C in tested range	N/A	18
2010	Lamba free assay	High concentrations lead to a 4-fold decrease in signal	N/A	Sample dilution	19
2010	LFI A	Reduction in T intensity at high analyte concentrations	No loss of T in tested range, but C disappears with increasing concentration	Sample dilution	20
2011	LFI A	Signal stops increasing in intensity with increased concentration	Loss of T at higher concentrations	Washing step	21
2011	One step immunoassay	High analyte concentrations saturate capture and detector mAbs, reducing chance of sandwich formation and decreasing signal intensity	C diminishes (minimally) and T is lost at higher concentrations	first Sample dilution	22
2012	LFI A	Loss of T signal at high analyte concentrations	C diminishes and T is lost at higher concentrations	first Sample dilution	23

2012	LFA	Reduction in T intensity at high analyte concentrations	Loss of T reported at higher concentrations	Sample dilution Bioreagent optimization	24
2012	LFA	Signal decrease at high analyte concentrations	Decrease in fluorescent T signal at high concentrations	Sample dilution	25
2013	LFA	High concentrations lead to false negative results	Decrease in T at high concentrations reported	Sample dilution	26
2013	Vertical flow immunoassay (VFA)	Excess analyte concentrations prevent binding to labeled-analyte-complex	N/A	Assay duration	27
2013	Urine pregnancy testing	Plotted immunoassay results resemble a hook when high antigen concentrations lead to a decrease in signal intensity	N/A	N/A	28
2014	LFA	Reduction in T intensity at high analyte concentrations	Decrease in T at high concentrations reported	Sample dilution	29
2014	3-line LFIA	False negatives from reduction in T intensity at high analyte concentrations	C diminishes first and reappears as T is lost at higher concentrations	Additional target lines	30
2014	Chemiluminescent lateral flow immunosensor	High concentrations lead to a decrease in signal	No loss of C or T in tested range	Timed reagent release	31
2014	Blood ELISA	High analyte concentrations saturate capture and detector mAbs, reducing chance of sandwich formation and decreasing signal intensity	N/A	Sample dilution Sample pooling	32
2014	LFA	High concentrations give low results	N/A	N/A	33
2015	Immunoassay	High analyte concentrations saturate capture and detector mAbs, reducing chance of sandwich formation and decreasing signal intensity	N/A	Sample dilution	34
2015	LFA	Excess of analyte saturates labelled mAb binding sites leading to steric hindrance which prevents signal development	N/A	Bioreagent optimization	35
2015	LFA	Failure of T and C development caused by saturation of labelled antibody by excess analyte	Decrease in T at high conc	Additional target lines	36

2016	Clinical ELISA	Excess of either antigen or antibody compromises the formation of immunocomplexes.	N/A	Sample dilution	37
2016	DNA nanoparticles	Capture and detector mAbs saturation leads to falsely low results. Excess of either antigen or antibody compromises the formation of immunocomplexes.	N/A	Nanoparticle binding to aggregated free target limits the hook effect	38
2016	LFA	High analyte concentrations result in false negatives	N/A	Additional target line	39
2016	LFA	High analyte concentrations give falsely low signals	N/A	Bioreagent optimization	40
2017	LFA	Erroneously low results due to antigen excess	N/A	Sample dilution	41
2017	LFA	At high analyte concentrations T stops increasing and starts decreasing because unlabeled analyte blocks binding sites on T	At high concentrations C is lost – affecting T/C, T not lost in tested range	Kinetic monitoring of T/C ratio	42
2017	Immuno-metric assay	Capture and detector mAbs separately bind analyte, preventing labeled-analyte-complex formation leading to decreased signal	N/A	Sample dilution	43
2017	Vertical flow immunoassay (VFI)	Increasing analyte concentration resulting in decreasing T signal	N/A	Assay duration	44
2017	Nucleic acid lateral flow	High doses of analyte induce dim signals and false negatives	Reduction in T at high concentrations	Additional target lines	45
2017	Vertical Flow Assay (VFA)	Excess analyte that does not bind with labeled-analyte-complex interferes with the interaction with T	N/A	Sequential reagent loading	46
2017	Review: LFIA	False negatives at high analyte concentrations	N/A	N/A	47
2018	ELISA	Paradoxically lower signal observed for undiluted samples compared with dilution sample	N/A	Sample dilution	48
2018	Hook-effect immuno-chromatographic assay (HEF-ICA)	Simultaneous saturation of capture and detector mAbs by free analyte leads to loss of T	Reduction in T at high concentrations	Timed reagent release	49
2018	QD fluorescent LFIA	Extreme analyte concentrations bind with T preventing the binding of labeled-analyte-complex	At high concentrations C is lost T not in tested range	Washing step	50
2018	LFA	Saturation of T binding sites with excess analyte	No loss of T or C reported in the tested range	LFIA geometry	51

2018	LFA	Low dilution factors lead to false negative results	Loss of T at high concentrations	Sample dilution	52
2018	LFA	Undiluted samples lead to falsely low results	N/A	Sample dilution	53
2018	LFA	High analyte concentrations lead to low T signals	Loss of C and T observed at high concentrations	Sample dilution	54
2018	LFA	Undiluted samples lead to falsely low results	N/A	Sample dilution	55
2019	Duplex LFA	Saturation of T with excess analyte prevents labeled-analyte-complex binding	Loss of upper T reported at high concentrations	Sample dilution	56
2019	Review paper (LFIA / flow through)	Excess of unlabeled analyte binds saturates T and prevents binding of labelled-analyte-complex leading to loss of T	N/A	Assay duration	57
2019	3-line LFA biosensor using aptamers	Excess of unlabeled analyte binds saturates T and prevents binding of labelled-analyte-complex leading to loss of T	Loss of upper T reported at high concentrations	Additional target lines	58
2019	LFA	False negatives at high analyte concentrations	At high concentrations C is lost T not lost in tested range	Timed reading of assay	59
2019	LFA	High analyte concentrations lead to free and labeled analyte competing for limited number of T binding sites leading to reduction in T intensity	Reduction in C seen at lower concentration than loss of T	Sample dilution	60
2020	One step immunosensor	Excessive antigen concentration or limited amount of labeled antibody leads to a competition of T binding	Loss of upper T reported at high concentrations	Additional target lines	61
2020	Multiplex LFA	Intensity of T is proportional to concentration in sample until high concentrations where there is a false decrease	N/A	Sample dilution	62
2020	LFA	Excess of unlabeled analyte binds saturates T and prevents binding of labelled-analyte-complex leading to loss of T	Reduction in T at high concentrations	Sequential reagent loading	63
2020	LFA	T signal reduces beyond a certain threshold antigen concentration	At high conc: develops faster than C; T/C initially increases and then decreases as T is saturated and C still increases	Computational model & time-lapse imaging of signal development	64

Protocol S6.1: Antibodies & Carbon Nanoparticle Labeling

Buffer preparation:

All buffers were made in water from a MilliQ-system (MQ) (>18.2 MΩ/cm; Millipore, Burlington, MA, USA). Bovine serum albumin (BSA) was purchased from Sigma-Aldrich (Sigma-Aldrich, Zwijndrecht, The Netherlands). Washing buffer (WB) - 5 mM borate buffer (BB) was prepared by diluting 100 mM sodium tetraborate (VWR, Leuven, Belgium), 100 mM boric acid (Merck, Darmstadt, Germany) to pH 8.8. Storage buffer (SB) – 100 mM BB (pH 8.8) with 1% BSA (w/v). Running buffer (RB) – 100 mM BB (pH 8.8) with 1% BSA (w/v) and 0.05% Tween-20 (v/v) (Merck, Darmstadt, Germany).

CNP-mAb labeling:

Assay	Capture mAb (T)	Detector mAb (CNP-mAb)
Peanut Assay [PA]	51-2A12	51-12D2
Hazelnut Assay 1 [HA1]	50-6B12	50-6B12
Hazelnut Assay 2 [HA2]	50-6B12	50-5H9

An anti-peanut mAb (51-12D2) and two different anti-hazelnut mAbs (50-6B12 and 50-5H9) were labelled as detector mAbs with 'Spezial Schwartz 4' carbon nanoparticles (CNPs; purchased from Degussa AG, Frankfurt; Germany) as has been previously reported^{60,65,66}. Antibodies were buffer exchanged into WB using Zeba™ Spin Trap columns (Thermo Scientific; Landsmeer, The Netherlands) before labeling with carbon nanoparticles (CNPs). A 1% suspension of CNPs was prepared by adding 1 mL of MQ Water to 10 mg carbon and sonicating for 10 min. The resulting 1% carbon suspension was diluted five times in 5 mM WB (pH 8.8) to obtain a 0.2% suspension. After sonicating the suspension for 5 min, 350 µL of purified anti-peanut (51-12D2) or anti-hazelnut (50-6B12 or 50-5H9) solution (1 mg/mL in 5 mM WB) was added to 1 mL (to make a total volume of 1.35 mL) of 0.2% carbon suspension and stirred overnight at 4 °C. Two equal aliquots (670 µL), were made from the suspension, and these were each supplemented with 500 µL WB, before centrifuging them for 15 min at 13,636× g at 4 °C. Following the removal of the supernatants, the pellets were re-suspended in WB, repeating this step over three cycles. After the final wash, we discarded the supernatants and pooled the pellets together with 1 mL storage buffer for storage at 4 °C until use.

Protocol S6.2: Lateral Flow Immunoassay Preparation

The LFIA used in this study were composed of a nitrocellulose (NC) membrane (140 seconds/travel 4 cm), cut to 4 cm length, and secured on a plastic backing with 4.5 cm of absorbent pad overlapping one end of the NC. The XYZ 3060 BioDot dispensing platform

(Irving, CA; USA, was used to spray the goat anti-mouse antibody (GAMaB) control line (0.25 mg/mL) 10 mm upfront from the absorbent pad. For the peanut LFIA [PA] the anti-peanut mAb (51-2A12 – 0.25 mg/mL in 5 mM BB) was sprayed at 10 mm upfront from the control line, for the first hazelnut assay [HA1] the anti-hazelnut mAb (50-6B12 – 0.25 mg/mL in 5 mM BB) was sprayed at 5 mm upfront from the control line, whereas for the second hazelnut assay [HA2] 50-5H9 mAb (0.25 mg/mL in 5 mM BB) was sprayed at 10 mm upfront from the control line. For the control-line-only LFIAs, GAMaB (0.25 mg/mL), was sprayed in a line at 10 mm upfront from the absorbent pad. Developed membranes were cut into 4 mm wide strips using the CM5000 Guillotine Cutter. All LFIAs were heat-sealed in foil packets with silica beads and stored at room temperature until use.

Protocol S6.3: Surface Plasmon Resonance Procedures

An amine coupling kit (containing 0.1 M N-hydroxysuccinimide (NHS), 0.4 M 1-ethyl-3-(3-dimethylamino propyl)carbodiimide hydrochloride (EDC), and 1 M ethanolamine hydrochloride (pH 8.5), pH scouting kit (containing 10 mM sodium acetate pH 4.0, 4.5, 5.0 & 5.5), HBS-EP buffer (pH 7.4, consisting of 10 mM 4-(2-hydroxyethyl)piperazine-1-ethanesulfonic acid, 150 mM sodium chloride, 3 mM ethylenediaminetetraacetic acid, 0.005% v/v surfactant polysorbate-20) and CM5 sensor chips were purchased from GE Healthcare (Uppsala, Sweden). A standard amine coupling procedure using the amine coupling kit was performed for antibody immobilization at 25°C onto a reusable CM5 chip. First, the optimum immobilization pH was determined using pH scouting in the Biacore 3000 application wizard software. To this end, antibodies were diluted to 0.05 mg/mL in 10 mM sodium acetate of varying pH (4.0-5.0). Goat anti-mouse antibody (GAMaB) solution was diluted to 0.05 mg/mL in 10 mM Sodium Acetate pH 5.0. The biosensor surface was activated by injecting a 1:1 mixture of EDC and NHS (v/v) across flow cells (35 µL at a flow rate of 5 µL/min) and aiming for 10,000 Response Units (RU). Antibodies were immobilized by attaching them to the activated carboxymethylated dextran surface via its exposed amine groups. Coupling to the chip was followed by blocking remaining active sites with ethanolamine (1 M).

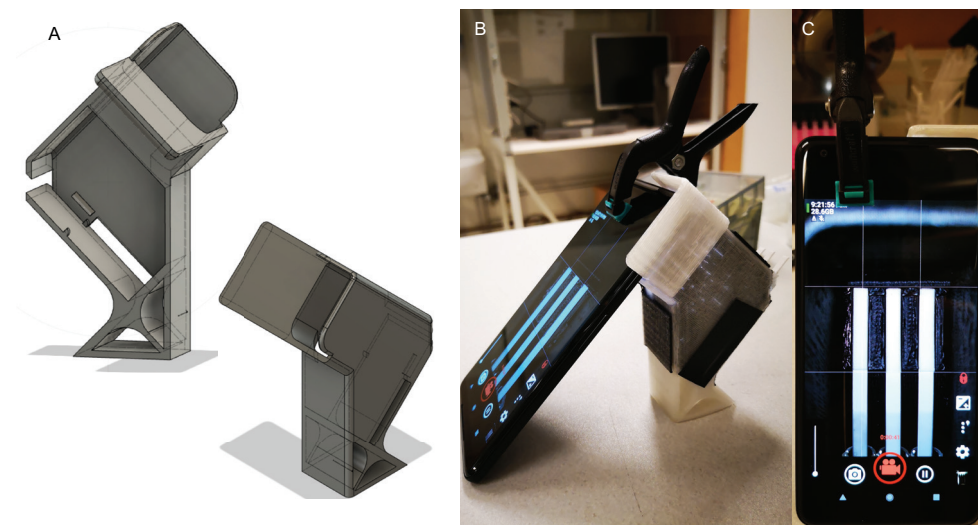


Figure S6.1. Smartphone holder for dynamic data acquisition of LFIA signal development. (A) Computer aided design of device holder. (B) Photograph of smartphone holder, with smartphone attached and real-time recording of 3 assays signal development. (C) Head on view of smartphone screen showing real-time signal development.

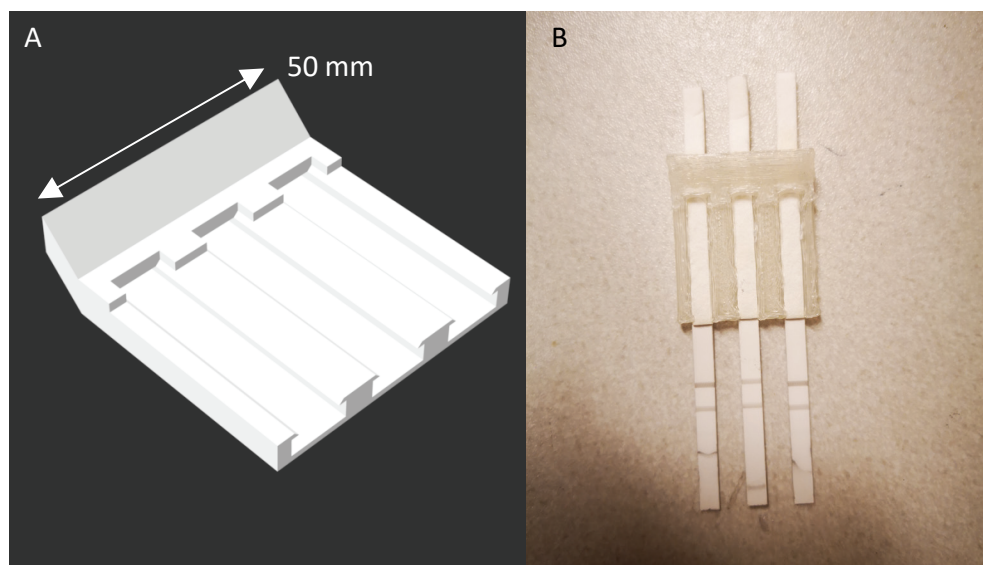


Figure S6.2. 3D-printed lateral flow immunoassay (LFIA) cartridge which allows 3 LFIAs to be recorded simultaneously. (A) computer aided design of the cartridge. (B) Photo of the 3D-printed LFIA cartridge, fitting 3 LFIAs.

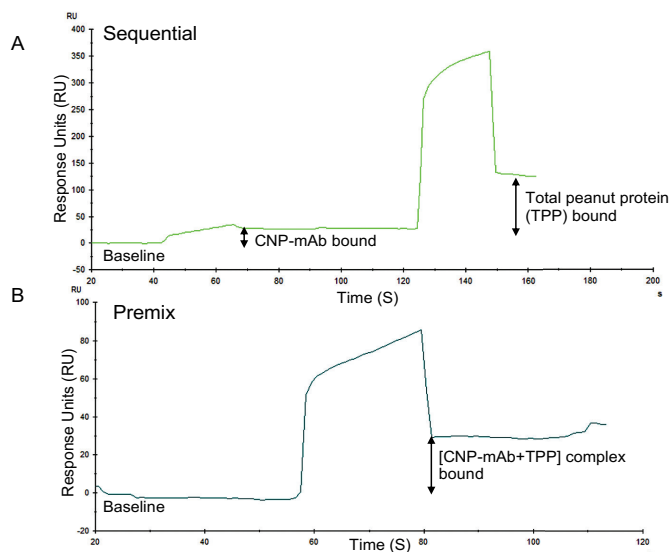


Figure S6.3. SPR sensorgrams showing sequential and pre-mix binding of carbon nanoparticle labeled antibodies (CNP-mAb) and total peanut protein (TPP) to the goat anti-mouse antibody (GAMaB). (A) Sequential binding: the first curve represents the binding of CNP-mAb (red-antibody) to the GAMaB (purple antibody) and the second curve represents TPP (blue circle) being captured by the CNP-mAb. (B) Pre-mix binding: the curve represents the association of the CNP-mAb-TPP complex for GAMaB.

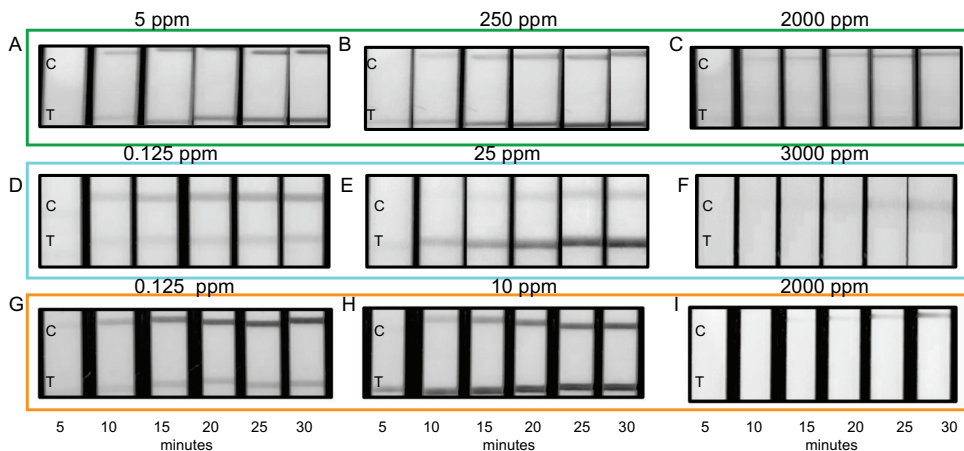


Figure S6.4. Photographs showing the development of test line (T) and control line (C) signal development over a 30-minute period. (A) Peanut Assay (PA) 5 ppm (B) PA 250 ppm (C) PA 2000 ppm (D) Hazelnut Assay 1 (HA1) 0.125 ppm (E) HA1 25 ppm (F) HA1 3000 ppm and (G) Hazelnut Assay 2 (HA2) 0.125 ppm (H) HA2 10 ppm (I) HA2 2000 ppm.

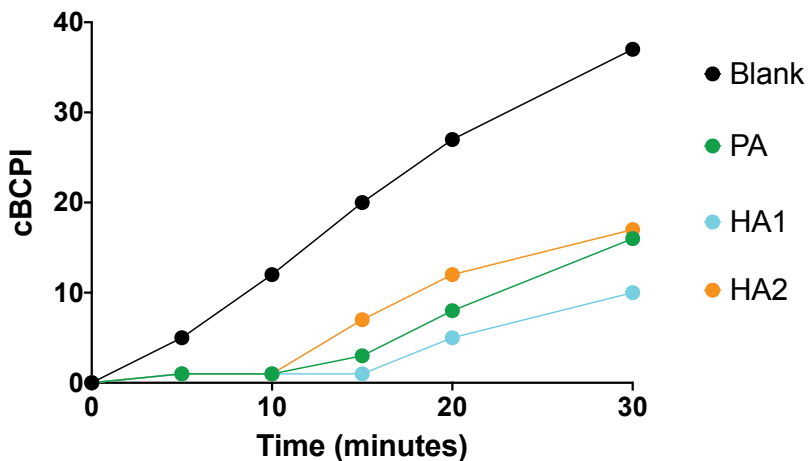


Figure S6.5. Control line-only lateral flow immunoassay time development for a blank sample (black), peanut assay (PA; 50 ppm; green), hazelnut assay 1 (HA1; 25 ppm; blue), hazelnut assay 2 (HA2 50 ppm; orange).

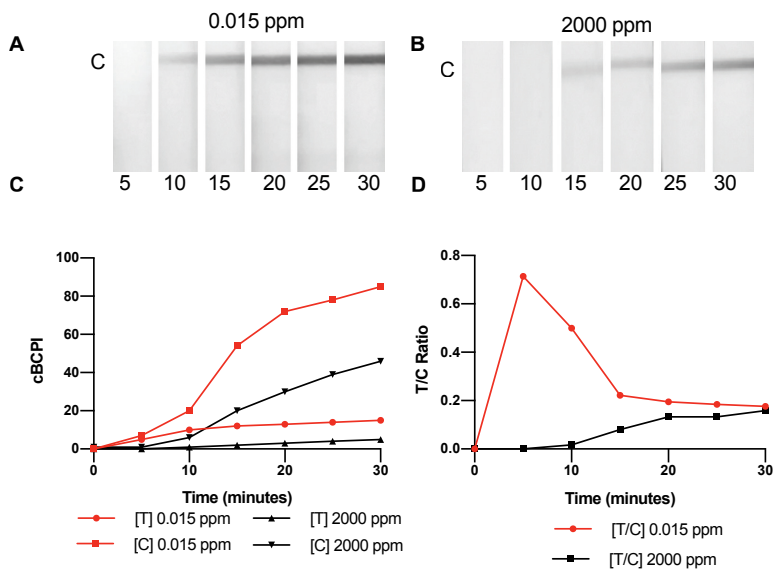


Figure S6.6. LFIA signal development over 30 minutes at 5-minute intervals in concentrations of (A) 0.015 ppm & (B) 2000 ppm of total hazelnut protein (C) the corrected blue channel pixel intensity (cBCPI) of test T and control C development at 0.015 ppm (red) and the C and T development (black). (D) the T/C development at 0.015 ppm and 2000 ppm.

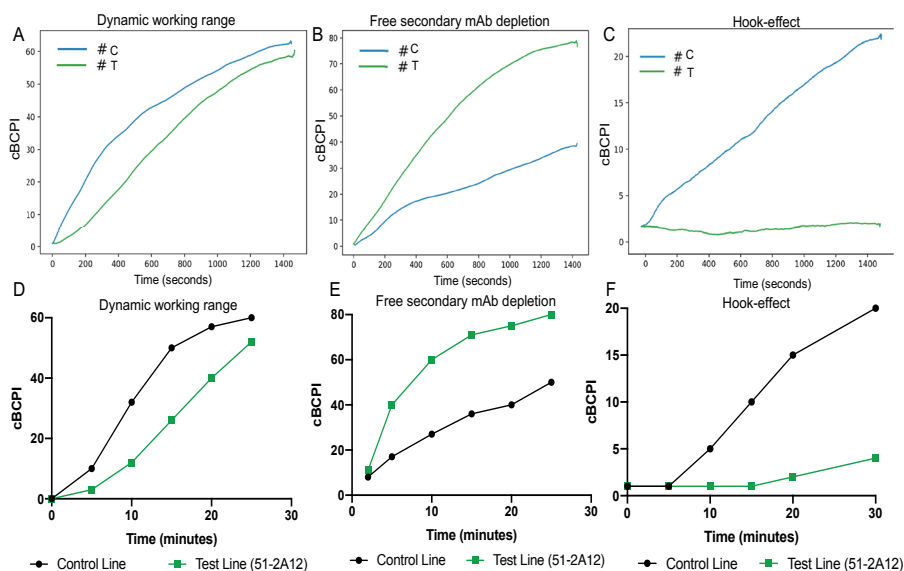


Figure S6.7. Dynamic LFIA signal development over 30 minutes. (A, B, C) Automatically generated kinetic profiles where the blue line represents the control line and the green line represents the test line at 1 ppm, 10 ppm and 2000 ppm total peanut protein (TPP) respectively. (D, E, F) Manually plotted time development curves where the black line represents the control line and the green line represents the test line at 1 ppm, 5 ppm and 2000 ppm TPP respectively.

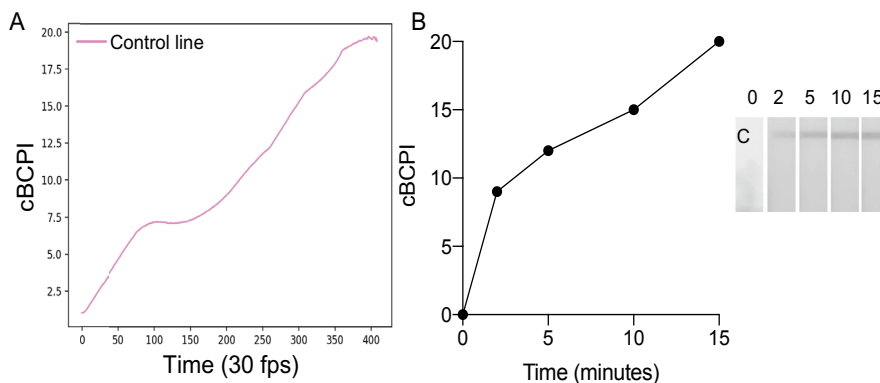


Figure S6.8. Dynamic monitoring of blank (0 ppm) LFIA signal development over 15 minutes. (A) Automatically generated binding profile where the pink line shows the control line, measurements are made every second (B) Manually plotted time-response profile and photographs showing control line development at 2, 5, 10 & 15 minutes.

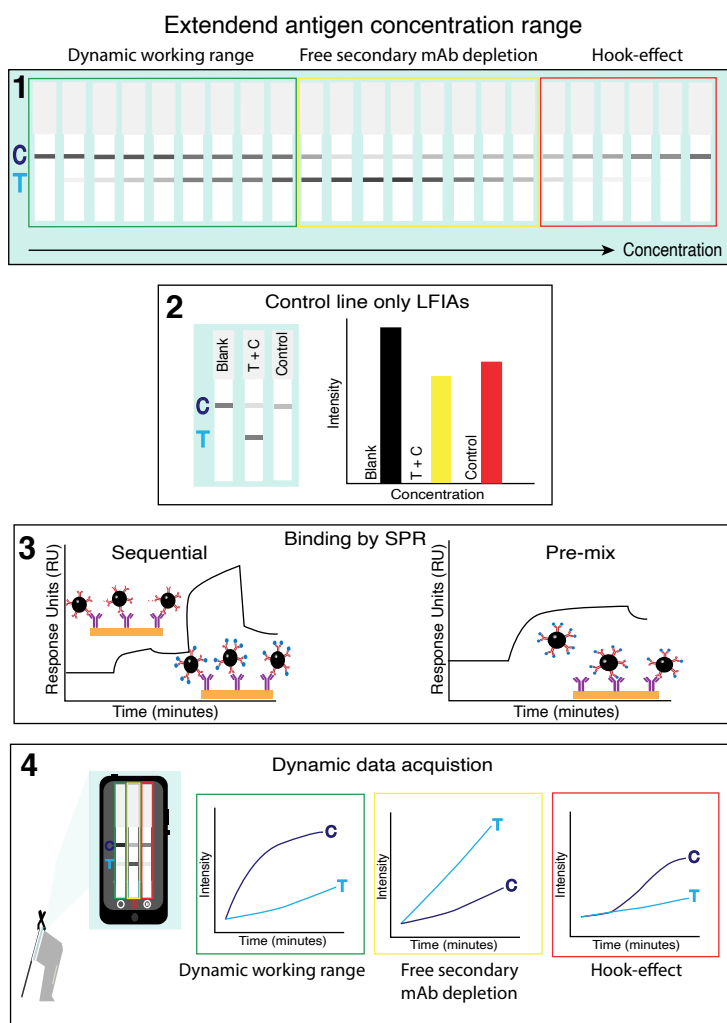


Figure S6.9. Schematic representation of the workflow of experiments for this study where the dynamic working ranges – green zone, free-secondary mAb depletion – yellow zone and hook-effect – red zone. First, lateral flow immunoassays (LFIA) are tested in an extended antigen concentration range. Next, LFIA in the yellow zone are tested in control line only experiments. After, the binding behaviors of the control antibody (purple) was tested using surface plasmon resonance (SPR), in sequential and pre-mix experiments. Finally, LFIA were dynamically monitored in the green, yellow and red zones to determine how their signal development is influenced by concentration, over time.

References

1. Miles, L.E.M.; Lipschitz, D.A.; Bieber, C.P.; Cook, J.D. Measurement of serum ferritin by a 2-site immunoradiometric assay, *Analytical Biochemistry* **1974**, *61*, 209-224, [https://doi.org/10.1016/0003-2697\(74\)90347-9](https://doi.org/10.1016/0003-2697(74)90347-9).
2. Rodbard, D.; Feldman, Y.; Jaffe, M.L.; Miles, L.E.M. Kinetics of two-site immunoradiometric ('sandwich') assays—II: Studies on the nature of the -high-dose hook effect, *Immunochemistry* **1978**, *15*, 77-82, [https://doi.org/10.1016/0161-5890\(78\)90046-9](https://doi.org/10.1016/0161-5890(78)90046-9).
3. Ryall, R.G.; Story, C.J.; Turner, D.R. Reappraisal of the causes of the "hook effect" in two-site immunoradiometric assays, *Analytical Biochemistry* **1982**, *127*, 308-315, [https://doi.org/10.1016/0003-2697\(82\)90178-6](https://doi.org/10.1016/0003-2697(82)90178-6).
4. Brensing, K.A.; Dahlmann, N.; Entzian, W.; Bidlingmaier, F., et al. Underestimation of LH and FSH hormone concentrations in a patient with a gonadotropin secreting tumor., *Hormone and Metabolic Research* **1989**, *21*, 697-698, DOI: 10.1055/s-2007-1009326.
5. Vaidya, H.C.; Wolf, B.A.; Garrett, N.; Catalona, W.J., et al. Extremely high values of prostate-specific antigen in patients with adenocarcinoma of the prostate; demonstration of the "hook effect", *Clin Chem* **1988**, *34*, 2175-2177.
6. Haller, B.L.; Fuller, K.A.; Brown, W.S.; Koenig, J.W., et al. Two Automated Prolactin Immunoassays Evaluated with Demonstration of a High-Dose "Hook Effect" in One, *Clinical Chemistry* **1992**, *38*, 437-438, 10.1093/clinchem/38.3.437.
7. Petakov, M.S.; Damjanović, S.S.; Nikolić-Durović, M.M.; Dragojlović, Z.L., et al. Pituitary adenomas secreting large amounts of prolactin may give false low values in immunoradiometric assays. The hook effect, *Journal of Endocrinological Investigation* **1998**, *21*, 184-188, 10.1007/BF03347299.
8. Barkan, A.L.; Chandler, W.F. Giant pituitary prolactinoma with falsely low serum prolactin: the pitfall of the "high-dose hook effect": case report, *Neurosurgery* **1998**, *42*, 913-915; discussion 915-916, 10.1097/00006123-199804000-00126.
9. Butch, A.W. Dilution Protocols for Detection of Hook Effects/Prozone Phenomenon, *Clinical Chemistry* **2000**, *46*, 1719-1720, 10.1093/clinchem/46.10.1719.
10. Pelkkikangas, A.-M.; Jaakohuhta, S.; Lövgren, T.; Härmä, H. Simple, rapid, and sensitive thyroid-stimulating hormone immunoassay using europium(III) nanoparticle label, *Analytica Chimica Acta* **2004**, *517*, 169-176, <https://doi.org/10.1016/j.aca.2004.04.043>.
11. Tate, J.; Ward, G. Interferences in immunoassay, *Clin Biochem Rev* **2004**, *25*, 105-120.
12. Garber, E.A.E.; Eppley, R.M.; Stack, M.E.; McLaughlin, M.A., et al. Feasibility of Immunodiagnostic Devices for the Detection of Ricin, Amanitin, and T-2 Toxin in Food, *Journal of Food Protection* **2005**, *68*, 1294-1301, 10.4315/0362-028x-68.6.1294.
13. Bowen, R.A.; George, D.T.; Hortin, G.L. False-Negative Result for Cocaine Metabolites on a Lateral-Flow Drug Test Slide Corrected by Dilution, *Clinical Chemistry* **2005**, *51*, 790-791, 10.1373/clinchem.2004.046607.

14. Koets, M.; Sander, I.; Bogdanovic, J.; Doekes, G., et al. A rapid lateral flow immunoassay for the detection of fungal alpha-amylase at the workplace, *Journal of Environmental Monitoring* **2006**, *8*, 942-946, 10.1039/B605389K.
15. Guglielmo-Viret, V.; Splettstoesser, W.; Thullier, P. An Immunochromatographic Test for the Diagnosis of Ricin Inhalational Poisoning, *Clinical Toxicology* **2007**, *45*, 505-511, 10.1080/15563650701354226.
16. Schweers, B.A.; Old, J.; Boonlayangoor, P.W.; Reich, K.A. Developmental validation of a novel lateral flow strip test for rapid identification of human blood (Rapid Stain Identification (TM)-Blood), *Forensic Science International-Genetics* **2008**, *2*, 243-247, 10.1016/j.fsigen.2007.12.006.
17. Old, J.B.; Schweers, B.A.; Boonlayangoor, P.W.; Reich, K.A. Developmental Validation of RSID™-Saliva: A Lateral Flow Immunochromatographic Strip Test for the Forensic Detection of Saliva, *Journal of Forensic Sciences* **2009**, *54*, 866-873, 10.1111/j.1556-4029.2009.01055.x.
18. Martín-Hernández, C.; Muñoz, M.; Daury, C.; Weymuth, H., et al. Immunochromatographic lateral-flow test strip for the rapid detection of added bovine rennet whey in milk and milk powder, *International Dairy Journal* **2009**, *19*, 205-208, <https://doi.org/10.1016/j.idairyj.2008.10.016>.
19. Levinson, S.S. Hook effect with lambda free light chain in serum free light chain assay, *Clinica Chimica Acta* **2010**, *411*, 1834-1836, <https://doi.org/10.1016/j.cca.2010.07.027>.
20. Boyle, T.; Njoroge, J.M.; Jones, R.L.; Principato, M. Detection of Staphylococcal Enterotoxin B in Milk and Milk Products Using Immunodiagnostic Lateral Flow Devices, *Journal of Aoac International* **2010**, *93*, 569-575.
21. Corstjens, P.L.A.M.; de Dood, C.J.; van der Ploeg-van Schip, J.J.; Wiesmeijer, K.C., et al. Lateral flow assay for simultaneous detection of cellular- and humoral immune responses, *Clinical Biochemistry* **2011**, *44*, 1241-1246, <https://doi.org/10.1016/j.clinbiochem.2011.06.983>.
22. Koets, M.; Renström, A.; Zahradnik, E.; Bogdanovic, J., et al. Rapid one-step assays for on-site monitoring of mouse and rat urinary allergens, *Journal of Environmental Monitoring* **2011**, *13*, 3475-3480, 10.1039/C1EM10658A.
23. Posthuma-Trumpie, G.A.; Wichers, J.H.; Koets, M.; Berendsen, L.B.J.M., et al. Amorphous carbon nanoparticles: a versatile label for rapid diagnostic (immuno)assays, *Anal Bioanal Chem* **2012**, *402*, 593-600, 10.1007/s00216-011-5340-5.
24. Qin, Z.; Chan, W.C.W.; Boulware, D.R.; Akkin, T., et al. Significantly Improved Analytical Sensitivity of Lateral Flow Immunoassays by Using Thermal Contrast, *Angewandte Chemie International Edition* **2012**, *51*, 4358-4361, 10.1002/anie.201200997.
25. Li, X.; Lu, D.; Sheng, Z.; Chen, K., et al. A fast and sensitive immunoassay of avian influenza virus based on label-free quantum dot probe and lateral flow test strip, *Talanta* **2012**, *100*, 1-6, <https://doi.org/10.1016/j.talanta.2012.08.041>.
26. Yadav, Y.K.; Fatima, U.; Dogra, S.; Kaushik, A. Beware of "hook effect" giving false negative pregnancy test on point-of-care kits, *J Postgrad Med* **2013**, *59*, 153-154, 10.4103/0022-3859.113838.
27. Oh, Y.K.; Joung, H.-A.; Kim, S.; Kim, M.-G. Vertical flow immunoassay (VFA) biosensor for a rapid one-step immunoassay, *Lab on a Chip* **2013**, *13*, 768-772, 10.1039/C2LC41016H.

28. Griffey, R.T.; Trent, C.J.; Bavolek, R.A.; Keeperman, J.B., et al. "Hook-like Effect" Causes False-negative Point-of-care Urine Pregnancy Testing in Emergency Patients, *The Journal of Emergency Medicine* **2013**, *44*, 155-160, <https://doi.org/10.1016/j.jemermed.2011.05.032>.
29. Lourens, A.; Jarvis, J.N.; Meintjes, G.; Samuel, C.M. Rapid Diagnosis of Cryptococcal Meningitis by Use of Lateral Flow Assay on Cerebrospinal Fluid Samples: Influence of the High-Dose "Hook" Effect, *Journal of Clinical Microbiology* **2014**, *52*, 4172-4175, 10.1128/jcm.01683-14.
30. Oh, Y.K.; Joung, H.-A.; Han, H.S.; Suk, H.-J., et al. A three-line lateral flow assay strip for the measurement of C-reactive protein covering a broad physiological concentration range in human sera, *Biosensors and Bioelectronics* **2014**, *61*, 285-289, <https://doi.org/10.1016/j.bios.2014.04.032>.
31. Joung, H.-A.; Oh, Y.K.; Kim, M.-G. An automatic enzyme immunoassay based on a chemiluminescent lateral flow immunosensor, *Biosensors and Bioelectronics* **2014**, *53*, 330-335, <https://doi.org/10.1016/j.bios.2013.10.004>.
32. Namburi, R.; Kancherla, V.; Ponnala, A. High-dose hook effect, *Journal of Dr. NTR University of Health Sciences* **2014**, *3*, 5-7, 10.4103/2277-8632.128412.
33. Zeng, N.; Hung, Y.S.; Li, Y.; Du, M. A novel switching local evolutionary PSO for quantitative analysis of lateral flow immunoassay, *Expert Systems with Applications* **2014**, *41*, 1708-1715, <https://doi.org/10.1016/j.eswa.2013.08.069>.
34. Cormano, J.; Mackay, G.; Holschneider, C. Gestational Trophoblastic Disease Diagnosis Delayed by the Hook Effect, *Obstetrics & Gynecology* **2015**, *126*, 811-814, 10.1097/aog.0000000000000860.
35. Liu, D.; Huang, Y.; Wang, S.; Liu, K., et al. A modified lateral flow immunoassay for the detection of trace aflatoxin M1 based on immunomagnetic nanobeads with different antibody concentrations, *Food Control* **2015**, *51*, 218-224, <https://doi.org/10.1016/j.foodcont.2014.11.036>.
36. Baumert, J.L.; Tran, D.H. In *Handbook of Food Allergen Detection and Control*, Flanagan, S., Ed.; Woodhead Publishing, 2015, pp 219-228.
37. do Carmo Dias Gontijo, M.; de Souza Vasconcellos, L.; Ribeiro-Oliveira, A. Hook effect and linear range in prolactin assays: distinct confounding entities, *Pituitary* **2016**, *19*, 458-459, 10.1007/s11102-014-0632-3.
38. Ruff, L.E.; Sapre, A.A.; Plaut, J.S.; De Maere, E., et al. Selection of DNA nanoparticles with preferential binding to aggregated protein target, *Nucleic Acids Research* **2016**, *44*, e96-e96, 10.1093/nar/gkw136.
39. Courtney, R.C.; Taylor, S.L.; Baumert, J.L. Evaluation of Commercial Milk-Specific Lateral Flow Devices, *Journal of Food Protection* **2016**, *79*, 1767-1774, 10.4315/0362-028x.Jfp-16-127.
40. Qi, X.; Huang, Y.; Lin, Z.; Xu, L., et al. Dual-Quantum-Dots-Labeled Lateral Flow Strip Rapidly Quantifies Procalcitonin and C-reactive Protein, *Nanoscale Research Letters* **2016**, *11*, 167, 10.1186/s11671-016-1383-z.
41. Campbella, J.P.; Heaney, J.L.J.; Shemar, M.; Baldwin, D., et al. Development of a rapid and quantitative lateral flow assay for the simultaneous measurement of serum kappa and lambda immunoglobulin free light chains (FLC): inception of a new near-patient FLC screening tool, *Clinical Chemistry and Laboratory Medicine* **2017**, *55*, 424-434, 10.1515/cclm-2016-0194.

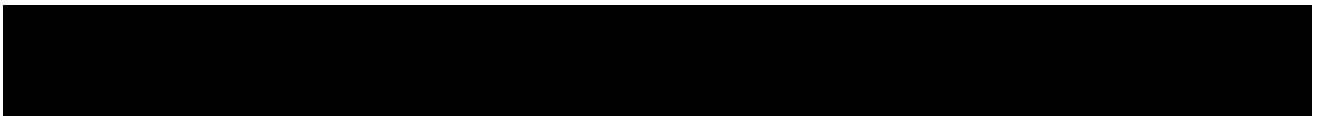
42. Rey, E.G.; O'Dell, D.; Mehta, S.; Erickson, D. Mitigating the Hook Effect in Lateral Flow Sandwich Immunoassays Using Real-Time Reaction Kinetics, *Anal Chem* **2017**, *89*, 5095-5100, 10.1021/acs.analchem.7b00638.
43. Ward, G.; Simpson, A.; Boscato, L.; Hickman, P.E. The investigation of interferences in immunoassay, *Clinical Biochemistry* **2017**, *50*, 1306-1311, <https://doi.org/10.1016/j.clinbiochem.2017.08.015>.
44. Eltzov, E.; Marks, R.S. Colorimetric stack pad immunoassay for bacterial identification, *Biosensors and Bioelectronics* **2017**, *87*, 572-578, <https://doi.org/10.1016/j.bios.2016.08.044>.
45. Hu, J.; Choi, J.R.; Wang, S.; Gong, Y., et al. Multiple test zones for improved detection performance in lateral flow assays, *Sensors and Actuators B: Chemical* **2017**, *243*, 484-488, <https://doi.org/10.1016/j.snb.2016.12.008>.
46. Park, J.; Park, J.-K. Pressed region integrated 3D paper-based microfluidic device that enables vertical flow multistep assays for the detection of C-reactive protein based on programmed reagent loading, *Sensors and Actuators B: Chemical* **2017**, *246*, 1049-1055, <https://doi.org/10.1016/j.snb.2017.02.150>.
47. Hsieh, H.V.; Dantzler, J.L.; Weigl, B.H. Analytical tools to improve optimization procedures for lateral flow assays, *Diagnostics* **2017**, *7*, <https://doi.org/10.3390/diagnostics7020029>.
48. Chen, J.; Chen, K.-H.; Wang, L.-M.; Zhang, W.-W., et al. High-dose HOOK effect in urinary DcR2 assay in patients with chronic kidney disease, *Clinical Biochemistry* **2018**, *58*, 32-36, <https://doi.org/10.1016/j.clinbiochem.2018.06.001>.
49. Oh, J.; Joung, H.-A.; Han, H.S.; Kim, J.K., et al. A hook effect-free immunochromatographic assay (HEF-ICA) for measuring the C-reactive protein concentration in one drop of human serum, *Theranostics* **2018**, *8*, 3189-3197, 10.7150/thno.24034.
50. Deng, X.; Wang, C.; Gao, Y.; Li, J., et al. Applying strand displacement amplification to quantum dots-based fluorescent lateral flow assay strips for HIV-DNA detection, *Biosensors and Bioelectronics* **2018**, *105*, 211-217, <https://doi.org/10.1016/j.bios.2018.01.039>.
51. Asiaei, S.; Bidgoli, M.R.; ZadehKafi, A.; Saderi, N., et al. Sensitivity and color intensity enhancement in lateral flow immunoassay tests by adjustment of test line position, *Clinica Chimica Acta* **2018**, *487*, 210-215, <https://doi.org/10.1016/j.cca.2018.10.001>.
52. Anfossi, L.; Di Nardo, F.; Cavallera, S.; Giovannoli, C., et al. Multiplex Lateral Flow Immunoassay: An Overview of Strategies towards High-throughput Point-of-Need Testing, *Biosensors (Basel)* **2018**, *9*, 10.3390/bios9010002.
53. Anfossi, L.; Di Nardo, F.; Profiti, M.; Nogarol, C., et al. A versatile and sensitive lateral flow immunoassay for the rapid diagnosis of visceral leishmaniasis, *Anal Bioanal Chem* **2018**, *410*, 4123-4134, 10.1007/s00216-018-1067-x.
54. Anfossi, L.; Di Nardo, F.; Russo, A.; Cavallera, S., et al. Silver and gold nanoparticles as multi-chromatic lateral flow assay probes for the detection of food allergens, *Anal Bioanal Chem* **2018**, 1905-1913, <https://doi.org/10.1007/s00216-018-1451-6>.
55. Lee, G.-h.; Arthur, I.; Leung, M. False-Negative Serum Cryptococcal Lateral Flow Assay Result Due to the Prozone Phenomenon, *Journal of Clinical Microbiology* **2018**, *56*, e01878-01817, 10.1128/jcm.01878-17.

56. Galan-Malo, P.; Pellicer, S.; Pérez, M.D.; Sánchez, L., et al. Development of a novel duplex lateral flow test for simultaneous detection of casein and β -lactoglobulin in food, *Food Chemistry* **2019**, *293*, 41-48, <https://doi.org/10.1016/j.foodchem.2019.04.039>.
57. Jiang, N.; Ahmed, R.; Damayantharan, M.; Ünal, B., et al. Lateral and Vertical Flow Assays for Point-of-Care Diagnostics, *Advanced Healthcare Materials* **2019**, *8*, 1900244, 10.1002/adhm.201900244.
58. Gao, Y.; Zhu, Z.; Xi, X.; Cao, T., et al. An aptamer-based hook-effect-recognizable three-line lateral flow biosensor for rapid detection of thrombin, *Biosensors and Bioelectronics* **2019**, *133*, 177-182, <https://doi.org/10.1016/j.bios.2019.03.036>.
59. Ma, Q.; Yao, J.; Yuan, S.; Liu, H., et al. Development of a lateral flow recombinase polymerase amplification assay for rapid and visual detection of *Cryptococcus neoformans/C. gattii* in cerebral spinal fluid, *BMC Infectious Diseases* **2019**, *19*, 108, 10.1186/s12879-019-3744-6.
60. Ross, G.M.S.; Salentijn, G.I.J.; Nielen, M.W.F. A Critical Comparison between Flow-through and Lateral Flow Immunoassay Formats for Visual and Smartphone-Based Multiplex Allergen Detection, *Biosensors (Basel)* **2019**, *9*, 10.3390/bios9040143.
61. Shin, S.; Choi, M.; Shim, J.; Park, S. Hook effect detection and detection-range-controllable one-step immunosensor for inflammation monitoring, *Sensors and Actuators B: Chemical* **2020**, *304*, 127408, <https://doi.org/10.1016/j.snb.2019.127408>.
62. Huang, L.; Tian, S.; Zhao, W.; Liu, K., et al. Multiplexed detection of biomarkers in lateral-flow immunoassays, *Analyst* **2020**, *145*, 2828-2840, 10.1039/C9AN02485A.
63. Ki, H.; Oh, J.; Han, G.-R.; Kim, M.-G. Glycation ratio determination through simultaneous detection of human serum albumin and glycated albumin on an advanced lateral flow immunoassay sensor, *Lab on a Chip* **2020**, *20*, 844-851, 10.1039/C9LC00967A.
64. Sathishkumar, N.; Toley, B.J. Development of an experimental method to overcome the hook effect in sandwich-type lateral flow immunoassays guided by computational modelling, *Sensors and Actuators B: Chemical* **2020**, *324*, 128756, <https://doi.org/10.1016/j.snb.2020.128756>.
65. Bremer, M.G.E.G.; Smits, N.G.E.; Haasnoot, W. Biosensor immunoassay for traces of hazelnut protein in olive oil, *Anal Bioanal Chem* **2009**, *395*, 119-126, 10.1007/s00216-009-2720-1.
66. Ross, G.M.S.; Bremer, M.; Wichers, J.H.; van Amerongen, A., et al. Rapid Antibody Selection Using Surface Plasmon Resonance for High-Speed and Sensitive Hazelnut Lateral Flow Prototypes, *Biosensors (Basel)* **2018**, *8*, 10.3390/bios804

CHAPTER 7

7

Discussion



General Discussion

Consumers are increasingly conscious about food safety; with the rising prevalence of food allergies, it is logical that we are witnessing a demand for portable, disposable, citizen science-based allergen detection. Combining easy to use sample preparation methods with paper-based immunoassays and ubiquitous detectors like smartphones, tablets or wearables paves the way for decentralized consumer testing. Advancements in 3D-printing and smartphone sensing capabilities have enabled the development of novel lab-on-a-chip devices for liquid handling and extraction with smartphone-based readout. The next scientific and technological challenge is to interconnect solid sample preparation (homogenization, solid-liquid extraction, filtration and dilution/amplification) with on-chip immunosensing and readout. The main aim of this thesis was to develop a miniaturized consumer-operable analytical device for automated, multiplex food allergen detection. In this chapter, the central themes of sample preparation, immunosensing and smartphone-detection are revisited; the potential, limitations and future recommendations regarding the devices developed in this thesis are discussed, and finally a perspective is given on the outlook for disposable devices in a broader societal context by discussing sensor developments for the on-going SARS-CoV-2 pandemic.

1 Sample Preparation

Emerging portable analytical devices are often limited by the need for time-consuming sample preparation which can substantially delay results. Sample preparation remains a challenge because consumers are unfamiliar with and cannot be expected to perform the necessary steps of sampling, homogenization, extraction and dilution¹. Obviously, the ideal situation for consumer applications would be no sample preparation, but currently, only photonic sensors or dipsticks testing already dilute liquid samples (e.g., urine, drinking water) are capable of sensing in this way. For many applications, sensing alone is insufficient, especially when the target is contained within a solid sample and that first needs to be extracted into a testable liquid.

Micro total analysis systems (μ TAS) or lab-on-a-chip (LOC) microfluidic devices can combine several laboratory sample preparation functions in a single chip. These devices have myriad advantages for integrated biosensing such as low sample/reagent use, short assay durations, automatization of different functions (e.g., sample handling, mixing, reagent storage) and multiplexing^{1,2}. As such, microfluidic systems are suited for miniaturizing laboratory-based sample preparation into consumer-friendly systems, with 3D-printing making their fabrication both time and cost efficient³. Recently, a number of 3D-printed devices have been reported for portable liquid sample handling⁴ including for DNA extraction⁵⁻⁸, solid-phase extraction of liquids^{9,10}, hydrogel/membrane separation^{11,12}; unibody arrays¹³ and multi-step handling similar to ELISA¹⁴. However, even devices using

liquid samples are rarely equipment free, still relying on pipettes to load or pre-dilute samples before analysis^{13,15}. Some devices have circumvented the need for additional laboratory equipment, instead enabling integration via connectable disposables such as syringes¹⁶ or silicon tubing allowing for finger pump controllable liquid handling¹⁷. Similarly, unibody lab on a chip (ULOC) devices can achieve autonomous volume metering with precision approaching that of laboratory pipettes (i.e., 2% error for 10 μ L), making on-chip dilution of liquid samples possible without additional laboratory equipment^{14,18-20}.

Conversely, rapid and portable solid-liquid extraction has proved inherently challenging; which might explain why so many integrated devices detect targets in liquid matrices like buffer, water, biological samples (e.g., bodily fluids), milk, juice or honey²¹. For food allergen detection, it is often necessary to first homogenize a solid food into a fine powder and incubate it in an extraction buffer before filtering out any large particles. Even then, the extract might need to be substantially diluted in running buffer before detecting via an immunoassay. The sample preparation methods developed in this thesis are summarized in Table 7.1. In Chapter 3, a standard laboratory extraction method was used, but obviously this would be unsuitable for consumer testing. The necessary equipment and extraction time were reduced in Chapter 4 making the method more feasible for on-site testing but was still a multi-step procedure requiring technical skills. This changed in Chapter 5 with the focus on the development of a pipette-free, consumer-operable sample preparation device.

Table 7.1. Sample preparation methods developed in this thesis

Chapter	Sample Preparation	Total Duration
3	Cookies homogenized using a food processor; ground sample incubated in buffer for 1 hour; samples centrifuged for 20 min; extract filtered through a series (3) of low-protein binding filters; sample manually diluted into assay working range	90 min
4	Cookies homogenized by shaking in a tube with ball-bearings; ground sample agitated with buffer in tube with ball-bearings for 1 min; extract filtered through a series (3) of low-protein binding filters; sample manually diluted into working range	10 min
5	Cookies homogenized by crushing with syringe plunger; ground sample incubated with buffer in syringe for 1 min; extract in syringe filtered through 3D-printed sieves; syringe interconnects with ULOC for autonomous dilution into working range	2 min

1.1 Homogenization & Extraction

Using CAD and 3D-printing enabled the rapid prototyping of the interconnectable sample preparation system detailed in Chapter 5 allowing for multiple iterative designs to be conceived and tested in a short time period. The key challenges were to homogenize,

extract, filter and then dilute solid samples in a consumer-operable way. The initial design for the homogenizer unit was a 3D-printed module that attached onto a generic glass pepper cracker allowing the module to use the cracker's mechanical grinding mechanism (see Figure 7.1A-E). A lid (Figure 7.1C) attached a syringe containing extraction buffer to the module (Figure 7.1E). When the user inserted a cookie into the glass chamber and turned the mechanism, powdered cookie entered the “extraction-syringe” where it was extracted for 1 min before passing through a filter. The handheld unit worked efficiently but its size, cost, and necessity to clean the glass chamber properly before re-use, prevented it from being fit-for-purpose for integrating with a disposable consumer device.

Taking inspiration from this successful syringe-based extraction and “lab-in-a-syringe” assays that automate liquid-phase micro-extraction²²⁻²⁴, the next design concept combined homogenization, solid-liquid extraction and filtration in a single disposable “sample-prep-in-a-syringe” device. Using CAD, a miniaturized grinder with dimensions to fit into the bottom of a generic 10 mL disposable syringe was designed (see Figure 7.1F). The cylindrical grinder was made from two separable parts with sharp teeth, so that when the parts were turned or pressed/retracted, the sample inside was crushed. To avoid the necessity for an additional attachment (i.e., a syringe filter holder containing a low-protein binding filter), sieves with a pore size of 5 μm were 3D-printed, laser cut to the syringe dimensions and inserted underneath the bottom grinder module in the syringe.

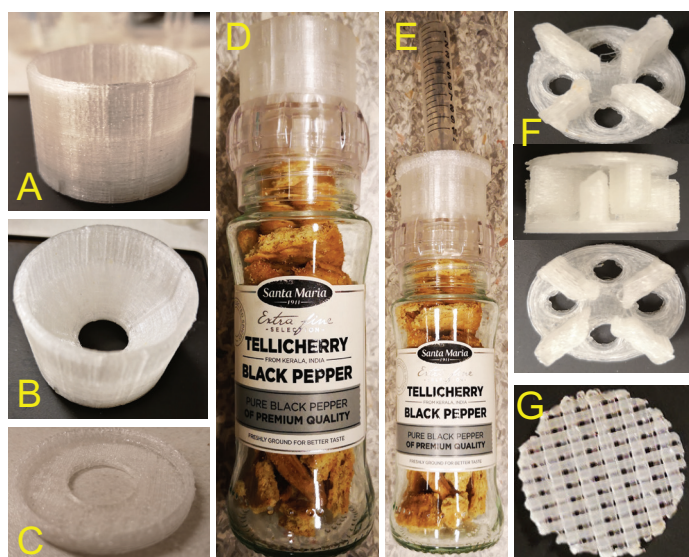


Figure 7.1. Developing the 3D-printed sample preparation unit; the body and lid of attachment (A-C), the pepper cracker with module attached (D) and syringe attached (E), the two-part grinder (F) the laser-cut sieves (G).

The “sample-prep-in-a-syringe” grinder module was successful, although when wet some of the sample became stuck to the grinder teeth. When testing the crushing capability with only the bottom half of the grinder and the syringe plunger, the cookie was crushed with similar effectiveness and less sample stuck in the teeth. Finally, the unit was assessed for its ability to homogenize a solid sample using just the syringe plunger against two 3D-printed sieves (see Figure 7.1G). Using this method, the cookies were effectively homogenized to reproducible particle sizes and the sieves prevented too large particles from leaving the unit, resulting in a system that took a fraction of the printing time and material cost compared with the grinder module. For this thesis, the final interconnectable sample preparation unit was developed for cookies and would likely need some adaptations to make it appropriate for other solid samples with different compositions.

1.2 Dilution

For allergen analysis, homogenization and extraction are only the first steps of sample preparation. Dilution of concentrated samples is a prerequisite for avoiding high concentration dependent effects such as the ‘hook-effect’ discussed in Chapter 6. Allergen extracts typically need to be diluted between 10-100 times before they are tested with paper-based immunoassays such as LFIA²⁵. As previously mentioned, some ULOC devices can automate on-chip dilution, offering comparable performance capabilities to pipettes¹⁴. ULOCs work by fitting silicone tubing to on-chip connectors that are each linked to an individual check-valve, this prevents sample backward-flow, allowing for unidirectional sample actuation. The silicone tubing attached to the connectors can be used as finger pumps or attached to a syringe like the extraction syringe described above. The original design for the ULOC device presented in Chapter 5 can be seen in Figure 7.2A. The initial dilutor ULOC had 6 unibody connector valves, allowing for the connection of the sample prep syringe, air transport syringe and reagent/buffer delivery tubing as well as an outlet that facilitated the attachment of a secondary silicon tubing/syringe.

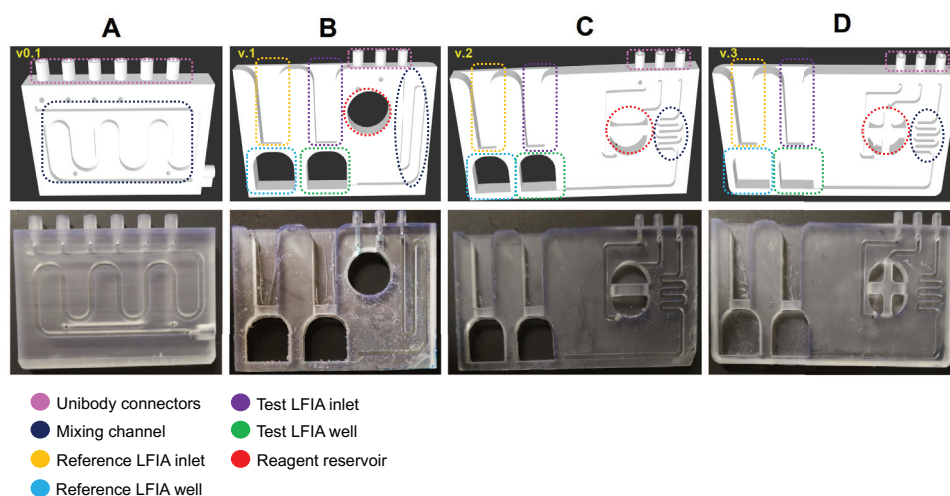


Figure 7.2. The design and development process for the ULOC dilutor showing the stl files and corresponding 3D-print; (A) the original design (v0.1), (B) the first design for integrating LFIAs (v.1); (C) the improved design (v.2); (D) the penultimate structurally improved design (v.3).

The dilutor had a comparable volume metering accuracy to pipettes (2.4% vs 2% error for 10 μL volume)^{26,27} enabling arbitrary sample dilution. While this prototype had excellent transport and dilution properties, it needed further integration with another module/component to execute the final paper-based immunoassay. Using CAD and 3D-printing it is possible to radically adjust a prototype's design, print it and test it within a single day. Before reaching the final v.4 prototype presented in Chapter 5, the ULOC went through 3 additional design iterations, as can be seen in Figure 7.2B-D. Subsequent ULOC designs reduced the number of unibody connectors to 3; 1 was used as the sample/air inlet and the other 2 were connected to each other by silicon tubing, allowing for the fluid pathway to be extended and preventing too much pressure build up upon sample injection due to its elastic nature. The key design features of the ULOC were the central reagent reservoir which allowed on-chip bioreagent storage, the microchannel for unidirectional sample transport, and the reference and the test wells connected to their corresponding LFIA inlets. In addition to the reagent reservoir being pre-filled with bioreagents, the reference well was pre-filled with the necessary reagents for a negative control measurement (i.e., running buffer and CNP-mAbs). In the final ULOC, the sample preparation syringe attaches to the first connector, extracted liquid is injected into the ULOC channel where it enters the reagent reservoir, the sample mixes with the pre-contained labelled antibodies and running buffer allowing for on-chip dilution of concentrated samples. Finally, the mixture is transported by the ULOC microchannel to the test well and an LFIA is inserted into the test LFIA inlet for immunodetection.

1.3 Future improvements

When interconnected, this disposable system goes beyond total sample preparation enabling the largely autonomous homogenization, solid-liquid extraction, filtration, dilution, transport and subsequent detection of allergenic proteins from cookie matrices, yet the current prototype described in chapter 5 faces some limitations. These include: the need to introduce extraction buffer, the use of an air-displacement syringe, the need to manually connect two syringes to the ULOC device, the ability to only run a single LFIA at one concentration (and a reference LFIA as a negative control), the analysis time of 5 - 25 minutes and having only been validated with solid bakery products. To prevent additional steps and plastic waste, future versions of the system should aim to either contain the extraction buffer within a compartment of the syringe or in an additional chamber on the ULOC. Additionally, the air displacement syringe could easily be replaced by retaining the silicone tubing attached to the connector from the sample-prep syringe, using this as a finger pump to actively transport the sample to the reagent reservoir. However, it should be noted that finger pumping has high inter-user variability and the air displacement syringe offers a more consistent pressure. Future versions could consider using a single syringe for extraction and transport, with a miniaturized solvent-selection valve aspirating either buffer from a reservoir contained on the ULOC or air from the outside. An additional advancement could involve a connection between the sample and reference wells, transforming the reference well into another detection well. If the additional well pre-contained a known volume of running buffer, when the already dilute extract passes from the first test well to the second test well, this would allow for an additional measurement to be made for a more dilute sample - this could be particularly relevant when considering establishing the dynamic working range of the assay, as is discussed in Chapter 6. Still, although the system works well with solid bakery products (different types of cookies) and liquid samples (plant-based milks, running buffer) it has not yet been tested with other solid sample matrices and it is feasible that more gelatinous foods might block the current 3D-sieve pores - future versions must consider whether adjustments to the pore sizes are necessary before utilizing the system. Finally, to truly determine the usability of device it should be tested by different consumer groups/ages outside of the laboratory, although it has already been successfully tested by a 15-year-old high school student.

2 Immunosensing

After sample preparation, the target can be detected via specific immunoreagents in a simplified immunoassay like those developed and described throughout this thesis.

2.1 Immunoreagents

The emergence of antibody engineering and phage-display has facilitated the flexible design of sensitive, selective, specific and standardized antibody clones and fragments, giving assay developers a broad choice of immunoreagents with diverse binding characteristics^{28,29,30}. Still, most commonly, a combination of specific monoclonal antibodies (mAbs) and species-specific IgG antibodies are used in sandwich format immunoassays. The mAbs used in a particular assay must be fit-for-purpose, so assay developers must carefully consider the desired assay performance properties before embarking on development. One of the most valued assay parameters is speed; to develop a rapid immunoassay it is necessary to select mAbs with favorable binding kinetics towards their target antigens. This can be done using a label-free SPR-based biosensor as was described in Chapter 3. Using a sensor chip functionalized with an Fc specific IgG, means antibodies are only captured via their Fc domains thus preventing steric hindrance, which is a major advantage for label-free screening of multiple mAbs. The Fc-functionalized assay offers several advantages including (1) on-chip affinity purification of crude mAbs from their culture media, (2) retention of the binding activity of the captured mAb because they are always captured in the correct orientation, and (3) shorter assay development times compared with assessing each mAb individually in direct characterization assays³¹

As such it was possible to use the Fc fragment to screen and select immunoreagents with desired characteristics for subsequent purification and application in LFIA. The binding speeds and sensitivities of the Fc selected mAbs were subsequently reflected in sandwich LFIA, giving the Fc method an edge over conventional affinity ELISA for LFIA-based mAb selection. Despite the success of the developed protocol compared with typical ELISA, it could be further advanced by using an SPR instrument with a higher-throughput capacity^{32,33}. A future improvement would be to also measure the binding speed of the Fc capture antibody before immobilizing it onto the sensor chip surface to ensure that the optimal capture reagent is used^{31,34}.

In addition to expediting screening of antibodies for immunoassay applications, Fc-specific fragments can be used as the capture antibody in clinical assays for directly detecting serological antibody responses^{35,36}, although it has been suggested that nanobodies may instead be more appropriate for such applications³⁷. With continued advances in antibody engineering, it is likely in the near future that most assays will exploit nanobodies as their capture recognition elements. Nanobodies recognize their antigen via a single binding domain-only, still achieving high affinity and specificity compared with conventional mAbs and have decreased likelihood of eliciting a false result, making them attractive considerations for the development of next generation immunoassays³⁷⁻³⁹.

2.2 Labels

Detector antibodies in sandwich immunoassays need to be labelled with particles that are collectively big enough to be visualized with the naked eye but not large enough to disrupt the antibody binding. The overwhelming majority of LFIA use gold nanoparticles (AuNPs) due to their stability, homogenous size distribution and easy interfacing with reflectance and digital lateral flow readers. More recently, carbon nanoparticles (CNPs) have emerged as an inexpensive alternative label in LFIA, not only do CNPs have excellent contrast in paper-based assays making them excellent for smartphone-detection but they can reach up to 10-fold lower limits of detection compared with AuNPs⁴⁰⁻⁴². Fluorescent nanoparticles are also reported to offer increased sensitivity compared with AuNPs³⁶. Quantum dots (QDs) are semiconductor nanoparticles that exhibit a fluorescent signal when excited under UV light. They have been used as labels in a wide range of immunoassays but require a UV light source and sometimes an optical filter to read⁴³⁻⁴⁵. However, emergence of affordable 3D-printing platforms has facilitated the development of portable UV readers and smartphone attachments that make QD's an attractive option for novel immunoassays⁴⁵⁻⁴⁹. Before selecting CNPs as the detector label in this thesis, both CNPs and QDs were compared for their applicability in passive flow-through assays like those developed in Chapter 4. Nitrocellulose membranes were functionalized with the same capture antibodies and tested with sample and the same detector mAb labeled with CNPs, or with QDs which gave a strong fluorescent signal when excited under UV (365 nm) light. Both detector labels gave similar sensitivities, but the QD-based assay needed to be read under UV light whereas the CNP based LFIA could be easily read by naked eye, giving it an advantage for consumer testing.

2.3 SPR-based Immunosensing

Surface plasmon resonance (SPR) based biosensors allow for the label-free measurement of biomolecular interactions in real-time and have been used to facilitate the high-throughput analysis of food allergens in multichannel or imaging instrumental set-ups⁵⁰. A recent review details the use of fiber-optic surface plasmon resonance (FOSPR), surface plasmon resonance imaging (SPRi), localized surface plasmon resonance (LSPR), and transmission surface plasmon resonance (TSPR) for the detection of food allergens⁵¹. Conventional SPR-sensors are limited by their cost, maintenance and necessity for trained personnel to operate; further they are generally lab-based, restricting their use as on-site sensors. Until recently, the complex optics and precise alignment of internal components needed for SPR-sensing hindered the development of truly portable SPR devices⁵². The ubiquity of touch-screen smartphones with powerful CPU's, high-pixel counts, integrated cameras and SPR compatible light sources paired with the emergence of accessible 3D-printing platforms has enabled plasmonic sensing by smartphone⁵³. Smartphone screen displays are sufficient for wide-angle illumination for configuring angle resolved SPR⁵⁴. In contrast, FOSPR, LSPR and SPRi sensing can be more practically achieved using the phone's rear-facing flash as the light source and camera as the sensor⁵⁵⁻⁶⁰.

2.3.1 Smartphone-based SPR

Unfortunately, only a limited number of portable SPR studies tested realistic sample matrices with the majority focusing on the detection of an analyte in buffer, and few reported benchmarking or cross-validation of the portable SPR system with an established SPR-instrument. Recently, Xiao et al. at Linköping University, developed a smartphone-based SPR sensor that uses white light (LED) to excite surface plasmons in three spectral domains at the red, green and blue bands of the LED and measures the total internal reflection SPR dips with the rear-facing smartphone camera (see Figure 7.3).

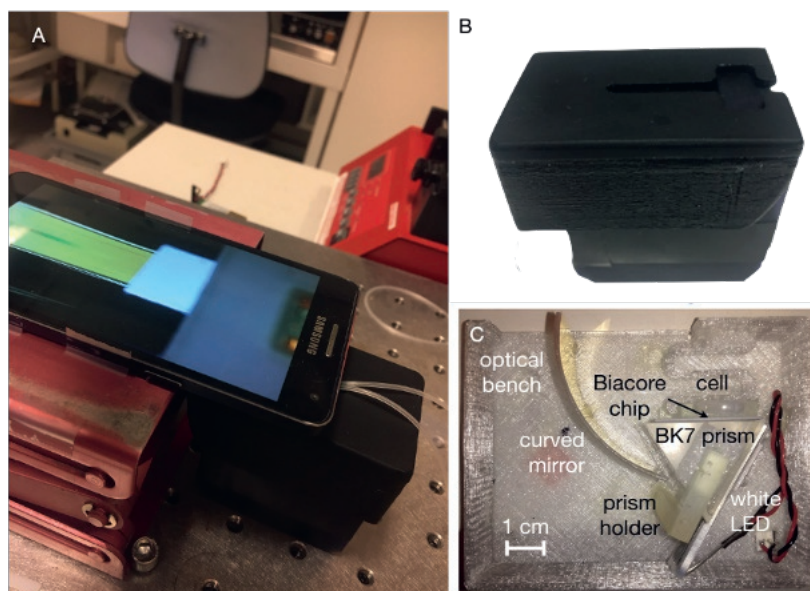


Figure 7.3. The smartphone-based prototype SPR platform; (A) photo of the SPR platform combined with a smartphone; (B) photo of the 3D-printed SPR platform (C) the inner components of the SPR platform. Photos credited to Xiao 2020.

To benchmark the prototype SPR sensor, its performance was directly compared using the same samples, immunoreagents and buffers against a commercial SPR instrument (Biacore 3000) for detecting total hazelnut protein (THP) in plant-based milks. The prototype sensor achieved a comparable sensitivity to the commercial instrument; see Figure 7.4 for a direct comparison of the overlaid sensorgrams for soymilk and plotted calibration curves for all tested plant milks for the two systems. The cross-validation of the prototype against a standard instrument with real samples shows that the novel sensor can already reach similar detection levels as a lab-based system. It should be noted that the commercial biosensor measures using response units (RUs) whereas the prototype

sensor uses “relative response” units, so the difference in scale observed in Figure 7.4 is to be expected. Further, the 3D-printed prototype-sensor is inexpensive (< \$5), portable and connectable with a smartphone making it well suited for on-site testing compared with much more expensive (\$100k +) desktop SPR instruments. However, the prototype sensor relies on a Biacore chip (\$300), which increases its cost. Still, these chips are reusable when effectively optimized, making this cost increase less relevant. Future improvements should aim to decrease assay run times as the current sensor still has much longer run times than a commercial SPR. Finally, on-site testing has many logistical challenges so to truly demonstrate the prototype sensor as a portable system, measurements should be made also outside of a lab environment⁵².

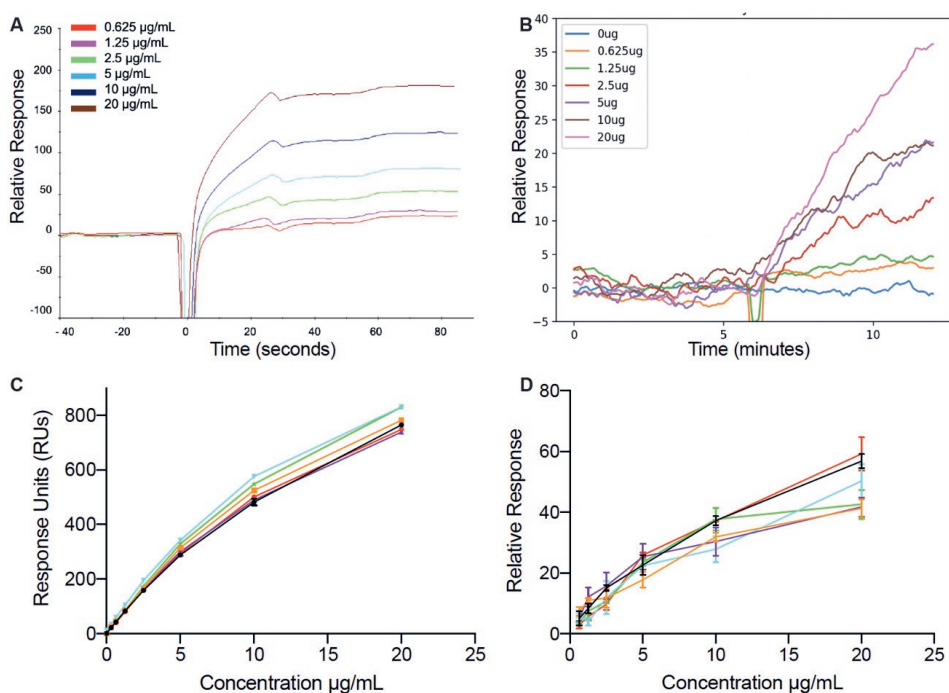


Figure 7.4. Performance comparison between a commercial Biacore 300 instrument and Xiao's smartphone-based prototype SPR-sensor. (A) Biacore: overlaid sensorgrams showing the detection of different concentrations of total hazelnut protein (THP) spiked in soymilk (0.625 – 20 µg/mL), (B) Prototype: overlaid sensorgrams showing the detection of different concentrations of total hazelnut protein (THP) spiked in soymilk (0.625 – 20 µg/mL), (C) Biacore: calibration curve showing the detection of a range of concentrations of THP in buffer and different plant-based milks as a function of RU. Error bars represent standard deviation ($n=3$). (D) Prototype: calibration curve showing the detection of a range of concentrations of THP in buffer and different plant-based milks as a function of relative response. Error bars represent standard deviation ($n=3$).

2.4 Paper-based Immunoassays

Paper-based immunoassays like LFIA are increasingly used by consumers and non-experts for on-site testing. Singleplex LFIAs like the hazelnut LFIA developed in Chapter 3 are by far the most widely distributed format due to their simplicity in fabrication and operation. But as is shown in Chapter's 4-6, LFIA is adaptable to multiplexing through the addition of multiple test regions allowing for the simultaneous detection of different analytes in a single sample. Despite these possibilities, the majority of line-based multiplex LFIAs are duplex or triplex assays with more high-throughput multiplexing typically being restricted to dotted arrays or alternative formats of paper-based analytical devices such as flow-through assays^{46,61-64}. Multiplex assays are notoriously challenging to optimize due to the potential for cross-interference, differences in sensitivity, specificity and binding kinetics of the different antibodies^{65,66}. The challenges of multiplex LFIA were first made apparent in Chapter 4 when developing and testing different paper-based immunoassay formats. When testing the multiplex LFIA at increasing antigen concentrations the hazelnut test line was lost at a lower concentration than the peanut test line was, indicating a difference in binding behaviors between the two antibodies.

Another challenge when developing consumer-operable assays is the pre-storage of immunoreagents. Most paper-based immunoassays store labeled antibodies in conjugate pads, which release the reagents when the pads are wetted. Other interesting examples of reagent storage in micro-paper analytical devices (μ PADs) use paper-microfluidics^{15,67,68}, inkjet printing^{69,70}, chemical etching⁷¹ and origami^{72,73} to pre-contain reagents. Still, most of these examples are complicated and not intended for consumer use, but the integration of 3D-printing and paper-based devices allows for greater freedom for reagent storage^{6,67,74}. Combining LFIA with a 3D-printed ULOC as described in Chapter 5 allowed pre-storage of CNP-mAbs in running buffer, enabling on-chip reagent storage and dilution of concentrated samples. Still, the long-term stability of the on-chip bioreagents was not studied here. Crucially, the purpose of the on-chip reagent reservoir was to automate equipment-free dilution of samples and mixing with reagents for subsequent LFIA detection. While the overall duration of the total analysis could still be improved, this is the first reported device that allows pipette-free dilution of concentrated samples into the appropriate assay dynamic working range for subsequent multiplex LFIA-based detection and takes approximately the same time as it would to manually dilute and detect the samples in the lab.

3 Smartphone Detection

Dedicated LFIA readers have been commercially available since the early 2000's and commonly use digital camera sensors combined with computer algorithms to provide

precise LFIA measurements. Large desktop readers that batch-measure multiple LFIAs were quickly replaced by handheld versions that allow for portable LFIA quantification. One affordable, handheld, standard LFIA reader is called “The Cube”; this device is described as an ‘electronic eye’ and reportedly removes the risk of error within LFIA testing. However, “The Cube” simply provides a binary (yes/no) result for the LFIA based on the appearance/lack of appearance of multiple test lines and then exports all test results to the cloud for subsequent data analysis. Further, until recently the device required LFIAs be housed in proprietary cassettes (cost approx. \$100 / cassette) substantially increasing the cost of assay development and requiring the end-user to physically insert/remove the LFIA from the cassette before/after each measurement. A similar “electronic eye” system is employed by the NIMA sensor. In the NIMA, each LFIA is contained in a window of the disposable sample-prep capsule, when the capsule is inserted into the NIMA device an in-built sensor reads and transmits the result to the device and to the user’s smartphone. While these examples can offer uniformity of results, both are only optimized to a single assay configuration and require different equipment for other LFIAs (i.e., the cube requires a new cassette per assay configuration and NIMA requires a whole new sensor for different analytes).

The use of smartphones as analytical detectors has boomed in recent years with their inbuilt cameras, powerful processing software and cloud connectivity making them attractive LFIA readers. The benefits of using smartphones cameras for reading optical immunoassays have been extensively explored throughout this thesis. Despite their clear advantages, it is well known that different smartphone cameras, or the same camera on different settings can substantially alter images⁷⁵. Additionally, smartphone manufacturers have their own proprietary imaging processing algorithms that automatically enhance the image quality⁷⁶. Studies comparing different smartphone models for colorimetric analysis report differences in sensitivity between the models^{77,78}, affirming the necessity to standardize smartphone image capture. In Chapter’s 4-6 the open-source android software ‘OpenCamera’ was used to lock the white balance, focus, flash and other settings of the camera to achieve a consistent sensing result. While the responses of camera sensors vary from one camera to the next, because the RGB values provided by any imaging device are device dependent⁷⁹, it was observed in Chapter 4 that using OpenCamera to standardize image capture allowed for near identical results between two different smartphone models. Future smartphone-based detectors should consider the application of such free software or an iOS equivalent in order to standardize smartphone image capture allowing for better comparisons to be made in this rapidly evolving field.

The use of 3D-printed embedded optics and references can extend the capabilities of smartphone cameras for sensing^{18,19}, but an alternative is to instead use the phone’s ambient light sensor (ALS). The ALS automatically adjusts the light intensity of a phone

screen according to the ambient lighting. Using a 3D-printed module attached directly to the ALS makes it possible to make a proximity-based measurement of the transmitted light intensity from an assay^{80,81}. Regardless of the sensor component used, the majority of reported smartphone-based tests still require off-line data processing, with only a limited number of publications reporting the development of a true smartphone app^{45,69,82,83}. In Chapter's 3-4, two freely downloadable apps were used for obtaining color values for image analysis. The first app (RGB color detector) gave RGB readings for a selected region and the second (Nix pro color sensor) translated the RGB values to cieLAB values. These values were then used to plot a calibration curve of cieLAB value as a function of analyte concentration. Despite this method working well, the conversion between the two color spaces was unnecessary and ultimately delayed the time-to-result. While the values were obtained using smartphone apps, it was not an automatic process and the results still needed to be processed on a laptop. Mostly, smartphones are used to record a photo/video that is then analyzed in ImageJ or a similar image processing software on a computer. This was one of the approaches applied in Chapter's 5-6. The other approach was to use a smartphone to record a video of the developing LFIA and then to pass this video to a computer-based python program for measurement of the test and control signal development. This method largely automated the time-development analysis of the LFIA, providing crucial information compared with endpoint analysis, and gave comparable results to the manual image processing of the same video frames using ImageJ, making it an attractive alternative to current approaches. Yet, this method still required the export of video data to a computer for further interpretation, therefore an off-line approach with on-smartphone processing was considered.

3.1 On-smartphone processing

As an off-line alternative with on-smartphone processing, a standalone prototype app that automatically interprets LFIA for allergen detection has been developed by Zhao et al. of Queen's University. Using object recognition, the app identifies the LFIA's physical positioning in a smartphone video and feeds these features into a prediction model for result interpretation, allowing for identification of LFIA control and test lines based on their physical positioning (see Figure 7.5).

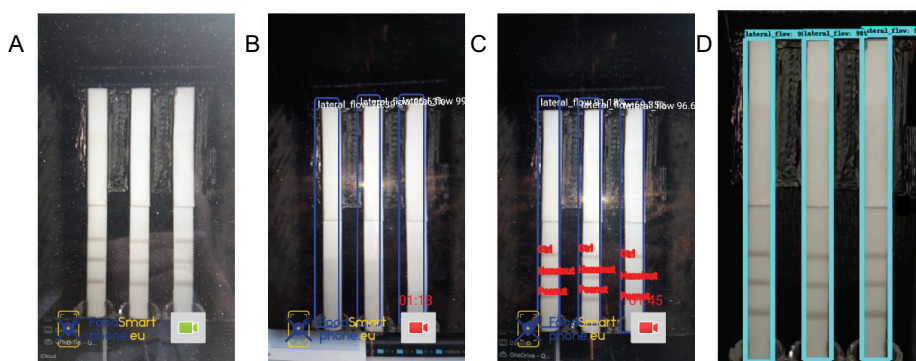


Figure 7.5. Screenshots and signal processing with smartphone app. (A) opening the app, (B) starting the video and automatically recognizing LFIA by their bounding boxes, (C) test results displayed on the screen. Figure credited to Zhao 2020.

Machine learning was used to train the app with a total of 4567 images generated from 10 videos (each showing the development of 3 LFIA) recorded using a smartphone attached to the 3D-printed holder developed in Chapter 5. While the app had 86.7% accuracy for determining positive/negative results in the multiplex LFIA, it was unable to recognize concentration dependent effects giving false results if the control or test lines did not behave as anticipated. Future improvements should focus on using a time-based threshold for signal development in order to avoid false negative results, as was reported in Chapter 6. If the App detects the control line signal first, followed by the test line, the LFIA is in the dynamic working range, if the App detects the test line signal before the control line, then the LFIA is in free secondary mAb depletion range and is already at high analyte concentrations. If no lines appear for the first ten minutes, and only then the signal starts developing, the LFIA is at hook-effect concentrations and false negatives are likely. A further improvement would be for the LFIA to be analyzed automatically in real-time as the video is recorded; the current app still requires a pre-recorded video to be exported to the developed app for analysis, preventing it from being a truly real-time method.

Smartphone-based analytical devices are still evolving and likely have not reached their full potential yet. Improvements can be expected in the coming years with phones having enlarged pixel arrays with reduced pixel sizes, improved camera pixel intensity and increasingly powerful processors⁸³. Increased touch screen sensitivity might even transform phone screens into analytical weighing scales for sample preparation⁸³. The upcoming roll-out of 5G technology is expected to accelerate next-generation mobile communication allowing for high-speed wireless data transfer and widespread accessibility even in remote regions⁸⁴ making network connectivity issues obsolete.

4 Outlook in a broader context: future disposables

The future potential of integrated disposable consumer immunodiagnostics in food safety, forensic, environmental and clinical testing appears limitless, just at a point in global history where such disposable devices will be tested to their limit. The ongoing global SARS-CoV-2 pandemic has emphasized the necessity for accurate consumer-operable home tests integrated with smartphone-detection for data analysis and transfer to relevant stakeholders (i.e., healthcare professionals). Current laboratory-based diagnostic testing solutions, which amplify and detect the virus' genetic material via polymerase-chain reaction (PCR), take around 8 hours to analyze and have a typical time-to-result of between 24-48 hours⁸⁵. Diagnosis can be further delayed by limited testing capacities. This delay is especially problematic when considering that the reliability of the PCR test depends on the day of infection that a sample was taken at; if a person is tested on the first day of infection the false negative rate is 100%⁸⁶. This false-negative rate reportedly falls to 67% on day 4, 38% on day 5 and 20% on day 8, before increasing to 21% again on day 9 of the infection and up to 66% on day 21⁸⁶. Depending on local testing capacities, availability of a vehicle and other additional barriers, it can take a week before an individual is screened for the disease. It is hardly surprising then that society is experiencing a growing distrust of scientists and governments. Even with the emergence of disposable LFIA for rapid screening for COVID, until testing is mandated, and the corresponding testing capacity is reached it is unlikely we will get a clear picture of the true extent of the disease⁸⁷.

Now would be the perfect time for globalized citizen science, using a smartphone-facilitated, decentralized-testing approach. Many consumers are already comfortable with using LFIA, with the home pregnancy testing market forecast to reach 0.36 billion USD by 2024 in Europe alone⁸⁸, and a home COVID test would not be much different. A simple smartphone app could guide the consumer how to collect the sample (e.g., finger-prick for blood or a swab for saliva) and apply it to the LFIA. The app would then guide the user how to record a photo of their developed/developing LFIA, providing users the net of a cube printed onto black cardboard and a "how to fold" video would allow for users to make their own light-box to photograph LFIA under controlled ambient light conditions. Using object recognition, the app would inform the user when the LFIA is in the correct location to record the photo, while dynamic data acquisition would monitor false compliance. To ensure accessibility, the app must have a user-operable interface and include instruction options in sign-language, multiple spoken languages and clear text. After the app has recorded the image/video, it should provide users with a binary positive/negative result before storing the user's data (linked with a specific barcode) and wirelessly transmitting to relevant stakeholders (healthcare professionals, government etc.). It would even be feasible to consider the app already being linked with global 'track and trace' apps enabling result-focused social distancing. Such global home-testing

would allow us to appreciate the true scale of SARS-CoV-2, and the affordability of these disposable tests could even mean that frontline individuals could perform testing daily. Still, many key issues would need to be considered before such an app could be possible, including privacy, accountability, misuse of citizen science and the risk of fraud.

Moreover, there is a neglected darker side to such a disposable solution. Currently, we produce 300 million tons of plastic annually, half of which is used for single-use items⁸⁹. This will likely increase with demand for plastic cassettes for disposable COVID tests. Although cassettes will be likely made from degradable materials such as polylactic acid (PLA), recycling these will be complicated by the biohazardous nature of the used LFIA. Although outer cassettes can easily be removed, cleaned and recycled, we cannot expect consumers to do this. Instead, we must consider feasible strategies to prevent compounding to our already enormous plastic waste. A potential quick fix could be to include a printed device that allows users to 'unclip' the cassette without handling the inner test. While such a device would also be made from plastic, it could be reusable for the duration of home testing and eventually recycled. Clearly, disposable testing is the future, but it should not come at the cost of making our (environmental) future disposable.

An alternative self-detection approach to disposable testing is continuous health care monitoring through wearable sensors. In recent years, numerous invasive and non-invasive wearable sensors have been developed including watches, patches, contact lenses and glasses^{1,84,90-92}. Still, these reusable electronics are often expensive preventing them from being accessible to many. Electronic or digital tattoos might present an affordable solution. These miniaturized labs are 3D-printed using circuit printed technologies onto flexible materials that can the user can directly wear on their skin⁹³. The tiny electrodes in the tattoos record and transmit wearer information to smartphones or other connectable devices and can work for several days consecutively, extending their life compared with single use tests.

5 Conclusions

In closing, this thesis has explored the emerging field of consumer-operable portable food safety analysis and outlined the necessary criteria for developing real-life consumer immunosensors. Surface plasmon resonance has been used to extensively study antibody-antigen binding characteristics allowing for the development of sensitive, disposable, single and multiplex paper-based immunoassays optimized for rapid testing. Smartphone cameras have been exploited as optical detectors with different off-line and on-smartphone image analysis methods being tested for semi-quantifying LFIAs both with and without 3D-printed auxiliary attachments. A novel smartphone-based dynamic

data acquisition method has been devised that allows for the differentiation between high-antigen concentration effects in LFIA that could prevent misinterpretation of false negatives. The first consumer-operable interconnectable system that allows for the total immunodetection of multiple food allergens from sample to smartphone has been successfully created. Finally, emerging technologies including portable SPR, machine-learning for on-smartphone processing, and wearable sensors have been discussed as well as the future of disposable analytical devices.

References

1. Dincer, C.; Bruch, R.; Costa-Rama, E.; Fernández-Abedul, M.T., et al. Disposable Sensors in Diagnostics, Food, and Environmental Monitoring, *Advanced Materials* **2019**, *31*, 1806739, 10.1002/adma.201806739.
2. Nahavandi, S.; Baratchi, S.; Soffe, R.; Tang, S.-Y., et al. Microfluidic platforms for biomarker analysis, *Lab on a Chip* **2014**, *14*, 1496-1514, 10.1039/C3LC51124C.
3. Waheed, S.; Cabot, J.M.; Macdonald, N.P.; Lewis, T., et al. 3D printed microfluidic devices: enablers and barriers, *Lab on a Chip* **2016**, *16*, 1993-2013, 10.1039/C6LC00284F.
4. Li, F.; Ceballos, M.R.; Balavandy, S.K.; Fan, J., et al. 3D Printing in analytical sample preparation, *Journal of Separation Science* **2020**, *43*, 1854-1866, 10.1002/jssc.202000035.
5. Agrawal, P.; Reifengerger, J.G.; Dorfman, K.D. 3D Printing-Enabled DNA Extraction for Long-Read Genomics, *ACS Omega* **2020**, *5*, 20817-20824, 10.1021/acsomega.0c01912.
6. Trinh, K.T.L.; Trinh, T.N.D.; Lee, N.Y. Fully integrated and slidable paper-embedded plastic microdevice for point-of-care testing of multiple foodborne pathogens, *Biosensors and Bioelectronics* **2019**, *135*, 120-128, <https://doi.org/10.1016/j.bios.2019.04.011>.
7. Yin, J.; Suo, Y.; Zou, Z.; Sun, J., et al. Integrated microfluidic systems with sample preparation and nucleic acid amplification, *Lab on a Chip* **2019**, *19*, 2769-2785, 10.1039/C9LC00389D.
8. Du, K.; Cai, H.; Park, M.; Wall, T.A., et al. Multiplexed efficient on-chip sample preparation and sensitive amplification-free detection of Ebola virus, *Biosensors and Bioelectronics* **2017**, *91*, 489-496, <https://doi.org/10.1016/j.bios.2016.12.071>.
9. Park, M.; Seo, T.S. An integrated microfluidic device with solid-phase extraction and graphene oxide quantum dot array for highly sensitive and multiplex detection of trace metal ions, *Biosensors and Bioelectronics* **2019**, *126*, 405-411, <https://doi.org/10.1016/j.bios.2018.11.010>.
10. Zhu, C.; Hu, A.; Cui, J.; Yang, K., et al. A lab-on-a-chip device integrated DNA extraction and solid phase PCR array for the genotyping of high-risk HPV in clinical samples, *Micromachines* **2019**, *10*, doi:10.3390/mi10080537.
11. Lockwood, S.Y.; Meisel, J.E.; Monsma, F.J., Jr.; Spence, D.M. A Diffusion-Based and Dynamic 3D-Printed Device That Enables Parallel in Vitro Pharmacokinetic Profiling of Molecules, *Anal Chem* **2016**, *88*, 1864-1870, 10.1021/acs.analchem.5b04270.
12. Kim, H.; Chung, D.-R.; Kang, M. A new point-of-care test for the diagnosis of infectious diseases based on multiplex lateral flow immunoassays, *Analyst* **2019**, *144*, 2460-2466, 10.1039/C8AN02295J.
13. Tang, C.K.; Vaze, A.; Rusling, J.F. Automated 3D-printed unibody immunoarray for chemiluminescence detection of cancer biomarker proteins, *Lab on a chip* **2017**, *17*, 484-489, 10.1039/c6lc01238h.
14. Suska, A.; Filippini, D. Autonomous lab-on-a-chip generic architecture for disposables with integrated actuation, *Scientific Reports* **2019**, *9*, 20320, 10.1038/s41598-019-55111-z.
15. Tsagkaris, A.S.; Migliorelli, D.; Uttl, L.; Filippini, D., et al. A microfluidic paper-based analytical device (μ PAD) with smartphone readout for chlorpyrifos-oxon screening in human serum, *Talanta* **2021**, *222*, 121535, <https://doi.org/10.1016/j.talanta.2020.121535>.

16. Anderson, K.B.; Lockwood, S.Y.; Martin, R.S.; Spence, D.M. A 3D Printed Fluidic Device that Enables Integrated Features, *Analytical Chemistry* **2013**, *85*, 5622-5626, 10.1021/ac4009594.
17. Wang, J.; Deng, K.; Zhou, C.; Fang, Z., et al. Microfluidic cap-to-dispense (μ CD): a universal microfluidic-robotic interface for automated pipette-free high-precision liquid handling, *Lab on a chip* **2019**, *19*, 3405-3415, 10.1039/c9lc00622b.
18. Comina, G.; Suska, A.; Filippini, D. Autonomous Chemical Sensing Interface for Universal Cell Phone Readout, *Angewandte Chemie International Edition* **2015**, *54*, 8708-8712, 10.1002/anie.201503727.
19. Comina, G.; Suska, A.; Filippini, D. 3D Printed Unibody Lab-on-a-Chip: Features Survey and Check-Valves Integration., *Micromachines* **2015**, *6*, 437-451.
20. Comina, G.; Suska, A.; Filippini, D. Low cost lab-on-a-chip prototyping with a consumer grade 3D printer, *Lab on a Chip* **2014**, *14*, 2978-2982, 10.1039/c4lc00394b.
21. Nelis, J.L.D.; Tsagkaris, A.S.; Dillon, M.J.; Hajslova, J., et al. Smartphone-based optical assays in the food safety field, *TrAC Trends in Analytical Chemistry* **2020**, 115934, <https://doi.org/10.1016/j.trac.2020.115934>.
22. Hárendarčíková, L.; Baron, D.; Šebestová, A.; Rozsypal, J., et al. True lab-in-a-syringe technology for bioassays, *Talanta* **2017**, *174*, 285-288, <https://doi.org/10.1016/j.talanta.2017.06.017>.
23. Maya, F.; Horstkotte, B.; Estela, J.M.; Cerdà, V. Lab in a syringe: fully automated dispersive liquid-liquid microextraction with integrated spectrophotometric detection, *Anal Bioanal Chem* **2012**, *404*, 909-917, 10.1007/s00216-012-6159-4.
24. Horstkotte, B.; Solich, P. The Automation Technique Lab-In-Syringe: A Practical Guide, *Molecules* **2020**, *25*, 1612, 10.3390/molecules25071612.
25. Galan-Malo, P.; Pellicer, S.; Pérez, M.D.; Sánchez, L., et al. Development of a novel duplex lateral flow test for simultaneous detection of casein and β -lactoglobulin in food, *Food Chemistry* **2019**, *293*, 41-48, <https://doi.org/10.1016/j.foodchem.2019.04.039>.
26. Shang, Z.; Zhou, X.; Li, C.; Zhou, X. Design of Micropipette System with High Precision for Small Enzyme Immunoassay Analyzer, *Journal of Shanghai Jiaotong University (Science)* **2019**, *24*, 605-615, 10.1007/s12204-019-2104-4.
27. Pushparaj, P.N. Revisiting the Micropipetting Techniques in Biomedical Sciences: A Fundamental Prerequisite in Good Laboratory Practice, *Bioinformation* **2020**, *16*, 8-12, 10.6026/97320630016008.
28. McCafferty, J.; Griffiths, A.D.; Winter, G.; Chiswell, D.J. Phage antibodies: filamentous phage displaying antibody variable domains, *Nature* **1990**, *348*, 552-554, 10.1038/348552a0.
29. Borrebaeck, C.A. Antibodies in diagnostics - from immunoassays to protein chips, *Immunol Today* **2000**, *21*, 379-382, 10.1016/s0167-5699(00)01683-2.
30. de la Cruz, S.; López-Calleja, I.M.; Alcocer, M.; González, I., et al. Selection of Recombinant Antibodies by Phage Display Technology and Application for Detection of Allergenic Brazil Nut (*Bertholletia excelsa*) in Processed Foods, *Journal of Agricultural and Food Chemistry* **2013**, *61*, 10310-10319, 10.1021/jf403347t.

31. Kamat, V.; Rafique, A.; Huang, T.; Olsen, O., et al. The impact of different human IgG capture molecules on the kinetics analysis of antibody-antigen interaction, *Analytical Biochemistry* **2020**, *593*, 113580, <https://doi.org/10.1016/j.ab.2020.113580>.
32. Yang, D.; Singh, A.; Wu, H.; Kroe-Barrett, R. Comparison of biosensor platforms in the evaluation of high affinity antibody-antigen binding kinetics, *Analytical Biochemistry* **2016**, *508*, 78-96, <https://doi.org/10.1016/j.ab.2016.06.024>.
33. Nguyen, H.H.; Park, J.; Kang, S.; Kim, M. Surface plasmon resonance: a versatile technique for biosensor applications, *Sensors (Basel)* **2015**, *15*, 10481-10510, 10.3390/s150510481.
34. Ndao, D.M.; Hickman, D.T.; López-Deber, M.P.; Davranche, A., et al. Binding Affinity Measurement of Antibodies from Crude Hybridoma Samples by SPR, *Bio-protocol* **2014**, *4*, e1276, 10.21769/BioProtoc.1276.
35. Brown, E.P.; Dowell, K.G.; Boesch, A.W.; Normandin, E., et al. Multiplexed Fc array for evaluation of antigen-specific antibody effector profiles, *J Immunol Methods* **2017**, *443*, 33-44, 10.1016/j.jim.2017.01.010.
36. Wang, J.; Meng, H.-M.; Chen, J.; Liu, J., et al. Quantum Dot-Based Lateral Flow Test Strips for Highly Sensitive Detection of the Tetanus Antibody, *ACS Omega* **2019**, *4*, 6789-6795, 10.1021/acsomega.9b00657.
37. Pinto Torres, J.E.; Goossens, J.; Ding, J.; Li, Z., et al. Development of a Nanobody-based lateral flow assay to detect active Trypanosoma congolense infections, *Scientific Reports* **2018**, *8*, 9019, 10.1038/s41598-018-26732-7.
38. Gonzalez-Sapienza, G.; Rossotti, M.A.; Tabares-da Rosa, S. Single-Domain Antibodies As Versatile Affinity Reagents for Analytical and Diagnostic Applications, *Frontiers in Immunology* **2017**, *8*, 10.3389/fimmu.2017.00977.
39. Kinimi, E.; Odongo, S.; Muyldermans, S.; Kock, R., et al. Paradigm shift in the diagnosis of peste des petits ruminants: scoping review, *Acta Veterinaria Scandinavica* **2020**, *62*, 7, 10.1186/s13028-020-0505-x.
40. Qiu, W.; Baryeh, K.; Takalkar, S.; Chen, W., et al. Carbon nanotube-based lateral flow immunoassay for ultrasensitive detection of proteins: application to the determination of IgG, *Mikrochim Acta* **2019**, *186*, 436, 10.1007/s00604-019-3508-4.
41. Qiu, W.; Xu, H.; Takalkar, S.; Gurung, A.S., et al. Carbon nanotube-based lateral flow biosensor for sensitive and rapid detection of DNA sequence, *Biosensors and Bioelectronics* **2015**, *64*, 367-372, <https://doi.org/10.1016/j.bios.2014.09.028>.
42. Posthuma-Trumpie, G.A.; Wichers, J.H.; Koets, M.; Berendsen, L.B.J.M., et al. Amorphous carbon nanoparticles: a versatile label for rapid diagnostic (immuno)assays, *Anal Bioanal Chem* **2012**, *402*, 593-600, 10.1007/s00216-011-5340-5.
43. Wilkins, M.D.; Turner, B.L.; Rivera, K.R.; Menegatti, S., et al. Quantum dot enabled lateral flow immunoassay for detection of cardiac biomarker NT-proBNP, *Sensing and Bio-Sensing Research* **2018**, *21*, 46-53, <https://doi.org/10.1016/j.sbsr.2018.10.002>.

44. Liang, Z.-Y.; Deng, Y.-Q.; Tao, Z.-Z. A quantum dot-based lateral flow immunoassay for the rapid, quantitative, and sensitive detection of specific IgE for mite allergens in sera from patients with allergic rhinitis, *Anal Bioanal Chem* **2020**, *412*, 1785-1794, 10.1007/s00216-020-02422-0.
45. Hou, Y.; Wang, K.; Xiao, K.; Qin, W., et al. Smartphone-Based Dual-Modality Imaging System for Quantitative Detection of Color or Fluorescent Lateral Flow Immunochromatographic Strips, *Nanoscale research letters* **2017**, *12*, 291-291, 10.1186/s11671-017-2078-9.
46. Liu, Z.; Hua, Q.; Wang, J.; Liang, Z., et al. A smartphone-based dual detection mode device integrated with two lateral flow immunoassays for multiplex mycotoxins in cereals, *Biosensors and Bioelectronics* **2020**, *158*, 112178, <https://doi.org/10.1016/j.bios.2020.112178>.
47. Paterson, A.S.; Raja, B.; Mandadi, V.; Townsend, B., et al. A low-cost smartphone-based platform for highly sensitive point-of-care testing with persistent luminescent phosphors, *Lab on a Chip* **2017**, *17*, 1051-1059, 10.1039/C6LC01167E.
48. Priye, A.; Ball, C.S.; Meagher, R.J. Colorimetric-Luminance Readout for Quantitative Analysis of Fluorescence Signals with a Smartphone CMOS Sensor, *Analytical chemistry* **2018**, *90*, 12385-12389, 10.1021/acs.analchem.8b03521.
49. Ludwig, S.K.J.; Tokarski, C.; Lang, S.N.; van Ginkel, L.A., et al. Calling Biomarkers in Milk Using a Protein Microarray on Your Smartphone, *PLoS One* **2015**, *10*, e0134360, 10.1371/journal.pone.0134360.
50. Pilolli, R.; Monaci, L.; Visconti, A. Advances in biosensor development based on integrating nanotechnology and applied to food-allergen management, *TrAC Trends in Analytical Chemistry* **2013**, *47*, 12-26, <https://doi.org/10.1016/j.trac.2013.02.005>.
51. Zhou, J.; Qi, Q.; Wang, C.; Qian, Y., et al. Surface plasmon resonance (SPR) biosensors for food allergen detection in food matrices, *Biosensors and Bioelectronics* **2019**, *142*, 111449, <https://doi.org/10.1016/j.bios.2019.111449>.
52. Masson, J.-F. Portable and field-deployed surface plasmon resonance and plasmonic sensors, *Analyst* **2020**, *145*, 3776-3800, 10.1039/D0AN00316F.
53. Guner, H.; Ozgur, E.; Kokturk, G.; Celik, M., et al. A smartphone based surface plasmon resonance imaging (SPRI) platform for on-site biodetection, *Sensors and Actuators B: Chemical* **2017**, *239*, 571-577, <https://doi.org/10.1016/j.snb.2016.08.061>.
54. Preechaburana, P.; Gonzalez, M.C.; Suska, A.; Filippini, D. Surface plasmon resonance chemical sensing on cell phones, *Angew Chem Int Ed Engl* **2012**, *51*, 11585-11588, 10.1002/anie.201206804.
55. Liu, Y.; Liu, Q.; Chen, S.; Cheng, F., et al. Surface Plasmon Resonance Biosensor Based on Smart Phone Platforms, *Scientific Reports* **2015**, *5*, 12864, 10.1038/srep12864.
56. Bremer, K.; Roth, B. Fibre optic surface plasmon resonance sensor system designed for smartphones, *Opt. Express* **2015**, *23*, 17179-17184, 10.1364/OE.23.017179.
57. Roche, P.J.R.; Fillion-Côté, S.; Cheung, M.C.K.; Chodavarapu, V.P., et al. A Camera Phone Localised Surface Plasmon Biosensing Platform towards Low-Cost Label-Free Diagnostic Testing, *Journal of Sensors* **2011**, *2011*, 406425, 10.1155/2011/406425.
58. Dutta, S.; Saikia, K.; Nath, P. Smartphone based LSPR sensing platform for bio-conjugation detection and quantification, *RSC Advances* **2016**, *6*, 21871-21880, 10.1039/C6RA01113F.

59. Fan, Z.; Geng, Z.; Fang, W.; Lv, X., et al. Smartphone Biosensor System with Multi-Testing Unit Based on Localized Surface Plasmon Resonance Integrated with Microfluidics Chip, *Sensors (Basel)* **2020**, *20*, 446, 10.3390/s20020446.
60. Lertvachirapaiboon, C.; Baba, A.; Shinbo, K.; Kato, K. A smartphone-based surface plasmon resonance platform, *Analytical Methods* **2018**, *10*, 4732-4740, 10.1039/C8AY01561A.
61. Huang, L.; Tian, S.; Zhao, W.; Liu, K., et al. Multiplexed detection of biomarkers in lateral-flow immunoassays, *Analyst* **2020**, *145*, 2828-2840, 10.1039/C9AN02485A.
62. Guo, M.; Wang, J.; Du, R.; Liu, Y., et al. A test strip platform based on a whole-cell microbial biosensor for simultaneous on-site detection of total inorganic mercury pollutants in cosmetics without the need for predigestion, *Biosensors and Bioelectronics* **2020**, *150*, 111899, <https://doi.org/10.1016/j.bios.2019.111899>.
63. Bartosh, A.V.; Urusov, A.E.; Petrakova, A.V.; Kuang, H., et al. Highly sensitive lateral flow test with indirect labelling for zearalenone in baby food, *Food and Agricultural Immunology* **2020**, *31*, 653-666, 10.1080/09540105.2020.1750570.
64. Bartosh, A.V.; Sotnikov, D.V.; Hendrickson, O.D.; Zherdev, A.V., et al. Design of Multiplex Lateral Flow Tests: A Case Study for Simultaneous Detection of Three Antibiotics, *Biosensors* **2020**, *10*, 17, 10.3390/bios10030017.
65. Anfossi, L.; Di Nardo, F.; Cavallera, S.; Giovannoli, C., et al. Multiplex Lateral Flow Immunoassay: An Overview of Strategies towards High-throughput Point-of-Need Testing, *Biosensors (Basel)* **2018**, *9*, 10.3390/bios9010002.
66. Tsai, T.-T.; Huang, T.-H.; Ho, N.Y.-J.; Chen, Y.-P., et al. Development of a multiplex and sensitive lateral flow immunoassay for the diagnosis of periprosthetic joint infection, *Scientific Reports* **2019**, *9*, 15679, 10.1038/s41598-019-52051-6.
67. Tsigkaris, A.S.; Pulkrabova, J.; Hajslova, J.; Filippini, D. A Hybrid Lab-on-a-Chip Injector System for Autonomous Carbofuran Screening, *Sensors (Basel)* **2019**, *19*, 5579, 10.3390/s19245579.
68. Reboud, J.; Xu, G.; Garrett, A.; Adriko, M., et al. Paper-based microfluidics for DNA diagnostics of malaria in low resource underserved rural communities, *Proc Natl Acad Sci U S A* **2019**, *116*, 4834-4842, 10.1073/pnas.1812296116.
69. Joh, D.Y.; Hucknall, A.M.; Wei, Q.; Mason, K.A., et al. Inkjet-printed point-of-care immunoassay on a nanoscale polymer brush enables subpicomolar detection of analytes in blood, *Proceedings of the National Academy of Sciences* **2017**, 201703200, 10.1073/pnas.1703200114.
70. Altundemir, S.; Uguz, A.K.; Ulgen, K. A review on wax printed microfluidic paper-based devices for international health, *Biomicrofluidics* **2017**, *11*, 041501-041501, 10.1063/1.4991504.
71. Eriksson, E.; Lysell, J.; Larsson, H.; Cheung, K.Y., et al. Geometric Flow Control Lateral Flow Immunoassay Devices (GFC-LFIDs): A New Dimension to Enhance Analytical Performance, *Research* **2019**, *2019*, *8*, 10.34133/2019/8079561.
72. Chen, C.-A.; Yeh, W.-S.; Tsai, T.-T.; Li, Y.-D., et al. Three-dimensional origami paper-based device for portable immunoassay applications, *Lab on a Chip* **2019**, *19*, 598-607, 10.1039/C8LC01255E.

73. Liu, W.; Cassano, C.L.; Xu, X.; Fan, Z.H. Laminated Paper-Based Analytical Devices (LPAD) with Origami-Enabled Chemiluminescence Immunoassay for Cotinine Detection in Mouse Serum, *Analytical Chemistry* **2013**, *85*, 10270-10276, 10.1021/ac402055n.
74. He, Y.; Gao, Q.; Wu, W.-B.; Nie, J., et al. 3D Printed Paper-Based Microfluidic Analytical Devices, *Micromachines* **2016**, *7*, 108, 10.3390/mi7070108.
75. Otero, C.; García-Porta, N.; Taberner, J.; Pardhan, S. Comparison of different smartphone cameras to evaluate conjunctival hyperaemia in normal subjects, *Scientific Reports* **2019**, *9*, 1339, 10.1038/s41598-018-37925-5.
76. Akkaynak, D.; Treibitz, T.; Xiao, B.; Gürkan, U.A., et al. Use of commercial off-the-shelf digital cameras for scientific data acquisition and scene-specific color calibration, *J. Opt. Soc. Am. A* **2014**, *31*, 312-321, 10.1364/JOSAA.31.000312.
77. Nelis, J.L.D.; Zhao, Y.; Bura, L.; Rafferty, K., et al. A Randomized Combined Channel Approach for the Quantification of Color- and Intensity-Based Assays with Smartphones, *Anal Chem* **2020**, 10.1021/acs.analchem.0c01099.
78. Nelis, J.L.D.; Bura, L.; Zhao, Y.; Burkin, K.M., et al. The Efficiency of Color Space Channels to Quantify Color and Color Intensity Change in Liquids, pH Strips, and Lateral Flow Assays with Smartphones, *Sensors (Basel)* **2019**, *19*, 5104, 10.3390/s19235104.
79. Charrière, R.; Hébert, M.; Trémeau, A.; Destouches, N. Color calibration of an RGB camera mounted in front of a microscope with strong color distortion, *Appl. Opt.* **2013**, *52*, 5262-5271, 10.1364/AO.52.005262.
80. Chen, Y.; Fu, Q.; Li, D.; Xie, J., et al. A smartphone colorimetric reader integrated with an ambient light sensor and a 3D printed attachment for on-site detection of zearalenone, *Anal Bioanal Chem* **2017**, *409*, 6567-6574, 10.1007/s00216-017-0605-2.
81. Fu, Q.; Wu, Z.; Xu, F.; Li, X., et al. A portable smart phone-based plasmonic nanosensor readout platform that measures transmitted light intensities of nanosubstrates using an ambient light sensor, *Lab on a Chip* **2016**, *16*, 1927-1933, 10.1039/C6LC00083E.
82. Coskun, A.F.; Wong, J.; Khodadadi, D.; Nagi, R., et al. A personalized food allergen testing platform on a cellphone, *Lab on a Chip* **2013**, *13*, 636-640, 10.1039/C2LC41152K.
83. Huang, X.; Xu, D.; Chen, J.; Liu, J., et al. Smartphone-based analytical biosensors, *Analyst* **2018**, *143*, 5339-5351, 10.1039/C8AN01269E.
84. Mejía-Salazar, J.R.; Rodrigues Cruz, K.; Materón Vásques, E.M.; Novais de Oliveira, O., Jr. Microfluidic Point-of-Care Devices: New Trends and Future Prospects for eHealth Diagnostics, *Sensors (Basel)* **2020**, *20*, 1951, 10.3390/s20071951.
85. Ng, K.H.; Bezak, E. Prejudice in science - Lessons from the coronavirus story, *Phys Med* **2020**, *75*, 83-84, 10.1016/j.ejmp.2020.06.011.
86. Kucirka, L.M.; Lauer, S.A.; Laeyendecker, O.; Boon, D., et al. Variation in False-Negative Rate of Reverse Transcriptase Polymerase Chain Reaction-Based SARS-CoV-2 Tests by Time Since Exposure, *Ann Intern Med* **2020**, *173*, 262-267, 10.7326/M20-1495.

87. Ragnesola, B.; Jin, D.; Lamb, C.C.; Shaz, B.H., et al. COVID19 antibody detection using lateral flow assay tests in a cohort of convalescent plasma donors, *BMC Research Notes* **2020**, *13*, 372, 10.1186/s13104-020-05212-0.
88. Boxer, J.; Weddell, S.; Broomhead, D.; Hogg, C., et al. Home pregnancy tests in the hands of the intended user, *Journal of Immunoassay and Immunochemistry* **2019**, *40*, 642-652, 10.1080/15321819.2019.1671861.
89. van Emmerik, T.; Schwarz, A. Plastic debris in rivers, *WIREs Water* **2020**, *7*, e1398, 10.1002/wat2.1398.
90. Koo, J.H.; Jeong, S.; Shim, H.J.; Son, D., et al. Wearable Electrocardiogram Monitor Using Carbon Nanotube Electronics and Color-Tunable Organic Light-Emitting Diodes, *ACS Nano* **2017**, *11*, 10032-10041, 10.1021/acsnano.7b04292.
91. Keum, D.H.; Kim, S.-K.; Koo, J.; Lee, G.-H., et al. Wireless smart contact lens for diabetic diagnosis and therapy, *Science Advances* **2020**, *6*, eaba3252, 10.1126/sciadv.aba3252.
92. Gao, W.; Emaminejad, S.; Nyein, H.Y.Y.; Challa, S., et al. Fully integrated wearable sensor arrays for multiplexed in situ perspiration analysis, *Nature* **2016**, *529*, 509-514, 10.1038/nature16521.
93. Wang, Y.; Qiu, Y.; Ameri, S.K.; Jang, H., et al. Low-cost, μm -thick, tape-free electronic tattoo sensors with minimized motion and sweat artifacts, *npj Flexible Electronics* **2018**, *2*, 6, 10.1038/s41528-017-0019-4.

—

S

Summary



Summary

This thesis described the design and development of prototypical portable analytical devices for multiplex food allergen immunodetection; from sample preparation all the way through to smartphone-based readout. Furthermore, it explored the fundamental binding mechanisms underlying sandwich format immunoassays including antibody-antigen interactions, affinity, cross-reactivity, kinetics and high antigen concentration-dependent effects such as the hook effect. In Chapter 1, the scene was set by introducing the need for disposable allergen immunoassays before providing general information about sample preparation, immunosensing, 3D-printing and smartphone-detection.

In Chapter 2, a comprehensive overview of immunochemical food allergen assays and detectors in the context of their user-friendliness was provided. It summarized traditional laboratory-based methods for food allergen detection such as enzyme-linked-immunosorbent assay, flow cytometry, and SPR, and the potential to modernize these methods by interfacing them with a smartphone readout system, before discussing the emergence of novel smartphone-based food-allergen detection methods that had specifically been designed with the intention of being consumer-friendly. The chapter outlined the criteria for consumer-friendly allergen detection devices as being rapid, affordable, sensitive, simple, multiplex and linked with a smartphone-based detector.

The concepts of assay speed and sensitivity were addressed in Chapter 3, where an SPR-based method was developed for screening and selecting crude anti-hazelnut antibodies based on their relative association rates, cross reactivity and sandwich pairing capabilities, for subsequent application in a rapid LFIA. The method allowed for the selection of antibodies with optimal binding characteristics which were also reflected when applied in sandwich format carbon nanoparticle based LFIA. One of the developed LFIA had a time-to-result of 30 seconds and a LOD of 0.1 ppm when detecting hazelnut in a real-life cookie matrix. A smartphone was used to record videos of the developing LFIA and endpoint images of the developed LFIA and two freely downloadable smartphone apps were then used to analyze the data.

The antibodies selected in Chapter 3 were applied in three different formats of multiplexed paper-based immunoassay in Chapter 4, namely active and passive flow-through assays, and lateral flow immunoassays with different test line configurations. All three formats of assay formats performed well, detecting total hazelnut protein (THP) and total peanut protein (TPP) in the low-ppm range in both spiked buffer and real-life cookie matrix, with the fastest assay time being 1 min and the slowest being 10 min. It was found that the LFIA were more reproducible and consumer-operable compared with the flow-through immunoassays, and a larger dilution of THP/TPP limited the occurrence of high-

concentration dependent effects. Two different smartphone models were used for the analysis of optimized assays, showing that using an app like OpenCamera to record smartphone images allowed for excellent agreement between the two different models. Additionally, the optimal LFIA configuration was validated as a screening method in spiked matrix extract, blank matrix extract ($n = 20$) and incurred spiked flour.

The optimized multiplex LFIA that was validated in Chapter 4, was integrated with interconnectable, 3D-printed sample preparation devices in Chapter 5. The chapter described the development and characterization of a novel, compact, inexpensive, and prototype immunosensor combining sample preparation and on-chip reagent storage for multiplex allergen lateral flow immunosensing. The handheld prototype allowed for the total homogenization of solid food samples, 1 minute solid-liquid allergenic protein extraction, 3D-printed sieve-based filtration, ULOC-enabled dilution, mixing, transport, and smartphone-based detection of hazelnut and peanut allergens in solid bakery products with limited operational complexity. A 3D-printed smartphone holder was developed to allow for detection of developing LFIAs under controlled lighting conditions. The multiplex lateral flow immunoassay (LFIA) detected allergens as low as 0.1 ppm in real bakery products; the already consumer-operable system demonstrated its potential for future citizen science approaches by being tested by an untrained user (teenager), proving its usability.

The 3D-printed smartphone holder presented in Chapter 5 was used to enable dynamic data acquisition and false negative monitoring of developing LFIA signals in Chapter 6. This chapter comprehensively studied how high antigen concentrations influence sandwich format immunoassays using LFIA and SPR and developed a smartphone-based video method for dynamic monitoring of high concentration effects in LFIA. Digital analysis of the video data allowed for clear differentiation between highly positive and false negative samples in order to indicate whether the LFIA was operating in the assays dynamic working range or at critically high concentrations. This chapter established that while the endpoint T/C ratio is an appropriate metric for semi-quantification of LFIAs within the dynamic working range, outside of this range when the test or control line is falsely diminished, the final T/C ratio is influenced.

The research presented in this thesis provides an important advancement in the development of portable analytical devices for integrated consumer-operable allergen detection and a means to monitor for false negative results in LFIA. In Chapter 7, the key themes of sample preparation, immunosensing and smartphone detection were re-examined; the major achievements and challenges of this thesis were dissected and an outlook to the future of disposable analytical devices were discussed.

CV

Curriculum Vitae



Curriculum Vitae



Georgina Maureen Ross was born on the 29th of November 1993 in London, United Kingdom. After completing her A-levels (Cheam High School & Sixth Form) in 2012, she started her bachelor's degree in Forensic Science at Bournemouth University (BU). Following her BSc, she received an academic excellence scholarship for studying a master's degree in Forensic Toxicology by Research at BU. Her MSc thesis focused on the development of a competitive LFIA for Ochratoxin A detection, for which she spent 2 months as a guest researcher in Birmingham at Abingdon Health Ltd. In May 2017, she started her PhD under the MSCA H2020 EU-funded project; FoodSmartphone. Her project focused on the

development of portable paper-based and 3D-printed immunoanalytical devices for the detection of multiple food allergens; the results obtained in the period between 2017-2020 are presented in this thesis. Since 2020, Georgina has worked as researcher in the Biosensors & Bioassays group of WFSR.

Publications

Ross, G.M.S., Filippini, D., Nielen, M.W.F., Salentijn, G.IJ., 2020. Unraveling the hook effect: a comprehensive study of high antigen concentration effects in sandwich lateral flow immunoassay. *Analytical Chemistry*. 92, 23, 15587-15595. doi: 10.1021/acs.analchem.0c03740

Ross, G.M.S., Filippini, D., Nielen, M.W.F., Salentijn, G.IJ., 2020. Interconnectable solid-liquid protein extraction unit and chip-based dilution for multiplexed consumer immunodiagnosics. *Analytica Chimica Acta*. 1140. 190-198. doi: 10.1016/j.aca.2020.10.018.

Ross, G.M.S., Salentijn, G.IJ., Nielen, M.W.F., 2019. A Critical Comparison between Flow-through and Lateral Flow Immunoassay Formats for Visual and Smartphone-Based Multiplex Allergen Detection. *Biosensors*. 9(4). doi: 10.3390/bios9040143

Ross, G.M.S., Bremer, M.G.E.G, Wichers, J.H., Van Amerongen, A., Nielen, M.W.F., 2018. Rapid Antibody Selection Using Surface Plasmon Resonance for High-Speed and Sensitive Hazelnut Lateral Flow Prototypes. *Biosensors*. 8(4), doi: 10.3390/bios8040130.

Ross, G.M.S., Bremer, M.G.E.G, Nielen, M.W.F., 2018. Consumer-friendly food allergen detection: moving towards smartphone-based immunoassays. *Analytical and Bioanalytical Chemistry*. 410, 5353- 5371. doi: 10.1007/s00216-018-0989-7

Publications (not included in this thesis)

Tsagkaris, A.S., Nelis, J.L.D., **Ross, G.M.S.**, et al 2019. Critical assessment of recent trends related to screening and confirmatory analytical methods for selected food contaminants and allergens. *Trends in Analytical Chemistry*. 121, 115688. doi: 10.1016/j.trac.2019.115688

Popular science

Ross, G.M.S., Tsagkaris, A.S, Suman, M. Nielen, M.W.F., Elliott., C.T. 2020. A smart era for food safety tests. *New Food Magazine*. 2. 24-26



A

Acknowledgements



Acknowledgements

The work presented in this thesis would have never been possible without the guidance, support and motivation from the brilliant people surrounding me. It is difficult to put into words how grateful I am for everything you have done, but I will try.

Firstly, I want to thank my promotor, Michel Nielen. You are truly inspirational; thank you for your humour, directness, guidance, opportunities and for continually challenging me during this project. I appreciate you listening to and encouraging my ideas. Your confidence in me has helped formulate my independence as a scientist. And of course, I will always be thankful that you helped me with my Irish citizenship.

I could not have asked for a better mentor than my co-promotor, Gert Salentijn. Since becoming my supervisor in 2019, I have appreciated our stimulating research discussions which often lead to interesting new ideas – Thanks for brainstorming with me! I value your candidness and feel that I can come to you for advice on any issue which is so important. Perhaps more importantly, I appreciate your sense of humour and ability to keep things lighthearted even during difficult times. Thank you for all the invaluable research, design, career and writing advice (especially during what the hook) – you have challenged me to become a better scientist.

Thanks to my first supervisor Monique Bremer for believing in me and allowing me to start my PhD. You encouraged me to think critically about my own work and did not lose patience when I tried to go in too many directions at once.

To my fantastic colleagues from Biosensors and Bioassays, Nathalie, Jeroen, Richard, Alexander, Liza, Rian and Mang Xu, thanks for fun in the lab and exciting experiments. Plus, thanks Adil and Will for giving me a helping hand during my hand injury. Also, a special thanks to Leen and Toine for employing me as a researcher during my PhD's final stages, I look forward to our ongoing work.

Thanks to all my colleagues at Wageningen Food and Biobased research. Notably, thanks to Aart van Amerongen for allowing me to work in your lab and for the discussions that helped formulate my first research paper. Jan Wichers - I cannot thank you enough for training me in LFIA development and CNP conjugation as well as for continuing to provide troubleshooting advice throughout my PhD!

Thanks to everyone at ORC for coming to my presentations, asking thought-provoking questions and providing valuable input. To address some ORC people individually, I want to thank Fred for the advice when starting my PhD and motivating me to network

at FAST. My PhD week group, Jordi, Sevil and Andrii for the continued laughs and Jorick, Esther and Ian for making me feel so welcome after first joining ORC.

I would especially like to thank Milou – you were always there for a coffee and a chat about our projects and social issues. You will always be Shakespeare in my head. Seeing how hard you worked has been a massive inspiration. I would trust very few people to take care of my snakes, and I will always be appreciative of you looking after Irwin for me!

To my paranymphs:

When I arrived in 2017, Nathalie made me instantly feel welcome and part of the team. You have continuously provided exceptional advice on all SPR related matters, which has helped me so much. You are such a positive person, and I really enjoy our conversations both inside and outside of research. I am looking forward to working with you more this next year and wish you all the luck finishing your own thesis (with LaTeX of course!).

Ariadni, when we interviewed you for FoodSmartphone, I already knew we would be friends. You are such a warm, vibrant, intelligent person who has made sharing an office with you a hilarious experience – even when Amazon listens in to our conversations. I appreciate always having someone to troubleshoot research with. I am excited to see you doing so well in your own PhD – I wish you every success.

Being part of a large research consortium through FoodSmartphone has been a transformative experience that was only possible through many people's dedication and funding from the MSCA EU H2020 program. First, thanks to our project co-ordinator Michel and project secretaries Wim Beek and Ingeborg van Leeuwen-Bol for keeping everything organized and for the lifetime supply of FoodSmartphone stickers. Thank you to all the project partners from WFSR, QUB, UCT, CSIC, LIU, Aquamarijn, CSEM, Barilla and Zeulab for the advice, discussions, secondments and summer schools. I am grateful to Jacob Baggerman and Ai Nguyen for training me in SEM during my secondment to Aquamarijn. I particularly want to thank my collaborators Michele Suman and Chris Elliott for the opportunity to publish a popular science article which further challenged my writing skills. Thank you to my past and present fellow ESRs, Vincent, Sahl, Raheel, Safiye, Klaudia, Ariadni, Julian, Chi, Javier, Jack, Aris and Jordi. I have valued the great collaborations, idea generation, presentations, beer-drinking and travel – I am sure we will work together again.

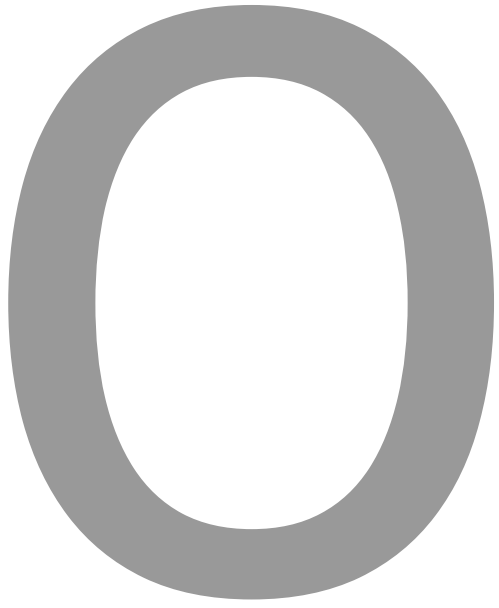
Thanks to Daniel Filippini and Anke Suska for making me feel so welcome in Sweden. Daniel, thank you for pushing me outside of my comfort zone, teaching me CAD/3D-printing, introducing me to programming, formulating research ideas with me and chatting about

photography. The lively discussions we had, the skills you taught me, and the collaborate research we produced has helped make me a more confident and competent researcher.

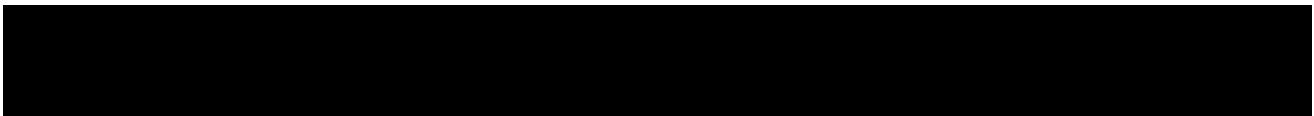
Finally, I want to thank my friends and family. You have always believed in me and encouraged me to reach my potential, thank you for your patience with my stress and chaotic schedule these past years. Bob, thank you for cooking me vegan food, exploring and getting tattooed with me. Charlotte, you are the best sister and friend I could ask for; thank you for being so perceptive and formidable, please never change.

This thesis would not have been possible without my parents', I cannot thank you enough for everything you have done for me. Dad, you have always provided support and the opportunity to grow – I could not have pictured being here when you took me to the BU open day back in 2011. Mum, you have always been my biggest motivator. Thank you for letting us read Animal Atlas every night; you stimulated me as a scientist and never dampened my curiosity or limited my imagination.

Connor, I cannot begin to express my gratitude for the love and encouragement you have provided during these 3 degrees. You have always pushed me to fulfil my dreams and supported me in moving to Wageningen for this PhD. You have helped me practice every presentation, celebrated my publications, empathized with my failed experiments and cursed with me after journal rejections. Thank you for everything, I love you.



Overview of completed training activities



Overview of completed training activities

Discipline specific activities	Organizer	Place	Year
1st FoodSmartphone summer school	VLAG	Wageningen	2017
WUR annual PhD symposium*	WUR	Wageningen	2018
Forum of Science & Technology (FAST)	TI-COAST	Veldhoven	2018
2nd FoodSmartphone summer school*	VSCHT	Prague	2018
Rapid Methods Europe*	RME	Amsterdam	2018
Swiss POC conference	CSEM	Chur	2018
Biodot Lateral Flow Workshop*	Biodot	Amsterdam	2018
World of Science & Technology*	WOTS	Utrecht	2018
Advanced Food Analysis	VLAG	Wageningen	2019
Food Allergy Forum*	FAF	Amsterdam	2019
Forum of Science & Technology (FAST)*	TI-COAST	Veldhoven	2019
AOAC International*	AOAC	Colorado	2019
NRL Food Allergen Workshop*	CER Group	Brussels	2019
Recent Advances in Food Analysis (RAFA)	RAFA	Prague	2019
Advanced course: 3D-printing of microfluidic components	LIU	Sweden	2019
Barilla industrial business training	Barilla	Online	2020
Smart Tech for Food (ST4F)*	CSIC	Online	2020
Rapid Methods Europe*	RME	Online	2021

General courses	Organizer	Place	Year
Scientific Writing	WGS	Wageningen	2017
Brain Training	WGS	Wageningen	2017
Efficient Writing Strategies	WGS	Wageningen	2017
VLAG PhD Week	VLAG	Baarlo	2018
Scientific Artwork	WGS	Wageningen	2018
Presenting with Impact	WGS	Wageningen	2018
Scientific Publishing	WGS	Wageningen	2018

Other activities	Organizer	Place	Year
Preparation of PhD research proposal	VLAG	Wageningen	2017
Weekly group meetings: Organic Chemistry*	ORC	Wageningen	2017-2020
Weekly group meetings: Biosensors*	WFSR	Wageningen	2018-2021
Miniaturization of Biosensing*	WFSR/ TI-COAST	Nijmegen	2018-2021
MSCA outreach: primary school workshop*	WFSR	London	2018
MSCA outreach: university lecture/workshop*	WFSR	Bournemouth	2018
TFTB-38 Imaging & Ubiquitous Biosensing	LIU	Sweden	2019
Weekly group meetings: Optical Devices Lab*	LIU	Sweden	2019

*represents oral presentation

The research described in this thesis was funded by the European Union's Horizon 2020 research and innovation program under the Marie Skłodowska-Curie grant agreement No 720325.

Printed by ProefschriftMaken